SLAC-329
UC-34D
(T/E)

Opportunities and Requirements for Experimentation at a Very High Energy e^+e^- Collider

C. Ahn, C. Baltay, T. L. Barklow, P. R. Burchat,
D. L. Burke, A. R. Cooper, C. Dib, G. J. Feldman,
J. F. Gunion, H. E. Haber, T. M. Himel, B. W. Lynn,
S. Komamiya, M. E. Peskin, A. Petersen, and R. J. Van Kooten

May 1988

Prepared for the Department of Energy
under contract number DE–AC03–76SF00515

Printed in the United States of America. Available from the National Technical Information Service, U. S. Department of Commerce, 5285 Port Royal Road, Springfield, Virginia 22161. Price: Printed Copy A10, Microfiche A01.

Authors' affiliations:

C. AHN, T. L. BARKLOW, D. L. BURKE, A. R. COOPER,
C. DIB, G. J. FELDMAN, T. M. HIMEL, S. KOMAMIYA,
M. E. PESKIN, A. PETERSEN, AND R. J. VAN KOOTEN*

Stanford Linear Accelerator Center
Stanford University, Stanford, California 94309

C. BALTAY†

Department of Physics, Columbia University
New York, N. Y. 10027

P. R. BURCHAT AND H. E. HABER‡

Institute for Particle Physics, University of California
Santa Cruz, California 95064

J. F. GUNION§

Department of Physics, University of California
Davis, California 95616

B. W. LYNN¶

Department of Physics, Stanford University
Stanford, California 94305

* Work supported by the Department of Energy, contract DE–AC03–76SF00515.
† Work supported by the National Science Foundation.
‡ Work supported by the Department of Energy, contract DE–AM03–76SF00010.
§ Work supported by the Department of Energy, contract DOE–AC03–76SF00098.
¶ Work supported by the National Science Foundation, contract NSF–PHY–86–12280.

Table of Contents

1. Introduction

Over the past fifteen years of high-energy physics, electron-positron annihilation has been the most productive of all reactions probing the fundamental interactions. The e^+e^- annihilation process is unique in offering at the same time copious production of novel particles, low backgrounds from more conventional physics, and the most efficient use of the energy which an accelerator provides. These features have allowed the detailed characterization of the charm and bottom quark-antiquark systems and the unambiguous discovery of gluon jets—the crucial ingredients in the establishment of Quantum Chromodynamics as the correct theory of the strong interactions—as well as the discovery of the tau lepton and the confirmation of the weak and electromagnetic properties of all of the quarks and leptons at high energy. Over the next few years, experiments will begin at SLC and LEP, and we anticipate new discoveries from the detailed study of the Z^0 resonance. It is time, then, to begin to think out how one might continue this mode of experimentation to still higher energies.

This document is the report of a committee convened by the Director of SLAC, Burton Richter, to set out the major physics goals of an e^+e^- collider in the energy range 600 GeV – 1 TeV, corresponding to the next feasible step in accelerator technology. The committee was charged with the task of outlining the main experiments that such a collider might carry out and the requirements which those experiments place on the accelerator design.

It is clear that a high-energy e^+e^- collider, even one with a center of mass energy below 1 TeV, will have great opportunity to address the central open questions of particle physics. At the moment, we seem to understand very well the laws which govern the basic strong, weak, and electromagnetic forces among quarks and

leptons. However, these laws apparently require the existence of a further particle or set of particles, the Higgs bosons, which mediate a new, so far undiscovered, force. This force is responsible for giving the W and Z bosons their masses, and also for generating the masses of the quarks and leptons. In theoretical models of the Higgs bosons, the new forces associated with this new sector become evident at energies below or of the order of 1 TeV. In many models, new types of fermions or weak bosons also become apparent at the energy scale set by the Higgs phenomenon. An e^+e^- collider will be able to search directly for the Higgs bosons and will also produce and make visible whatever other new species might exist within its energy range.

Along with this promise, however, come new problems associated with the move to higher energies. The most important consideration for any study of particle physics at very high energy is that increased luminosity is required to do almost any interesting experiment. Though there do exist speculative theoretical scenarios under which modest luminosities would suffice, most theoretical models predict that the cross sections for new physics will be of the order of the elementary QED point cross section:

$$1\ \mathrm{R} = \frac{4\pi\alpha^2}{3s} = \frac{86.8\ \mathrm{fb}}{[E\ (\mathrm{TeV})]^2}\ . \tag{1.1}$$

To produce 10^3 events per year of a reaction with the point cross section at a center of mass energy of 1 TeV requires a luminosity of 10^{33} cm^{-2}sec^{-1}. This feature alone provides a substantial challenge to accelerator designers. We expect that the combined requirements of high luminosity and high energy cannot be met without introducing some complication in the conduct of experiments. To avoid large synchrotron radiation losses, the accelerator will need to be a linear collider rather than a storage ring. To achieve high luminosity, the bunches of electrons and positrons which collide must then be exceedingly small and highly focussed. This implies, in turn, that the nonlinear interactions of these bunches at the collision point will be extremely large, leading to significant synchrotron radiation ("beamstrahlung") and probably to significant disruption of the bunches during the collision process.

One of the goals of this study was to assess the new experimental problems that this energy smearing and other obstacles of the machine design would entail. It is one of our main conclusions that these new complications need not significantly hinder experiments. Because the basic environment provided by e^+e^- annihilation is so simple, it is not difficult to design searches for new particles which are clean and efficient. As long as the luminosity is high enough, we believe that we can carry out clear and definitive experiments.

The plan of this report is as follows: In the remainder of this chapter, we will review the advantages of the e^+e^- annihilation reaction in more detail and give some comparisons between a high-energy e^+e^- collider of the type that we will discuss and a large proton-proton collider such as the proposed Superconducting Supercollider. In Chapter 2, we will summarize the main results of our study which bear on accelerator design, discussing in some detail appropriate guidelines for energy, luminosity, and the quality of the experimental environment. We will also emphasize here the importance of longitudinal polarization as an analysis tool in this energy regime. In Chapter 3, we will review the general characteristics of e^+e^- annihilation events within the standard model in the energy region we will discuss.

The remaining sections of this report will discuss in some detail the four physics issues which we see as the most important topics to be addressed by e^+e^- annihilation experiments in this energy region. Chapter 4 will discuss the most straightforward experiments for the new collider, searches for new quarks and leptons. Chapter 5 will discuss the search for the Higgs boson. In Chapters 6 and 7 we will discuss two possible probes of modifications of the standard weak interaction gauge theory: Chapter 6 will discuss the physics associated with the appearance of a new Z^0 resonance. Chapter 7 will discuss the pair-production of W bosons, emphasizing the use of this reaction as a precision test of weak interaction theory. Finally, in Chapters 8 and 9, we will discuss two specific examples of searches for new particles associated with a possible new sector of forces at TeV energies. Chapter 8 will discuss the search for supersymmetric particles in high-energy e^+e^-

collisions. Chapter 9 will discuss the search for charged Higgs bosons and other signs of an extended Higgs sector. In each of these discussions, we will present both the theoretical importance of the study and the detailed experimental technique by which it can be carried out.

Our work in this report builds on previous studies of e^+e^- physics at very high energy which have been presented in refs. 1–6. Some of the work of our committee has been reported in more pedagogical form in the contributions by two of our members to the 1987 SLAC Summer Institute proceedings. Of these, ref. 7 summarizes the basic theoretical results on high-energy e^+e^- annihilation, including a careful discussion of the physics underlying the formulae, and ref. 8 gives a heuristic overview of the experimental considerations. These two articles might provide the reader a useful complement to the analyses which we report here.

1.1. The Advantages of e^+e^- Annihilation

We have already noted the important role that e^+e^- reactions have played in the development of particle physics. We will now review more specifically the special qualities of this reaction responsible for its great success. We will argue in the body of this report that these qualities will remain valid for the very high energy experiments that we consider here.

The central feature of high-energy e^+e^- collisions, from which all other essential properties follow, is that the particular process in which the electron and positron annihilate into new species—despite its small cross section—can be cleanly separated from other possible e^+e^- reactions. In the current energy regime of PEP and PETRA, the annihilation process competes only with the two-photon reaction and with purely electromagnetic processes such as Bhabha scattering. Since two-photon processes characteristically involve only a small fraction of the total available center of mass energy, but with no imbalance of transverse momentum, and since, in any event, the two-photon cross sections are not large, it has been

possible to remove these events from searches for new physics with relatively simple cuts. This has allowed searches for a wide range of possible new particles in which the cuts applied have relatively high efficiency but remove virtually all background.[9–11]

In the energy regime we will consider in this report, several new reactions come into play. In addition to processes involving photon-photon collisions, one can have reactions in which one or both of the the electron and positron emit W bosons. The radiative annihilation into a Z^0 boson has a relatively large cross section. Production of W and Z boson pairs becomes a major part of the annihilation cross section. It remains true, however, that the annihilation and non-annihilation events are kinematically well separated. The photon and W bremsstrahlung processes result in final states with total mass only a fraction of that available from the annihilation processes. The photon and W reactions can even be separated from one another by their transverse momentum spectra; this observation turns out to be crucial for Higgs boson searches. The final picture that we reach is one in which the additional processes available in e^+e^- reactions add richness but do not interfere in an important way with the crucial isolation of novel annihilation processes.

Once the annihilation channel has been separated from other possible processes, one can begin to take advantage of its two special virtues. The first is that of isotropy: Pair production due to the annihilation process is roughly isotropic in the lab frame, so that the natural angular cuts which detectors impose do not significantly decrease signals for new physics. The second advantage is that of democracy: Almost all particles pair-produced as final states of e^+e^- annihilation are produced with cross sections of the same order of magnitude:

$$\sigma(e^+e^- \to X\overline{X}) \;=\; \mathcal{A}\cdot(1\mathrm{R})\;, \tag{1.2}$$

times phase space, where $\mathcal{A}$ is a number between 0.25 and 5 and (1R) is the point cross section. The result (1.2) is true for pair-production of quarks and leptons, and

for charged bosons and other exotic species. It also holds for $e^+e^- \to \gamma\gamma$, e^+e^-, W^+W^-, $Z\gamma$, and ZZ, if one considers only the angular region $20° < \theta < 160°$ which excludes the large forward and backward peaks. Familiar and exotic physics processes appear with comparable probability. This result means that, in searches for some new species, the ratio of signal to background begins at roughly 1:1, even before detailed cuts on the nature of the final state are imposed. It is easy, then, for exotic processes to stand out in the data.

Carrying this argument one step further, the most important background processes turn out to be rather simple in form—quark-antiquark pair production with a bit of gluon radiation, or simple W^+W^- production; thus, the backgrounds are straightforward to characterize and remove. This means that new physics can be studied using the full range of its final states, rather than only those signatures which are particularly striking. For example, we find that one of the most efficient ways to find heavy leptons at a high-energy e^+e^- collider is to search for their decay to hadrons, plus missing neutrinos. One of our most important conclusions is that W and Z bosons may be identified by calorimetric mass determination using their hadronic final states. This gives a powerful experimental tool for tracking the weak bosons, which appear prolifically both in the signals and in the backgrounds for new physics.

An additional potential advantage of e^+e^- reactions at the high energies we consider here is the availability of longitudinal electron polarization as a probe of the reactions one observes. All e^+e^- annihilation reactions have some dependence on beam polarization, due to the interference between the virtual photon and virtual Z^0 contributions. In the regime of center of mass energies above 150 GeV, these contributions have comparable size, and so the polarization effects should be quite large. Certain processes, such as $e^+e^- \to W^+W^-$, have an exceptionally large polarization-dependence and can be removed or enhanced by the choice of electron polarization.

Leaving aside the question of the small size of cross sections, then, e^+e^- col-

liders provide an ideal environment for discovering and characterizing new physics. The best features of this environment, which have been exploited so successfully by experiments at currently accessible energies, will remain valid after the further step in energy that we consider here.

Our main goal in this report is to illustrate and amplify the central argument set out in this section. By examining the standard model background processes, and then by working through specific searches for a variety of novel states, we will illustrate the cleanliness and simplicity of e^+e^- physics in the high energy regime. We will show that straightforward analysis techniques identify new particles in a wide range of their final states, and with high efficiency, while substantially removing the background. This conclusion assures us that e^+e^- experiments will be capable of producing larges samples of exotic states which may then be probed in considerable detail, to address questions of branching fractions, mixing effects, and other specific aspects of the coupling pattern which might be important in fixing the role of these states within a grander pattern.

1.2. e^+e^- vs. pp Colliders

To complete this introduction, we would like to comment on the relation of high energy e^+e^- colliders to high energy hadron colliders in the exploration of the next scale of physics. In the Chapter 2, we will describe in specific terms the importance of searching for a new sector of particles and interactions in the energy region 100 GeV – 1 TeV. We consider this the central enterprise of high energy physics over the next fifteen to twenty years. Proton-proton and electron-positron colliders have different and complementary roles in this search.

Hadron colliders have been used to great effect in exploratory studies spanning a wide range of energy, concentrating on processes with particularly large or distinguishable cross sections. The Υ resonance and the W and Z bosons were discovered by using the energy distributions of proton constituents to scan for a resonance and by using leptonic decay modes to make the resonant events visible. The fundamental couplings of QCD have been made manifest at the CERN

collider in the very large cross section process of high transverse momentum jet production. Similar experiments can be imagined for higher energies. Indeed, for every hypothesis on the nature of the new interactions expected at TeV energies, there is some characteristic effect which should be visible at a 20–40 TeV pp collider.[12] Design studies for an accelerator of this type have been carried out both in the United States and in Europe, and the proponents of these machines are now actively seeking funds to begin construction. It now seems clear that either the American machine, the Superconducting Supercollider (SSC), or the European one, the Large Hadron Collider (LHC) at CERN, will be funded for completion in the late 1990's. Either of these devices will have the potential to explore broadly for new effects in the energy region around 1 TeV, and either might well produce the crucial piece of evidence for the general nature of new physics at those energies.

On the other hand, we do not believe that pp experiments alone will suffice to unravel the physics of the TeV energy scale. As we will stress in the next chapter, the problem which must be solved is not simply the matter of verifying a few parameters but is, rather, a profound question about new fundamental interactions. Hadron colliders have only a limited ability to answer detailed questions about this new physics. The contrast to the picture which we have set out in the previous section is striking. At pp colliders, cross sections due to conventional physics are large, and the final states resulting from these processes are complex. Searches for new physics can be carried out only by looking for distinctive final states, and, even here, some promising channels are removed by unexpected backgrounds. Polarization of the initial protons is essentially completely degraded at the level of the quarks and gluons which initiate new elementary processes. Thus, the many handles described in the previous section for the detailed characterization of new phenomena will be available only in experiments at an e^+e^- collider.

We have argued that a high energy e^+e^- collider is important to the needs of fundamental physics over the next twenty years. But we would like to add that, over an even longer term, such a collider will have a still more essential role. The enormous scale and cost of the SSC make clear that this will be the last proton

synchrotron built along conventional lines. But beyond the question of the cost and practicality of accelerators, pp collisions suffer a more fundamental limitation at energies higher than that of the SSC. On the one hand, the cross sections for parton-parton subprocesses decrease as $E_{\rm CM}{}^{-2}$ as the energy of the subprocess

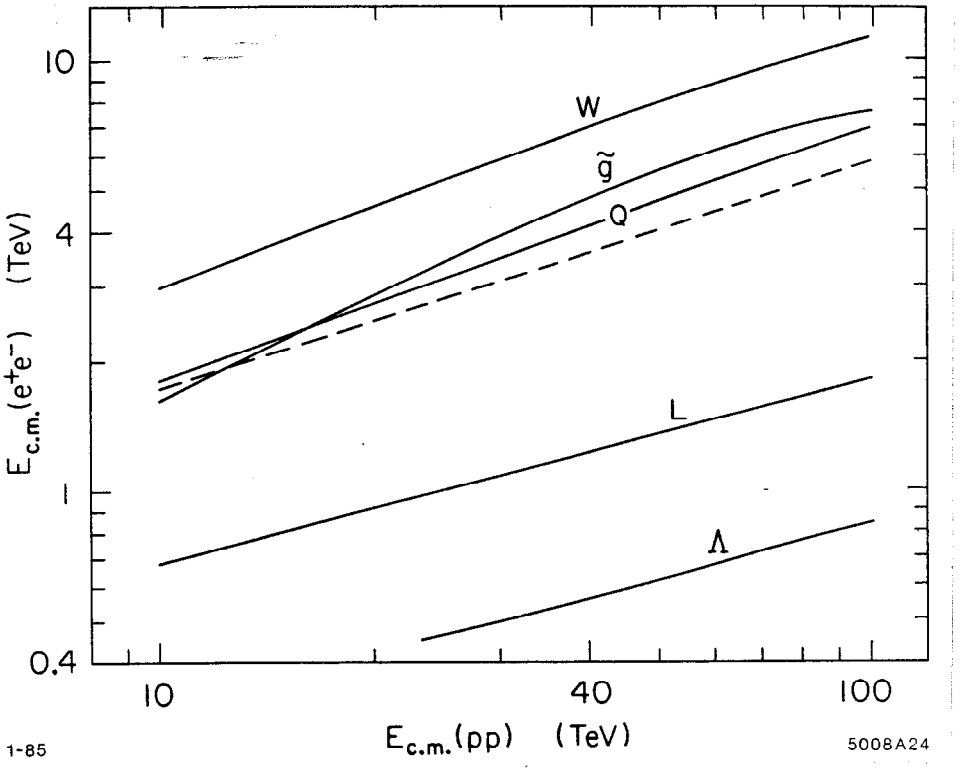

Figure 1. Comparison of effective center of mass energies of e^+e^- and pp colliders for discovering various hypothesized new particles, assuming a maximum pp luminosity of 10^{33} cm^{-2}sec^{-1}, from ref. 3. The searches considered are those for new vector bosons, supersymmetry partners, heavy quarks, heavy leptons, and fermion compositeness. The dashed line represents eq. (1.3).

is increased. On the other hand, the large size of the proton-proton inelastic cross section leads to severe experimental problems of radiation damage and event pileup at luminosities greater than 10^{33} cm^{-2}sec^{-1}; these problems become much

worse if one changes the form of the accelerator from a large synchrotron to, for example, a pp linear collider. This means that one cannot achieve the full promise of higher energy pp collisions by raising the luminosity to access rarer subprocesses. A comparison of the discovery reach of an e^+e^- collider to that of a pp collider with fixed luminosity, based on the work of ref. 12, is shown in Fig. 1. The figure justifies the empirical law

$$E_{\rm CM}(e^+e^-) \sim \sqrt{E_{\rm CM}(pp)/3}\ , \tag{1.3}$$

with both energies in TeV.

The future of high-energy physics, then, belongs to the electron-positron colliders. Accelerator physicists around the world are now assembling the techniques needed to build high-energy colliders using high-gradient linear electron accelerators incorporating the efficient power sources and tiny beam spot sizes necessary to achieve high luminosity. This is essentially a new line of accelerator technology, one which is only now receiving its first practical test in the Stanford Linear Collider project. The machine which we will discuss in this report would represent the next step after the SLC in the evolution of this technology to higher energies. From here on, we will emphasize the importance of this machine in its own right in addressing the key issues that confront us now. But one should keep in mind also that this machine provides the unique avenue to further technical progress in pushing back the frontier of fundamental physics.

2. Requirements for the New Collider

In this chapter, we will discuss the design of an e^+e^- collider for the 600 GeV–1 TeV energy range, from the viewpoint of experimentation. We will present an overview of the basic physics goals that we see for experimentation in this range, organized in terms of the constraints that the experimental program places on the collider itself. The conclusions about points of physics that we set out in this chapter will be supported by detailed analysis in Chapters 3–9.

Our most important recommendations concern energy and luminosity. Here, we have reached no surprising conclusions: We recommend that the center of mass energy of the collider be as high as can be managed in a feasible step—1 TeV, if possible. Even so, we note that many interesting milestones in speculative theories are passed already at the lower center of mass energy of 600 GeV. We recommend that special attention be given to obtaining as high a luminosity as possible. Though we will give some examples of physics processes which can be studied in event samples of a few fb^{-1}, we believe that a mature physics program at 1 TeV would require an event sample of the order of 30 fb^{-1}, corresponding to 2500 events of a process with cross section 1 R. Even if this sample were obtained over several years, it would require an actual delivered luminosity in excess of 10^{33} $\text{cm}^{-2}\text{sec}^{-1}$. We emphasize that these two requirements are linked: Since the basic cross sections decrease as E^{-2}, an increasing luminosity is needed to exploit the potential offered by increased energy. (If the energy of the machine were kept to the lower value of 600 GeV, the equivalent event sample size would be 10 fb^{-1}.)

The least trivial conclusion of our study is that many of the features of the environment of e^+e^- reactions which lead to their extreme cleanliness at current energies can be relaxed substantially without compromising the most important

experiments. Operation of a linear collider at high luminosity will entail sizable synchrotron radiation in the collision region ('beamstrahlung') and a complicated final-focus system. These features will lead to a substantial smearing of the center of mass energy of annihilation events and also to problems in working at very forward angles. These effects will certainly make experiments more difficult, but we find that neither significantly affects the ability of e^+e^- collider experiments to search for new physics.

An additional factor which we call to the attention of accelerator designers is that of polarization. We feel that longitudinal polarization of electrons will be an essential tool in the study of e^+e^- reactions in this energy region, so that one should plan for such polarization as an integral part of the collider design. We see no barrier to maintaining substantial polarization through the beam transport and collision processes at an e^+e^- linear collider.

2.1. ENERGY

We will begin by describing the physics goals of the collider which pose definite requirements for its center of mass energy. We should begin with the statement that we do not find an ironclad argument that 600 GeV, or even 1 TeV, in the center of mass will necessarily suffice to uncover the next scale of physics. On the other hand, we do find compelling the idea that the decade or so in energy above 100 GeV contains a new sector of physical forces waiting to be discovered. We believe that the search for this new sector of fundamental physics should be the major goal of the particle physics community and should be carried on with all available techniques. The machine we envision here will dramatically extend the region of this search in e^+e^- reactions, by a factor of 5 beyond the highest LEP energies. In this section, we will review the argument for new physics in this energy region and survey specific speculative models of its nature. We will see that these models typically predict dramatic new phenomena which would be visible to a 1 TeV e^+e^- collider.

We should first explain why theoretical predictions, even of a very general character, are relevant at all to the motivation for a new accelerator. During the early years of high-energy physics, and continuing through the early 1970's, the promise of an additional factor of 3 in center of mass energy was considered sufficient justification for a new machine. And, indeed, while we explored the interesting and complex region of center-of mass energies up to 4 GeV, this argument was reasonable, and even compelling. Arguments which were apparently more well-reasoned, based on detailed theories of the extrapolation to higher energies, proved to be completely off the mark. But by the time PEP and PETRA began to operate, the situation had changed in an essential way. At these energies, we have apparently discovered the start of the asymptotic region, promised by the standard gauge theory of strong, weak, and electromagnetic interactions, in which all e^+e^- reactions are well described by simple gauge boson exchanges. Within the standard model, this state of affairs continues to arbitrarily high energy. New physical phenomena can arise only from the breakdown of this elegant and broadly (if not all-) inclusive theory.

However, the great success of the standard model requires us to seriously consider all of its implications, both positive and negative. One of these is that the standard model gauge theory is incomplete in itself; to derive from the standard model its successful implications for the structure of the weak interactions, one must add to it additional structure with characteristic energy below 1 TeV. The masses of weak bosons, quarks, and leptons arise, in the standard model, from the interaction of these particles with Higgs bosons, or with some other external agent which causes the spontaneous breaking of the $SU(2) \times U(1)$ gauge symmetry. We will refer to this new system generically as the Higgs sector. The standard model is hardly explicit about its form; the Higgs sector can be realized in any of a large number of ways, from a weakly coupled theory of one scalar field to a new set of strong interactions in all their complexity. We know only, from the value of the W boson mass, that one characteristic parameter of this theory is of the order of 250 GeV. But it rests on firm theoretical grounds that the standard model cannot

break its own symmetry, or generate its own masses, with only the set of fundamental interactions we know today. Something large and profound is missing, and we must find it.

It is clear, then, that the Higgs sector exists and is waiting to be discovered. Unfortunately, it is less clear exactly where to look. Very little can be said about this question on general grounds, and so we must survey the range of theoretical models. We encourage the reader, however, to take the remainder of this section only as rough guide, because specific, model-dependent predictions outside the sphere of confirmed theory are no more likely to be correct than the corresponding predictions of the 1960's.

Theories of the Higgs sector fall generally into three classes: minimal, weak-coupling, and strong-coupling models. In the minimal models, the Higgs sector is as small as possible: It consists of one self-interacting $SU(2)$ doublet scalar field or a system indistinguishable from this one in the energy range below 1 TeV. In this model, the Higgs mechanism causes three of the four degrees of freedom of this field to be absorbed as the longitudinal polarization states of the weak bosons. All that remains beyond the weak bosons themselves is one neutral particle with scalar couplings to matter. Throughout our report, when we speak of a (singular) Higgs boson, we will be referring to this particle. Weak-coupling models complicate this structure by adding more particles. This addition may be a simple modification, in which the Higgs sector is built up of a set of $SU(2)$ doublet fields, or a more complex generalization involving new matter particles and gauge bosons. The most ambitious scheme of this type is given by postulating supersymmetry, a symmetry between fermions and bosons which, in practice, requires doubling the whole set of known elementary particles. Strong-coupling models involve building up the Higgs sector using some new strong interactions. Models involving technicolor forces, and models in which the quarks and leptons are composite structures, are generally of this type.

The three classes of models have quite different experimental signatures. In the

minimal scenarios, one must search for the unique neutral Higgs boson. The mass of this boson is not especially well predicted by the theory; it could be anywhere below 1 TeV. In the weak-coupling scenarios, one must search for some type of new particles with electroweak quantum numbers—new quarks and leptons, their scalar partners, charged Higgs bosons, or gauge fermions. In the most optimistic scenario, one might also find new Z^0 bosons. In general, these particles will be in the mass range of a few hundred GeV. In the strong-coupling scenario, the scale of the new strong interactions is normally above 1 TeV. However, these interactions usually have visible effects below 1 TeV; these may occur through corrections to the predictions of the standard model for simple electroweak processes, or through particles, the analogues of π and K for these new strong forces, which naturally have masses well below the forces' natural scale. Let us consider these three scenarios in turn and ask what indication each gives for the energy of the proposed collider.

Minimal Higgs Boson. Consider first the minimal scenario. Here the signal of new physics is precisely one elusive particle. The mass of this particle is linked to its self-coupling λ through the relation:

$$m_{\rm H} = \sqrt{\lambda}\,\langle\Phi\rangle \ , \tag{2.1}$$

where $\langle\Phi\rangle$ is the Higgs field vacuum expectation value. In this scheme, the W boson mass is given by the relation

$$m_W = g\,\langle\Phi\rangle/2 \ , \tag{2.2}$$

and thus we can compute

$$\langle\Phi\rangle = 246 \text{ GeV} \ . \tag{2.3}$$

In more general models of the Higgs sector, the W boson mass is always given by the formula (2.2), with $\langle\Phi\rangle$ some more general parameter of the Higgs sector carrying

mass dimensions. The value of $\langle\Phi\rangle$ is essentially the only definite information we have about the Higgs sector. This value sets the energy scale of any new physics postulated to explain the origin of the weak boson masses.

Unfortunately, this information is never sufficient. Its shortcoming is made clear, in the minimal models, from the fact that we have no idea of the size of the Higgs field self-coupling. Reasonable theoretical bounds on this number allow Higgs boson masses as large as 1 TeV. It is worth asking what experiment will tell us about this value over the next ten years. Experiments at the Z^0 should be sensitive to a minimal Higgs boson of mass below 40 GeV.[13] The extension of LEP to 200 GeV in the center of mass should allow experiments to comb the mass region up to 80 GeV.[14] Beyond that point, further constraints will come from the SSC or the LHC. However, the search for the Higgs boson in hadron collider experiments depends crucially on the final state of Higgs decay and thus, in turn, on the mass of this particle. If the mass of the Higgs boson is greater than $2m_Z$, the dominant decay modes are those to W^+W^- and Z^0Z^0. Of the various possible final states in this decay, only the case of a decay to Z^0Z^0 in which both Z bosons decay leptonically may be considered an unambiguous signature, but that reaction should be quite clean for Higgs boson masses below 600 GeV.[15] For larger masses, the Higgs becomes so strongly coupled to its decay products that it is too wide to be distinguished as a resonance; Chanowitz and Gaillard have shown, however, that the coupling to this heavy Higgs produces a significant distortion of the observable WW and ZZ scattering cross section.[16] If the mass of the Higgs is below $2m_Z$, the search for this particle becomes more difficult. Gunion, Kane, and Wudka[17] have suggested a set of methods for observing the Higgs boson in this mass range through minor decay modes, for example, $H^0 \to \gamma\gamma$. But the dominant decay of these Higgs bosons to quark pairs would be completely obscured by strong-interaction background processes.

A high-energy e^+e^- collider would neatly complement the capabilities of the hadron collider experiments. We will show in Chapter 5 that an e^+e^- collider with center of mass energy 1 TeV will be sensitive to Higgs bosons from the LEP region

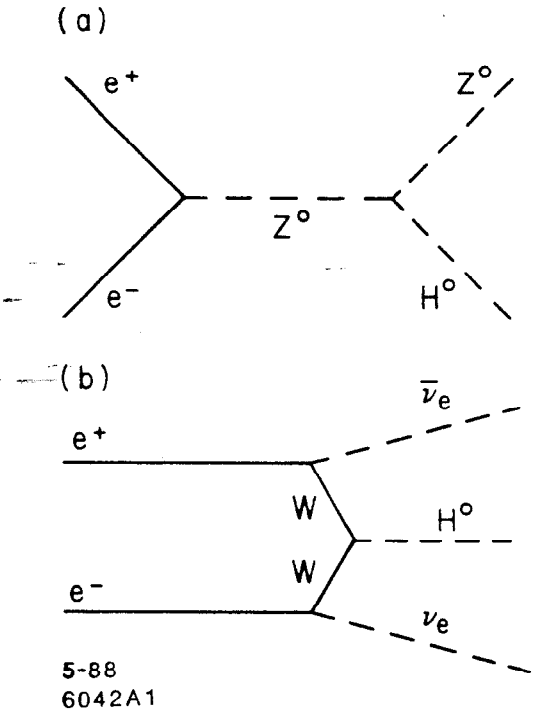

Figure 2. Two reactions which produce the Higgs boson in high-energy e^+e^- collisions.

up to masses of roughly 500 GeV, including almost the whole of the troublesome region below the W^+W^- threshold. The only serious difficulty arises when the Higgs boson mass is very close to m_W. In the whole range, the Higgs boson can be reconstructed with high efficiency in its major decay modes. If one intends this collider to cover as much of the Higgs mass range as possible, then clearly one should press the machine to energies as high as possible. If one wishes to concentrate on the problem of covering the intermediate mass regime, we find that the preferred machine energy is still 800 GeV – 1 TeV. This value follows from the following considerations, argued out in full in Chapter 5: At a high-energy e^+e^- collider, the Higgs boson can be sought in either of the reactions shown in Fig. 2. The first of these reactions, $e^+e^- \to H^0Z^0$ may be used either without reconstruction of the Higgs, by identifying the Z^0 and applying the beam energy constraint, or by reconstructing both the Higgs and the Z^0. The first method

is the one traditionally mentioned in discussions of Higgs searches, but we have found that the second method can be carried out straightforwardly. This method has the advantages of higher efficiency and insensitivity to energy smearing by beamstrahlung. Unfortunately, the cross section for $e^+e^- \to H^0Z^0$ is never large; it is of the order of 0.1 R even when all Z^0 and Higgs final states can be used in the analysis.

On the other hand, the second reaction shown in Fig. 2—WW fusion—has a large cross section, about 1 unit of R at 1 TeV. The process is quite distinguishable from backgrounds, unless the Higgs is closely degenerate with the W and Z bosons. This reaction does require that the Higgs be reconstructed, but, since the reaction puts the Higgs into an isolated kinematic region, this is generally straightforward. We find no difficulty in using WW fusion to identify a Higgs boson which decays dominantly into $t\bar{t}$, or even $b\bar{b}$, and the reaction continues to be effective above the W pair threshold.

The broad range of energy covered by SSC gives this machine special sensitivity to the case of a heavy Higgs boson. Chanowitz[18] has claimed that, for any possible realization of the Higgs sector, the SSC can give some evidence of its nature if this machine can operate at its most ambitious luminosity of 10^{33} cm^{-2}sec^{-1}. Chanowitz's argument applies also to e^+e^- colliders, but only at center of mass energies of 2 TeV or above. However, we will argue below that some signatures of the large Higgs mass scenario can be observed even in 1 TeV e^+e^- collisions.

Heavy Quarks and Leptons. Before discussing the search for more interesting Higgs sectors of the weak-coupling type, we would like to address the question of the expected masses of new quarks and leptons. These masses are also tied to the value of the Higgs field vacuum expectation value, through the relation

$$m_f = \frac{\lambda_f}{\sqrt{2}} \langle \Phi \rangle \ . \tag{2.4}$$

Quarks become strongly coupled to the Higgs sector, in the sense that the leading order of perturbation theory for quark-quark scattering violates its unitarity

bounds, at quark masses of 550 GeV.[19] In principle, any quark masses up to this value are equally well allowed, and there is no difficulty of principle for quarks to have still larger masses. Most probes of the quark mass spectrum through radiative corrections are sensitive to the mass difference within a weak doublet $(m_U - m_D)$ rather than the quark mass itself. Thus, it is quite likely that e^+e^- experiments through LEP II will not give a bound on undiscovered heavy quarks stronger than the constraint that they are above threshold. The Tevatron experiments, at a luminosity of 10^{30} cm^{-2}sec^{-1}, should be sensitive to new quarks up to 200 GeV.[20] The SSC or LHC should be sensitive to new quarks in the full allowed mass range, but only through their semileptonic decay modes.

An e^+e^- collider of energy 1 TeV can survey the whole spectrum of quarks with modest coupling to the Higgs sector, almost up to the unitarity limit of ref. 19. We will argue in Chapter 7 that they can even search for higher mass states through an indirect effect, the perturbation of the cross section for W pair production due to the anomalously large radiative corrections induced by these heavy flavors. Thus, a 1 TeV collider has a powerful reach in searching for new heavy fermions.

Beyond this general consideration, we would like to note also a remarkable, though more speculative, theory of the fermion-Higgs couplings which leads to an even more accessible milestone. Several authors, beginning with Pendleton and Ross[21] and Hill[22] have noted that the standard-model renormalization-group equation for the quark-Higgs coupling has a fixed point at a certain value where the growth of the coupling due to QCD renormalization is balanced by the decrease of the coupling due to its self-interaction. This fixed point value depends on the number of heavy flavors but generally corresponds to a quark mass between 150 and 200 GeV. It is actually the generic case, in models with heavy fermions, that several new quark generations appear at this fixed-point value. This multiple appearance of new fermions would be accessible to a collider with center of mass energy above 500 GeV.

Weak-Coupling Scenarios. Now let us turn our attention to other manifes-

tations of a weak-coupling sector which generates the Higgs bosons. In this case it is unfortunately difficult to make any concrete statement about preferred energies, because models of this type generally have a large number of unknown free parameters. Supersymmetric models of the standard gauge theory have probably been studied more thoroughly than other models of this class, and the constraints of supersymmetry serve to limit their predictions. These models will then provide a reasonable context for our analysis.

Even supersymmetric models of a minimal structure contain numerous parameters beyond those of the standard model. One must provide at least two different parameters which characterize the mass scale of supersymmetry breaking, plus a number of unknown dimensionless couplings associated with the coupling of ordinary matter to the sector which breaks supersymmetry. We will discuss these parameters more concretely in Chapter 8. If none of the dimensionless couplings are excessively large, the parameter $\langle\Phi\rangle$ will be tied to the scale of supersymmetry breaking. In this case, the supersymmetry breaking parameters will have a mass scale of a few hundred GeV and so the supersymmetric partners of the quarks, leptons, and gauge bosons will also have masses of this order. The panoply of predicted new particles is exceptionally rich; a typical mass spectrum is shown in Fig. 3. It is our impression, obtained by surveying many published models, that, in the bulk of the parameter space available to supersymmetric models, some superpartners are below 200 GeV in mass and most superpartners are below 400 GeV. These models could be studied in some detail by a 1 TeV collider. Not all supersymmetric models obey this general rule; in fact, Claudson, Hall, and Hinchliffe[23] have constructed otherwise perfectly reasonable models in which no observable superpartners have masses below 900 GeV. But a 1 TeV collider covers a large segment of the overall parameter space. We should note that the structure inherited from supersymmetry places additional constraints on more conventional elements of the Higgs sector. Several authors have noted that, under mild assumptions, all supersymmetric models of the weak-interaction symmetry breaking contain a Higgs boson with mass below about 100 GeV.

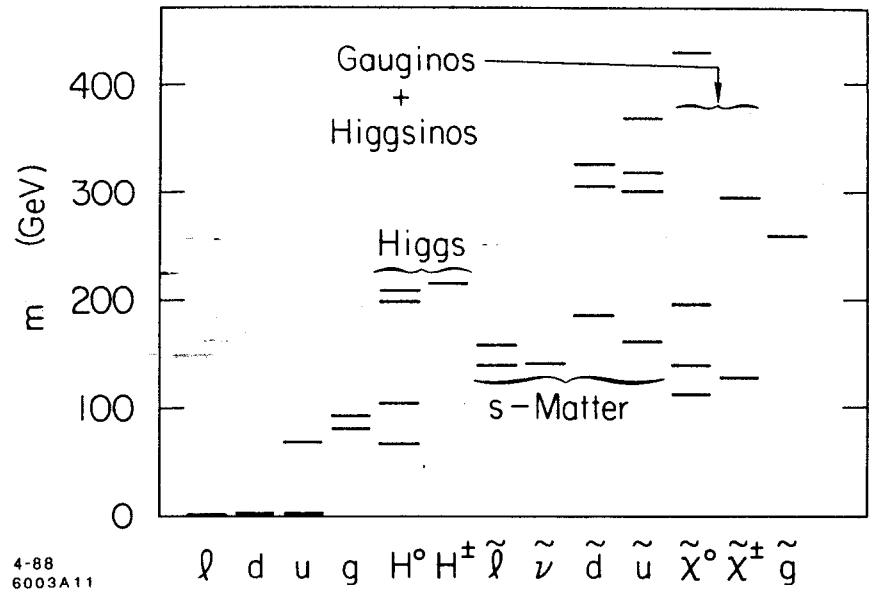

Figure 3. Spectrum of particles in a supersymmetric model of the fundamental interactions, at a randomly chosen point in the space of model parameters.[24]

The existence of a second Z^0 boson, which would appear as a dramatic resonance in e^+e^- annihilation, is a very real possibility in extensions of the standard model. Such bosons appear almost ubiquitously, for example, in 'superstring-inspired phenomenology'. Despite this, we know of no compelling arguments for the range of masses of such particles, beyond the obvious statement that, in supersymmetric models, they are near the scale of supersymmetry breaking. If such a boson should exist below the maximum energy of an e^+e^- collider, it will provide a new resonance, with a dramatic enhancement of the e^+e^- annihilation total cross section by a factor of 10^3. We will describe the physics of such a resonance in Chapter 6. Even at higher masses, a new Z^0 is still visible through its effect on asymmetries in fermion pair production. We will show in Chapter 6 that, with a 1 TeV collider, it is possible not only to discover the presence of a new Z^0 at a mass up to about 3 GeV but also to measure its couplings to fermions.

Strong-Coupling Scenarios. Finally, we turn to models in which the Higgs sector arises from a new set of strong interactions. In these models, one could

hope to observe the new interactions directly or to observe new particles required by the form of these interactions. Let us discuss first the possible appearance of new particles, the analogues of π and K mesons for these interactions. If these new interactions are similar to QCD in being built around a strongly-coupled gauge theory, it is almost unavoidable that this system will have spontaneously broken global symmetries and, therefore, approximate Goldstone bosons. These bosons receive zero mass from the new strong interactions, but they normally receive some mass from their electroweak, or more exotic, couplings. The situation has been worked out in some detail for a particular class of models, labelled 'technicolor' models,[28] in which the new interactions are taken to precisely mimic QCD. Such models may contain a pair of charged bosons which are very light, so that they should have been visible at PEP and PETRA energies. But in other models of this type, the first exotic states are colored particles with mass of the order of 200 GeV and couplings similar to those of Higgs bosons, coupling to color octet combinations of quarks or to quark-lepton pairs.[29] These bosons should be well within the reach of a 1 TeV collider.

If the new strong interactions couple directly to quarks and leptons, their direct effects are also easily visible at manageable energies. Eichten, Lane, and Peskin[30] pointed out that such new interactions correct the form of the cross sections for pair-production and Bhabha scattering by adding contact terms to the standard-model amplitudes. Because the standard model contributions are of order α, the strong contact terms can stand out in relief. Experiments at PEP and PETRA were potentially sensitive to contact interactions arising from a strong interaction scale 30 times or more larger than the center of mass collision energy. We expect that a similar level of sensitivity is possible at these higher energies. A 500 GeV collider could not only discover contact interactions corresponding to mass scales up to 10 TeV but also give some information on the space-time structure of these interactions. Further discussion of this issue may be found in refs. 7 and 31.

On the other hand, new strong interactions which couple only to the Higgs sector may be more difficult to detect at an e^+e^- collider with center of mass

energy 1 TeV. It is possible that such interactions would produce no dramatic deviations from the standard model; a scenario of this type has been presented by Lee, Quigg, and Thacker.[32] In this model, the interactions of the Higgs sector are strong only in the $J = 0$ partial wave, and this channel is difficult to access in e^+e^- collisions at energies below 2 TeV. However, in technicolor models, and presumably in more general models with strong coupling among the Higgs particles, the new interactions form a vector resonance analogous to the rho meson of the familiar strong interactions. We will show in Chapter 7 that this resonance affects the cross section for pair production of longitudinally polarized W bosons. In some scenarios, the position of the resonance can be below 1 TeV; this produces a significant enhancement of the e^+e^- cross section, with peak value 25 R. Even in the minimal scenario for technicolor, where the resonance position is 1.8 TeV, the perturbation of the W boson pair production cross section is quite significant at center of mass energies of 1 TeV.

Summary. We have now surveyed the range of theoretical models which have been put forward to explain the physics of $SU(2) \times U(1)$ symmetry breaking. These models range from austere ones to quite intricate schemes. In any comprehensive survey, we would expect to find some theoretical models which cannot be tested even with a large step in energy, and we have been careful to point out examples of such models for the machine we propose. But it is striking what a wealth of phenomena predicted to appear in association with the weak interaction symmetry breaking can be expected at e^+e^- center of mass energies below 1 TeV.

To this detailed summary of models, we would like to add a further, very general argument. We have seen that the structure of the Higgs sector can easily become complex, with a sizable multiplet of new particles. At first sight, it seems that the simplest models of the Higgs sector are to be preferred. But on closer examination, one finds that it is only the more complex models that actually explain the breaking of $SU(2) \times U(1)$, rather than just parametrizing this symmetry breaking. In these more complex models, the weak interaction symmetry breaks through the breaking of some symmetry which is bound up with the structure

of the new sector. In supersymmetric models, for example, supersymmetry plays this role. This more fundamental symmetry can protect many other particles from obtaining masses, and so its breaking readily creates a multiplet of particles with masses at the weak interaction scale. Such a set of new particles, a 'TeV multiplet', is thus a generic feature of models of the weak interaction symmetry breaking. The extended argument that we have given in this section may be simply cast as the statement that these particles are expected to appear in e^+e^- annihilation, and, most probably, in just the region that would be explored by an e^+e^- collider of center of mass energy 1 TeV.

Two Postscripts. We should make two additional comments on the problem of setting the center of mass energy of the new collider. Both stem from the fact that our arguments are general in character, a feature which has led us to recommend a large step in machine energy over LEP. If we knew in advance, or discovered in the course of experiments at the collider, that the threshold for new physics occurred well below 1 TeV, it would be worthwhile to work as close to this threshold as allows a reasonable phase space for new particle production. If the new physics includes a new Z^0 resonance, this point is obvious. But even if the new physics is seen only in continuum production of novel particles, lowering the energy gives an advantage because cross sections for particle production are roughly constant in R units, and the R unit falls steeply with energy. It is likely, then, that one would often wish to run this new collider at energies below the maximum energy for which it is designed. In this respect, we expect that the usage of this new collider will follow the pattern of SPEAR and CESR rather than that of PEP and PETRA.

This expectation makes it essential to plan in advance for the ability to vary the energy of the collider. We hope that it will be possible to operate this machine at any center of mass energy between 300 GeV and the maximum energy of the design. Fortunately, the conditions on a change of the energy are not very severe. First, because cross sections increase as the energy is lowered according to an $E_{\rm CM}^{-2}$ dependence, we only insist that the luminosity of the machine not decrease faster

than E^2. Second, it should never be necessary to operate this collider in a scanning mode. We will argue in Chapter 6 that a collider with appreciable energy spread through beamstrahlung is already automatically conducting a scan in energy, and that this scan is sufficient to discover a new Z^0 boson at any energy accessible to the collider. We know no examples of interesting but less prominent resonances to be expected in this energy region. It will suffice, then, to fix the energy of the collider for each running year and to schedule all changes in this energy for major shutdown periods.

If the threshold of new physics is discovered before the design of the new collider is complete, the collider can be optimized for that energy region. A particularly exciting possibility is that this threshold will be discovered in the SLC or Tevatron experiments which are now beginning their data-taking. The Tevatron, in particular, can produce evidence for supersymmetric partners of quarks and gluons up to about 150 GeV and can unambiguously indicate the location of a new Z^0 boson up to about 500 GeV. If the first of these discoveries were made, an e^+e^- collider of center of mass energy 400 GeV and luminosity 5×10^{32} cm^2/sec would be optimal for the detailed characterization of the new phenomena. In the second case, one could use the same lower energy, and even a much lower luminosity. We will describe the experiments of interest for these scenarios in Chapters 6 and 8. In either case, the collider required would be less of a technical challenge than the 1 TeV machine, and should be cheaper to construct and operate. On a longer time scale, the discoveries of the SSC or LHC may also provide guidance on the energy scale of this new collider. Whatever new phenomena the hadron machines uncover, must, we feel, be brought into the clearer light of e^+e^- reactions in order to be fully understood. This process might well give accelerator builders a clearer, and perhaps also a technically simpler, goal.

2.2. LUMINOSITY

Let us now turn to our recommendations for the luminosity of the new collider. We insist that the new collider be built to guarantee large samples of integrated luminosity, of the order of 30 fb^{-1}, or 2500 R^{-1}, at 1 TeV. Such large event samples may not be needed in the first, exploratory, stages of the experimental program, but they will certainly be required to allow a mature program of particle searches. We have identified theoretical scenarios in which new physics enters with cross sections much larger than the unit of R. We will discuss these scenarios briefly later in this section. However, in the absence of direct experimental evidence for these scenarios, we believe it would be foolish to use them as bases for the collider design. The new machine, then, should be designed to search for new phenomena with cross sections of the order of a unit of R.

There are two ways that one can estimate the minimum reasonable samples of integrated luminosity. The first of these is a rough argument based on the history of experiments at PEP and PETRA. In Table 1, we list a selection of papers from PETRA which excluded important possibilities for hypothetical particles, along with the luminosity samples on which these papers were based. Results from PEP generally came later, but the program of particle search experiments at PEP was certainly mature by the summer of 1984, when PEP had collected 50 pb^{-1} of data at 29 GeV, a sample corresponding to 5000 R^{-1}. Our estimate of the luminosity requirements for the new collider accords with this experience.

We have tested this rough argument by detailed analysis of a variety of particle search experiments which one would expect to carry out at this new collider. In the Monte Carlo studies of particle search experiments discussed in the body of this report, we have limited ourselves to luminosity samples of 30 fb^{-1}. The reader can glean from this detailed discussion our general conclusion that a sample of this size would allow us to do justice to the physics of e^+e^- collisions at the machine energy, whereas a substantially smaller sample would not.

To complete this discussion of luminosity, we would like to discuss briefly the

Table 1. A sampler of PETRA particle searches.

	Experiment	Excluded for	$\int \mathcal{L}$
Heavy lepton L	MARK J[33]	$m < 16$ GeV	520 R^{-1}
Slepton $\tilde{e}, \tilde{\mu}$	CELLO[34]	$3 < m < 16$ GeV	800 R^{-1}
Higgs: $H^+ \to \tau^+ \overline{\nu}$	MARK J[35]	$m < 15$ GeV	3000 R^{-1}
Higgs: $H^+ \to c\overline{s}$	TASSO[36]	$m < 13$ GeV	5400 R^{-1}

two scenarios which predict large enhancements of the cross section for e^+e^- annihilation. These entail the appearance of a new Z^0 boson or the appearance of strong interactions for leptons with a characteristic scale below 6 TeV. The phenomenology of the new Z^0 will be discussed in some detail in Chapter 6. In short, however, we expect that it should have a ratio of width to mass of a few percent, roughly the same as for the conventional Z^0. This leads to peak cross sections enhanced by a factor of about 10^3 over the expectation of the standard model, over a narrow region of 10 GeV in energy. For Z^0 masses up to 500 GeV, it is likely that this resonance would be discovered in advance at the Tevatron collider. If the new Z^0 mixes substantially with the familiar Z^0, the precision determination of fermion couplings to the Z^0 should give evidence for the existence of this state at some mass below 1 TeV, although the precise value of the mass will not be uniquely determined. If the new Z^0 does not mix with the familiar one, and if it is too heavy to be seen at the Tevatron, it may not be apparent in any experiment before this new collider begins operation. This last scenario has a window of modest size. If the existence of the resonance is not known in advance, it would be a mistake to anticipate the presence of this resonance in setting the luminosity of the collider. On the other hand, we have already noted that it would be straightforward, given the luminosity we have requested, to discover a new Z^0 anywhere in the energy region of the machine by sitting at the maximum energy and using the natural energy spread of the machine to make a scan.

In this summary of the properties of a new Z^0, we have assumed that it is possible to realize in an experiment the large increase in cross section expected theoretically at the resonance peak. At first sight, this seems unrealistic, since beamstrahlung will spread the center of mass energies of collisions over a range of energies of order 10–30% of the nominal operating point. However, we have found that realistic beamstrahlung spectra[37] leave a substantial fraction of the collisions within 2% of the nominal machine energy, even while the rest of the events are spread into a long tail. This peak at the full machine energy contains 25–50% of the events, depending on the machine design. This phenomenon allows one to make use of any resonance which is discovered, realizing this same fraction of the peak cross section, without adjusting the machine design. Backgrounds from continuum production processes will not be negligible, but they will be readily subtracted. In principle, one might imagine adjusting the running conditions to decrease the energy spread; however, any adjustment which decreases the luminosity substantially would not be worthwhile.

The second scenario which gives large cross sections involves lepton strong interactions; this case is much less extreme in character. If we assume that the scale of lepton strong interactions is below 6 TeV, one expects lepton cross sections to stop falling with the R unit at an energy of a few hundred GeV and then to rise to roughly ten times the standard model cross section at a center of mass energy of 1 TeV. This scenario is discussed further, from a theoretical viewpoint, in ref. 7. One will be able to confirm or rule out this scenario in advance, since lepton strong interactions at this level have a small but noticeable effect on Bhabha scattering in the region just above the Z^0. Indeed, current experiments at PEP and PETRA restrict the scale of lepton strong interactions to be above 2 TeV, a value already quite far above the Higgs vacuum expectation value (2.3).

Though neither of these two scenarios is out of the question, and even though some theorists would consider the existence of a second Z^0 likely, neither can be guaranteed. Any other option, unfortunately, gives us small cross sections which put luminosity at a premium.

2.3. Environment

Because of the very stringent requirement we have put forward for the luminosity, we have considered relaxing other standards which have previously been considered a natural part of the environment of e^+e^- annihilation. In storage rings, the condition that the colliding beams be stored stably restricts the energy spread of collisions to a value smaller than 1 part in 10^3. Mini-beta quadrupoles may obstruct experimentation somewhat at small angles, but most experimental arrangements allow some type of low-angle tagging device. It would be wonderful if the design of a linear collider could allow the same tight definition of the center of mass energy and the same ease of small-angle particle detection. Unfortunately, it is likely that both of these features must be compromised to achieve a high luminosity. The requirement of maximizing the luminosity pushes one into the regime of strong nonlinear interaction between the bunches, large disruption, and substantial beamstrahlung radiation. It also requires a delicately positioned set of final focus quadrupoles; these should be small objects in themselves but may require a massive support structure. We have investigated the extent to which one can accept these compromises in the experimental environment if this is necessary to achieve higher luminosity. In particular, we have asked whether it is still possible to carry out the crucial new particle searches if the e^+e^- collision energy has a substantial spread, or if experiments must exclude regions of solid angle in the forward and backward direction. We conclude that, while these disturbances in the environment require more carefully planned experimentation, they do not seriously detract from the substantial advantages which e^+e^- annihilation offers.

A new feature of experimentation which becomes relevant in this energy region helps to counter the degradation of the environment. We expect detectors at this high-energy collider to rely heavily on calorimetry. They will be optimized to detect jets and to measure jet and jet-jet invariant masses. With this in mind, we have concentrated in our study on analysis methods which make use of jet energies and angles to replace the information of the center of mass frame. In addition,

two aspects of the physics itself relax the requirements for the environment. First, most interesting events, signal and background, contain W and Z bosons. One can understand a large fraction of the events in which these bosons decay hadronically by reconstructing the bosons using jet analysis. Second, searches for events with missing energy at a TeV collider generally involve large values of the unbalanced transverse momentum, due to neutrino emission or intermediate virtual W bosons. Thus, the requirements on forward tagging in such experiments are much less severe than in comparable searches at PEP.

To study the importance of this degradation of the environment, we have modeled these effects as a part of our Monte Carlo study of particle search experiments. To assess the effect of beamstrahlung, we have assigned the colliding electron and positron energies chosen from a realistic beamstrahlung energy distribution. Three such distributions were computed for our study by P.-S. Chen, using a beam-beam interaction simulation code written by K. Yokoya.[37] This code includes multiple photon radiation during the collision of the electron and positron bunches and computes in detail the disruption of the two bunches through their interaction. The parameters of the bunches were based on realistic sets of machine parameters, corresponding to a nominal collision energy of 1 TeV and luminosities in excess of 10^{33} cm^{-2}sec^{-1}. The three distributions gave mean fractional energy losses $\delta = 0.1, 0.26, 0.4$. One should note that this measure does not capture the full information contained in the distribution; some contributions to backgrounds depend mainly on the length and flatness of the low-energy tail, which is sensitive to the precise machine parameters. One should also recall that about 30% of the e^+e^- annihilations are still occurring with almost no energy loss. The intermediate case is plotted as a distribution of the center of mass energy of e^+e^- collisions in Fig. 4. We performed exploratory studies with all three distributions but found that they did not, in the end, give very different conclusions. Our final, detailed analyses were all done with the intermediate distribution shown in Fig. 4.

We found that the inclusion of beamstrahlung presented a serious challenge to the design of experiments by creating new sources of background. However, in every

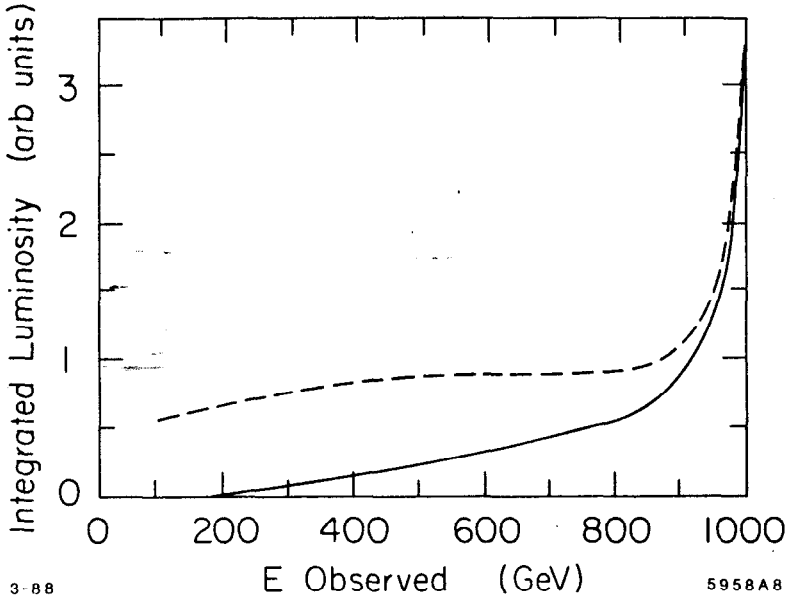

Figure 4. A typical spectrum of center of mass energy in e^+e^- collisions in the presence of beamstrahlung, computed for a collider of nominal energy 1 TeV.[37] The dashed curve represents the spectrum multiplied by E^{-2} to approximate the cross section for e^+e^- annihilation. Note that 30% of the events have a collision energy within 1% of the full 1 TeV.

case that we analyzed in detail, these problems could be substantially or completely overcome by careful refinement of the search technique. The use of calorimetric jet reconstruction came to play a central role in many of our analyses. Often, we found that additional, formally redundant cuts needed to be applied to the data to remove events from the tail of the beamstrahlung distribution. However, once a suitable set of cuts had been identified, we found that the signals we sought could be extracted without a significant degradation in their significance and with very little loss in efficiency. Among the analyses we report, only the search for charged Higgs bosons set out in Chapter 9 uses a beam energy constraint, and there it provides only a qualitative guide to resolving combinatoric problems. Even this analysis can tolerate a 25% loss of total center of mass energy. In the remainder of the search experiments we discuss, and in the reconstruction and precision measurement of the W pair production cross section that we will present in Chapter 7, our analyses are

actually boost-invariant and so are insensitive to beamstrahlung both as a formal matter and in our actual experience.

The question of whether forward angles can be permitted to be inaccessible to experiments should actually be broken into two different questions. First, one might in principle want to make detailed measurements at forward angles, to study two-photon physics or W pair production. For this, one would like to extend the tracking and calorimetry as close as possible to the beam direction. We do not see these as important goals for the new collider. It will be interesting to study W pair production, but the aspects of this reaction which most crucially test the standard model and its variants concern its shape in large-angle scattering. The strong forward peak is generated entirely by the production of transversely polarized W's by neutrino exchange; this contribution is essentially model-independent and it is not theoretically controversial. When we consider W pair production as a background to new particle search experiments, we find that it is always advantageous to cut away the forward and backward regions in order to minimize this background. We do not expect, then, that there are important experiments which require full detector capabilities down to small angles.

On the other hand, there are circumstances in particle search experiments in which one would like to veto events with particles in the forward and backward regions. We have studied the severity of a constraint on small-angle particle detection by insisting, in all of our analyses, that particles closer than 10° to the beam direction should simply be ignored. The experiments most sensitive to this restriction are experiments which depend on missing transverse momentum signatures, the Higgs boson search described in Chapter 5 and the searches for neutral supersymmetric states described in Chapter 8. In both cases, we find that this restriction can be tolerated, since the typical angles of recoil particles in background processes are quite large, though it is of some experimental advantage to be able to at least count charged tracks down to very small angles.

It is worth restating the main point of this discussion: We have emphasized

already the central importance of high luminosity to any experimentation at a high-energy e^+e^- collider. If it is necessary to seriously decrease the quality of the experimental environment as the price of achieving high luminosity, that is a price that we are willing to pay. The intrinsic simplicity of the physics of e^+e^- annihilation insures that that price is almost never too high.

2.4. POLARIZATION

Our final recommendation for the design of the new collider is that it should be constructed, from the beginning, to allow the electron beam to be longitudinally polarized. This would be a difficult requirement for a synchrotron, but in a linear collider this is mainly a matter of taking care in the design to smooth the path along which the beam is transported. We hope that the electron longitudinal polarization can be maintained without a significant perturbation of the collider design. The beam-beam interaction in the collision process involves strong fields which can precess the electron spin, but this should lead only to a 10% depolarization.[8]

In the energy region that we are discussing for this machine, polarization takes on a significance which it does not have at lower energies. The reason for this is that the weak interactions are essentially handed, and at energies above 100 GeV, the weak interactions contribute as strongly as the electromagnetic interactions to the basic reactions in e^+e^- collisions. Putting this another way, the standard model considers the left- and right-handed electrons to be fundamentally distinct species; the electron mass appears only because the Higgs sector produces a small mixing between these species. These considerations lead to a substantial polarization dependence even for standard model processes. This point is illustrated in Table 2, where we list the polarization asymmetries for a variety of standard and nonstandard e^+e^- reactions. Given the ubiquity of W bosons in signal and background, we would like especially to note the phenomenon shown in Fig. 5: The cross section for $e^+e^- \to W^+W^-$ falls by a factor of 30 when one switches from left- to right-handed electrons, even in the backward direction where the neutrino exchange diagram does not dominate. The fact that polarization-dependence is

Table 2. Polarization asymmetries for e^+e^- reactions.

	$A_{\rm pol}$
Standard Model:	
$e^+e^- \to u\bar{u}$	0.34
$e^+e^- \to d\bar{d}$	0.62
$e^+e^- \to W^+W^-$	0.94
$e^+e^- \to Z^0Z^0$	0.32
Superpartners:	
$e^+e^- \to \tilde{u}_L\bar{\tilde{u}}_L$	0.94
$e^+e^- \to \tilde{u}_R\bar{\tilde{u}}_R$	−0.60
Higgs Physics:	
$e^+e^- \to \nu\bar{\nu}H^0$	1.00
$e^+e^- \to H^+H^-$	0.65

intrinsically embedded in the structure of the standard model has two important consequences: First, polarization gives a new, independent handle on standard model backgrounds. The background from W pair production, for example, can be essentially eliminated by adjusting the polarization. But, more importantly, if the left- and right-handed electrons are independent species in the standard model, they are likely to be treated independently also by any new interactions that might appear for the first time in this energy region. The measurement of the polarization-dependence of new physics will then be an important clue to its origin. In Chapter 6, we will illustrate this point in great detail for the specific case of a new Z^0 boson.

We note parenthetically that the full information from longitudinal polarization can be obtained without polarizing the positron beam. The reason for this is that helicity-flip annihilation cross sections are very small at high energy in the standard model and in all its reasonable variants. The interaction vertex which

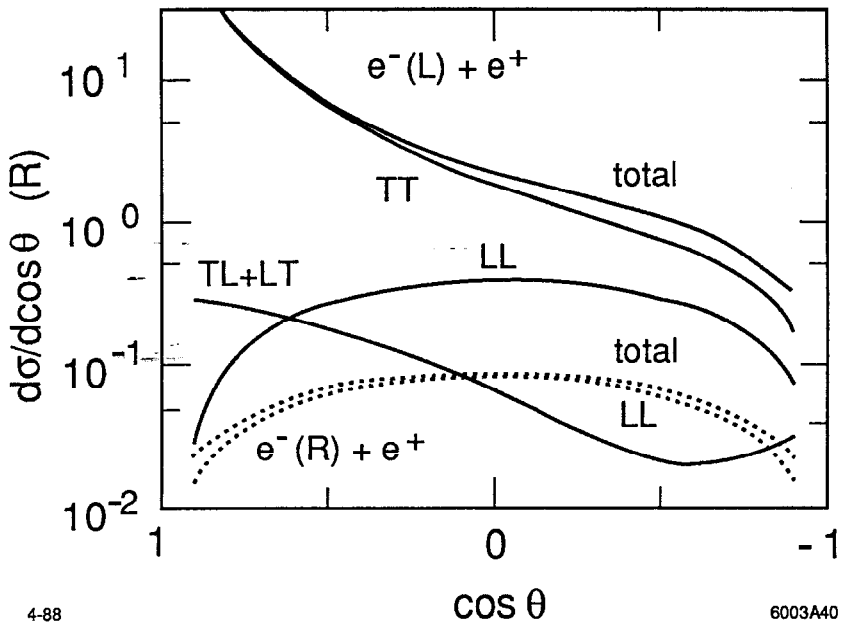

Figure 5. Differential cross sections for $e^+e^- \to W^+W^-$ at $\sqrt{s} = 1$ TeV, computed for left- and right-handed polarized electrons on unpolarized positrons.

would allow a left-handed electron to annihilate a left-handed positron also potentially contributes to the amplitude for mixing of left- and right-handed electrons which produces the electron mass. The fact that the electron mass is very small compared to the Higgs vacuum expectation value (2.3) indicates that these couplings are suppressed. The simplest estimate for the cross section for helicity-flip annihilation is $\sigma \sim (m_e/E_{\rm CM})^2 \sim 10^{-12}$ units of R. (In some models the rate is larger, but not sufficiently to counter this strong suppression.) Peripheral processes such as the two-photon process do arise from collision of left-handed electrons with left-handed positrons, but these are mainly backgrounds. The one exception to the rule, the process of double-Z^0-bremsstrahlung followed by Z^0 fusion to form a Higgs, has a cross section which is numerically small. Thus, we expect that a polarized electron beam will naturally pick out of the positron beam with which it collides those particles of the opposite polarization state. This will be true even if the positron beam is completely unpolarized. It is true that reaction rates would double if the positron beam could itself be correctly polarized. If this could be

done without a compensatory loss of luminosity, it would be worthwhile, on the same footing as any other technique for increasing the event sample.

3. General Characteristics of Events at $\sqrt{s} = 1$ TeV

In this chapter, we will discuss the various classes of events which the standard model predicts for an e^+e^- collider with an energy well above the Z^0 resonance. This discussion will provide a reference point for the discussion of new particle searches to be given in Chapters 4–9. One of our goals will be to set out the basic parameters of events in this energy region—particle multiplicities, thrust, acoplanarity, track densities, etc. We will discuss separately the features of each type of standard-model process and explain how each process can be independently characterized.

At current energies of e^+e^- reactions, the cross section is built up entirely from Bhabha scattering, e^+e^- annihilation, and two-photon processes. At energies well above the Z^0, the first two of these classes receive new contributions from virtual Z^0 exchange. In addition, entirely new classes of reactions appear. The annihilation processes $e^+e^- \to W^+W^-$, $e^+e^- \to Z^0\gamma$, and $e^+e^- \to Z^0Z^0$ become dominant mechanisms of hadron production. The second of these processes contributes also a peripheral component, the reaction of e^+e^- annihilation to a Z^0 plus a hard collinear photon, which becomes the most important source of low-multiplicity events. These new event topologies give a new complexity to the backgrounds. We will argue, however, that this increased complexity is still quite manageable. We will show that all of these processes can be characterized and isolated using detectors of the same quality as those currently being constructed for Z^0 physics.

Our discussion will give particular stress to the study of weak boson pair production. This process has special importance for our study, because it gives the most important background to new particle search experiments, which generally involve looking for missing energy due to neutrinos or other exotica. In addition,

many of the signatures of new states involve the production of W bosons in association with hadrons or leptons. We will therefore spend some time discussing the special features of weak boson production and the practical problems of reconstructing W and Z bosons.

3.1. The Standard Detector

All of the results that we will present for standard model processes assume a specific model for the configuration of the detector and a specific distribution of events in center of mass energy and longitudinal momentum generated by beamstrahlung. We begin by explaining these basic assumptions of our analysis.

The properties of the detector were chosen as an idealization of the expected performance of the SLD detector now under construction at SLAC.[38] We consider this the minimal performance of a detector which might be used at this new accelerator. Since the emphasis in our analysis is on calorimetry, we generally ignore tracking information for hadrons, though in some analyses charge-counting is useful for removing background. We also ignore, in our formal analyses, the information which would be supplied by a vertex detector, though we will note at appropriate points in our discussion of new physics which backgrounds can be reduced by systematic τ or b quark tagging. Similarly, all of our Monte Carlo work assumes unpolarized electron beams; we will note the effect of polarization where it is relevant.

To simulate the effect of the detector, we smear the particle momenta generated by Monte Carlo simulations of signals and backgrounds in the following manner: For muons and electrons, we assume that the angle of the track is well determined by a tracking chamber. For muons, the energy of the track is smeared by a Gaussian distribution with a standard deviation given by

$$\frac{\Delta E}{E} = 3 \times 10^{-4} \cdot E \,, \tag{3.1}$$

with E in GeV, for E above 2 GeV. This resolution should be achievable with a drift chamber of radius 1.8m, 72 position measurements with 200 μm resolution, a

magnetic field of 1.0T, and a tight vertex constraint. For electrons, we apply the same smearing for relatively low energies and the calorimetric formula

$$\frac{\Delta E}{E} = \frac{8\%}{\sqrt{E}}, \tag{3.2}$$

with E in GeV, for energies above 40 GeV. We assume that the charges of electrons and muons can be assigned unambiguously.

Photons and charged and neutral hadrons are treated indiscriminately as clusters of calorimetric energy. Tracks within 4° of one another are combined; then the combined tracks are smeared in a square box of size ± 2°. The energies of these tracks are smeared by

$$\frac{\Delta E}{E} = \frac{50\%}{\sqrt{E}}. \tag{3.3}$$

In the Higgs boson search analysis, we added a 2% constant offset to the formulae (3.2), (3.3). This made almost no difference to the results.

Finally, we are very conservative about the obstruction of the detector near the beam direction by the final focus quadrupoles and the apparatus needed to support them. Tracks within 10° of the beam axis are simply ignored.

Monte Carlo events were generated for a collider of nominal center of mass energy 1 TeV unless we explicitly note otherwise. The Monte Carlo events were generated with distribution in center of mass energy and longitudinal momentum given by one of the beamstrahlung spectra computed by Chen and Yokoya,[37] as described in the previous chapter. The bulk of our analysis was done with the intermediate case shown in Fig. 4, corresponding to a mean fractional energy loss of $\delta = 0.26$. This beamstrahlung simulation included the effects of multiple synchrotron radiation and realistic disruption for an e^+e^- machine operating at 1 TeV and 3×10^{33} cm^{-2}sec^{-1}. The simulation also included the correct distribution of longitudinal momenta produced by the multiple photon emission. On top of this distribution, initial-state radiative corrections were applied according to the prescription of Berends, Kleiss, and Jadach.[39]

3.2. Peripheral Processes

An e^+e^- collider in the energy range we consider gives two sources of peripheral, low momentum transfer events. First, there is the two-photon process, for which the cross section has been growing logarithmically from low energies while the annihilation cross sections have been falling as $E_{\rm CM}^{-2}$. Second, the process

$$e^+e^- \rightarrow Z^0 + \gamma \tag{3.4}$$

has a large cross section when the photon is collinear with the beam direction. However, neither of these processes is particularly important as backgrounds to annihilation processes, since both may be characterized, and cut out of interesting data sets, by their properties of low multiplicity and low transverse momenta. Two-photon reactions, and photon-electron reactions, form more significant backgrounds to physics processes which themselves involve significant missing energy, such as the process of Higgs boson production by W fusion, $e^+e^- \rightarrow \nu\overline{\nu}H^0$, which will be analyzed in Chapter 5. As a part of our discussion of Higgs boson searches, we will examine the background provided by two-photon reactions in some detail. For the moment, though, we would like simply to show that these reactions are cleanly separated from the annihilation events.

Using the Lund Monte Carlo, we have generated events resulting from $\gamma\gamma \rightarrow q\overline{q}$ (with 6 light flavors) and $\gamma\gamma \rightarrow W^+W^-$, with the photon spectrum given by a Weiszacker-Williams distribution folded with the electron or positron spectrum due to beamstrahlung. The pair-production cross section for quark pairs is given by the familiar expression

$$\frac{d\sigma}{d\cos\theta} = \frac{2\pi\alpha^2}{s} \cdot \left(\frac{\cos\theta}{1-\cos^2\theta}\right) \cdot 3 \cdot \sum_f Q_f^4 \,, \tag{3.5}$$

where $\cos\theta$ is the angle in the photon-photon center of mass frame. The production

cross section for W pairs is[40]

$$\frac{d\sigma}{d\cos\theta} = \frac{3\pi\alpha^2}{\pi s}\cdot\beta\cdot\left\{1-\frac{4}{1-\beta^2\cos\theta}\cdot\left(\frac{4}{3}+\frac{2m_W^2}{s}\right)\right. \\ \left. +\left(\frac{4}{1-\beta^2\cos\theta}\right)^2\cdot\left(\frac{2}{3}+\frac{2m_W^4}{s^2}\right)\right\}, \tag{3.6}$$

where $\beta = (1-4m_W^2/s)^{\frac{1}{2}}$. Our plots correspond to a luminosity sample of 10 fb^{-1}. In Figs. 6 and 7, we plot the distribution of two-photon events in terms of two variables which will be crucial in our analysis of annihilation events: the total invariant mass of hadrons, electrons, and photons in the event, as reconstructed by the calorimeter, and the angle between the thrust axis and the beam direction. It is clear that all but a few of the $q\bar{q}$ events appear below 150 GeV in invariant mass, and above $|\cos\theta_{thr}| = 0.8$. This labels these events as distinctly different from annihilation events at large effective $\sqrt{s}$. The W pair events are slightly more central (remember that their threshold in invariant mass is 165 GeV) but come at a much lower rate.

The second peripheral process, radiation of a forward photon followed by e^+e^- annihilation at the Z^0 resonance, has a cross section given by

$$\sigma(e^+e^-\to\gamma Z^0) = \frac{4\pi\alpha^2}{s}\cdot\left[\frac{(\frac{1}{2}-\sin^2\theta_w)^2+(\sin^2\theta_w)^2}{2\sin^2\theta_w\cos^2\theta_w}\right]\cdot\frac{1+m_Z^2/s^2}{(1-m_Z^2/s)}\cdot\log\left(\frac{s}{m_e^2}\right) \tag{3.7}$$

This corresponds to a cross section of 31 units of R for a collider with its full luminosity at 1 TeV, and more than 40 units of R after beamstralung and detector cuts are taken into account. However, these events have a very characteristic form: The observed hadronic invariant mass peaks neatly at the mass of the Z^0 (when the Z^0 decay products are not themselves lost down the forward hole), and the reconstructed Z^0 bosons are highly boosted, to $\gamma \approx 11$. These events were included in our Monte Carlo simulations among the radiative corrections to $e^+e^-\to q\bar{q}$.

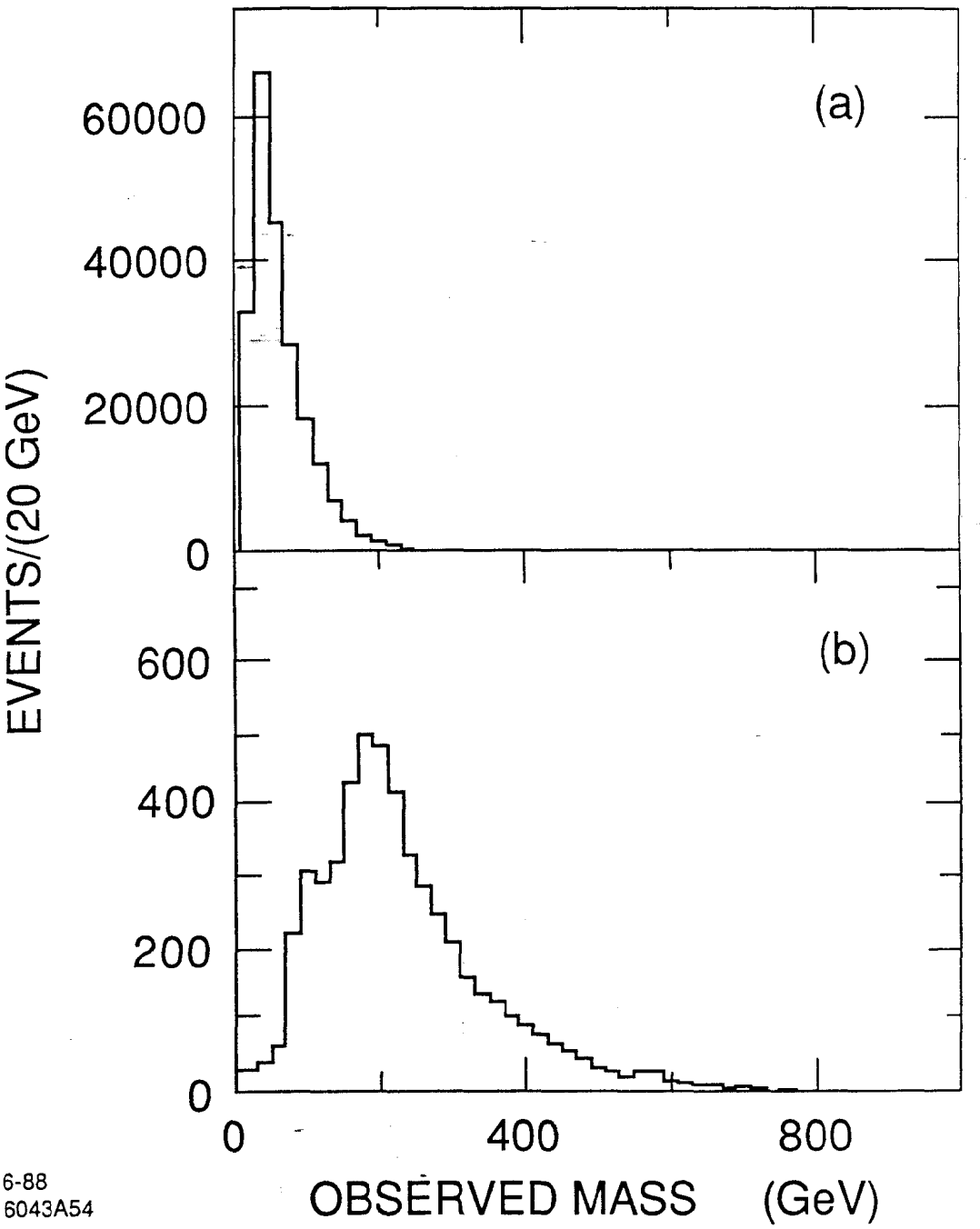

Figure 6. Distribution of observed invariant masses for two-photon reactions: (a) $\gamma\gamma \to q\bar{q}$, (b) $\gamma\gamma \to W^+W^-$. The distributions are normalized to e^+e^- integrated luminosity of 10 fb^{-1}.

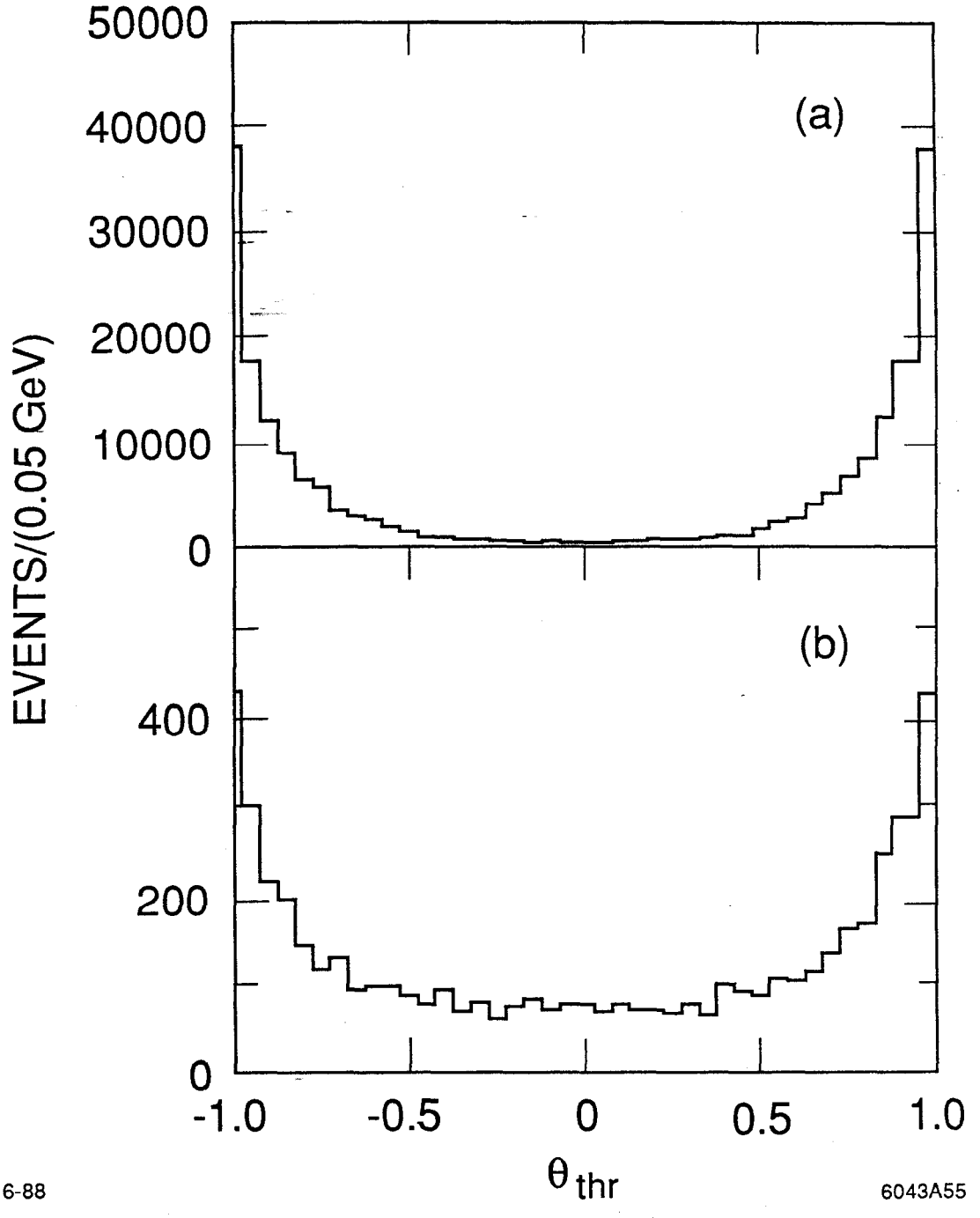

Figure 7. Distribution of the direction of the thrust axis, in the photon-photon center of mass frame, for two-photon reactions: (a) $\gamma\gamma \to q\bar{q}$; (b) $\gamma\gamma \to W^+W^-$. The distributions are normalized to an event sample of 10 fb^{-1}.

They will appear distinctly in the results on $e^+e^- \to q\bar{q}$ that we will present in section 3.4, and we will see there that they are cleanly eliminated by the most basic cuts.

3.3. Annihilation Reactions: Cross Sections

We now turn to the most important class of standard model reactions for our study, the e^+e^- annihilation processes. At energies of 1 TeV in the center of mass, we must consider not only the familiar processes of e^+e^- annihilation to quark pairs but also new processes of weak boson pair production. In this section, we will present the theoretical expectations for each of these reactions within the standard model. In the next section, we will present the results of our Monte Carlo study which translate these theoretical results into concrete estimates of expected backgrounds.

The familiar processes of e^+e^- annihilation into quark and lepton pairs remain major components of the e^+e^- cross section well above the Z^0. The only significant new feature of these reactions, within the standard model, is that the processes of annihilation into a photon and into a Z^0 become comparable in magnitude and interfere. In the total cross section, the Z^0 effect is generally small, since the electron couples relatively weakly to the Z^0. (One should note, though, that fermions with small electric charge, such as d quarks, have their relative production substantially enhanced.) But the interference between the photon- and Z^0-exchange contributions is visible through the presence of large forward-backward and polarization asymmetries.

The cross section for e^+e^- annihilation into a fermion pair, for some fermion f, is given by

$$\frac{d\sigma}{d\cos\theta} = \frac{\pi\alpha^2}{2s} N_c \Big\{ [|f_{LL}|^2 + |f_{RR}|^2]\cdot(1+\cos\theta)^2 + [|f_{LR}|^2 + |f_{RL}|^2]\cdot(1-\cos\theta)^2 \Big\} , \tag{3.8}$$

where

$$
\begin{aligned}
f_{LL} &= -Q + \frac{(-\frac{1}{2} + \sin^2\theta_w)(I_3 - Q\sin^2\theta_w)}{\sin^2\theta_w \cos^2\theta_w} \frac{s}{s - m_Z^2} \\
f_{RL} &= -Q + \frac{(\sin^2\theta_w)(I_3 - Q\sin^2\theta_w)}{\sin^2\theta_w \cos^2\theta_w} \frac{s}{s - m_Z^2} \\
f_{LR} &= -Q + \frac{(-\frac{1}{2} + \sin^2\theta_w)(-Q\sin^2\theta_w)}{\sin^2\theta_w \cos^2\theta_w} \frac{s}{s - m_Z^2} \\
f_{RR} &= -Q + \frac{(\sin^2\theta_w)(-Q\sin^2\theta_w)}{\sin^2\theta_w \cos^2\theta_w} \frac{s}{s - m_Z^2} .
\end{aligned}
\tag{3.9}
$$

The factor N_c accounts the number of colors and the QCD correction to the cross section; it is

$$
N_c = \begin{cases} 1 & \text{for leptons} \\ 3 \cdot (1 + \frac{\alpha_s}{\pi} + \ldots) & \text{for quarks} \end{cases} . \tag{3.10}
$$

In this formula, the form factors isolate the contributions from separate helicity states; for example, f_{LR} gives the amplitude for $e_L^- e_R^+$ to annihilate to $f_R \overline{f}_L$. (In both the initial and the final state, helicity conservation dictates that the helicity of the antiparticle must be opposite to the helicity of the particle. Fig. 8 shows the expected form of the annihilation cross section, to μ pairs and to hadrons, in the standard model. Figs. 9 and 10 show the expected forward-backward and polarization asymmetries for $e^+e^- \to \mu^+\mu^-$, $b\bar{b}$, and $t\bar{t}$. Note the large size of the expected effects. In Table 3, we summarize the predicted values of the total cross section and the asymmetries for pair production of each fermion species, for $s >> m_Z^2$. The cross sections include an enhancement factor resulting from the renormalization of α

$$
\left(\alpha(100\ \text{GeV})/\alpha(0)\right)^2 = \left(\frac{1}{128}\right)^2 \Big/ \left(\frac{1}{137}\right)^2 = 1.146\ ; \tag{3.11}
$$

recall that the definition (1.1) of the R unit involves $\alpha(Q^2 = 0)$.

Table 3 indicates that the total cross section for e^+e^- annihilation to neutrino pairs of each generation is 0.25 units of R. This would already pose a serious background for experiments searching for $e^+e^- \to$ (nothing), a signature interesting for supersymmetry searches and in other contexts. But, actually, the background

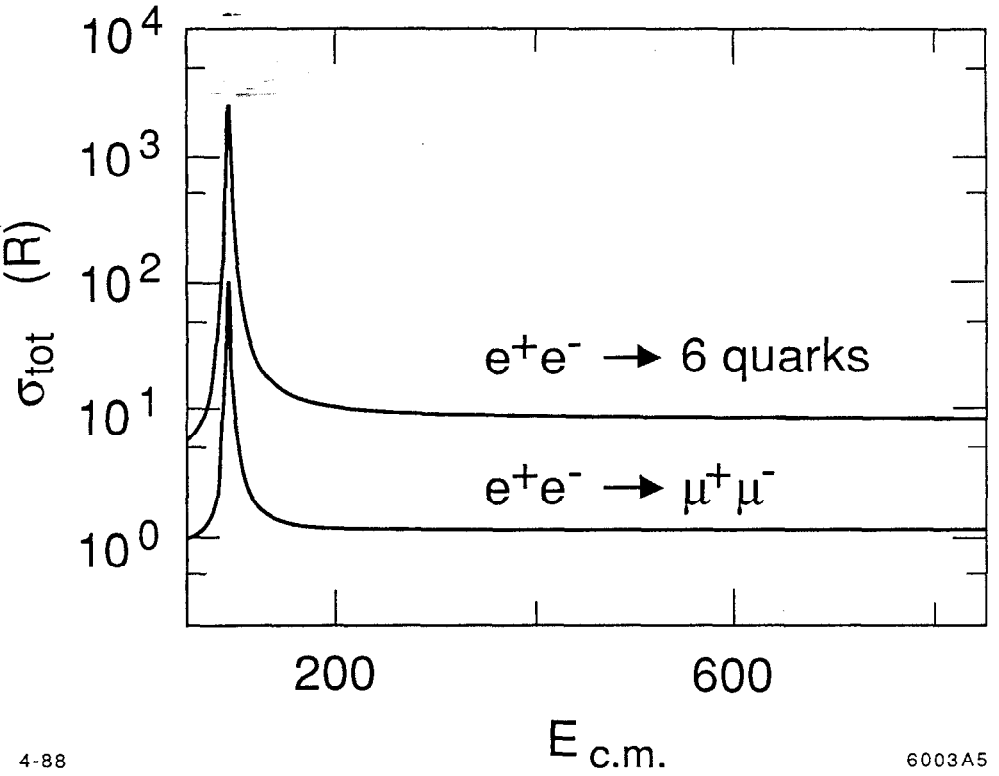

Figure 8. Total cross section for e^+e^- annihilation to hadrons and to μ pairs in the standard model.

problems for this signature are much worse, since the process $e^+e^- \to \nu_e\overline{\nu}_e$ can proceed not only by s-channel Z-exchange but also by t-channel W exchange.[41] In Fig. 11, we plot the total standard model cross section for $e^+e^- \to \nu\overline{\nu}$ as a function of center of mass energy.

The most important new processes which appear in e^+e^- reactions well above the Z^0 resonance involve the pair-production of weak vector bosons. The total cross

Table 3. Total cross sections (in units of R) and asymmetries for fermion pair production in e^+e^- annihilation well above the Z^0, computed for $\sin^2\theta_w = 0.23$.

	σ_{tot}	A_{FB}	A_{pol}
u	2.13	0.60	0.34
d	1.10	0.64	0.62
ℓ^-	1.29	0.47	0.07
ν	0.29	0.12	0.15

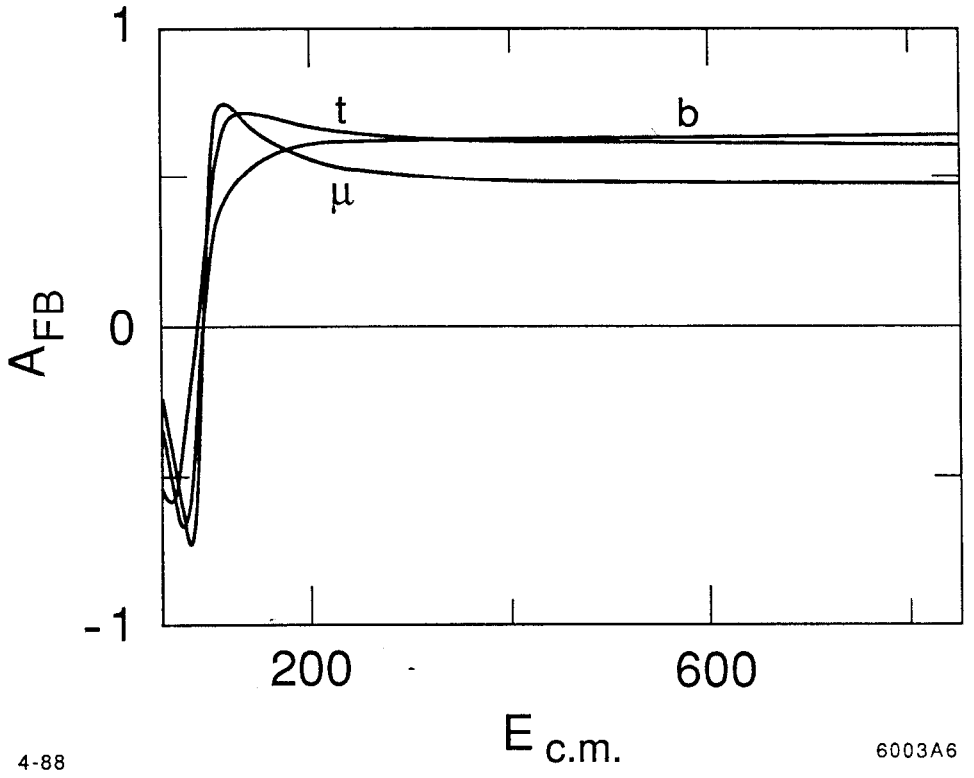

Figure 9. Forward-backward asymmetries for the production of μ, b and t pairs, in the standard model.

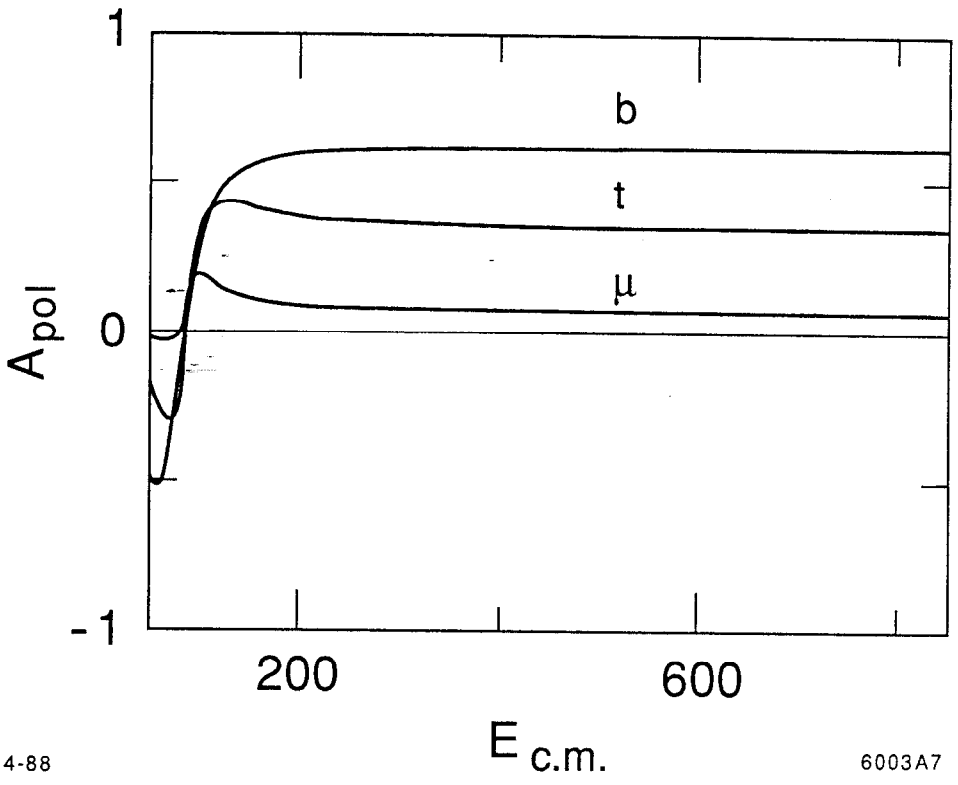

Figure 10. Polarization asymmetries for the production of μ, b, and t pairs, in the standard model.

section for this pair-production is enormous by the standards of e^+e^- annihilation: 20–30 units of R. These pair-production processes are interesting in their own right as dramatic predictions of the standard model. The reaction $e^+e^- \to W^+W^-$ provides particularly interesting tests of the standard model, which we will discuss in detail in Chapter 7. For the moment, though, our main concern will be that, since these processes form a large part of the total annihilation cross section, and since they involve heavy final-state particles, they provide the most important backgrounds to new particle searches.

Let us begin by displaying the standard model cross sections for these processes. As a point of reference, the cross section for $e^+e^- \to \gamma\gamma$, to leading order in α and ignoring the electron mass, is given by

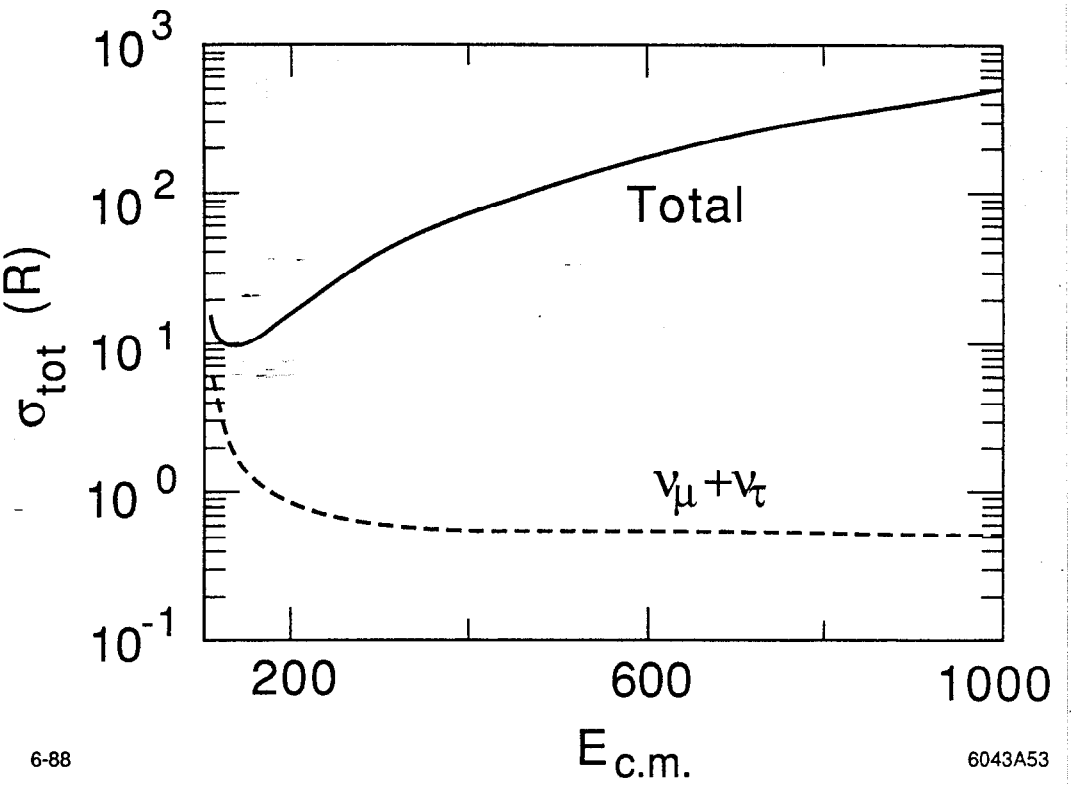

Figure 11. Total cross section for $e^+e^- \to \nu\bar{\nu}$ in the standard model, computed for 3 lepton generations.

$$\frac{d\sigma}{d\cos\theta}(e^+e^- \to \gamma\gamma) = \frac{\pi\alpha^2}{s}\left(\frac{u}{t} + \frac{t}{u}\right), \tag{3.12}$$

where $t = -\frac{1}{2}s(1 - \cos\theta)$, $u = -\frac{1}{2}s(1 + \cos\theta)$. The cross sections for $Z^0\gamma$ and Z^0Z^0 production have a similar form:[42]

$$\frac{d\sigma}{d\cos\theta}(e^+e^- \to Z^0\gamma) = \frac{\pi\alpha^2}{s}\left(\frac{(\frac{1}{2} - \sin^2\theta_w)^2 + (\sin^2\theta_w)^2}{2\sin^2\theta_w\cos^2\theta_w}\right)\cdot\left(1 - \frac{m_Z^2}{s}\right) \cdot\left(\frac{(u - m_Z^2)^2 + (t - m_Z^2)^2}{ut}\right), \tag{3.13}$$

where $t = -\frac{1}{2}(s - m_Z^2)(1 - \cos\theta)$, $u = -\frac{1}{2}(s - m_Z^2)(1 + \cos\theta)$;

$$\frac{d\sigma}{d\cos\theta}(e^+e^- \to Z^0Z^0) = \frac{\pi\alpha^2}{s}\left(\frac{(\frac{1}{2}-\sin^2\theta_w)^4+(\sin^2\theta_w)^4}{2\sin^2\theta_w\cos^2\theta_w}\right)\cdot\left(1-\frac{4m_Z^2}{s}\right)^{\frac{1}{2}}$$
$$\cdot\left(\frac{u}{t}+\frac{t}{u}+4m_Z^2\frac{s}{ut}-m_Z^4(\frac{1}{t^2}+\frac{1}{u^2})\right), \tag{3.14}$$

where $t = -\frac{1}{2}(s - [s(s-4m_Z^2)]^{\frac{1}{2}}\cos\theta) + m_Z^2$, $u = -\frac{1}{2}(s + [s(s-4m_Z^2)]^{\frac{1}{2}}\cos\theta) + m_Z^2$. The formulae (3.12) and (3.14) should be integrated only over $\cos\theta > 0$ to obtain the total cross section. The leading-order formula for $e^+e^- \to W^+W^-$ is considerably more complicated.[43,44] We will present this formula, and dissect it,

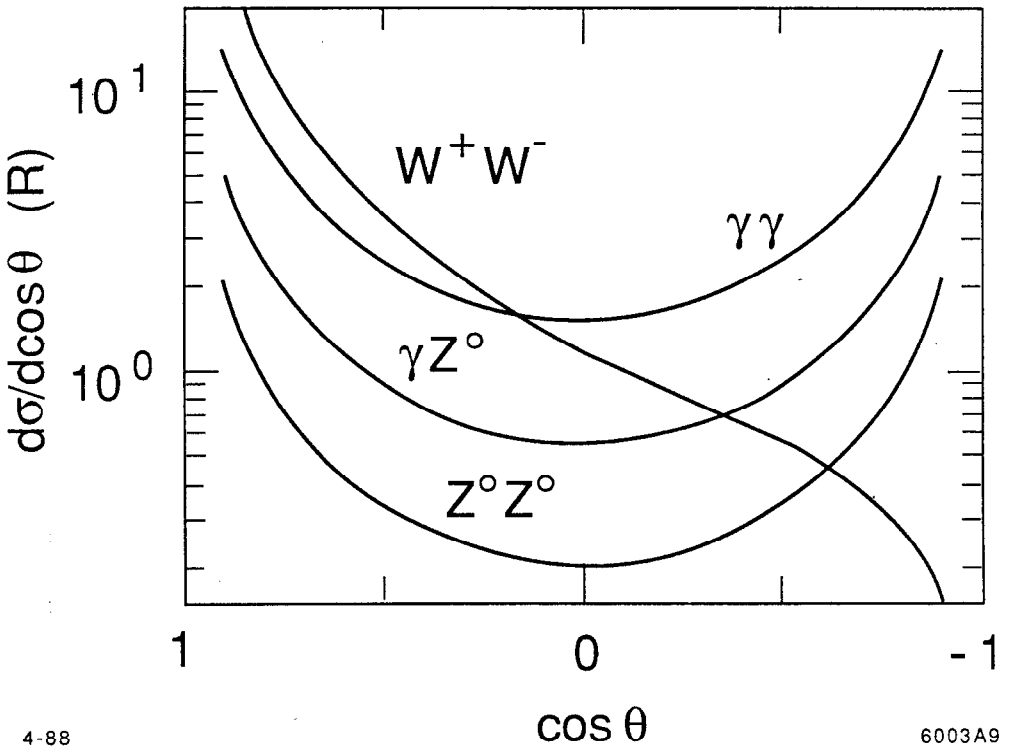

Figure 12. Differential cross sections for e^+e^- annihilation into vector boson pairs at $\sqrt{s} = 1$ TeV.

in Chapter 7. The theoretical differential cross sections for the four boson pair-production processes are displayed (in units of R) in Fig. 12.

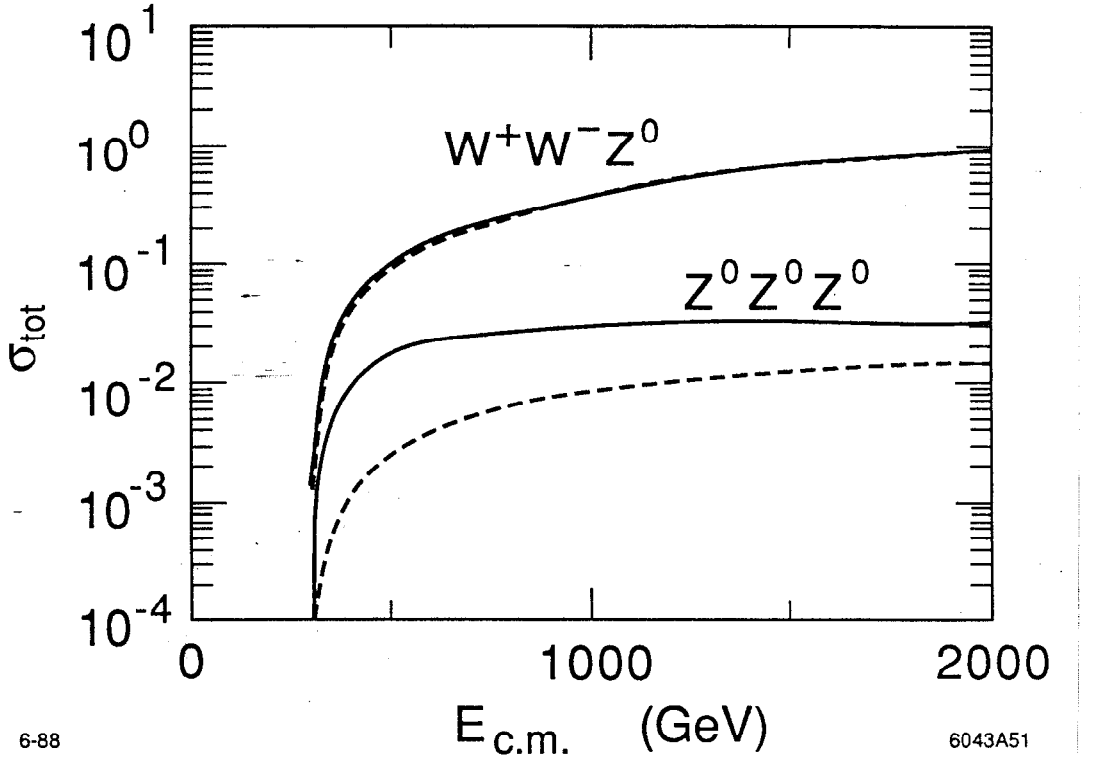

Figure 13. Total cross sections for the reactions $e^+e^- \to W^+W^-Z^0$ and $e^+e^- \to 3Z^0$, in the standard model. The solid curve assumes a Higgs boson mass $m_H = 300$ GeV; the dashed curve assumes $m_H = 100$ GeV.

Because of the large size of 2-boson production cross sections, one should expect that 3-boson reactions will sometimes be relevant. The reactions $e^+e^- \to W^+W^-Z^0$ and $e^+e^- \to 3Z^0$, in the case where one Z^0 decays to neutrinos, contribute directly to searches for new particles which decay to weak bosons plus missing energy. The total cross sections for these two processes as a function of energy are shown in Fig. 13. For the situation where one Z^0 decays to neutrinos, we would like to know the invariant mass of the system that remains. The distribution of this two-boson invariant mass, at $\sqrt{s}$= 1 TeV, is shown in Fig. 14. In general, these processes make only very small background contributions.

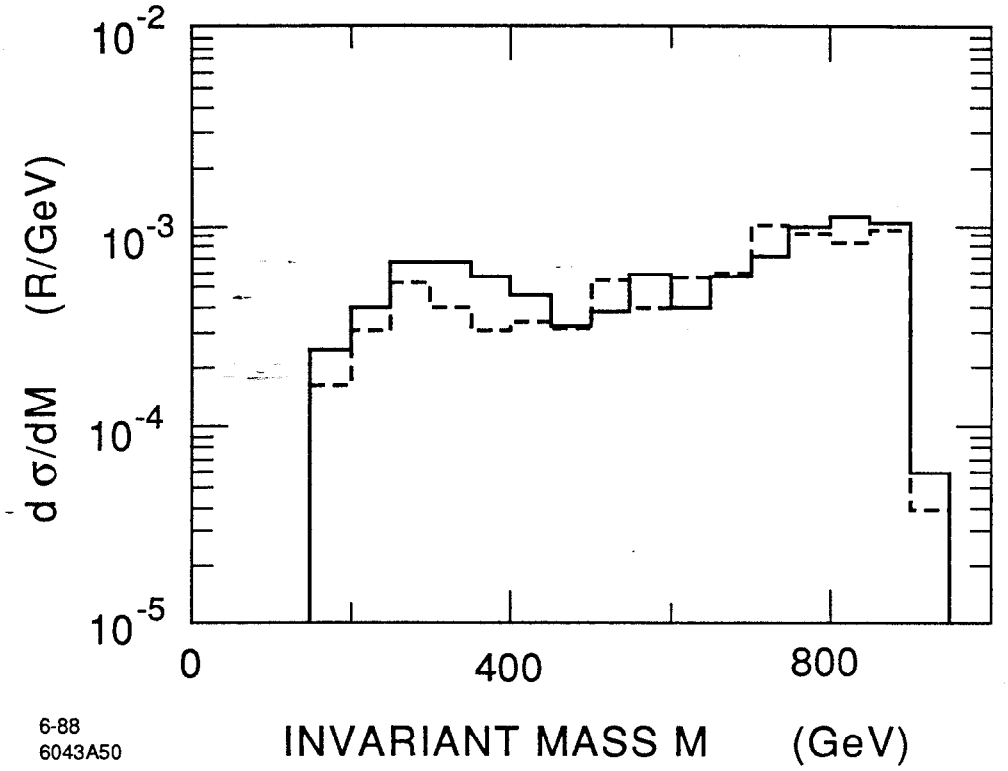

Figure 14. Invariant mass distribution for vector boson pairs in e^+e^- annihilation to three bosons at $\sqrt{s} = 1$ TeV: (a) W^+W^- mass distribution in $e^+e^- \rightarrow W^+W^-Z^0$, (b) Z^0Z^0 mass distribution in $e^+e^- \rightarrow 3Z^0$. The solid histogram is the result for $m_H = 300$ GeV, the dashed histogram is the result for $m_H = 100$ GeV.

3.4. Annihilation Reactions: Simulation

All of the e^+e^- annihilation processes which result in hadronic final states are potentially serious backgrounds to new particle searches. Whether one considers events resulting from $q\overline{q}$ production or weak boson pair production, the detected states have a central angular distribution and large deposited energy. In the $q\overline{q}$ reaction, gluon radiation can give jets of large invariant mass and, sometimes, substantial aplanarity. In later chapters, we will study specific particle searches and detail cuts which reduce the background from standard model annihilation processes. In this section, though, we would like to give an introduction to these background events and to explain how they should appear in our model detector.

We have explored this question by modelling the hadronization of quark pairs using the Lund Monte Carlo, version 6.3.[45] We definitely need to use a parton shower model in the 1 TeV region, rather than relying simply on exact matrix element computations, because even at PEP/PETRA energies we often have more than 4 jets in an event with a reasonable jet resolution. Although the Lund shower model (version 6.3) fits the PEP and PETRA data almost perfectly,[46] we are not sure that predictions of this model are reliable in the 1 TeV region. The model is based on the leading log approximation, with the soft and collinear gluon interference effects approximated to by the parton's angular ordering. Because of the leading log approximation, cross sections for the hard gluon emission processes are not reliable. For example, the hard three jet event rate is overestimated, compared to the prediction based on the exact matrix element.* To obtain the correct parton momentum distribution predicted by the exact $O(\alpha_s)$ calculations, the first $q\bar{q}g$ branching is modified so that the angular and energy distributions are constrained to be just those given by the $O(\alpha_s)$ exact calculation. Of course, this modification is not sufficient. If a soft gluon is emitted at the first branching and a hard one is emitted at the second branching, then there is no correction for this hard gluon emission. Therefore, we should not believe that the results of the models are exact.

The process of weak boson pair production is modelled by a Monte Carlo program written by Kleiss,[48] which includes the decay matrix elements of the W and Z bosons to fermions and correctly accounts the Breit-Wigner line shapes of these heavy states. Events from the tails of the Breit-Wigner distributions contribute disproportionately to backgrounds for new particle searches. The decays of W and Z are computed used the Lund fragmentation scheme.

Our simulation assumes 6 light quarks, including a top quark of mass 40 GeV,

* The rate of hard three jet events is underestimated by the Webber leading log parton shower model, ref. 47. This difference might depend on the gauge used for the two models. Although the physical quantities must be gauge invariant at infinite orders of the perturbative calculations, it is not surprising to have a different result at lower orders because the models are based on the leading log approximation.

Table 4. Effect of beamstrahlung on cross sections for Standard Model Processes.

Process	Cross section (fb)	
	Without Beamstrahlung	*With Beamstrahlung*
$e^+e^- \to W^+W^-$	2310	3570
$e^+e^- \to Z^0Z^0$	127	200
$e^+e^- \to q\bar{q}$	438	4050

and a nominal center of mass energy of 1 TeV. The simulation includes the effects of beamstrahlung and the idealized detector described previously. As we noted in Section 3.2, the simulation includes the process $e^+e^- \to Z^0\gamma$ as a part of the radiative corrections to quark pair production. The distributions shown in the figures presented below are correctly normalized to an integrated luminosity of 10 fb^{-1} unless it is specified otherwise.

We first address the gross distribution of events in energy and in the direction of the produced hadrons. One might expect that radiative corrections and beamstrahlung would lower the cross section for high-energy e^+e^- annihilation. This effect is counterbalanced, though, by a substantial number of events at lower center of mass energies, annihilating through the larger cross section available there. Our simulation gives a distribution of events which is roughly flat in hadronic invariant mass, in which the events with total hadronic invariant mass above 800 GeV account for almost all of the nominally expected luminosity, and this sample is enhanced by events with lower invariant mass. A comparison of the effective cross sections for the major physics processes with and without beamstrahlung is given in Table 4. All annihilation events with effective center of mass energy above 300 GeV are potentially useful for some physics analyses and should be kept in the data sample. On the other hand, we would like to discard events of very low energy, and events with large boosts which would not be well measured by the detector.

Fig. 15(a) shows the distribution of the reconstructed hadronic invariant mass

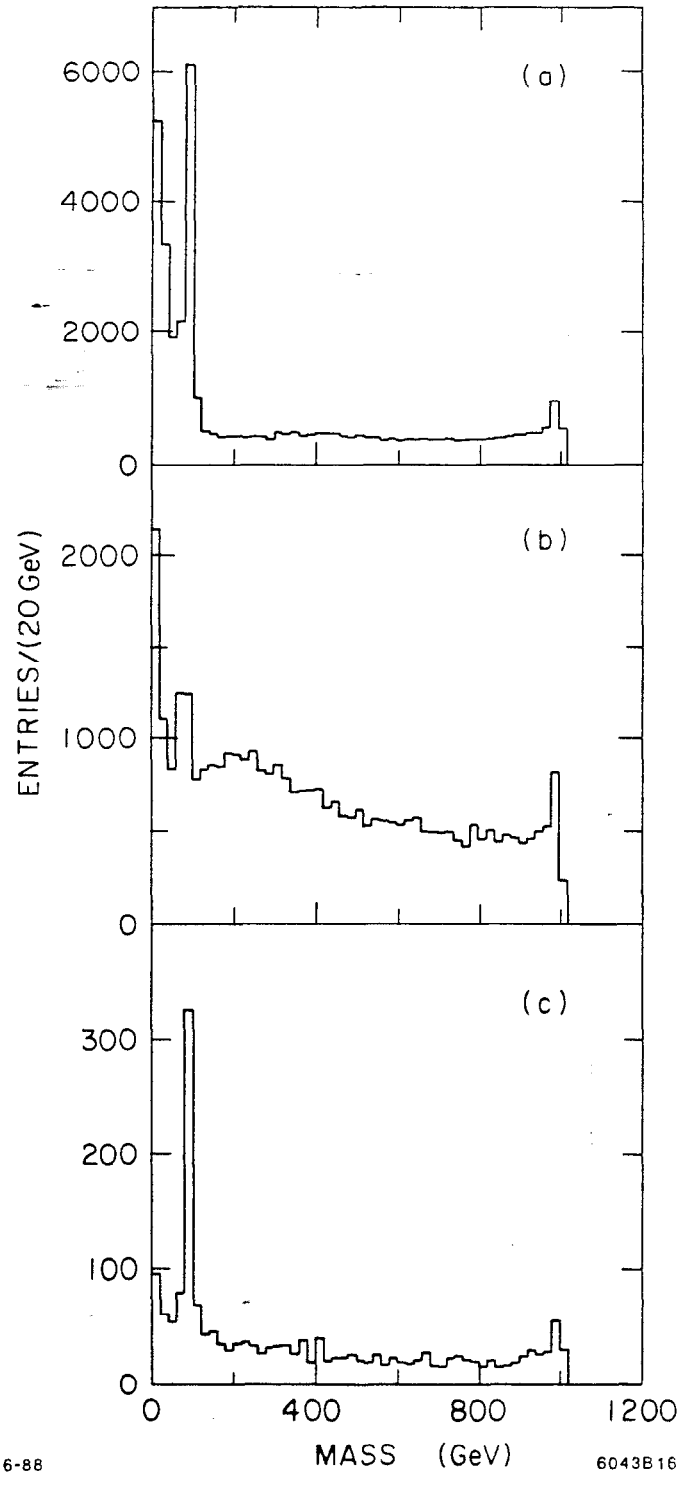

Figure 15. Distribution of the observed invariant mass for e^+e^- annihilation to (a) $q\bar{q}$, (b) W^+W^-, (c) Z^0Z^0, at $\sqrt{s} = 1$ TeV.

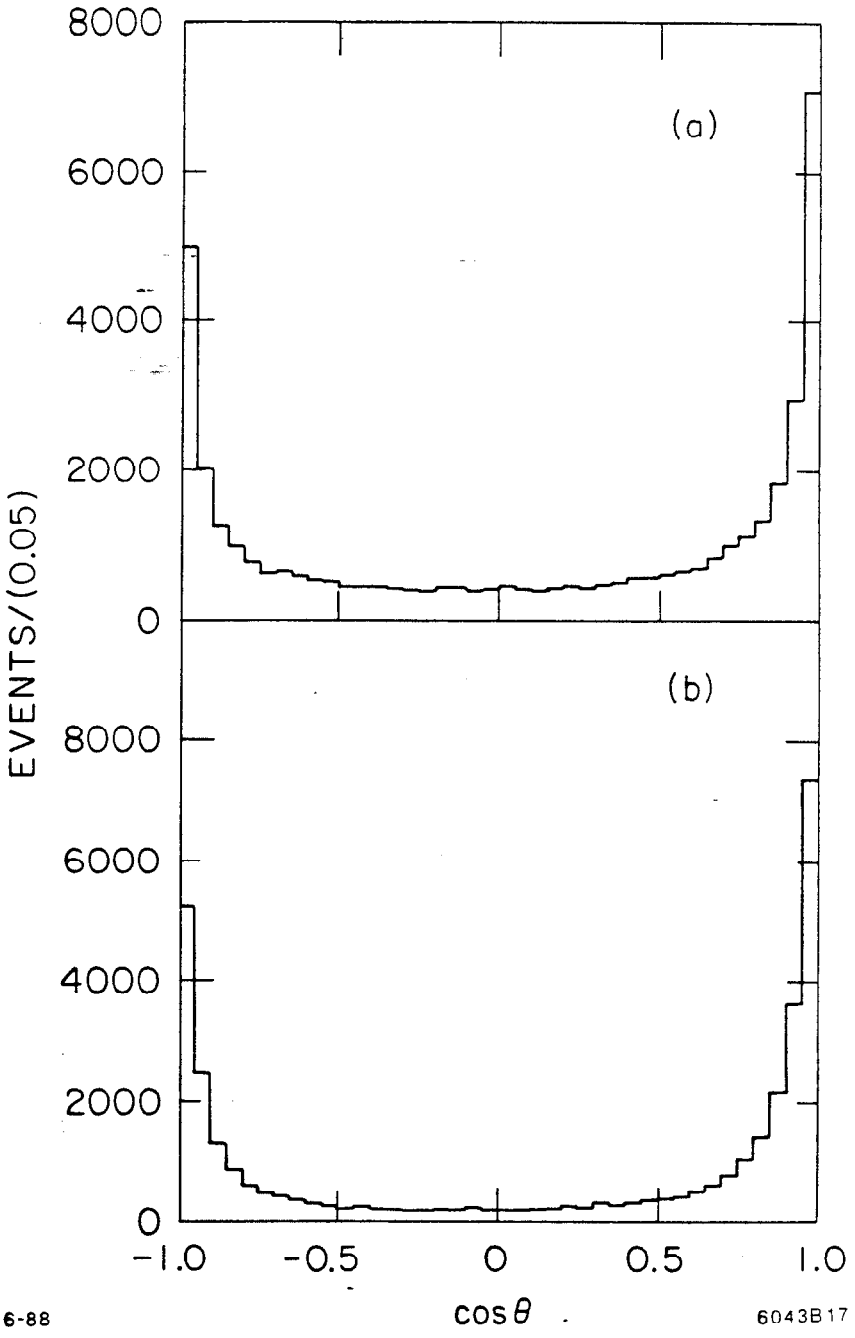

Figure 16. Distribution of the direction of the thrust axis for e^+e^- annihilation events at $\sqrt{s} = 1$ TeV: (a) $q\overline{q}$, (b) W^+W^-.

for $q\overline{q}$ events, showing the effect of beamstrahlung and detector smearing. The sharp peak at the Z^0 mass is due to the process, discussed in the previous section, of radiation down to the Z^0 by emission of a forward photon. The analogous distribution for W pair events is shown in Fig. 15(b). This distribution has a peak around the mass of the W, due to events in which the other W is lost down the 10° hole. The corresponding distribution for Z pair events, shown in Fig. 15(c), shows an even stronger peak at the Z mass, mainly due to events in which the other Z decays to $\nu\overline{\nu}$, a mode with a 20% branching fraction. In general, the distributions we will discuss are quite similar in appearance for W and Z pair events; normally, we will show only the W plot, since the Z pair production cross section is smaller by almost a factor of 10.

Fig. 16 shows the distribution of the direction of the thrust axis for $q\overline{q}$ and W pair events; in both cases, this distribution is strongly peaked forward and backward about the beam axis. For the $q\overline{q}$ events, the strong peaking is purely due to radiative corrections and beamstrahlung; for W pairs, the effect has a physics contribution in the peaking of the differential cross section. To select events for further analysis, we require that the measured invariant mass in the event be greater than 200 GeV, to eliminate the highly radiative events, and that the direction of the thrust axis satisfy $|\cos\theta_{thr}| < 0.8$, to insure that the event is indeed well measured. Similar cuts are included in the particle search analyses. About 70% of the events are removed by these two cuts.

The properties of the standard model events which survive these cuts are displayed in Figs. 17–27. Fig. 17 shows the distribution of charged particle multiplicity for $q\overline{q}$ and W pair events. The average multiplicities of $q\overline{q}$, W pair, and Z pair events in our sample are 42, 29, and 32, respectively. Note that the multiplicities are significantly lower for the vector boson events. This reflects a similarity between vector boson production at 1 TeV and τ pair production at PEP and PETRA energies; in both cases, the process preserves the multiplicity spectrum from a lower energy scale. Fig. 18 gives the distribution of charged tracks as a function of angle. (This figure reflects 2 fb^{-1} of data.) Despite the lower multiplicity of the

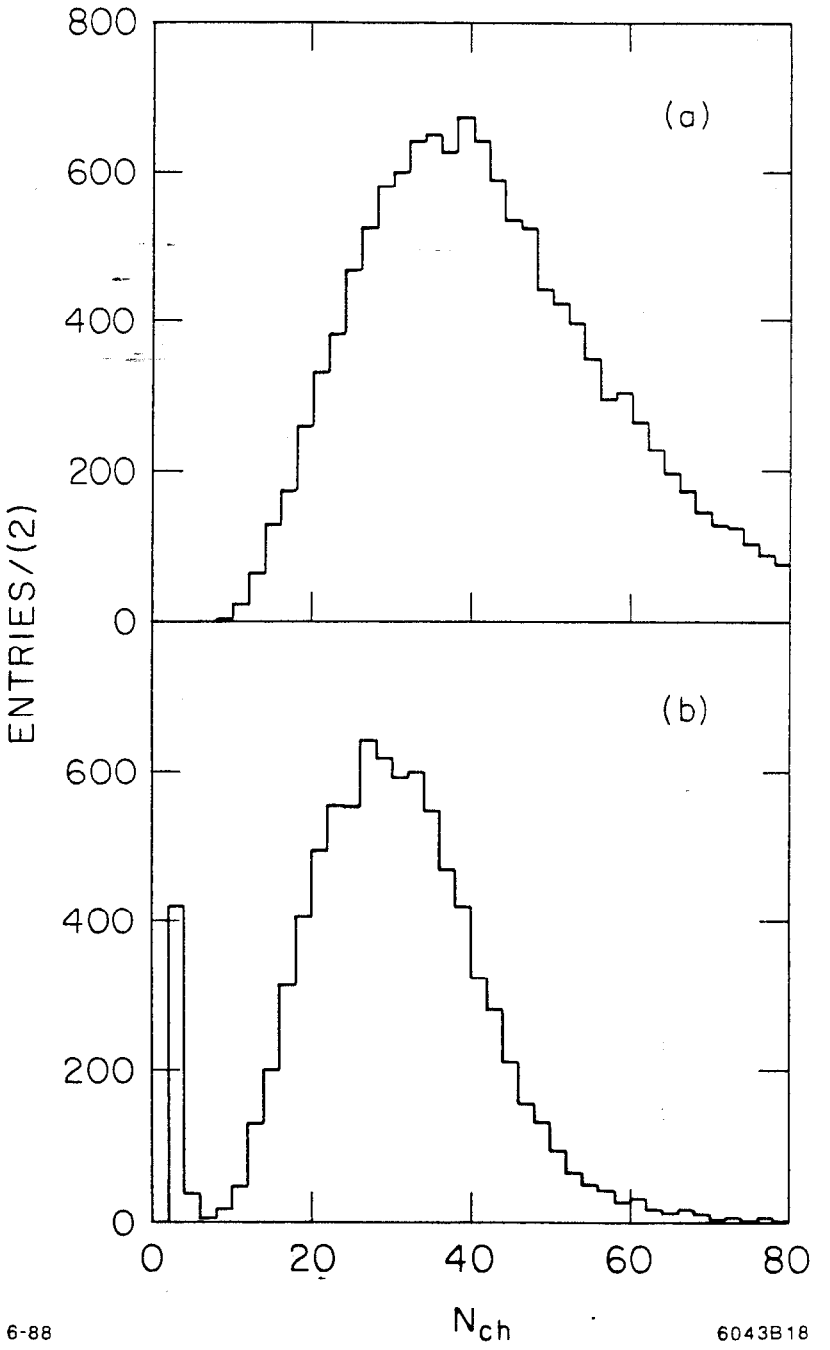

Figure 17. Distribution of the observed charge multiplicity for e^+e^- annihilation events at $\sqrt{s} = 1$ TeV: (a) $q\overline{q}$, (b) W^+W^-. In this figure, and in all of the remaining figures in this chapter, the events included are required to have a measured invariant mass greater than 200 GeV and a thrust axis direction satisfying $|\cos\theta_{thr}| < 0.8$.

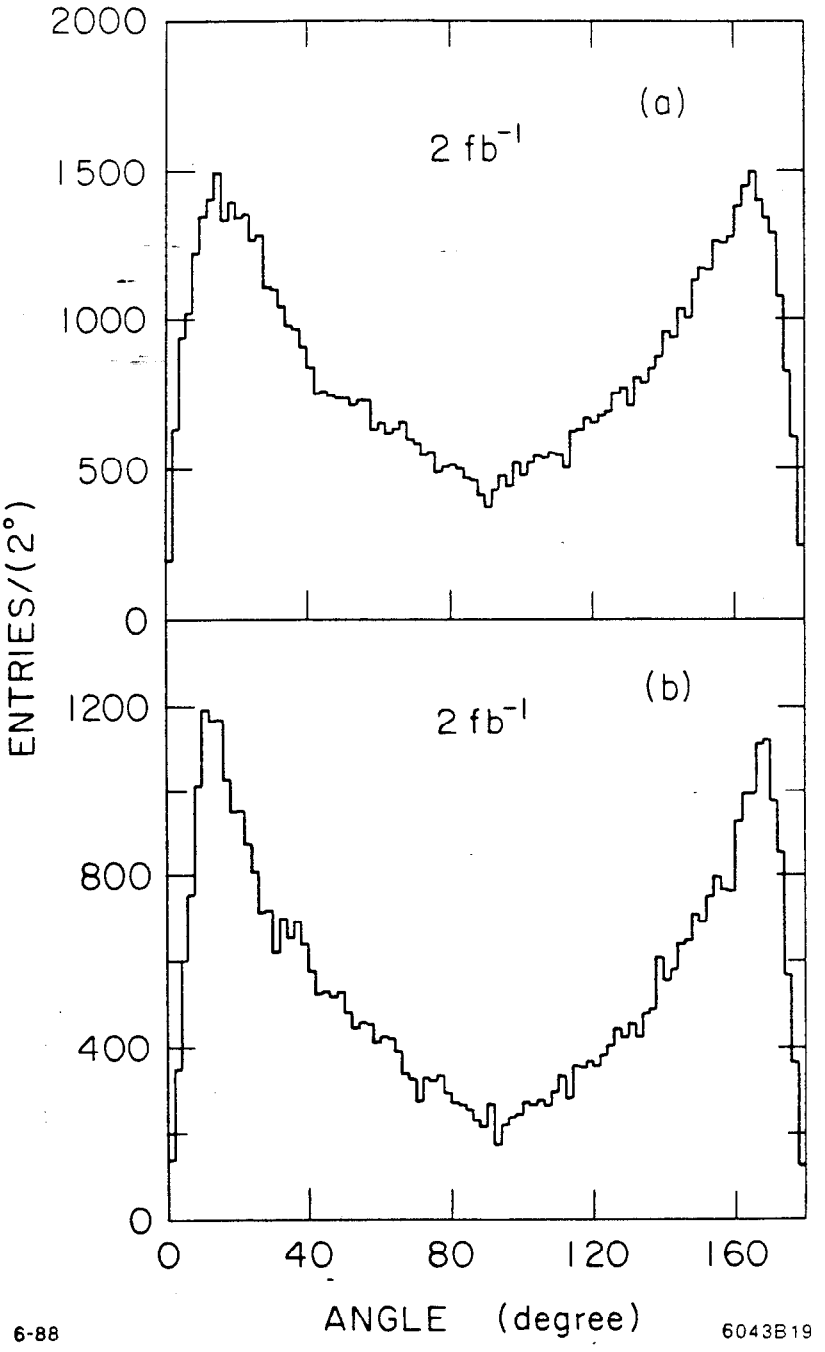

Figure 18. Density of charged tracks as a function of angle, for e^+e^- annihilation events at $\sqrt{s}$= 1 TeV: (a) $q\overline{q}$, (b) W^+W^-. This figure corresponds to an event sample of 2 fb^{-1}.

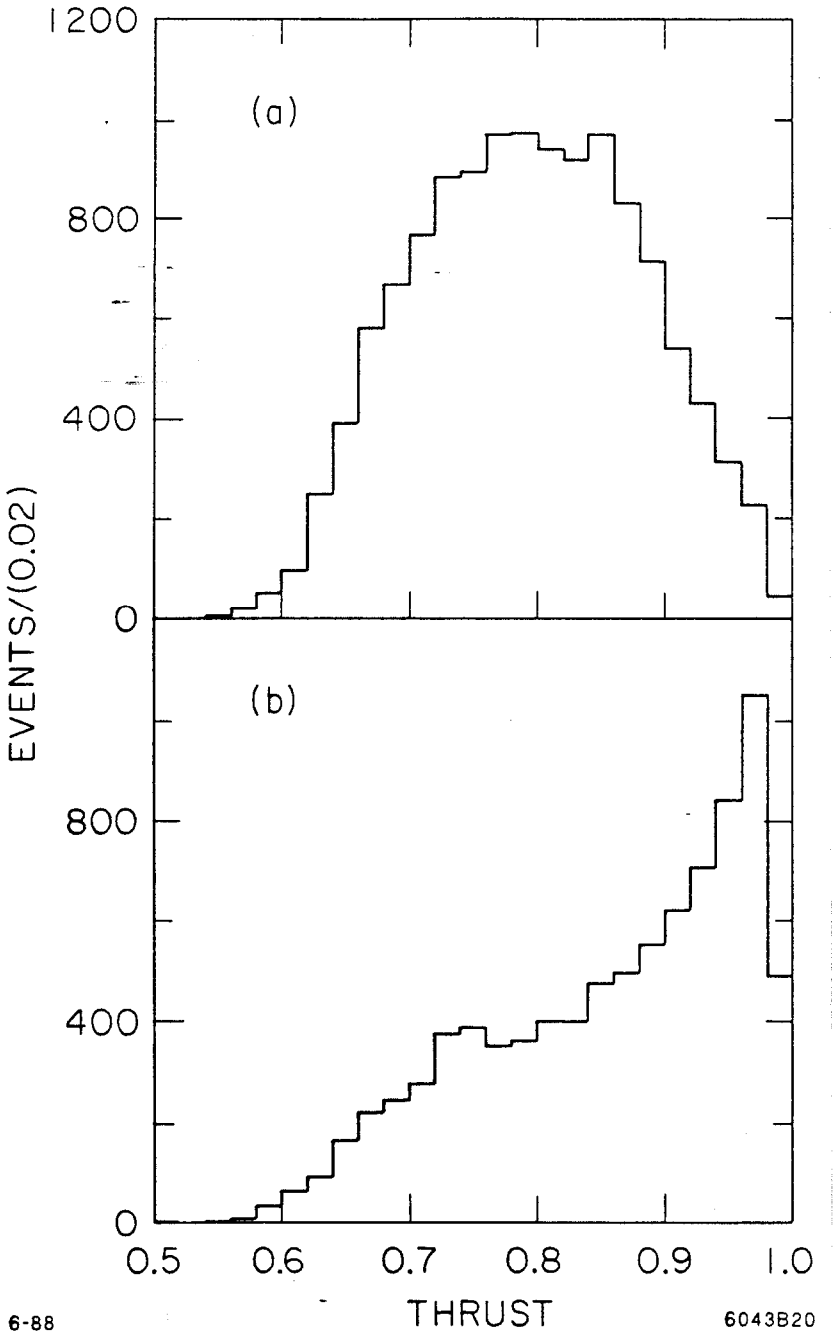

Figure 19. Distribution of thrust for e^+e^- annihilation events at $\sqrt{s} = 1$ TeV: (a) $q\overline{q}$, (b) W^+W^-.

W pairs, the tracking requirements for these events are no less severe than those for quark pair events. Fig. 19 gives the thrust distribution. The average thrust of $q\overline{q}$ events is 0.79; for W and Z pair events, the average thrust is 0.86 and 0.83, respectively.

The next two figures display the properties of these events in terms of jet masses. One possible way to obtain a jet mass spectrum is to divide the event into two hemispheres by a plane perpendicular to the thrust axis, assign all of the calorimetric energy deposition in each hemisphere to the same jet, and then compute the observed mass of each jet. Applying this procedure to the $q\overline{q}$, W, and Z pair events, we find the the jet mass distributions shown in Fig. 20. A more sophisticated procedure associates energy deposition into clusters using a clustering algorithm. We used an iterative procedure which assigned to each pair of clusters (i,j) at a given stage a quantity y_{ij} given by

$$y_{ij} \;=\; 2E_iE_j(1-\cos\theta_{ij})\;, \tag{3.15}$$

where the E_i are cluster energies and θ_{ij} is the angle between the two clusters. This variable is a combined measure of the opening angle and momentum imbalance of the two particles (or clusters) i and j. At each step, one combines the two clusters of the pair with the minimum value of y_{ij}. The iteration proceeds until a specified minimum value of y is reached or until a specified number of clusters is formed. Specifying that the state should be reduced to two clusters yields, for $q\overline{q}$, W, and Z pair events, the distributions of cluster masses shown in Fig. 21. The $q\overline{q}$ events, in both the thrust and cluster analyses, give substantial jet masses, due to gluon radiation. The additional peaks at zero and at the Z^0 mass come from the process $e^+e^- \rightarrow Z^0 + \gamma$, with the γ reconstructed as a zero-mass, zero-multiplicity jet.

In both jet mass distributions made for the W and Z pair events, the boson mass peak is clearly visible. The efficiency for reconstructing the boson masses to an accuracy of ± 15 GeV is about 40% for W and 45% for Z events. Since the branching fraction of the W to a quark pair is about 70%, the efficiency for

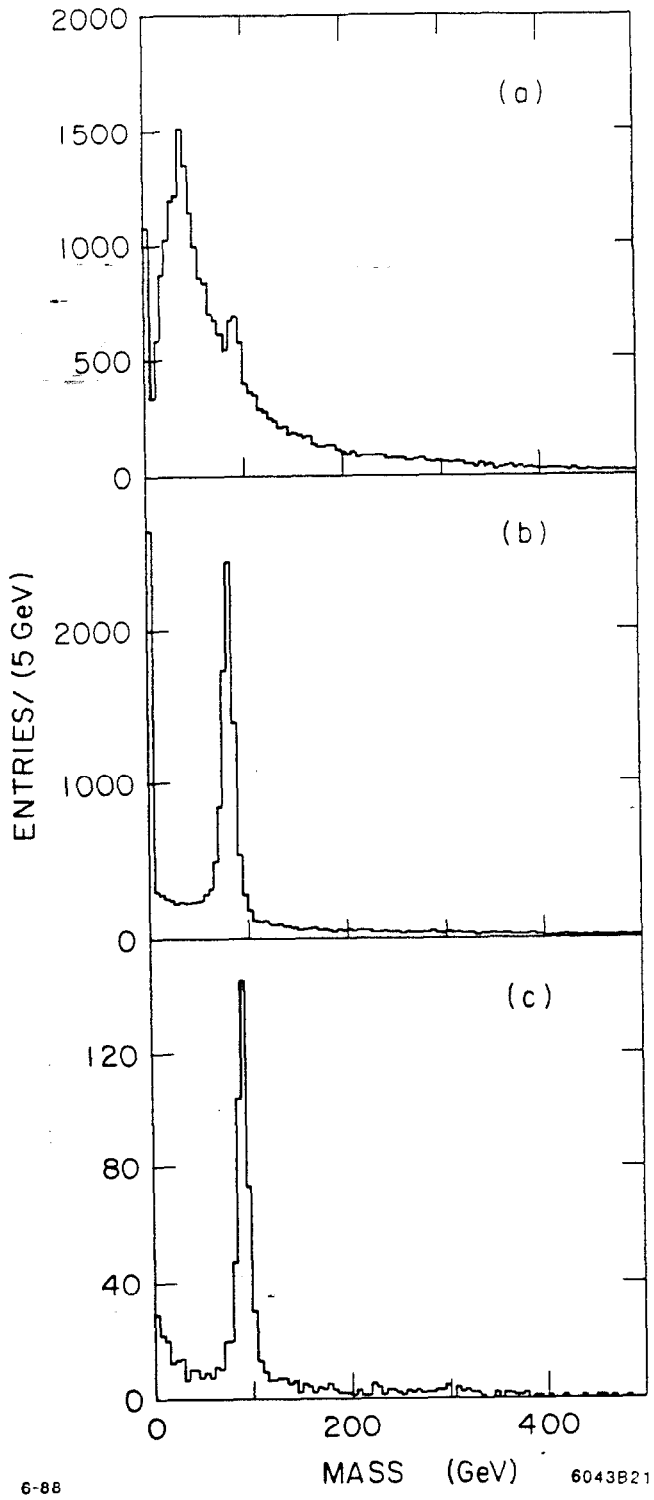

Figure 20. Distribution of reconstructed jet masses, using the hemisphere definition, for e^+e^- annihilation events at $\sqrt{s} = 1$ TeV: (a) $q\bar{q}$, (b) W^+W^-, (c) Z^0Z^0.

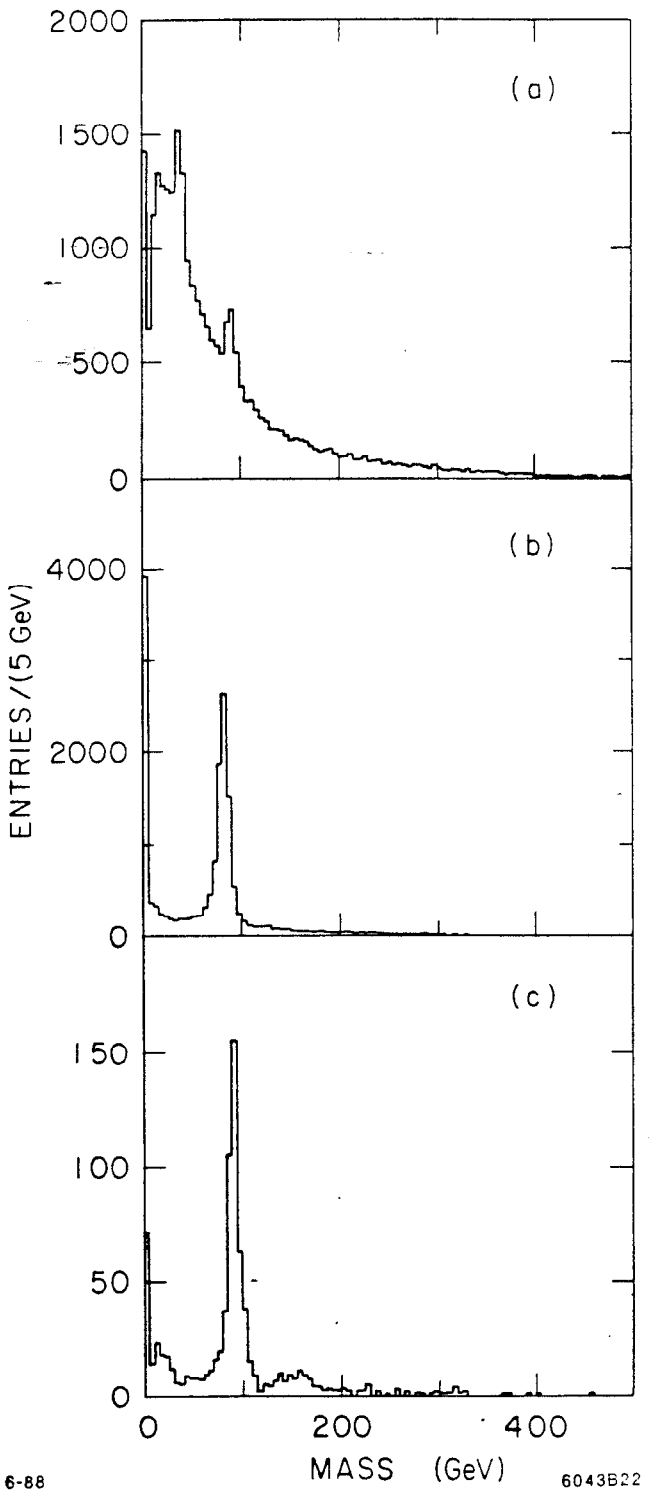

Figure 21. Distribution of reconstructed jet masses, using the cluster definition, for e^+e^- annihilation events at $\sqrt{s} = 1$ TeV: (a) $q\overline{q}$, (b) W^+W^-, (c) Z^0Z^0.

reconstructing the mass of a W which has decayed hadronically is about 57%. Similarly, about 56% of the Z bosons which decay to a quark or charged lepton pair are reconstructed accurately. The decays of the W to $\ell\overline{\nu}$ produce the additional peak in the lowest bin of the jet mass distribution. The enhancement at low mass in the Z plot comes from events in which one Z^0 decays to $\nu\overline{\nu}$ and the decay products of the other Z^0 are reconstructed as two jets.

Another way to view the jet mass distributions is to form scatter plots of the reconstructed invariant mass of one jet in each event relative to that of the other. These plots are shown in Figs. 22, 23, and 24 for $q\overline{q}$ and W and Z pair events, respectively, for a number of events corresponding to integrated luminosities of 2 fb^{-1} in the first two cases and 10 fb^{-1} in the last. The jet masses in these plots were determined as the masses in hemispheres defined normal to the thrust axis. In Fig. 23, we see strong bands along the two axes corresponding to events in which one W decayed hadronically and the other decayed leptonically. These last clusters are not present in the results for Z pair production shown in Fig. 24. There, the mismeasured jets are scattered more uniformly over the plot. The $q\overline{q}$ plot shows clusters along the axes due to $Z^0\gamma$ production. Notice that the distribution of high-mass $q\overline{q}$ jets tends to zero as both jet invariant masses become large, and that it is already quite small when both masses are of order m_W.

Fig. 25 displays the distribution of missing transverse momentum. This distribution, however, is not always an accurate indicator, since the main source of missing transverse momentum is the mismeasurement of the energy of a jet by the calorimeter. The missing transverse momentum then points in the direction of the thrust axis. To eliminate this source of background, one might wish to study the component of missing momentum perpendicular to both the beam direction and the thrust axis. The distribution of this quantity is shown in Fig. 26. Alternatively, one can study the acoplanarity angle, the angle between the two planes determined by the net momentum of each hemisphere and the beam direction. The distribution of this angle is shown in Fig. 27. By any measure, the events with quark pair production are dominated by two-jet events, and only the tails of

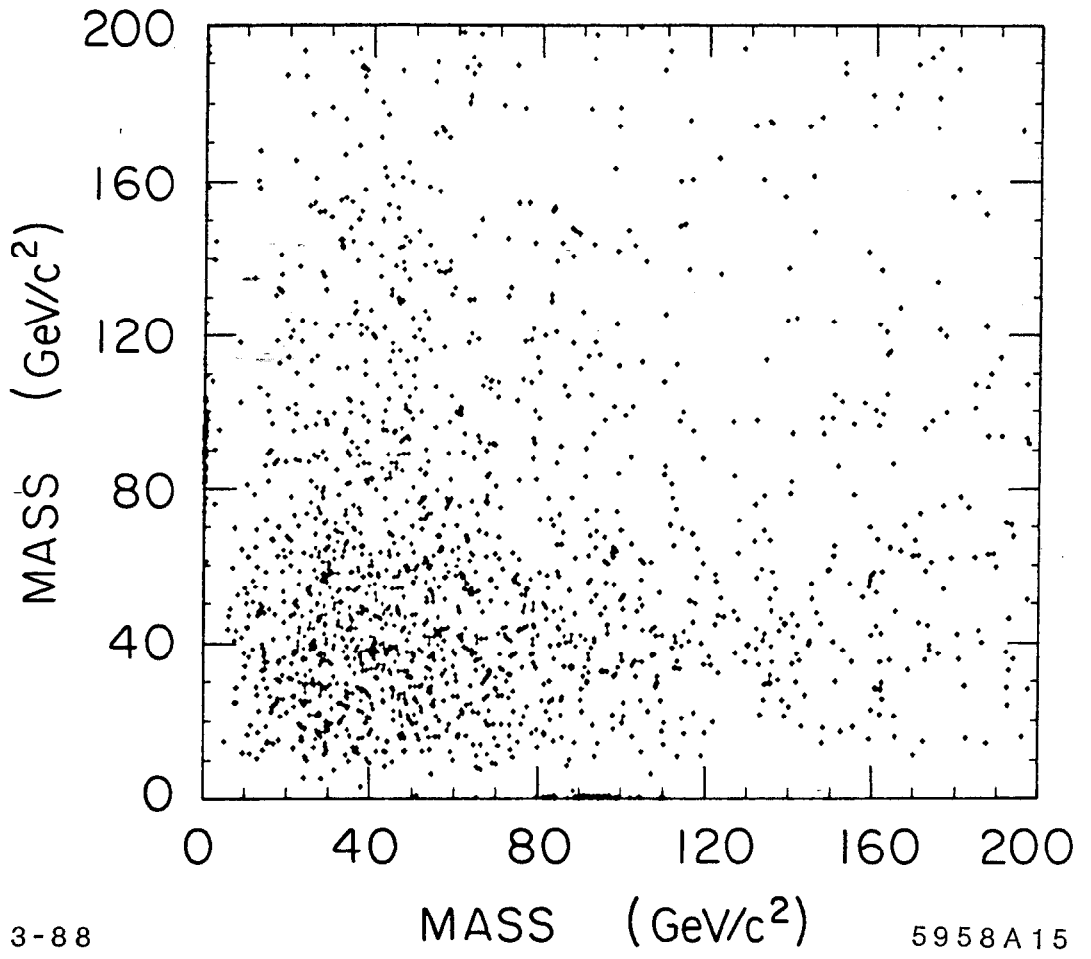

Figure 22. Scatter plot of the two jet masses in each event, for $e^+e^- \to q\overline{q}$ events at $\sqrt{s} = 1$ TeV. The jet masses are defined as in Fig. 20. This figure corresponds to an event sample of 2 fb^{-1}.

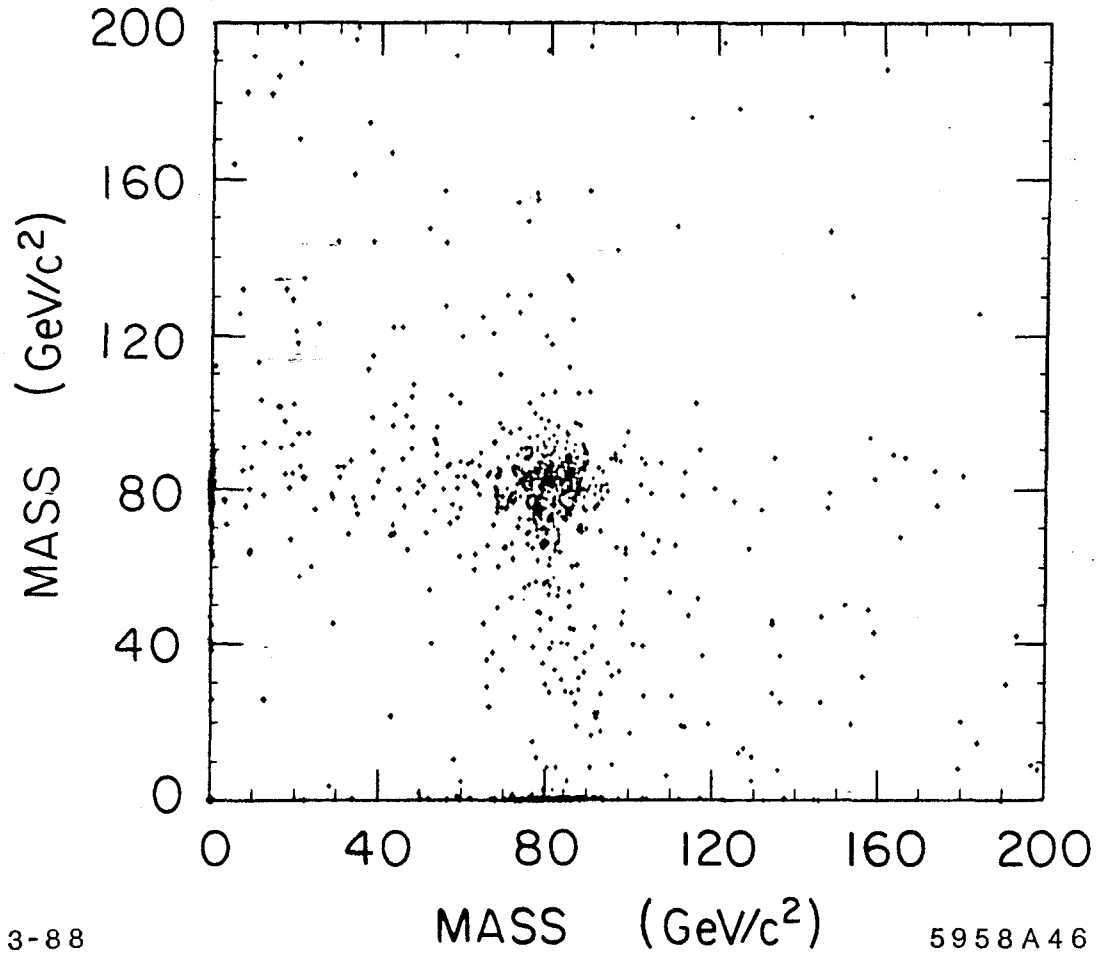

Figure 23. Scatter plot of the two jet masses in each event, for $e^+e^- \to W^+W^-$ events at $\sqrt{s} = 1$ TeV. The jet masses are defined as in Fig. 20. This figure corresponds to an event sample of 2 fb^{-1}.

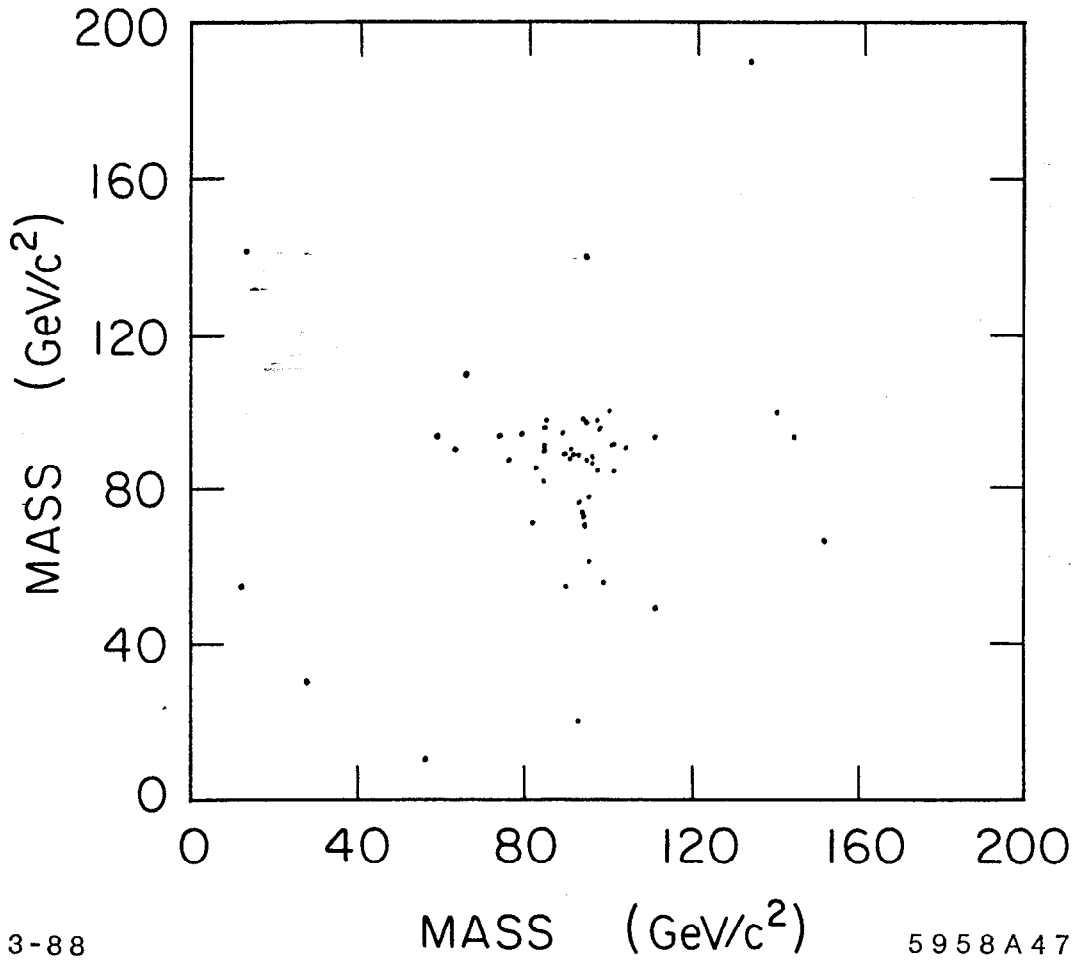

Figure 24. Scatter plot of the two jet masses in each event, for $e^+e^- \to Z^0Z^0$ events at $\sqrt{s} = 1$ TeV. The jet masses are defined as in Fig. 20. This figure corresponds to an event sample of 10 fb^{-1}.

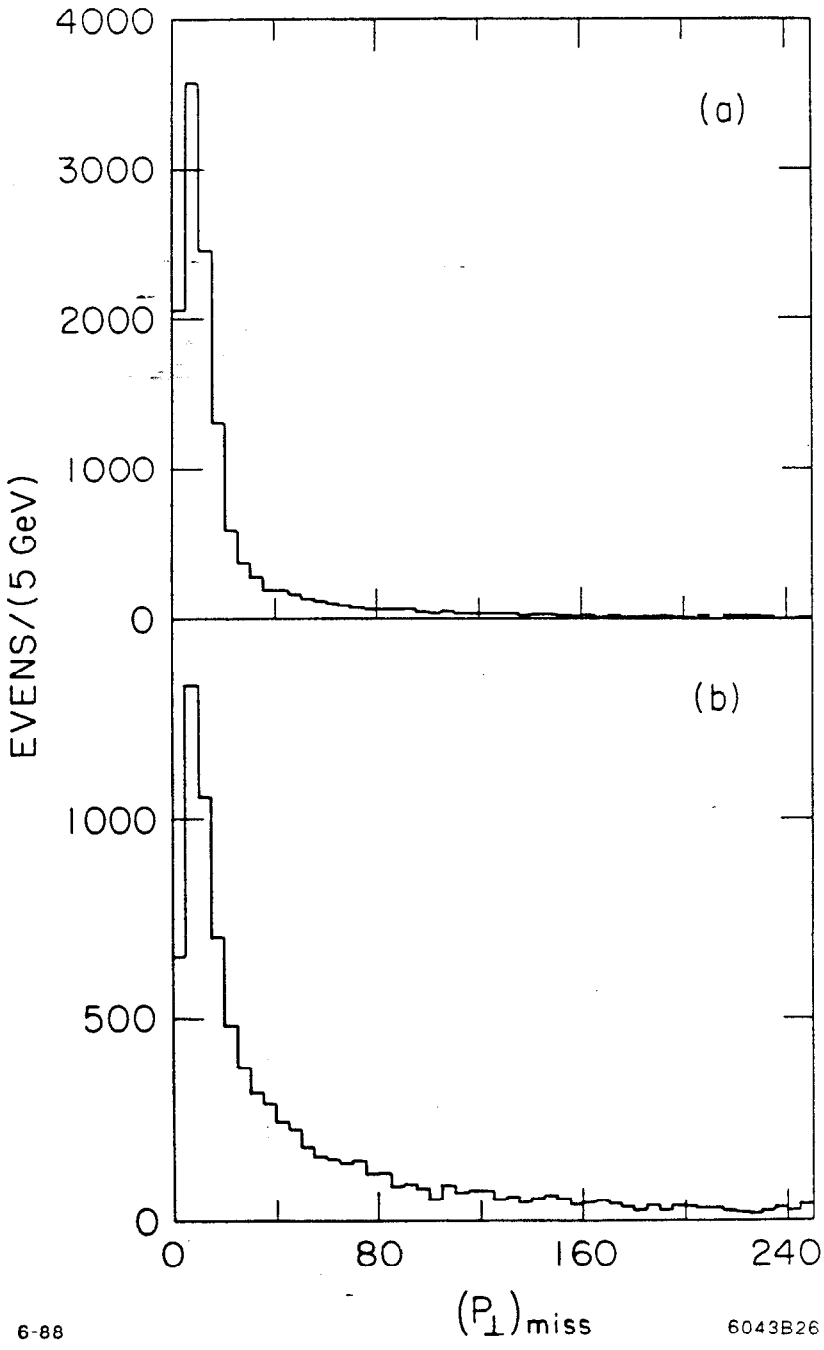

Figure 25. Distribution of apparent missing transverse momentum, for e^+e^- annihilation events at $\sqrt{s} = 1$ TeV: (a) $q\bar{q}$, (b) W^+W^-.

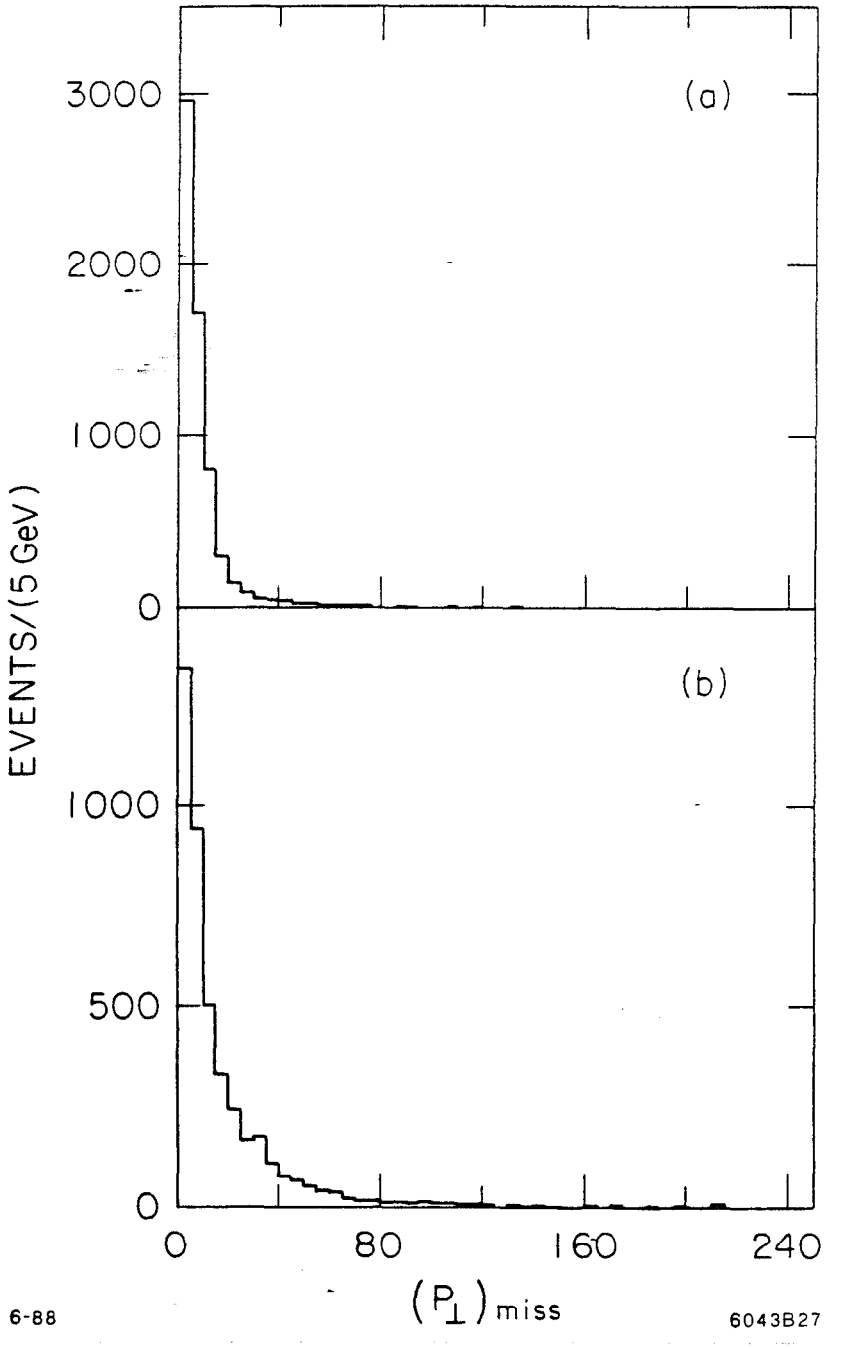

Figure 26. Distribution of apparent missing momentum normal to both the beam axis and the thrust axis, for e^+e^- annihilation events at $\sqrt{s} = 1$ TeV: (a) $q\bar{q}$, (b) W^+W^-.

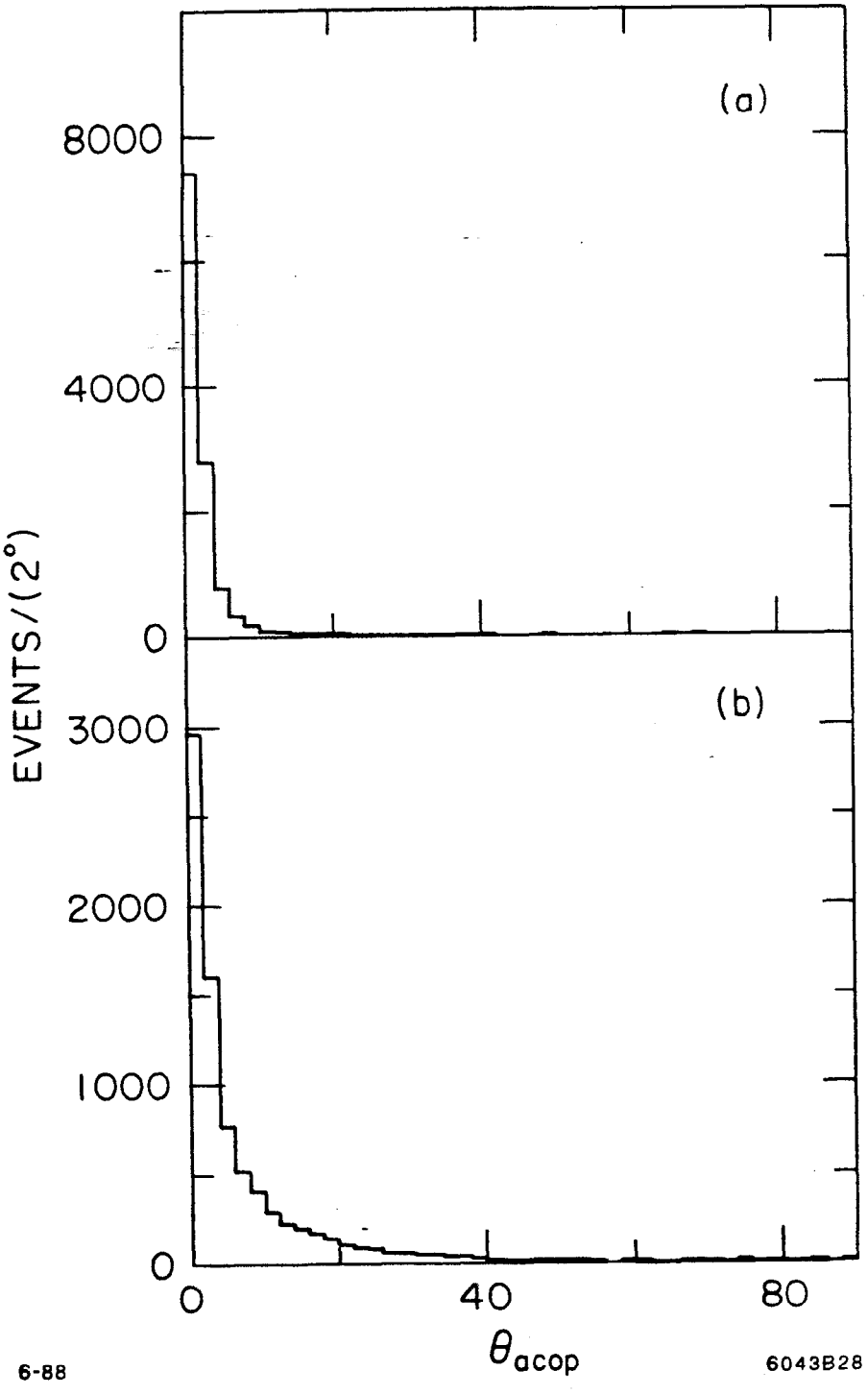

Figure 27. Distribution of acoplanarity angles between the thrust vectors of the two hemispheres, for e^+e^- annihilation events at $\sqrt{s} = 1$ TeV: (a) $q\bar{q}$, (b) W^+W^-.

distributions simulate the production of high-mass states. The vector boson pair events are just as highly coplanar.

3.5. W AND Z IDENTIFICATION

We will conclude our discussion of standard model processes with some comments on the distinguishablity of W and Z pair production from other standard

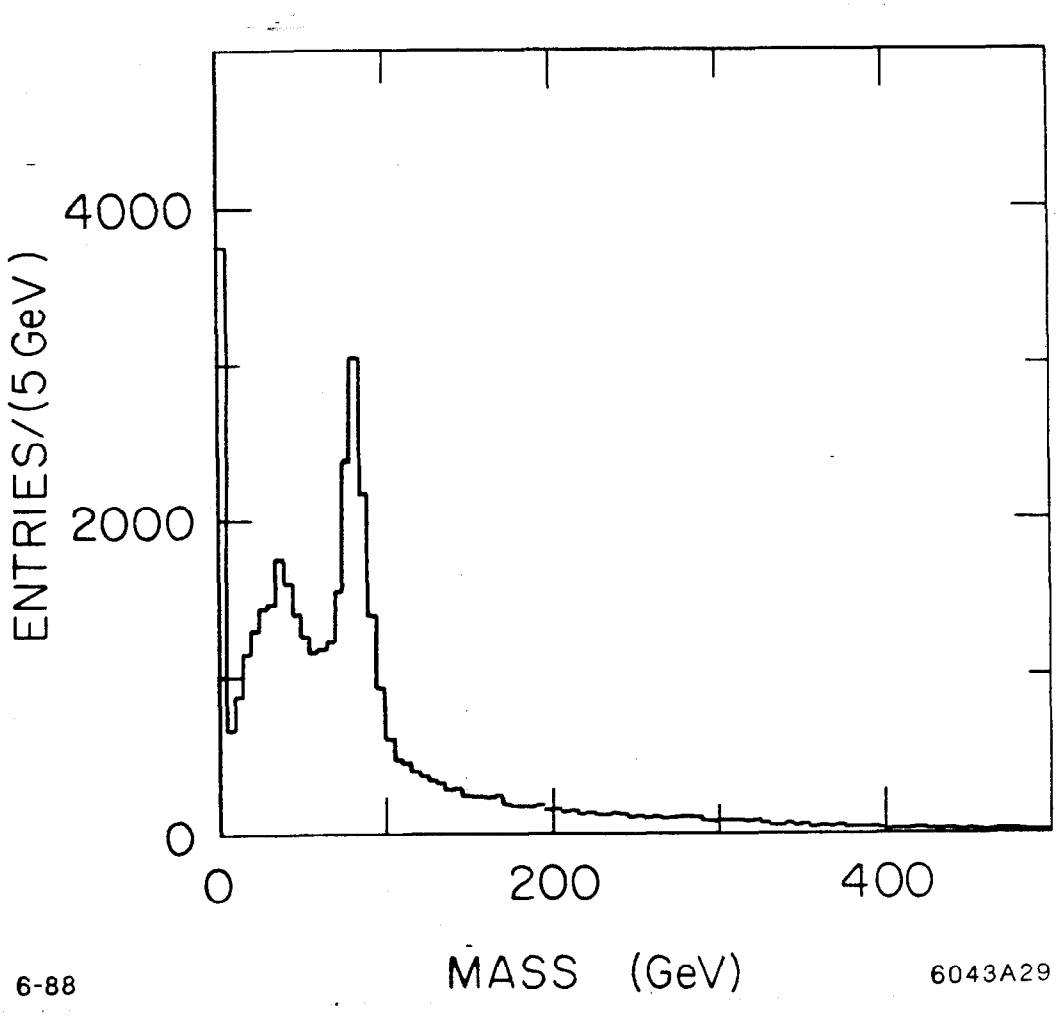

Figure 28. Distribution of jet masses for the full sample of events with e^+e^- annihilation to $q\bar{q}$, W^+W^-, and Z^0Z^0, corresponding to 10 fb^{-1} of data. The jet masses are defined as in Fig. 20.

model processes, and the ease of identifying individual W and Z bosons. Since some of the most important processes in the standard model, and also—as we will see—many of the important signatures for new particles, involve W and Z boson production, it is crucial that one should be able to tag the W and Z bosons in each event. Since these bosons decay to hadronic states 70% of the time, one would pay a high price in efficiency if it were not possible to reconstruct weak vector bosons

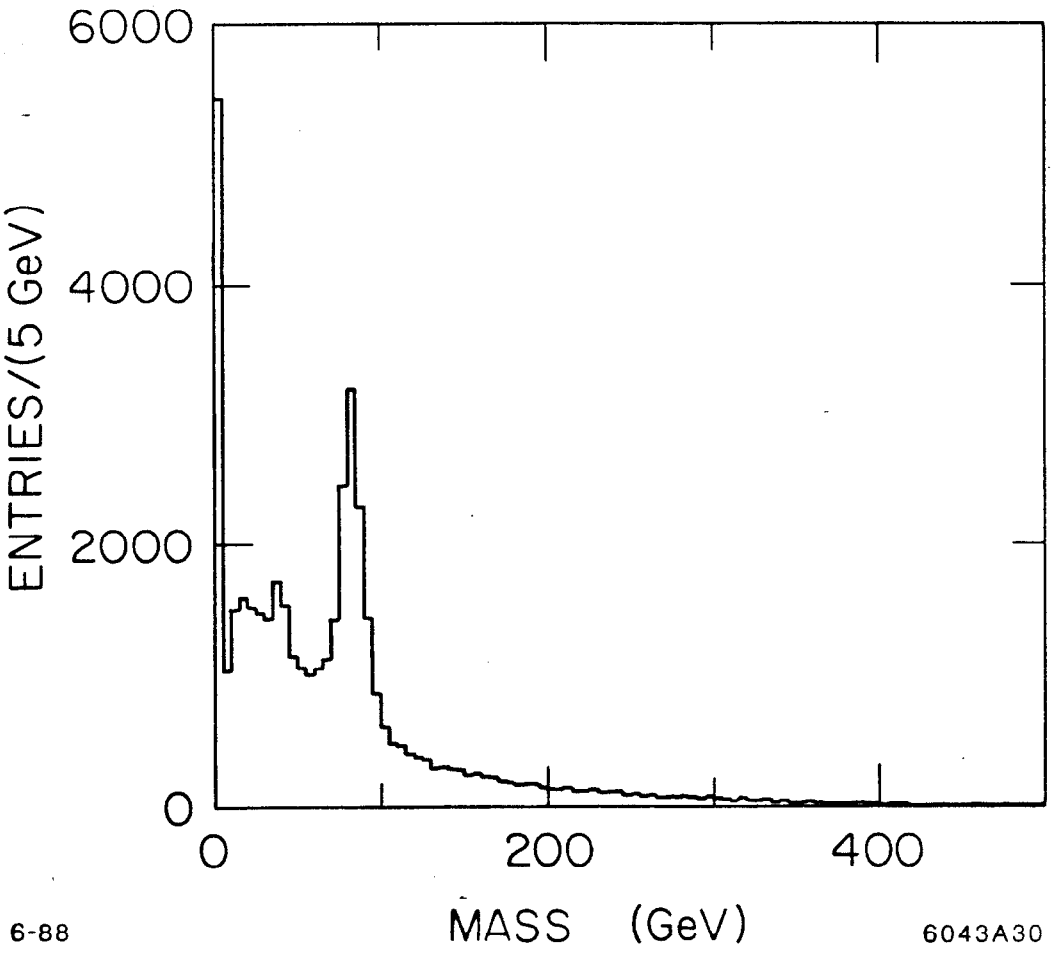

Figure 29. Distribution of jet masses for the full sample of events with e^+e^- annihilation to $q\bar{q}$, W^+W^-, and Z^0Z^0, corresponding to 10 fb^{-1} of data. The jet masses are defined as in Fig. 21.

in their hadronic decay modes. In hadron colliders, as is well known, it is difficult to identify W and Z bosons through their hadronic decays because of the large background from quark and gluon hard scattering. This has been shown already in the direct analysis of CERN collider data.[49] At the SSC, the situation is expected to be even worse: Not only can one not reconstruct W pair events in which both W's decay hadronically, but, for continuum W pair production, even events where one W decays leptonically are swamped by background.[50] (For the specific case

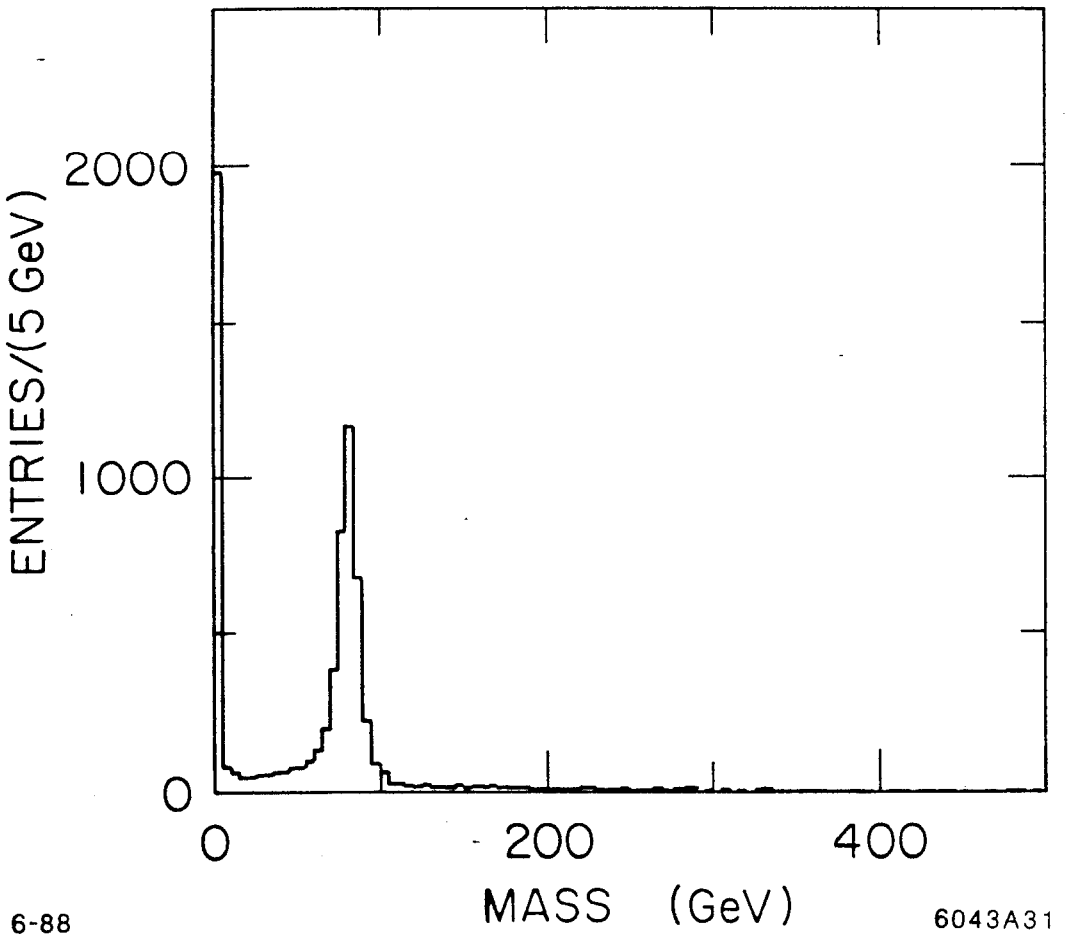

Figure 30. Distribution of jet masses in W^+W^-events for which the opposite jet has a mass between 73 and 93 GeV. The jet masses are defined as in Fig. 21.

of $H^0 \to W^+W^-$, methods have been proposed to overcome this background in the case of one leptonic W decay.[51]) In contrast to this situation, we have found that the identification of weak bosons by jet analysis is completely straightforward at a high-energy e^+e^- collider, even if one takes into account beamstrahlung and detector smearing.

The special character of vector boson jets among the products of general standard model processes is illustrated in Figs. 28 and 29. For the first of these figures,

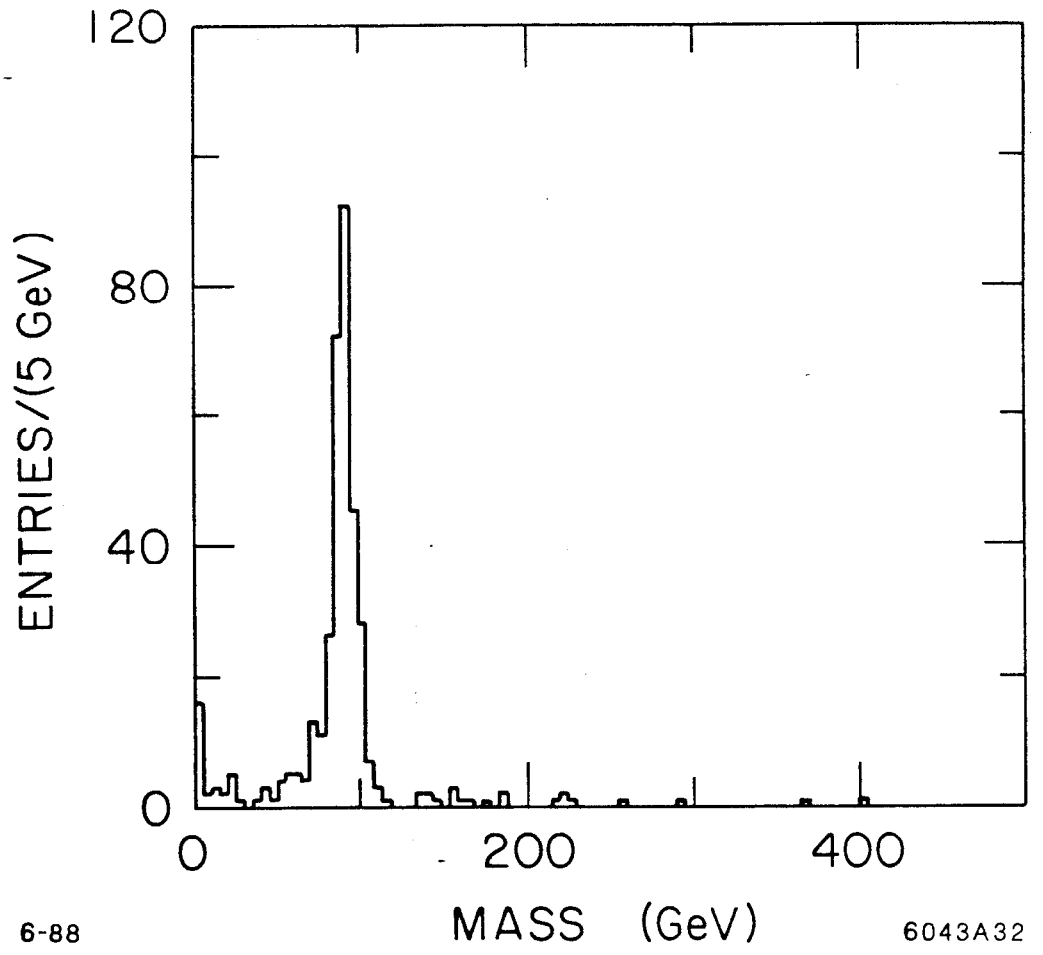

Figure 31. Distribution of jet masses in Z^0Z^0 events for which the opposite jet has a mass between 82 and 102 GeV. The jet masses are defined as in Fig. 21.

all of the events from our background simulations of W, Z, and quark pair production are subjected to the thrust analysis described previously: For all events with mass greater than 200 GeV and thrust direction such that $|\cos\theta_{thr}| < 0.8$, the event is divided into two hemispheres and the invariant mass of each hemisphere is computed. The W stands out on this plot; the Z is lost in the tail of the W only because of its relatively small pair-production cross section. Fig. 29 shows the corresponding analysis for the cluster method of jet identification.

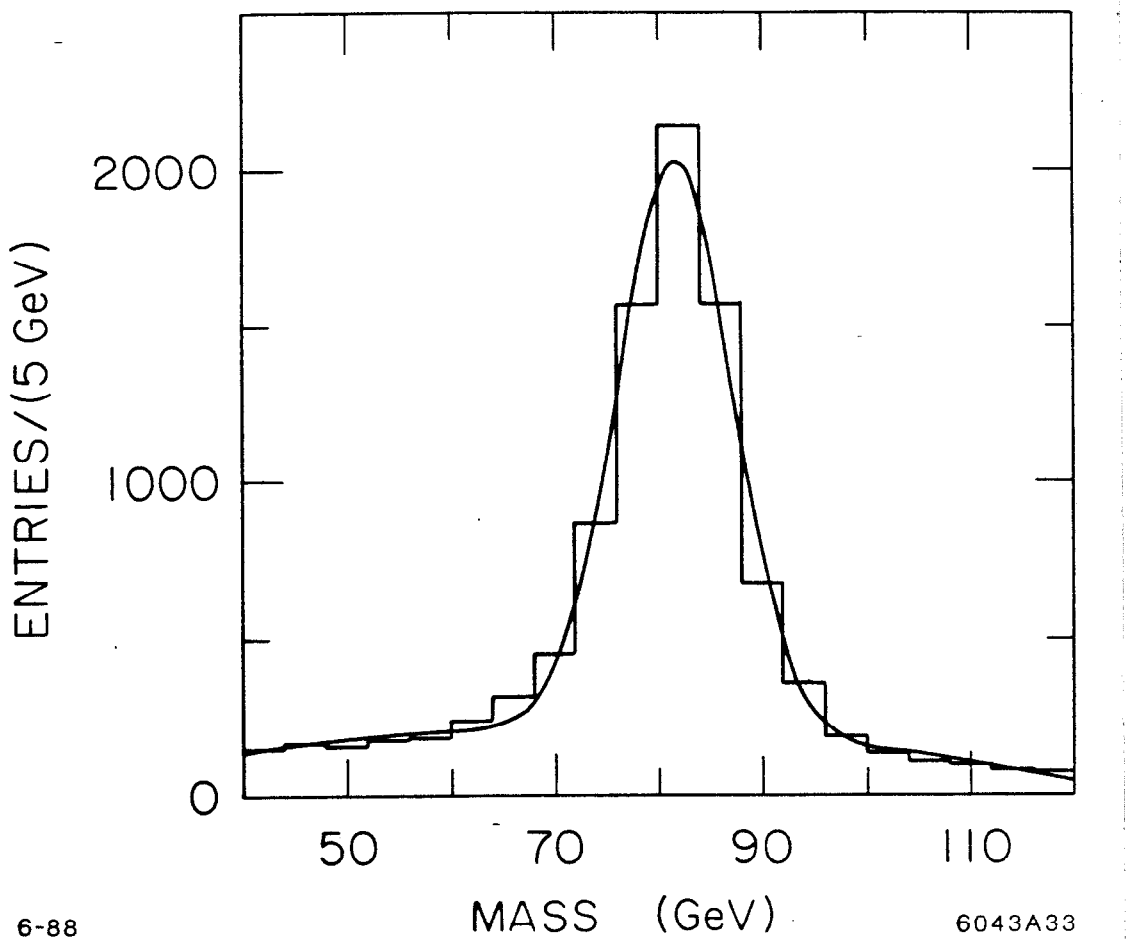

Figure 32. Gaussian fit to the W boson mass peak in Fig. 30.

To complement this analysis, we would like to show how well the weak boson masses are reconstructed by our model detector, in the presence of beamstrahlung and smearing. We can take advantage of one handle to clean up the distributions slightly. Since weak bosons are produced in pairs, the background to W and Z identification will be reduced if one chooses events which are consistent with boson pair production. Fig. 30 shows the mass of one jet in W pair events for which the opposite jet has a mass between 73 and 93 GeV from the cluster analysis. The distribution is only slightly cleaner than that of Fig. 21(b), because decays of the

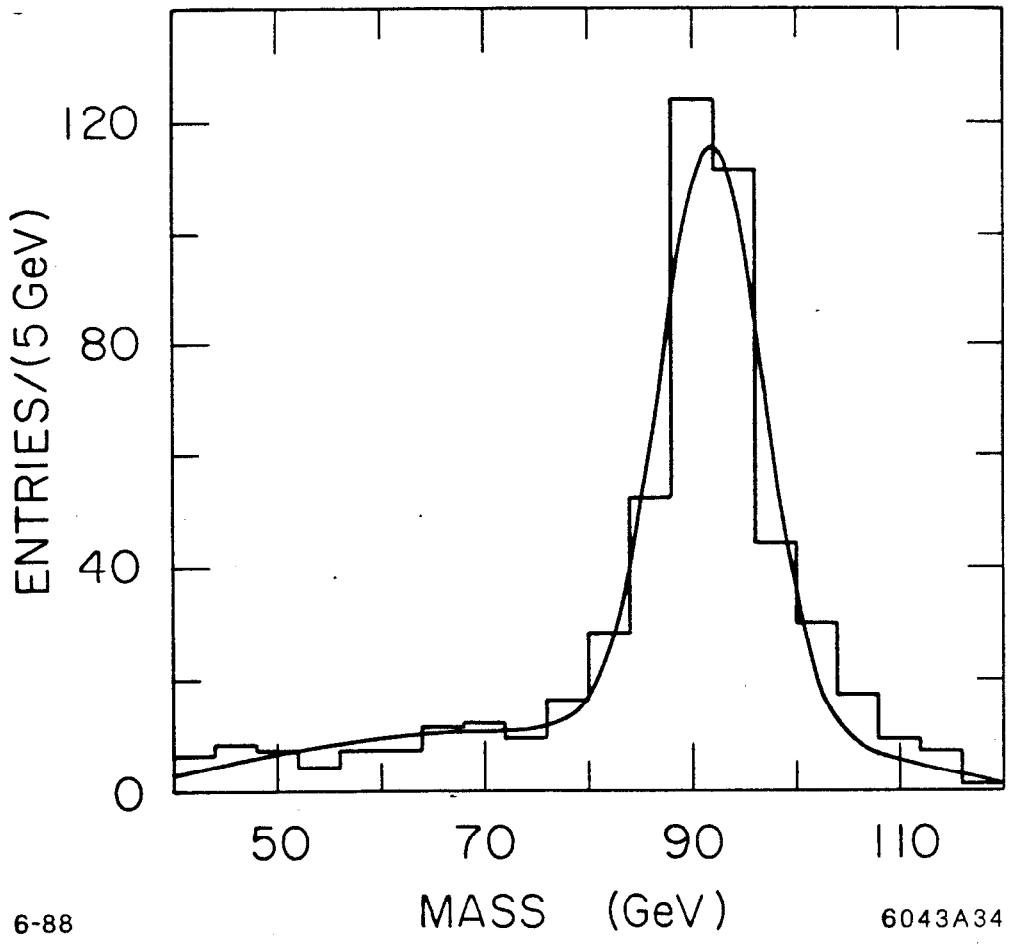

Figure 33. Gaussian fit to the Z^0 boson mass peak in Fig. 31.

W to $\ell\overline{\nu}$ are still included in the plot. Fig. 31 shows the mass of one jet in Z pair events for which the opposite jet has a mass between 82 and 102 GeV. In this case, there is some noticeable improvement over the simple jet analysis, because the events in which one Z^0 decays to neutrinos have been eliminated. In Figs. 32 and 33, we replot these jet mass distributions for W and Z in 4 GeV bins, together with a fit of each histogram to a Gaussian distribution plus a third order polynomial. The fit gives a mean of 81.6 ± 0.2 GeV with a standard deviation of 5.5 GeV for the W peak, and a mean of 91.8 ± 0.5 GeV with a standard deviation of 4.9 GeV for the Z^0 peak. The central values compare favorably with the nominal W and Z mass values used in the simulation, 83 and 93 GeV, respectively.

This analysis gives us confidence that we can use the new collider to study the standard and exotic sources of weak bosons with high efficiency.

4. New Quarks and Leptons

The greatest successes of e^+e^- colliders to date have come in the discovery of new heavy quarks and leptons. We might then expect that, in the higher-energy regime that we consider here, new quarks and leptons also produce dramatic and easily interpreted signatures. In this chapter, we will present methods for detecting new quarks and leptons and show that this is in fact quite easily done. Significant evidence for the existence of a new quark or a new lepton can be obtained with event samples as small as 300 R^{-1}. Once such a particle is identified, a broad program of investigation would be launched: One should determine accurate values for its mass and its weak and electromagnetic couplings and search also for decays involving forces outside the standard model. This extended program is in principle straightforward to carry out at an e^+e^- collider, if larger event samples (of order 10^3 R^{-1}) are available.

In the next section, we will discuss the motivation for expecting new quarks and leptons in the region of masses of a few hundred GeV. The new fermions which may appear could be either members of standard sequential generations or objects with more exotic quantum numbers. For definiteness, though, we have restricted our detailed analysis of signals and backgrounds to the case of sequential generations. We expect that these new fermions will be able to decay weakly by producing an on-shell W boson. The decay rate for a sequential fermion of mass M by real W emission is

$$\Gamma(Q \to Wq) = \frac{\alpha M}{16 \sin^2 \theta_w} \cdot |V_i|^2 \cdot \left(\frac{M}{m_W}\right)^2 \cdot \left(1 + 2\frac{m_W^2}{M^2}\right) \cdot \left(1 - \frac{m_W^2}{M^2}\right)^2 , \quad (4.1)$$

where V_i is a weak mixing angle. Unless V_i is extremely small (less than 10^{-5}), this process completely dominates the decays. The signature of a new fermion, then, is

the appearance of W pairs below the full beam energy, accompanied by additional quark jets or missing neutrinos.

Though we will not present a detailed procedure for characterizing a new quark or lepton, we should note that there is much additional information at hand. First, the new species should be produced with substantial forward-backward and polarization asymmetries. For sequential quarks and leptons, above a narrow threshold region, these asymmetries are just those given in Table 3. Additional information on the spins of the produced fermions can be found from their decay angular distributions: If f is the fraction of right-handed fermions produced into a given solid angle, the distribution of angles χ—measured in the fermion rest frame—between the fermion and W directions of motion is given by

$$\frac{d\Gamma}{d\cos\chi} \sim f(1-\cos\chi) + (1-f)(1+\cos\chi) . \tag{4.2}$$

(Unlike the situation for light fermions, this spin information is not lost in the hadronization process, since the decay time, the inverse of (4.1), is here much smaller than a hadronization time. We should note, however, this same calculation tells us that quarkonium resonances are irrelevant in this energy region, since the large width (4.1) smears them beyond recognition.) Finally, since the W mass peak is well resolved by calorimetry, one can determine directly whether the new fermion has additional decay modes involving other new particles, such as charged Higgs bosons.

4.1. Setting: Multiplets, Mirrors, and Fixed Points

There are many reasons for suspecting that there exist new fermions with masses in the general range of a few hundred GeV. The most basic reason, however, is the considerable latitude given for such heavy species within the standard model. As we noted in the introduction to this report, fermion masses arise from the

fermion-Higgs Yukawa couplings according to

$$m_f = \frac{\lambda_f}{\sqrt{2}} \langle \Phi \rangle \ , \tag{4.3}$$

where $\langle \Phi \rangle$ is the Higgs field expectation value (2.3). The quark which is now the heaviest known, the b, has a coupling $\lambda_b \sim 2 \times 10^{-2}$; a 50 GeV top quark would have $\lambda_t \sim 2 \times 10^{-1}$. We know of no reason why the couplings λ_f cannot be as large as order 1; that being so, we recognize that there is a great deal of room for new heavy quarks and leptons to appear. Such new fermions do indeed appear in a variety of theoretical models, with quantum numbers that depend on the exact structural assumptions made. Let us now review a few of those models.

New heavy quarks are required in some models which explain the hierarchy of fermion masses as being generated by some flavor-changing (horizontal) interactions. In such schemes, one generation of quarks and leptons may be relatively strongly coupled to the Higgs sector, and the Yukawa couplings of the other generations are derived from this one by the corrections which appear in successive orders of the expansion in horizontal interactions. These schemes usually require the new generations to have the standard quantum numbers.

A second class of models focusses on the origin of parity violation in the weak interaction. In the standard model, parity violation is put in from the beginning by the assumption that the coupling of weak bosons to fermions is chiral. Many authors, however, have proposed that the weak interactions have couplings which are intrinsically parity symmetric, but that the fermions with left- and right-handed weak interactions acquire different masses. Two representative schemes are given in Refs. 52 and 53. This structure arises naturally in schemes of grand unification in which the grand unifying group is a large orthogonal group: $O(10)$, $O(14)$, or $O(18)$. In these models, each conventional generation has a 'mirror' with the opposite parity coupling to weak bosons; all of these mirrors must have masses at most of order a few hundred GeV. The mirror fermions can be characterized by the fact that they have different production asymmetries from ordinary fermions[54]

Table 5. Properties of e^+e^- annihilation into fermion pairs with nonstandard weak quantum numbers.

	σ_{tot}	A_{FB}	A_{pol}
Mirror:			
u	2.13	−0.60	0.34
d	1.10	−0.63	0.62
ℓ^-	1.29	−0.47	0.67
Vectorlike:			
D	0.41	0	−0.60
N	0.57	0	0.16
E	1.39	0	0.65

These asymmetries are listed in Table 5. Again, the factor (3.11) has been included in the total cross sections.

A third class of models involves new fermions as relics of higher schemes of grand unification. In such models, the group of grand unification is larger than the minimal $SU(5)$, and thus the basic multiplet contains more states than a simple generation of quarks and leptons. Some of these extra states might also be protected by symmetry from acquiring masses much larger than the weak scale.[55] For example, in models in which the grand unifying group is E_6, the basic fermion multiplet is 27-dimensional and contains an extra charge $(-\frac{1}{3})$ quark and a lepton doublet with vector (rather than V–A) coupling to the W. The total cross sections and asymmetries expected for these species (above their threshold regions) are also presented in Table 5. These fermions are especially likely to survive to the weak scale if an extra neutral weak boson from among the generators of E_6 is also light. This assumption adds dramatic consequences to the physics and so merits a separate discussion. We will describe the physics associated with new Z^0 resonances separately in Chapter 6.

In addition to these specific scenarios which require new heavy fermions, there is a general consideration which leads us to expect new heavy quarks to appear at a specific value of the mass. As Pendleton and Ross[21] and Hill[22] discovered, the renormalization of quark-Higgs Yukawa couplings involve two competing effects which might be expected, for some flavors, to come into balance. The QCD renormalization makes these couplings increase as one descends from very high energies (for example, from the scale of grand unification) to the weak-interaction scale. The renormalization due to Higgs exchange makes the couplings decrease. The balance point is an attractive fixed point. Bagger, Dimopoulos, and Massó[56] have made a systematic study of quark masses within grand unified theories and have shown that this fixed point pulls in all quarks with sufficiently strong Yukawa couplings at the grand unification scale; the criterion would correspond more naively to quark masses of order 80 GeV. These considerations predict that several new generations of quarks may appear with masses very close to this fixed point value:

$$m_U \approx m_D \approx \frac{2\sqrt{2}}{3} g_s^2 \langle \Phi \rangle \cdot \frac{1}{\sqrt{N_H}} \sim \frac{300 \text{ GeV}}{\sqrt{N_H}} , \tag{4.4}$$

corresponding to a mass in the range 150–200 GeV, depending on the number of heavy flavors.

Finally, we should recall one consideration which provides a guide to how large fermion masses may be. Chanowitz, Furman, and Hinchliffe[19] have shown that the the leading-order diagrams for quark-quark scattering grow large as the quark mass (and, thus, the quark-Higgs coupling) is made large, and that these diagrams violate unitarity when the quark mass approaches

$$m_Q = \frac{4\sqrt{2}\,\pi}{5G_F} = 550 \text{ GeV} . \tag{4.5}$$

This sets the mass scale at which quarks become strongly coupled to the Higgs sector. It is not excluded that quarks and leptons might be heavier than this value, but in that case their behavior would be modified by these new strong

interactions, so that the dynamics of these quarks would resemble a theory of strongly interacting Higgs bosons rather than the simple picture that we are using here. As the masses of these quarks approach 1 TeV, such models go over smoothly into technicolor models of the Higgs sector.

4.2. Identification of a New Quark

Let us now descend from these theoretical considerations and concentrate on the simplest cases of new sequential quarks and leptons. We would like to present data analysis methods for finding these objects at an e^+e^- collider and to estimate the size of the event samples required. We will show that the new fermions can be isolated with analysis techniques which are simple and efficient. Applied to the 30 fb^{-1} data samples that we eventually envision for a working collider, these techniques would give large samples of tagged events which could be used to work out the detailed couplings of the new species.

Let us begin by considering the case of a single new quark, a b', which decays to a light quark plus a W boson, and the case of a new weak doublet (t', b'). We will report results for the relatively low masses $m_b = 150$ GeV, $m_t = 200$ GeV. This should be considered as a worst case among possible new quark searches, since the signatures of the b' and t' become more distinctive as the mass is raised. Our numerical results reflect a Monte Carlo-generated event sample corresponding to 30 fb^{-1} at $E_{\text{CM}} = 1$ TeV.

One can imagine two possible ways of detecting the reaction $b' \to W^- + q$. First, one might concentrate on events in which the W bosons decay hadronically and look for the large mass of the state in each hemisphere. This signature leads to a very simple analysis, with high efficiency for accepting b' events and therefore high statistics. One might worry that the method entails a large background arising from light quark pair production with hard gluon emission, and that this background would be difficult to estimate precisely. However, this concern can be dealt with by tagging the W bosons from the quark decay. A second method is to

concentrate on events in which one W decays leptonically. This method is much less efficient but leads to a completely clean signal.

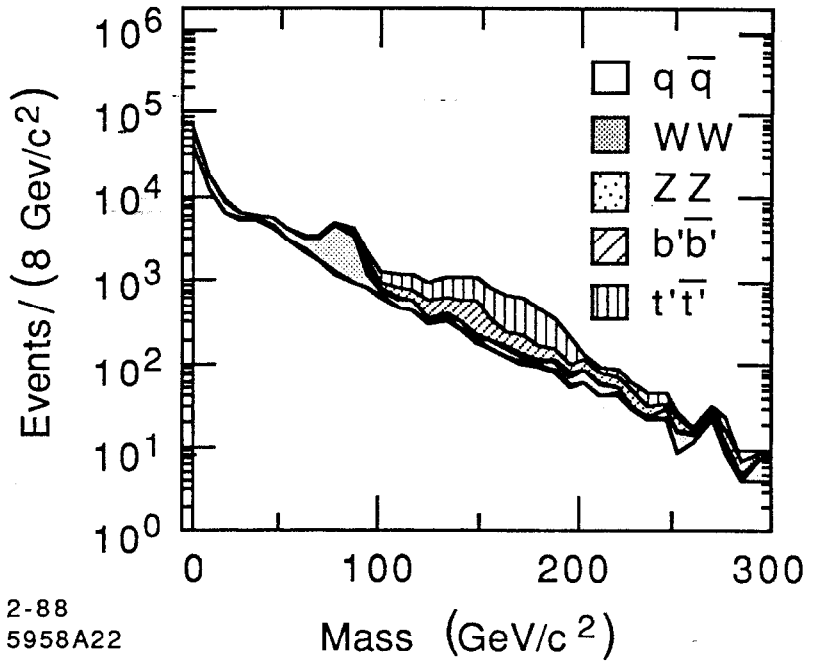

Figure 34. Smaller of the two values of the reconstructed mass in a hemisphere for b' and t' pair production, and for the major background processes.

For both of these analyses, some preliminary selection of events is required to reduce the large sample of peripheral reactions and forward W pair production. We thus begin by boosting each event along the e^+e^- collision axis to set the total measured longitudinal momentum to zero, and then placing a cut that the boosted thrust axis should have $|\cos\theta| < 0.8$. We have seen in the previous chapter that this procedure removes the large forward peak in W and Z pair production, reducing the large total cross section (20 units of R) to a manageable 3 units of R. It is also effective in removing highly radiative, and thus poorly measured, light quark pair events.

From this sample, one can straightforwardly divide each event into two hemi-

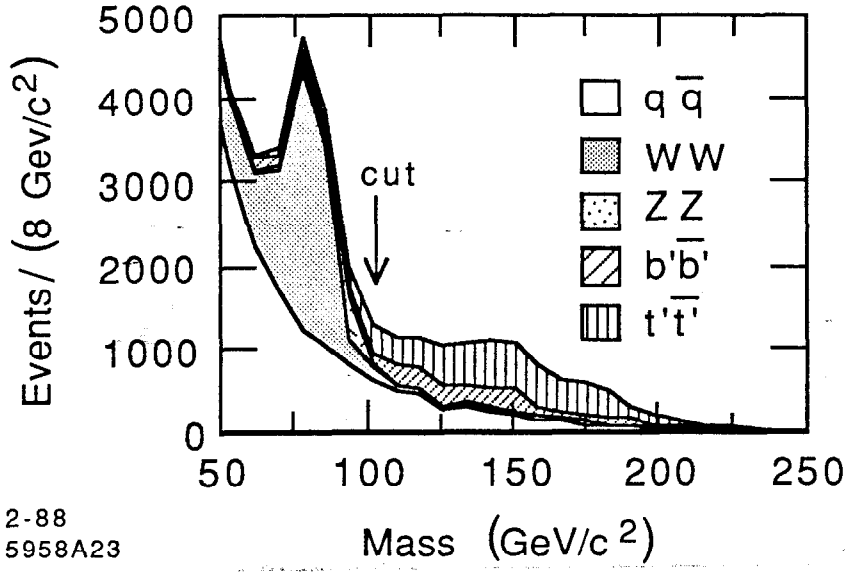

Figure 35. Distribution of smaller hemisphere masses from Fig. 34, plotted on a linear scale.

spheres normal to the thrust axis and compute the mass determined by calorimetry from each hemisphere. In Figs. 34 and 35, we plot the distribution of the smaller of the two mass values. As we saw in Fig. 28, the W and Z mass peaks are readily evident in this distribution, and beyond this point the standard model background cuts off sharply. At large values of the mass, the dominant background comes from light quark pair production events in which the quarks radiate two gluons. We should assign some model-dependent uncertainty to this continuum. The figure shows, however, that the b' quark appears as a distinct, though rounded, peak on this background.

To cleanly separate signal from background, we insist that the high-mass hadronic systems we have found contain W bosons. It suffices to reconstruct one W boson from jets identified in the calorimeter. We subjected the event sample of the previous paragraph to a cluster analysis, as decribed in eq. (3.15), to form clusters with a minimum separation of $y = (18\ \mathrm{GeV})^2$. We then required the presence of at least 5 clusters, with at least 2 in each hemisphere. Finally, we required

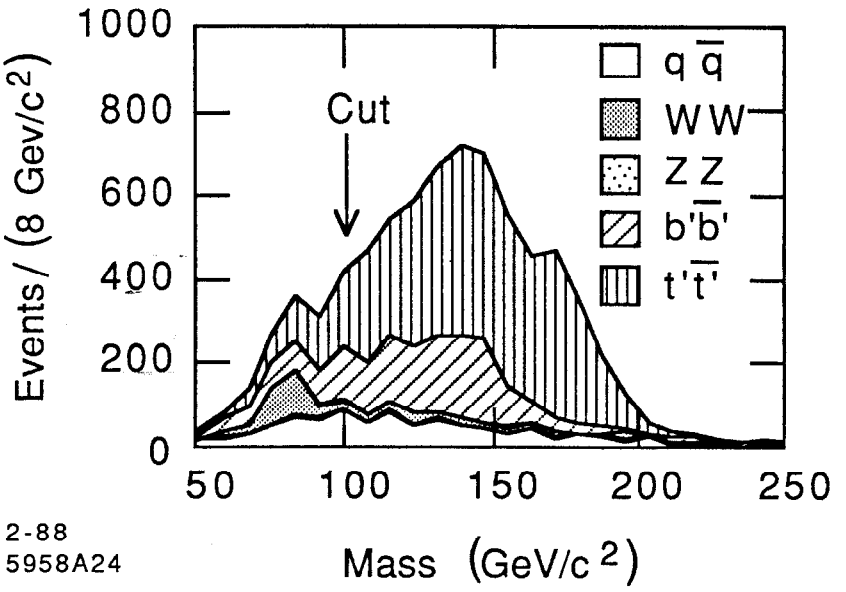

Figure 36. Smaller of the two values of the reconstructed mass in a hemisphere for b' and t' pair production, and for the major background processes, for events in which a W boson can be identified in one hemisphere.

that the event contain one hemisphere with at least 3 clusters in which 2 of these clusters sum to a mass between 72 and 92 GeV. The events passing these cuts are plotted in Fig. 36 as a function of the smaller reconstructed invariant mass for a hemisphere. Both the b' and the t' stand out cleanly from the background.

The results of this analysis are shown in numerical form in Table 6. The events tabulated are those which passed the cuts defined in the previous paragraph, with the additional cut that the minimum hemisphere mass plotted in Fig. 36 be greater than 104 GeV. What is most impressive about this plot is not the large ratio of signal to background but the efficiency with which the interesting events are selected. About a third of the $b'\bar{b}'$ events, and almost half of the total number of heavy quark events, are preserved in the analysis. Thus, this simple procedure supplies a substantial sample of tagged heavy quark events for more detailed investigations.

The second search method we had listed above was to search for isolated leptons

Table 6. Results of heavy quark search using cluster analysis.

	Events	Overall Efficiency	Signal / Background
Background:			
$q\bar{q}$	603	0.005	
W^+W^-	233	0.002	
Z^0Z^0	9	0.0015	
Total:	845		
Signals:			
$b'\bar{b}'$	1289	0.33	1.5
$b'\bar{b}' + t'\bar{t}'$	5291	0.46	6.3

Table 7. Results of heavy quark search using isolated leptons.

	Events	Overall Efficiency	Signal / Background
Background:			
$q\bar{q}$	8.2	7×10^{-5}	
W^+W^-	2.4	2×10^{-2}	
Z^0Z^0	0.5	8×10^{-5}	
Total:	11.1		
Signals:			
$b'\bar{b}'$	70	0.018	6.3
$b'\bar{b} + t'\bar{t}'$	286	0.025	19.5

resulting from heavy quark decay. To apply this analysis, we return to the sample of events which passed the preliminary selection criteria described above, and apply the further condition that the minimum invariant mass in a hemisphere is greater than 104 GeV. We then place cuts to pick out an isolated muon or electron. To do this, we define a cone around the lepton which should be essentially free of deposited energy. To suppress background events which result from W pair events in which one W decays leptonically, we set both a maximum and a minimum size for this cone, and also limit the momentum range of the lepton. The precise form of the optimized cuts is as follows: We insist that 5 GeV $< p_\ell <$ 100 GeV. We then parametrize the isolation of the lepton by an angle ϑ_{is}, the half-angle of the cone about the lepton which encloses 1 GeV of energy deposition. Events with semileptonic b' decays produce leptons with ϑ_{is} in the range 20–40°. If we now accept only those events with an identified lepton in the correct momentum range for which $15° < \vartheta_{is} < 45°$, we find the contributions from signal and background shown in Table 7. The efficiency of the procedure is unfortunately quite low, but the technique entails essentially no background. An event sample 5 times smaller (6 fb^{-1}) would still contain the b' signal as a 3 σ effect; the t' signal would be be a 3 σ effect even with 1.5 fb^{-1}.

Both of the analysis methods we described are completely insensitive to beamstrahlung and the limited angular acceptance of the detector. In part, this is the result of the fact that we cut out from the beginning events with the new quarks produced in the forward direction because the W pair backgrounds are large there. However, some of this insensitivity is due to the fact that we concentrate on kinematic variables which are independent of frame.

4.3. Identification of a New Lepton

We now turn to the problem of identifying a new charged lepton. As in the previous section, we will concentrate on the simplest case: A single new charged sequential lepton, decaying to a W boson and a neutrino. We will ignore the mass of the neutrino; the analysis remains unchanged if the neutrino is massive as long

as it is much lighter than the W. Once again, the Monte Carlo study we report corresponds to a data sample of 30 fb^{-1} at $E_{\rm CM} = 1$ TeV, and to a new lepton mass of 250 GeV.

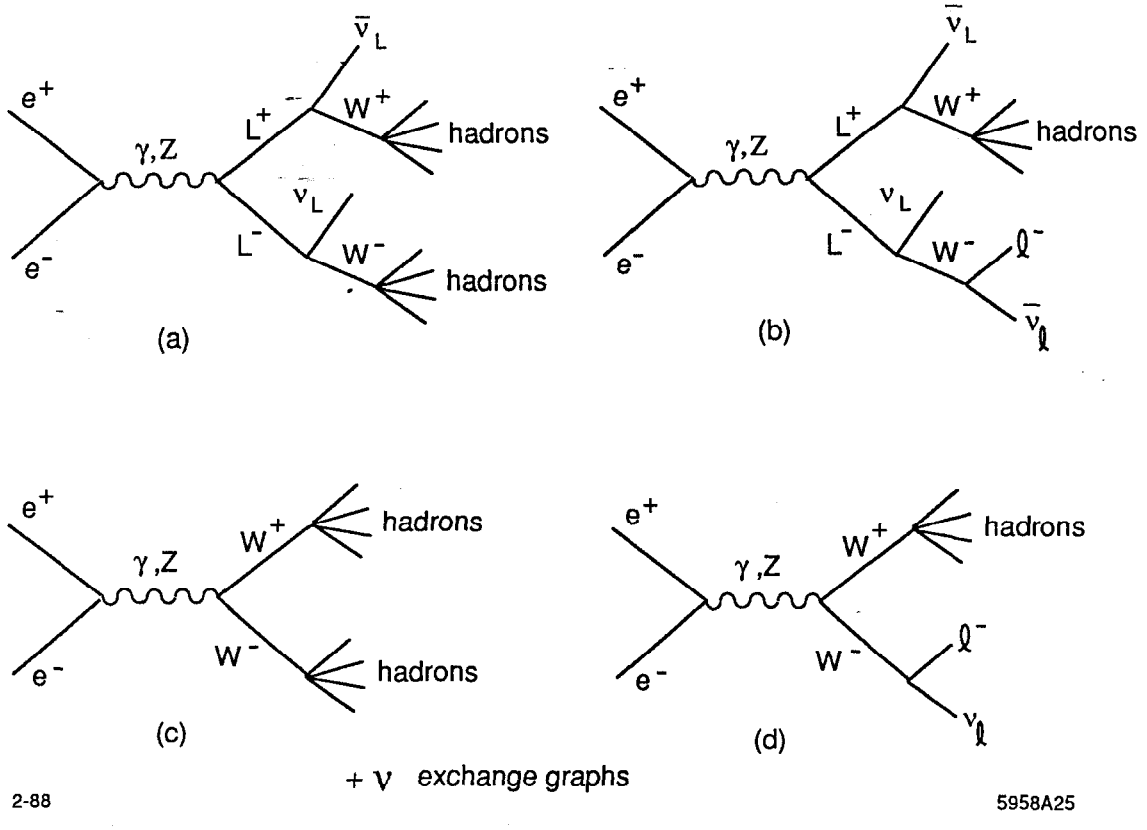

Figure 37. Final states resulting from L^+L^- and from W^+W^- production: In (a) and (c), both W bosons decay hadronically; in (b) and (d), one W boson decays leptonically.

The decays of the new heavy lepton will produce two distinct signatures: First, a charged lepton plus missing energy, second, a hadronic jet plus missing energy (see Fig. 37). Both decay modes have associated backgrounds coming from W pair production. Heavy lepton pair production events in which both leptons decay leptonically will clearly be difficult to isolate from W pair events, since in this case the background also has large missing energy. We will see that the heavy lepton

signal becomes quite clean when one considers decays with hadrons on one side and improves further for events with hadronic decays on both sides. The idea that one should look for heavy leptons through their hadronic decays seems astounding to those of us who have studied particle search analyses for hadron colliders. For us, this is an excellent illustration of how the simplicity of e^+e^- events aids powerfully in searching for new physics.

We consider first the case in which one heavy lepton decays hadronically and the other decays leptonically. In this case, all of the visible hadrons are produced from a W boson decay and should reconstruct to the W mass. The dominant backgrounds come from W pair events of this same topology, as shown in Fig. 37(d). We cannot discriminate these events on the basis of total energy, because beamstrahlung produces W pair events with large missing energy. However, the missing neutrinos in the heavy lepton decay produce an aplanarity in those events which cannot be mocked up by beamstrahlung. To apply this observation, we make the following cuts: We insist that each event should have a single identified lepton with $p_\perp > 50$ GeV, isolated so that energy less than 1 GeV is deposited in a cone of half-angle 45°about the lepton direction. We insist, further, that the deposited hadronic energy, considered as a single jet, correspond to a measured mass in the range 72 GeV $< m_j <$ 92 GeV. Fig. 38 shows the hadronic mass distribution before the second cut is applied; the W mass peak stands out cleanly. An additional cut must be applied to remove the substantial background from W pair events: We assume that each event corresponds to W pair production and try to reconstruct the missing neutrino according to procedure given in Section 7.2. This procedure usually gives an imaginary value of $p_{\nu z}$ for events which do not fit the W pair hypothesis, and we keep only those events. Now use the lepton momentum vector and the thrust axis of the hadronic system to construct two planes and define an acoplanarity angle. Fig. 39 shows the distribution of this angle due to signal and background. For acoplanarity angles greater than 30°, the W pair background is quite small, while the heavy lepton is still contributing substantially.

If both heavy leptons decay hadronically, the final state contains two well-

separated clusters of hadrons, each of which should reconstruct to a W boson. This allows a much cleaner and more efficient search procedure. Since the hadron calorimetry now captures all decay products of both W bosons, the signature of

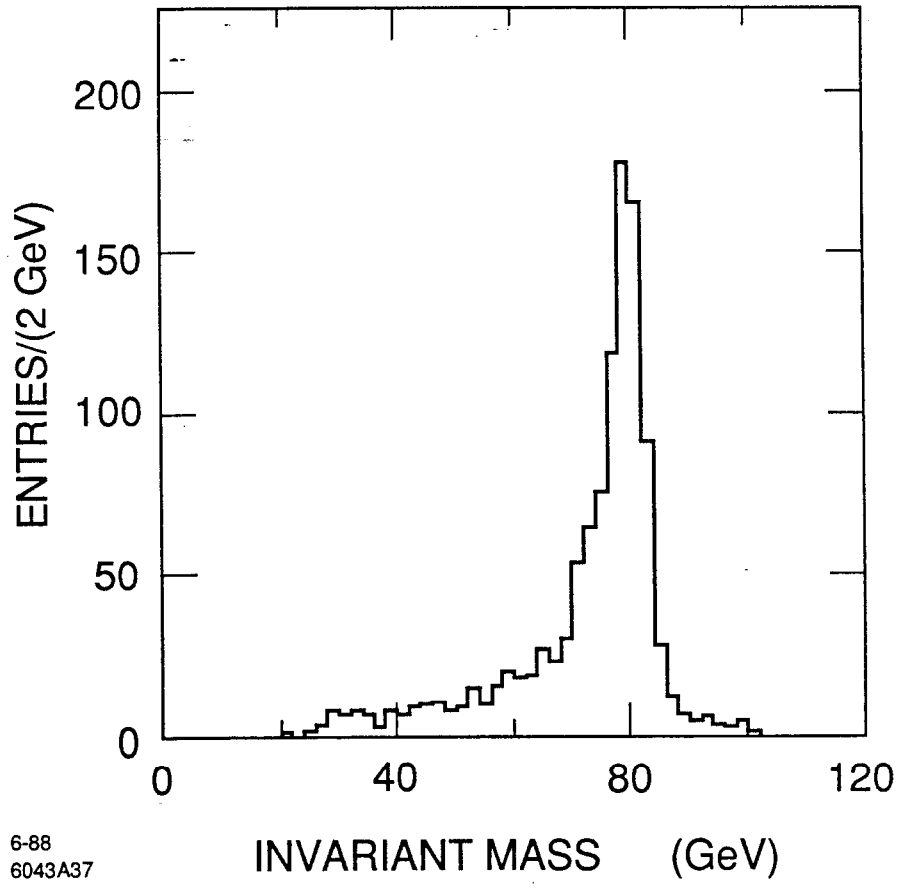

Figure 38. Invariant mass distribution of observed hadrons in L^+L^- events with an isolated lepton.

missing transverse energy clearly distinguishes the lepton pair production events from W pair background. The new lepton signal is most easily isolated by analyzing these events as W pair production and then asking that the W bosons be acoplanar. Specifically, we apply the following cuts: First, boost the event along the thrust axis to balance measured longitudinal momentum, and remove events for which

$|\cos\theta| < 0.8$. Then divide the event into 2 hemispheres normal to the thrust axis and require the measured mass of hadrons in each hemisphere to be in the range 72 GeV $< m <$ 92 GeV. As we saw in our discussion of W pair production, the

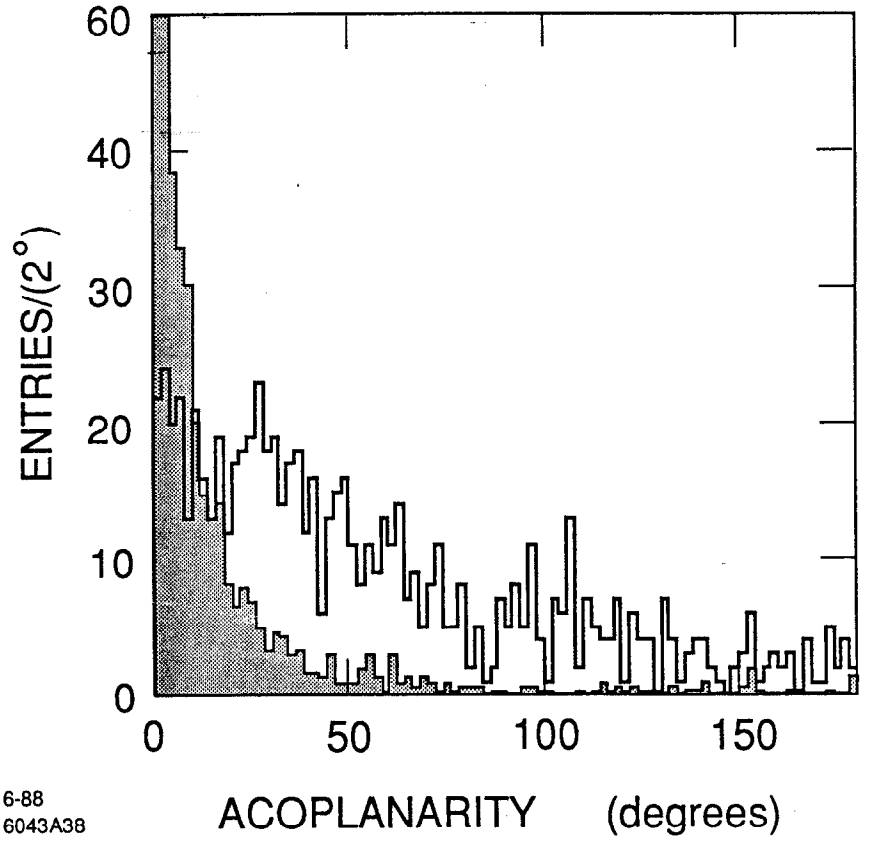

Figure 39. Distribution of acoplanarity angle between the lepton and the hadronic thrust axis, for L^+L^- events (unshaded histogram) and W^+W^- events (shaded histogram) with one hadronic and one leptonic W decay.

W bosons form a prominent feature on the jet mass distribution and are readily isolated. Once we have selected events with both hadronic jets reconstructing to W bosons, we can recompute the thrust axis in each hemisphere and use these two vectors to define two planes and an acoplanarity angle. The distribution of this

angle, for the signal and for the standard model background processes included in our Monte Carlo simulation, is shown in Fig. 40. The W pair background is essentially absent for acoplanarity angles greater than 10°. Additional background

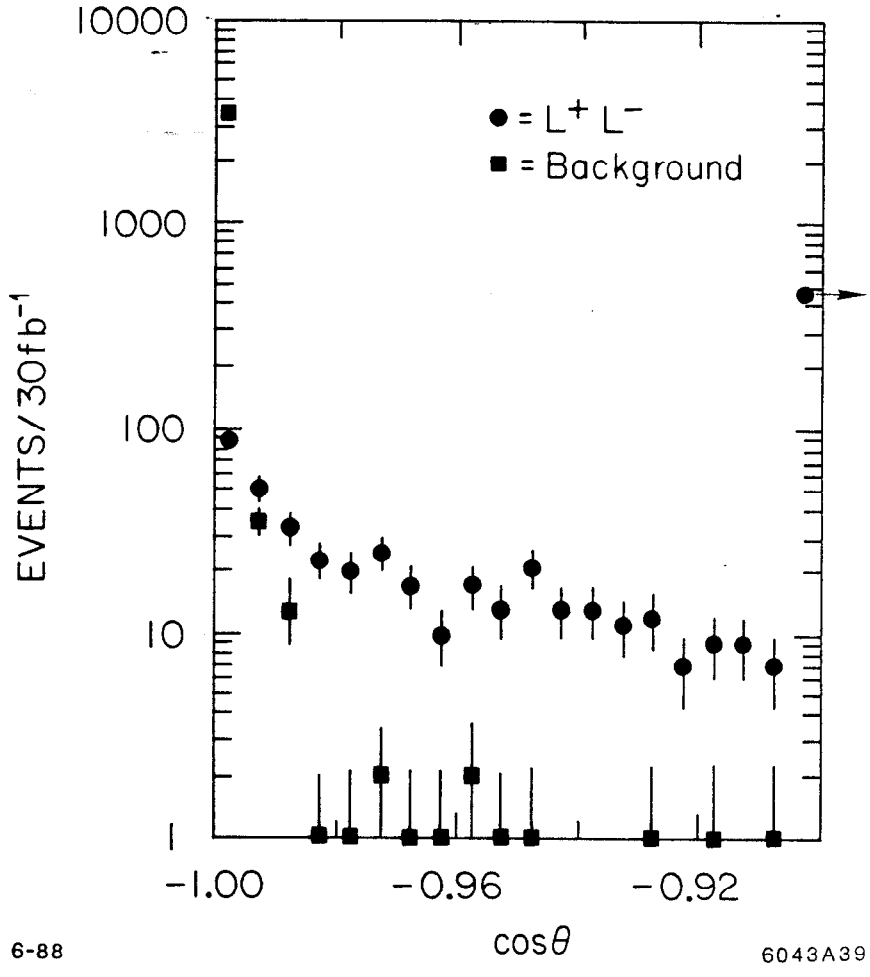

Figure 40. Distribution of acoplanarity angle between the thrust axes in the two hemispheres, for L^+L^- W^+W^- events in which both W bosons decay hadronically.

processes beyond those discussed in Chapter 3 come from $e^+e^- \rightarrow W^+W^-\nu\overline{\nu}$, $e^+e^- \rightarrow W^+W^-Z^0$, and vector boson pair production in two-photon reactions. We have ignored the two-photon processes because they peak at such low mass.

The acoplanarity distribution due to $e^+e^- \rightarrow W^+W^-Z^0$, with the Z^0 decaying to neutrinos, is shown in Fig. 41. It also gives a very small contribution. The W fusion process, which we take from the calculations of Gunion and Tofighi-Niaki,[57]

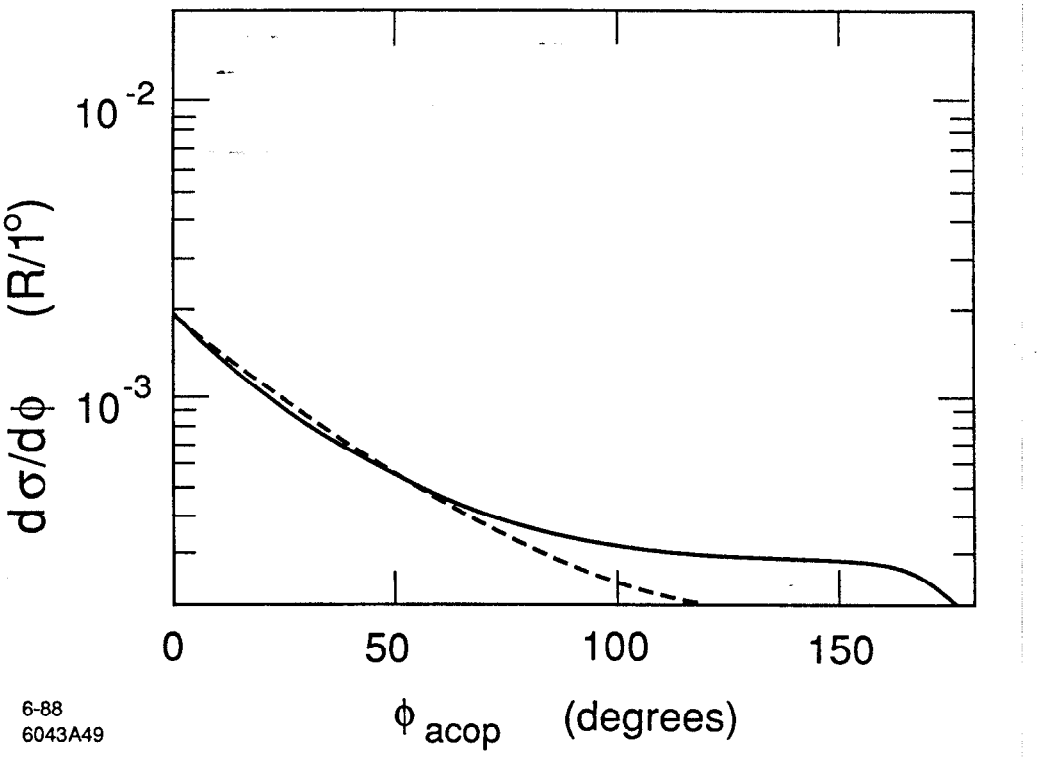

Figure 41. Distribution of acoplanarity angle between the two W bosons in the process $e^+e^- \rightarrow W^+W^-Z^0$, with the Z^0 decaying to neutrinos. The results are given in units of R per degree and include the branching ratio for the Z^0 decay to unobserved states. The two curves assume two values of the Higgs boson mass: 100 GeV (dashed) and 300 GeV (solid).

gives the largest of these contributions. But even this is quite small compared to the effect of the heavy lepton. In Fig. 42, we plot the final W^+W^- mass spectrum resulting from our analysis, and the corresponding spectrum due to the $e^+e^- \rightarrow W^+W^-\nu\bar{\nu}$.

To estimate the event sample needed to discover a heavy lepton, we should

Table 8. Results of heavy lepton search using hadronic decays.

	Events	Overall Efficiency	Signal / Background
Background:			
$q\bar{q}$	2	2×10^{-5}	
W^+W^-	13	13×10^{-5}	
Z^0Z^0	1	16×10^{-5}	
$W^+W^-\nu\bar{\nu}$	41	0.11	
Total:	57		
Signals:			
L^+L^-	680	0.11	11.9

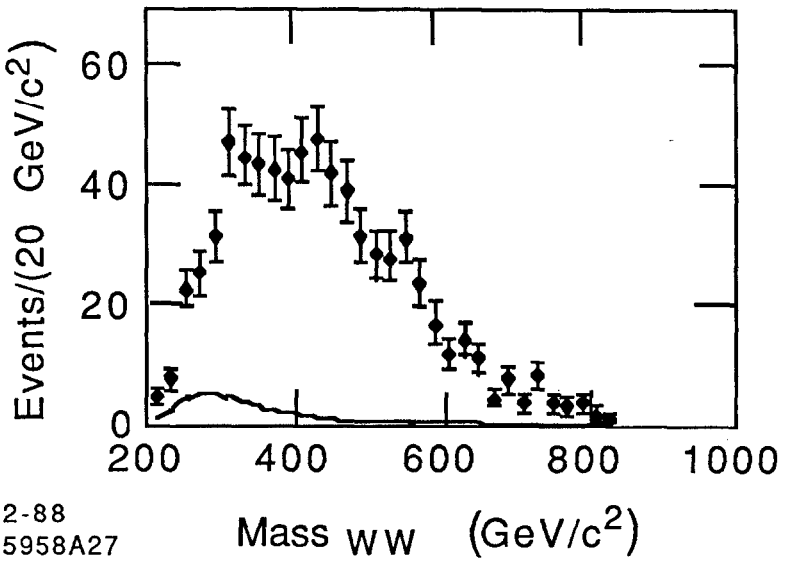

Figure 42. Final invariant mass spectrum of observed W pairs from L^+L^- production. The solid curve shows the background contribution from $e^+e^- \rightarrow W^+W^-\nu\bar{\nu}$.

recount the statistics of the analysis represented by Fig. 42. Let us, then, apply the cuts described in the previous paragraph plus the requirement that the acoplanarity angle be greater than 10°. This cut is very efficient for lepton pair events but

admits only 0.3% of the remaining W pair events. The contributions of signal and background are listed in Table 8. The final ratio of signal to background is outstanding; the signal would be apparent in any measureable sample of heavy lepton pair events, even in data samples as small as 1 fb^{-1}.

5. Higgs Boson Searches

The next proposed particle that we will discuss—the Higgs boson—stands much closer to the core of the standard model. In the standard theory of weak interactions, the masses of all quarks, leptons, and gauge bosons are supplied by spontaneous symmetry breaking. Nothing is known experimentally about the mechanism of this symmetry-breaking, beyond the size of the symmetry-breaking condensate given in eq. (2.3). We know of no sensible models, however, in which this symmetry-breaking arises from the dynamics of known particles. Some new particle or new sector—the Higgs sector—is required.

We have already discussed in Chapter 2 the variety of possible models of this new sector. Some involve a new set of strong interactions at some scale in the TeV region; others involve numerous new particles interconnected by couplings of a fairly arbitrary form. There is, however, a uniquely simple model of the Higgs sector which gives precise predictions for its experimental properties. This is the model in which the Higgs sector is represented by a single elementary weak-doublet scalar field, with a renormalizable self-coupling:

$$\mathcal{L} \;=\; D_\mu \phi^\dagger D^\mu \phi \;+ \mu^2 \phi^\dagger \phi \;-\; \frac{\lambda}{2} (\phi^\dagger \phi)^2 \;, \tag{5.1}$$

where D_μ is the covariant derivative which gives the coupling to weak gauge bosons. At the leading order of perturbation theory in λ, the field ϕ acquires a vacuum expectation value:

$$\langle \phi \rangle \;=\; \frac{1}{\sqrt{2}} \begin{pmatrix} 0 \\ \langle \Phi \rangle \end{pmatrix} \;, \tag{5.2}$$

in the notation of eqs. (2.1)–(2.3), producing masses in accordance with the formulae listed there. Three of the four real scalar components of ϕ are absorbed

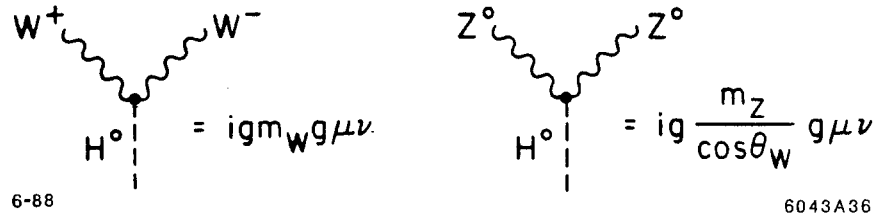

Figure 43. Vertices coupling H^0 to the W and Z bosons.

as longitudinal components of the W^+, W^- and Z^0 bosons, and only one neutral scalar field is left over as an independent physical state. We will refer to this neutral particle as the Higgs boson H^0. More complicated models of the Higgs sector include additional particles with their own signatures. However, all of these models either include some particle with approximately the same couplings as the H^0 or contain strong interactions at TeV energies such as the H^0 would induce if it were very heavy.

The ϕ self-coupling λ is completely unknown. Since this coupling determines the Higgs boson mass through eq. (2.1), this mass is also not known a priori. A rough upper bound is set by the fact that the Higgs sector becomes strongly interacting when $m_{\rm H} \sim 1$ TeV.[32] This gives a considerable territory to be explored.

To date, all searches for the H^0 have been negative. But this is not very surprising: The couplings of the Higgs boson to quarks and leptons are proportional to the quark and lepton masses, according to (2.4). This means that the Higgs boson is very difficult to produce if one starts from light quarks or leptons, the conventional forms of matter. This logic would lead us to expect, on the other hand, that heavy vector bosons should readily produce Higgs bosons. In fact, (5.1) contains the vertices shown in Fig. 43, which represent large couplings of the H^0 to the W and Z bosons. We have already seen that high-energy e^+e^- colliders produce vector bosons copiously; we should, then, expect that e^+e^- reactions are also rich sources of Higgs bosons. We will see, in fact, that a high-energy e^+e^- collider can explore for the H^0 effectively through most of its kinematic range.

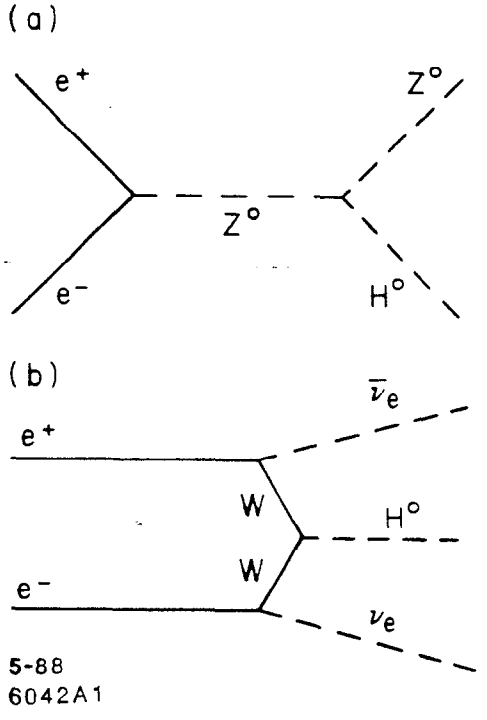

Figure 44. Feynman diagrams for Higgs production at a high energy e^+e^- collider.

The dominant production mechanisms for a neutral Higgs boson at a high-energy e^+e^- collider are the reactions $e^+e^- \to Z^0H^0$ and $e^+e^- \to \nu_e\overline{\nu}_eH^0$. The Feynman diagrams for these processes are shown again in Fig. 44. For e^+e^- center of mass energies $\sqrt{s}$ which are large compared to the particle masses involved, the cross section[32,58] for $e^+e^- \to Z^0H^0$ decreases as s^{-1} while the cross section[59] for $e^+e^- \to \nu_e\overline{\nu}_eH^0$ increases logarithmically with s. Numerical evaluations of these cross sections, for a range of Higgs masses, at $\sqrt{s} = 1$ TeV are given in Table 9. Cross sections for standard model background processes are supplied for comparison. Table 9 also shows the effect of beamstrahlung on these cross sections. The cross section for $e^+e^- \to \nu_e\overline{\nu}_eH^0$ is larger than that for $e^+e^- \to Z^0H^0$ by a factor of about 17 for a Higgs mass of 100 GeV and by a factor of about four for a Higgs mass of 500 GeV.

Because of the larger cross sections for $e^+e^- \to \nu_e\overline{\nu}_eH^0$, we find that, for most Higgs masses, this channel gives the largest signal with the highest signal-

Table 9. Higgs boson cross sections at an e^+e^- center of mass energy of 1 TeV, with and without the effects of beamstrahlung.

Process		Cross Section (fb) *Without Beamstrahlung*	Cross Section (fb) *With Beamstrahlung*
	$m_H = 100$ GeV	12.4	35
	$m_H = 150$ GeV	12.0	25
	$m_H = 300$ GeV	9.8	13
	$m_H = 500$ GeV	5.6	4
$e^+e^- \rightarrow Z^\circ H^\circ$	$m_H = 50$ GeV	12.7	43
	$m_H = 100$ GeV	216	163
	$m_H = 150$ GeV	147	124
	$m_H = 300$ GeV	70	53
	$m_H = 500$ GeV	23	13
$e^+e^- \rightarrow \nu_e\overline{\nu}_e H^\circ$	$m_H = 50$ GeV	234	196
$e^+e^- \rightarrow W^+W^-$		2310	3570
$e^+e^- \rightarrow Z^\circ Z^\circ$		127	200
$e^+e^- \rightarrow q\overline{q}$		127	200
$e^+e^- \rightarrow e^+\nu_e W^-$		9440	8770

to-background ratio. The one exception is a Higgs with mass near that of the $W^\pm$ or the Z^0. Backgrounds created by the processes $e^+e^- \rightarrow e^+\nu_e W^-$ and $e^+e^- \rightarrow \nu_e\overline{\nu}_e Z^0$ (shown in Fig. 45(b)) are kinematically similar to $e^+e^- \rightarrow \nu_e\overline{\nu}_e H^0$ and will dominate the signal unless advantage can be taken of the decay properties of the Higgs. Although backgrounds to $e^+e^- \rightarrow Z^0H^0$ from $e^+e^- \rightarrow W^+W^-$ and $e^+e^- \rightarrow Z^0Z^0$, shown in Fig. 45(a), will also be large in this mass region, this production mechanism should offer a cleaner signature than the $e^+e^- \rightarrow \nu_e\overline{\nu}_e H^0$ process, albeit with a smaller cross section.

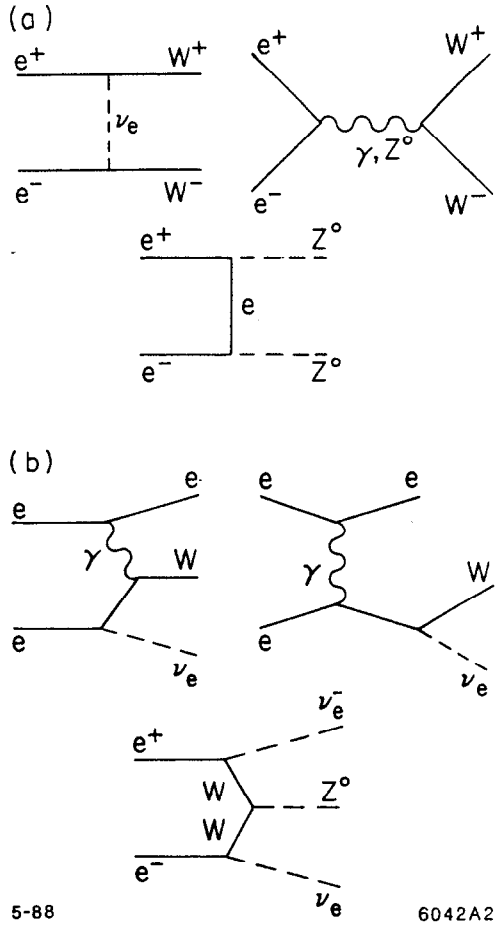

Figure 45. Feynman diagrams for background processes that appear in searches for Higgs production at a high energy e^+e^- collider: (a) annihilation processes, (b) γ and W bremmstrahlung processes.

Our analysis divides naturally into two segments, according to the mass of the Higgs: We distinguish the cases of a heavy Higgs ($m_H \gtrsim 2m_W$), from the so-called intermediate-mass Higgs ($m_H \lesssim 2m_W$). After presenting these two analyses, we comment on methods that may be used to enhance the effectiveness of searches for Higgs particles with masses near those of the W and Z^0.

5.1. Heavy Higgs Particles

If the mass of the Higgs exceeds twice the W mass, then the process $e^+e^- \to \nu_e\overline{\nu}_e H^0$ will be the most favorable source for its discovery. With our assumption that the top quark mass is less than the mass of the W, the Higgs will decay essentially 100% of the time to W^+W^- and Z^0Z^0. We note that if the mass of the top quark is larger than m_W, then the decay $t \to Wb$ will proceed immediately, and the W will carry most of the momentum of the top quark; thus, the alternative decay $H^0 \to t\bar{t}$ will look very similar to the direct decay of the Higgs to W-pairs.

The signature of the Higgs is a final state of two W bosons which are typically not coplanar due to the transverse momentum generated by the W boson propagators present in the production mechanism. We define acoplanarity as the angle between the two planes that each contain the beam axis and one jet axis. Acoplanarity of zero degrees implies that the two jet axes are pointing in opposite directions in a projection perpendicular to the beam axis. It is very useful to work with momenta in the plane perpendicular to the beam axis in the presence of beamstrahlung, because the beamstrahlung provides a boost for the event along the beam axis but not perpendicular to it. The basic philosophy of our analysis is to search for events in which both W bosons decay to hadrons with little or no energy carried away by neutrinos or other particles that are not observed in the detector. The topology and kinematics of the signal are then used to eliminate backgrounds from QCD and two-photon processes and from $e^+e^- \to W^+W^-$ events in which a neutrino in the decay chain creates a significant acoplanarity angle.

To analyze this method in detail, we simulate events of Higgs production by W fusion and compare them to the backgrounds discussed in Chapter 3, using always the standard detector defined there. The simulation of signal and background includes the effects of beamstrahlung. In all of the analyses described in this chapter, we first boost all smeared four-vectors along the z-axis until the vectorial sum of all the z-components of momenta is zero. A thrust analysis is then performed in

this boosted frame, and the event is rejected if the angle between the thrust axis and the beam, θ_{thr}, does not satisfy the condition $|\cos\theta_{thr}| < 0.8$. This procedure ensures that the event is well contained in the detector and preferentially rejects processes with differential cross sections which are sharply peaked along the beam axis (for example, $e^+e^- \to W^+W^-$, $e^+e^- \to Z^0Z^0$, and $e^+e^- \to q\bar{q}$).

A cluster analysis is performed with the detected particles in which the cluster-finding algorithm is constrained to divide the event into exactly two clusters. The invariant mass and the vectorial sum of the momenta for each cluster is calculated. We then select events in which the acoplanarity of these cluster momenta is greater than 10° and in which the mass of the minimum-mass cluster lies between 66 and 94 GeV and that of the maximum-mass cluster lies between 75 and 110 GeV. We use a W mass of 83 GeV, and the detector simulation indicates that this value should be reconstructed with 13% (FWHM) resolution.

To further reduce backgrounds due to events with large beamstrahlung radiation and/or missing particles, we select events in which the direction of the missing momentum satisfies $|\cos\theta_{miss}| < 0.9$, where θ_{miss} is the angle between the beam axis and the missing momentum in the laboratory frame. We also reject events in which the total visible energy is greater than 600 GeV. This cut removes backgrounds but is extremely efficient for retaining the signal events. The invariant mass of all particles that are detected in events that pass these requirements is calculated and shown in Fig. 46(a) and 46(b) for Higgs masses of 300 and 500 GeV, respectively. The estimated background, shown as a dashed histogram, includes contributions from $e^+e^- \to W^+W^-$ and $q\bar{q}$ and from two-photon processes. All distributions correspond to an integrated luminosity of 30 fb^{-1}. The number of signal events surviving the cuts is 125 for a 300 GeV Higgs and 46 for a 400 GeV Higgs; either would easily be observed above the background. Higgs particles with masses above 500 GeV become more difficult to observe because the production cross section decreases with mass and because the width of the Higgs itself increases as m_H^3.

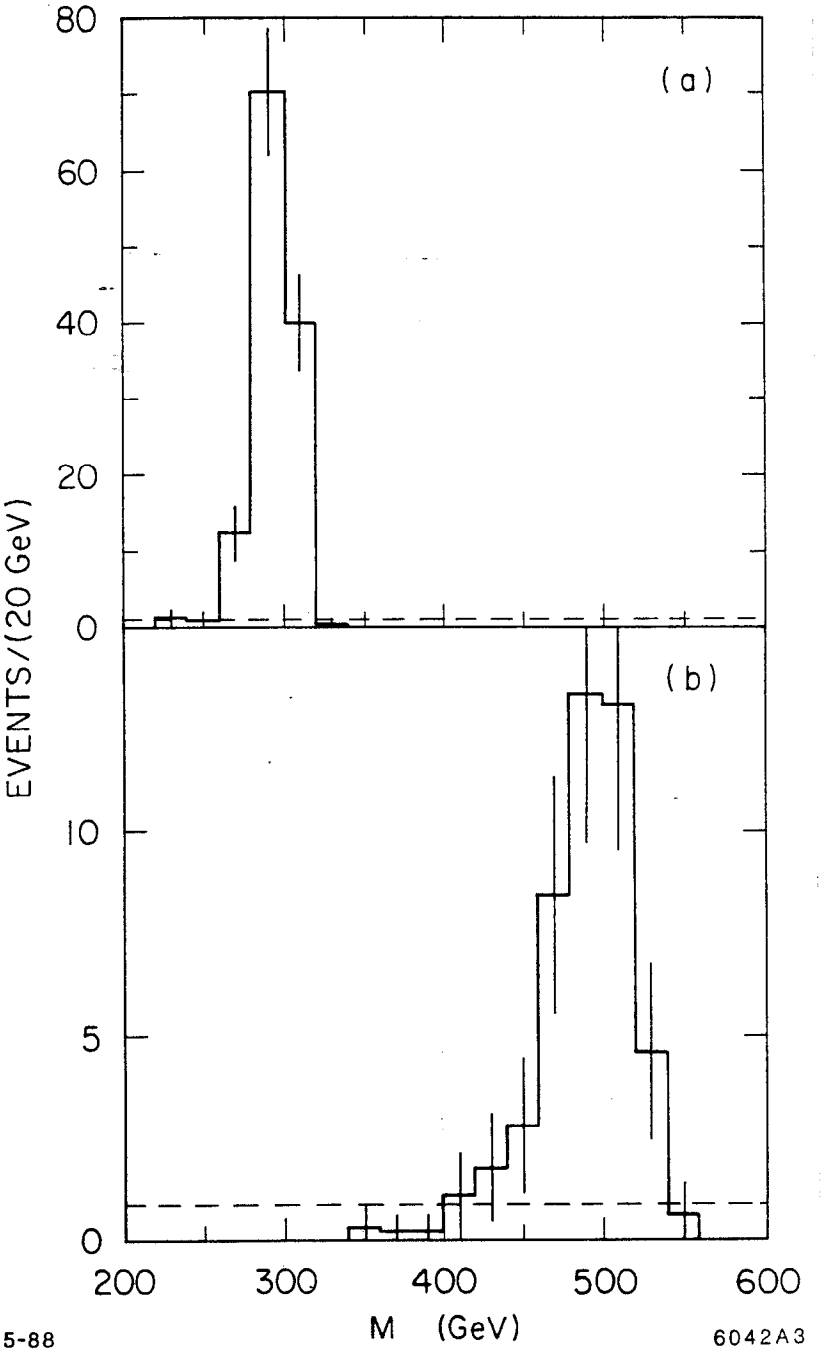

Figure 46. Reconstructed mass distributions, after selection criteria, for (a) a Higgs mass of 300 GeV and (b) a Higgs mass of 500 GeV. The Higgs is produced in the process $e^+e^- \rightarrow \nu_e\overline{\nu}_e H^0$. The dotted line corresponds to the expected background.

5.2. Intermediate Mass Higgs Particles

A Higgs boson with mass less than twice m_W will decay to the most massive quark-antiquark pair that is kinematically allowed. With our assumptions this will be either a top or bottom pair depending on the mass of the Higgs. In either case, the mass of each jet in the decay will be less than a vector boson mass.

The philosophy of our analysis of the $e^+e^- \to \nu_e\overline{\nu}_e H^0$ reaction with $m_H < 2m_W$ is to search for events that contain two acoplanar low-mass jets. Again, we test this method by simulation of signal and background using the standard conditions of Chapter 3. Some of the selection criteria are very similar to the heavy Higgs analysis. We select events in which $|\cos\theta_{thr}| < 0.7$ and $|\cos\theta_{miss}| < 0.9$ where θ_{thr} and θ_{miss} are defined in the previous section. We reject events if the visible energy is less than 100 GeV or greater than 400 GeV. We do a two-cluster analysis and select events in which the acoplanarity of the clusters is greater than 10° and in which the minimum-mass cluster has an invariant mass greater than 1 GeV (to reject leptonic decays of the $W^{\pm}$) and the maximum-mass cluster has an invariant mass less than 50 GeV.

Finally, events are accepted only if the missing momentum transverse to the beam is greater than 50 GeV and the number of charged particles outside the 10° hole around the beam axis is between 10 and 36. The reconstructed invariant mass distributions in events with a Higgs of mass 50 GeV and a Higgs of mass 120 GeV are shown in Fig. 47(a) and 47(b), respectively. The probability that an event of the type $e^+e^- \to \nu_e\overline{\nu}_e H^0$ will pass the above selection criteria varies between about 35% and 50% depending on the mass of the Higgs and the decay mode of the Higgs. (For example, this efficiency depends on the value chosen for the top quark mass.)

The background shown in Fig. 48 is dominated by the process $e^+e^- \to e^+\nu_e W^-$ and its charge conjugate, which we computed using the formulae of Gabrielli.[60] It also contains contributions from all of the standard model processes described in Chapter 3, and from the reaction $e^+e^- \to \nu_e\overline{\nu}_e Z^0$, which oc-

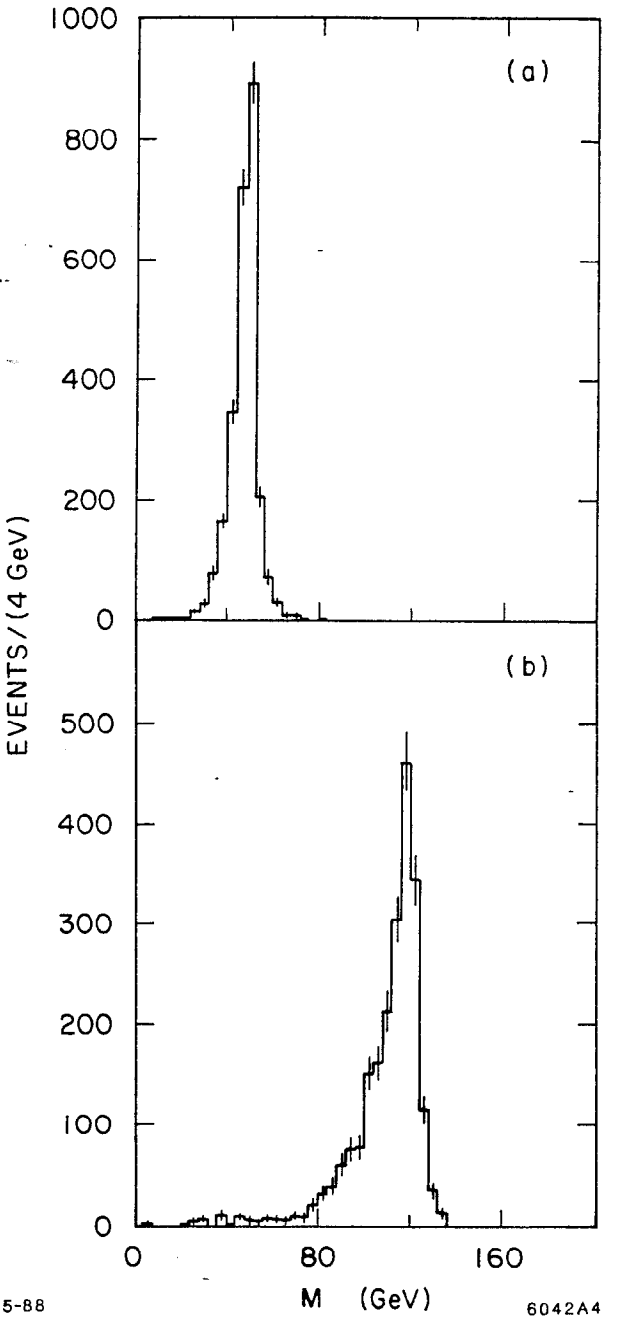

Figure 47. Reconstructed mass distributions, after selection criteria, for (a) a Higgs mass of 50 GeV and (b) a Higgs mass of 120 GeV. The Higgs is produced in the process $e^+e^- \rightarrow \nu_e\overline{\nu}_e H^0$.

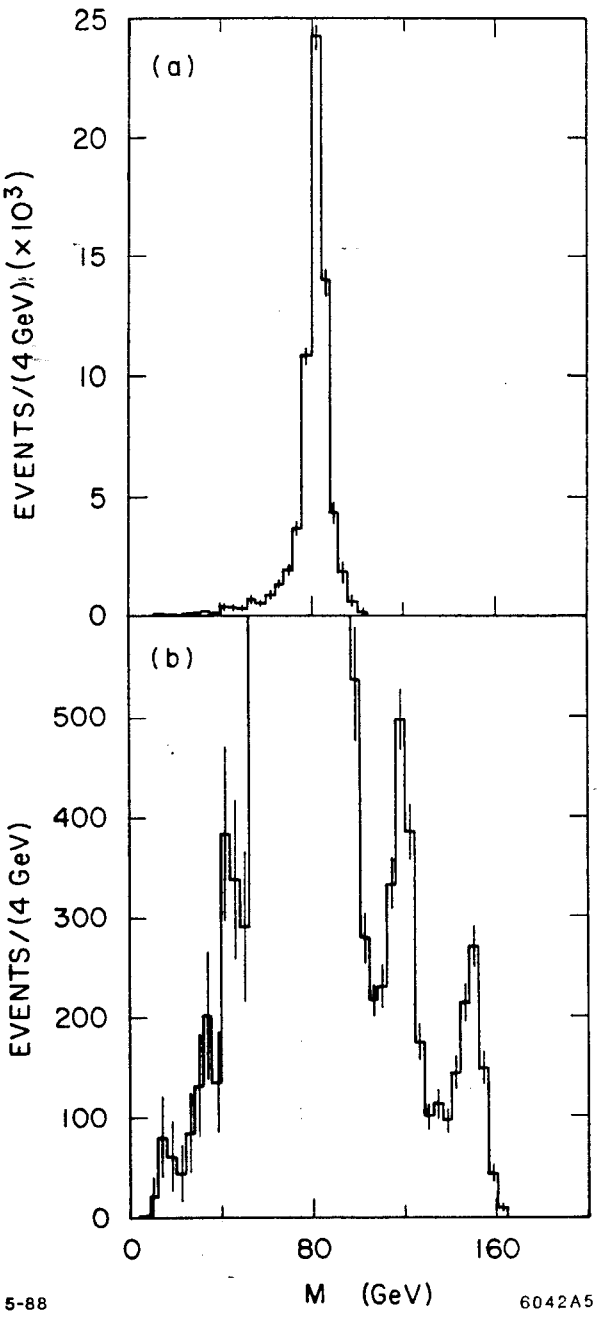

Figure 48. (a) Reconstructed mass distribution of background events that pass all selection criteria used to search for the Higgs in the reaction $e^+e^- \rightarrow \nu_e\overline{\nu}_e H^0$. This distribution is dominated by the process $e^+e^- \rightarrow e^+\nu_e W^-$ but includes a small contribution from the process $e^+e^- \rightarrow \nu_e\overline{\nu}_e Z^0$. (b) Reconstructed mass distribution for background events with signals from 120 GeV and 150 GeV Higgs particles added.

curs with a cross section that is approximately 3 times the Higgs cross section at $m_H = m_Z$.[61] Both figures correspond to an integrated luminosity of 30 fb^{-1}. The peak bin for the background distribution contains about 25 to 50 times as many events as the peak bin for the signal. It should be possible to discover a Higgs with $|m_H - m_W| > 30$ GeV with no further analysis, but as can be seen in the figure, the visibility of Higgs particles with masses closer to m_W depends critically on the resolution of the detector.

The background from $e^+e^- \to e^+\nu_e W^-$ is very difficult to distinguish from the $e^+e^- \to \nu_e\overline{\nu}_e H^0$ signal because the two processes are kinematically similar. This is demonstrated in Fig. 49 in which the transverse momentum distribution of the $W^\pm$ or H^0 is shown. There are, however, several features of the Higgs decay that might be exploited to enhance the signal with respect to the background. If it is possible to identify heavy quarks in the final state, then the predominance of top or bottom quarks in the Higgs decay will be a powerful signature. We have not addressed this issue further, but it is clear that the ability to place a precise vertex detector near the interaction point is extremely desirable.

We also note that the number of detectable charged particles in the final state will be even for the process $e^+e^- \to \nu_e\overline{\nu}_e H^0$, but odd for the process $e^+e^- \to e^+\nu_e W^-$ since the $e^\pm$ in the final state will typically disappear down the beam pipe. If we define the number of detected charged tracks in the event to be the number outside the 10° holes around the beam axis, then we find that approximately 90% of the signal and only 10% of the background events have an even number of charged tracks. The mass distribution for signal plus background is shown in Fig. 50 for events with an even number of detectable tracks. This is the most optimistic improvement in signal-to-background that could be expected unless it is possible to increase the acceptance of the detector. The situation will be less favorable in reality due to tracking inefficiencies created by overlap of particle trajectories, the decays of charged pions and kaons, and asymmetric photon conversions.

We have also investigated the production mechanism $e^+e^- \to Z^0H^0$ which has

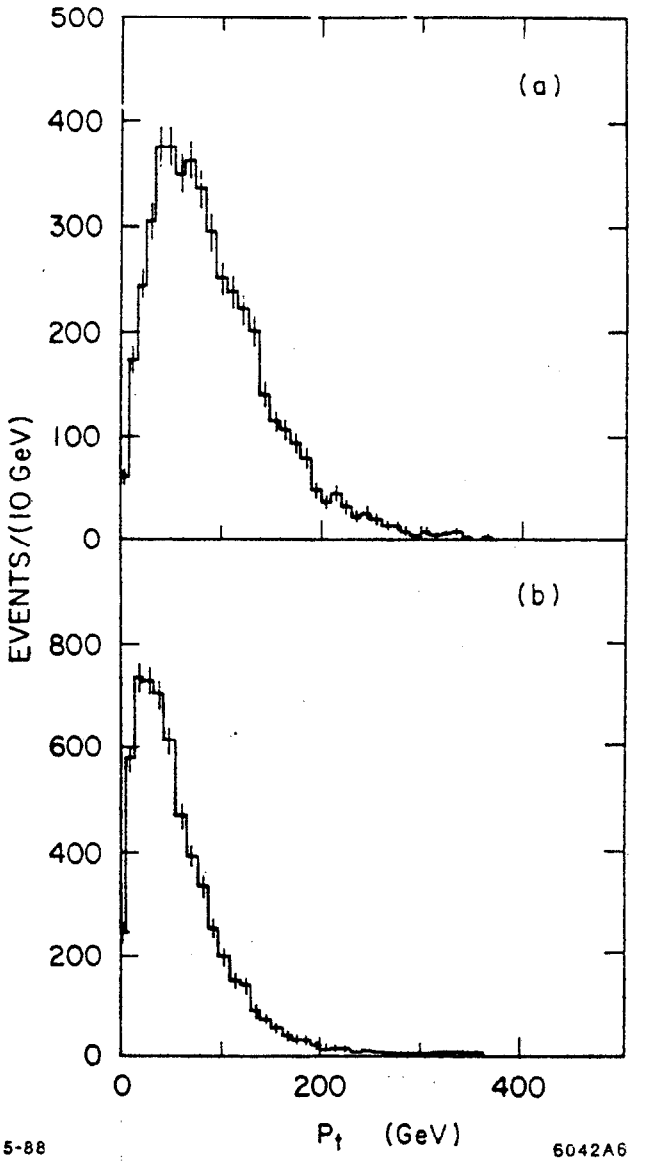

Figure 49. Transverse momentum (a) of the Higgs produced in the reaction $e^+e^- \rightarrow \nu_e\bar{\nu}_e H^0$ and (b) of the $W^\pm$ produced in the reaction $e^+e^- \rightarrow e^+\nu_e W^-$.

been previously analysed[13,14] at lower center of mass energies. The cross section for this process is substantial only at lower Higgs masses. (See Table 1.) The signature for this mode is two coplanar jets, one of which has the mass of the Z^0. We select events in which $|\cos\theta_{thr}| < 0.8$ since the distribution of the angle of

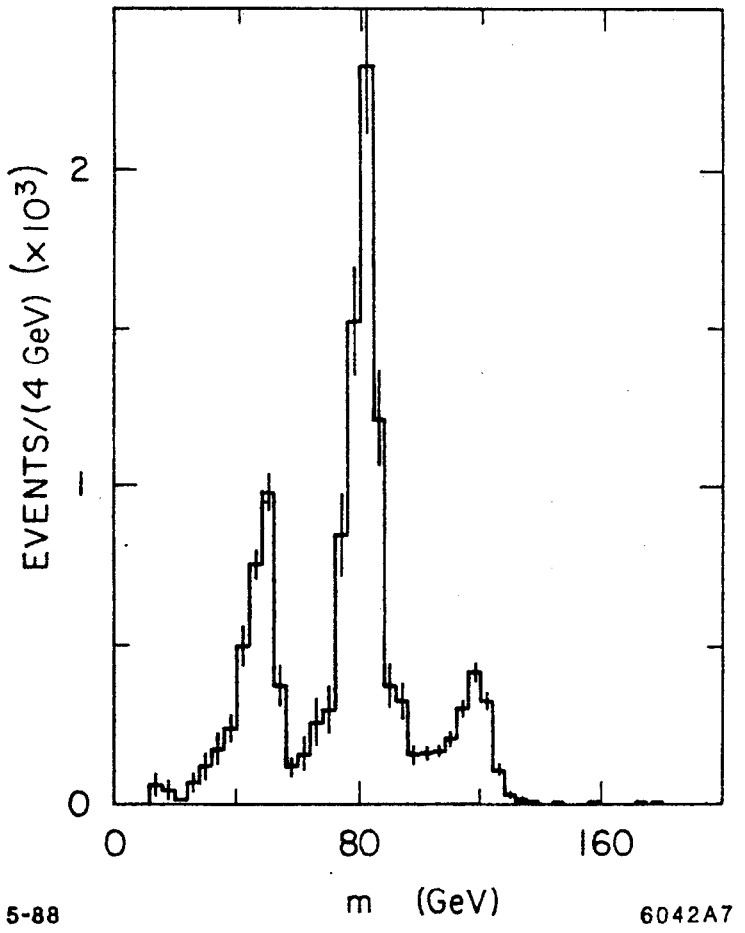

Figure 50. Reconstructed mass distribution for Higgs masses of 50 and 120 GeV plus background for events with an even number of charged tracks outside 10° holes around the beam axis.

emission of the Z^0 or H^0 with respect to the beam is peaked at 90°. We reject events if the visible energy is less than 400 GeV. We then do a two-cluster analysis and select events in which the acoplanarity of the clusters is less than 5°. To search for a Higgs boson with mass less than the Z^0 mass, we select events in which the mass of the maximum-mass cluster is between 88 and 98 GeV. To search for a Higgs boson with mass greater than the Z^0 mass, we select events in which the mass of the minimum-mass cluster is between 85 and 100 GeV. The probability that an event of the type $e^+e^- \rightarrow Z^0H^0$ will pass the above selection criteria is

about 23%, 19% and 29% for a Higgs mass of 50, 100, and 120 GeV, respectively.

The invariant mass distributions for signal events and background events are shown in Figs. 51 and 52, respectively. Each figure represents an integrated luminosity of 30 fb^{-1}. The signals in Fig. 51(a) and 51(b) correspond to Higgs masses of 50 and 120 GeV, respectively. Each distribution contains about 300 events. The backgrounds in Fig. 52(a) and 52(b) correspond to the selection criteria for a Higgs mass less than the mass of the Z^0 and greater than the mass of the Z^0, respectively. The backgrounds include contributions from $e^+e^- \rightarrow q\bar{q}$, $e^+e^- \rightarrow Z^0Z^0$, and $e^+e^- \rightarrow W^+W^-$ with no one dominant source. It is evident that outside the mass range 75 to 100 GeV the peak signal-to-background ratio is about one. In the mass range 75 to 100 GeV, the signal-to-background ratio is between one-quarter and one-third. As we noted previously, it may be possible to improve the clarity of the signal by identification of the heavy quarks favored in the decay of the Higgs.

We have shown, then, that the signal for a neutral Higgs boson with mass below 500 GeV, and more than 30 GeV away from the W masss, is clear at an e^+e^- collider with a nominal center of mass energy of 1 TeV. The signal is dominated by Higgs production through the W^+W^- fusion process $e^+e^- \rightarrow \nu_e\bar{\nu}_e H^0$.

For a Higgs mass near the mass of the $W^\pm$, there is a large background to the W^+W^- fusion process from $e^+e^- \rightarrow e^+\nu_e W^-$. For $m_H = m_W$, the signal-to-background ratio is about 1 : 30. However, there are two ways to reduce this background:

1. Heavy quark identification — the Higgs will decay almost exclusively to $t\bar{t}$ or $b\bar{b}$ pairs.

2. Charged track counting — an efficient charged track counter would provide significant reduction in the background.

The Higgs production mode $e^+e^- \rightarrow Z^0H^0$ does not provide very significant signals at a 1 TeV e^+e^- collider for most Higgs masses. However, this channel provides important cross checks and verifications if the Higgs signal is seen elsewhere,

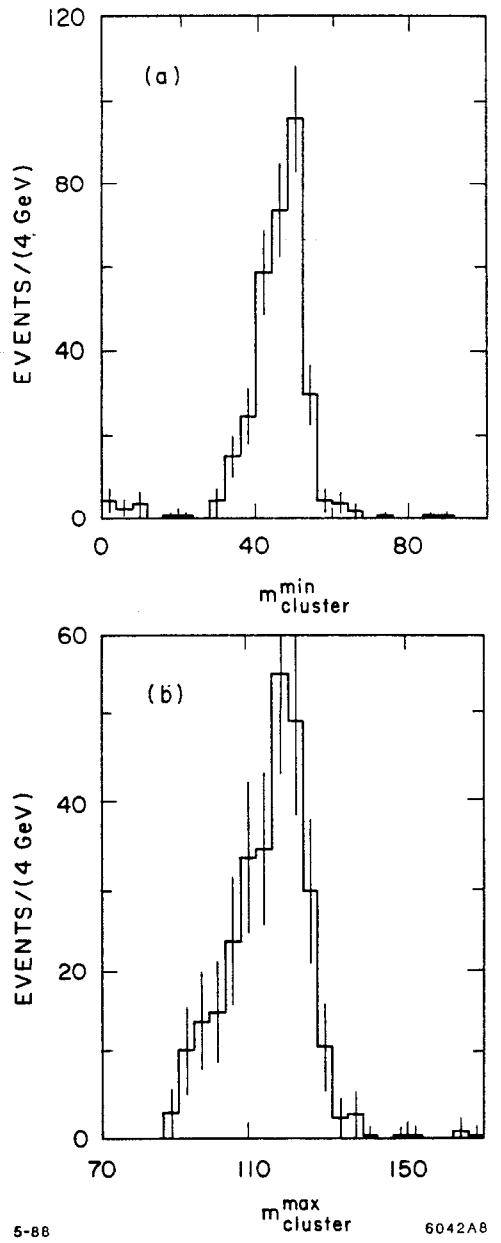

Figure 51. Reconstructed mass distributions, after selection criteria, for (a) a Higgs mass of 50 GeV and (b) a Higgs mass of 120 GeV. The Higgs is produced in the process $e^+e^- \rightarrow Z^0H^0$.

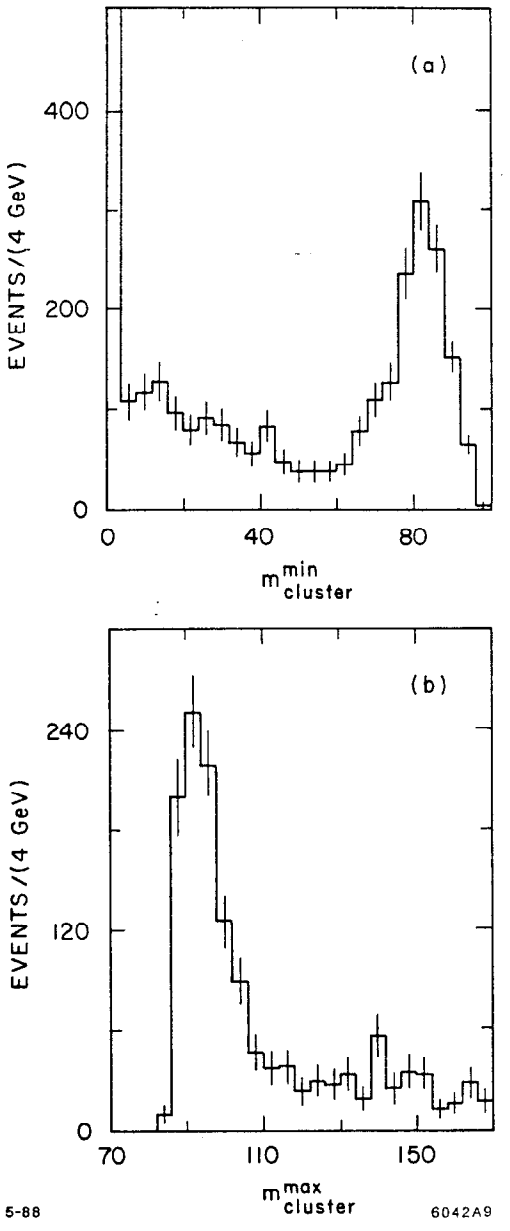

Figure 52. Reconstructed mass distributions of background events that pass all selection criteria used to search for the Higgs in the reaction $e^+e^- \rightarrow Z^0H^0$ (a) for $m_H < m_Z$, (b) for $m_H > m_Z$.

and will provide a visible signal if the Higgs mass is near to the mass of the W or Z^0.

6. New Z^0 Bosons

The most dramatic of all phenomena proposed for e^+e^- physics in the region below 1 TeV is the appearance of a new Z^0 boson. In just the way that the familiar Z^0 affects physics in the energy range about 100 GeV, a new boson would completely alter the pattern of fermion pair-production cross sections and asymmetries. On its resonance peak, the cross section for pair production would be enhanced by a factor of 10^3 above the standard model expectation.

We have not made a complete study of the physics program for a new Z^0, because we do not feel that the considerations of this physics should guide the design of a high-energy collider. If in fact no new resonance exists, a machine designed strictly to operate at such a resonance would not be able to carry out any of the other experiments listed in this report. On the other hand, if a new resonance is present, it will greatly enhance the physics potential of a TeV-energy collider. A collider of this type, operating at the resonance peak, would be the ideal tool to analyze the coupling of the new boson to the other elementary fermions and bosons, and thus to elucidate the new force of nature that the new boson represents. In this section, we wold like to review the basic phenomenology of a new resonance in order to indicate how rich a program of experiments would be available. Our discussion will make clear that, if such a new vector boson is discovered in the next few years, the design requirements for the collider we are discussing could be scaled back considerably, since the experimental program we will discuss could be carried out even at luminosities of 10^{31} cm^{-2}sec^{-1} or less, and at the resonance energy, which might be well below 1 TeV.

6.1. Setting: Extensions of Grand Unification

There are two very different motivations for expecting a new Z^0 boson in the energy range below 1 TeV, one based on theoretical prejudice, the other on ignoring theoretical prejudice. On one hand, many models of the grand unification of the fundamental interactions involve large gauge groups which allow extra neutral bosons, and it is not difficult for these bosons to gain mass only at the weak scale. On the other hand, the experimental constraints on such new bosons are very weak, since these bosons would be seen only as small corrections to neutral current processes. From this viewpoint, the door is almost completely open for a new-resonance to appear.

Let us first discuss the current constraints on a new neutral vector boson. In principle, such a boson could be seen directly, as the familiar Z^0 has been, as a resonance in lepton pair production in $p\overline{p}$ collisions. However, the sensitivity of this technique currently reaches only a little beyond the conventional Z^0.[62] Stronger constraints come from the careful analysis of weak neutral current data. An important part of those constraints is the requirement that the new boson not lower the mass of the familiar Z^0 by mixing in such a way as to upset the standard model relation between m_Z, G_F and $\sin^2\theta_w$. These constraints have been worked out in detail by Amaldi, *et. al.*[63] Their bounds, for various hypotheses on the couplings of the new weak boson (to be explained below) are shown in Fig. 53. The figures make clear that, almost independently of the nature of its couplings, a new weak boson is freely allowed if its mass is above 250 GeV, as long as it does not mix appreciably with the familiar Z^0.

Over the next five years, we will learn more about the existence of new Z^0 bosons, since the Tevatron collider at Fermilab reaches deeply into the possible parameter space. In Fig. 54, we plot the values of the mass of a new Z^0 which would correspond to 5 events of $p\overline{p} \to e^+e^- + X$ due to production and decay of a new gauge boson, in the class of models to be discussed below. The two levels of energy and luminosity assumed are those projected for the Tevatron collider in its

present configuration and with an upgrade planned for the early 1990's. It seems likely that we will know before the design of a new e^+e^- collider must be finalized

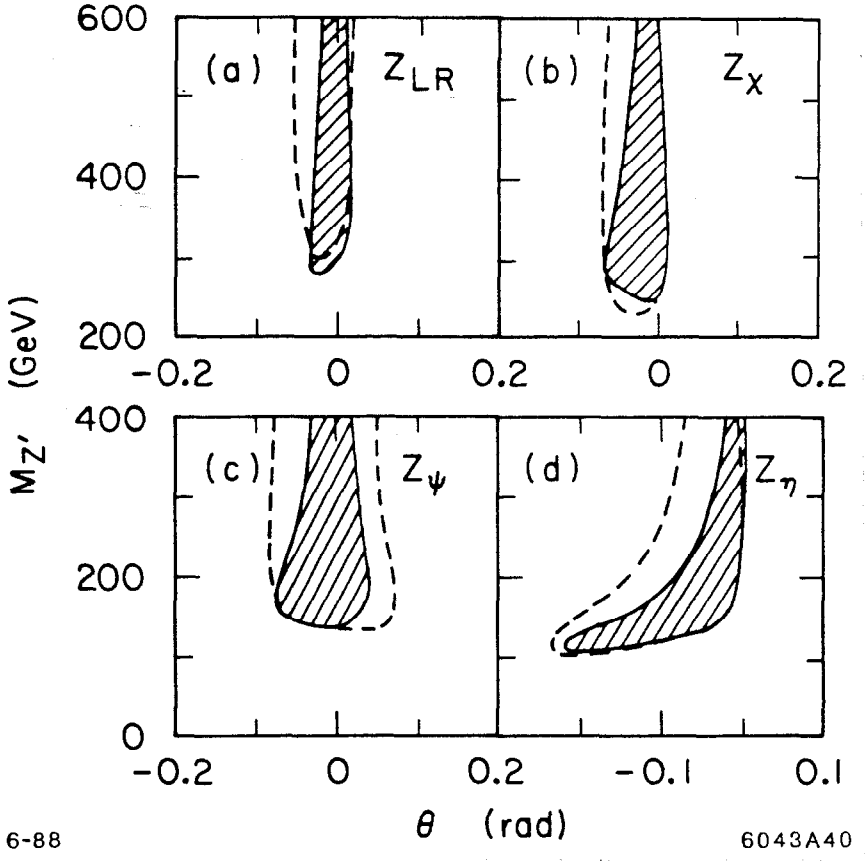

Figure 53. Allowed regions for the mass of a Z' and its mixing angle with the familiar Z^0, from ref. 63: (a) for $SU(2)_L \times SU(2)_R$ models, (b), (c), (d) for the three coupling schemes χ ψ, η defined at the end of this section. The two boundaries correspond to two assumptions on the Higgs bosons which break $SU(2) \times U(1)$; the solid boundaries assume Higgs doublets only.

whether there is a new Z^0 below 400 GeV. On a longer time scale, the SSC or the LHC should map out the presence of new vector bosons to masses of 4 TeV or above.[12]

It is important to note that the constraints on a new charged vector boson are

much more severe, at least in the most natural hypothesis that this charged boson can mediate $(V+A)$ weak interactions. Direct experiments on muon decay rule out the presence of $(V+A)$ interactions in that process to a level corresponding to a

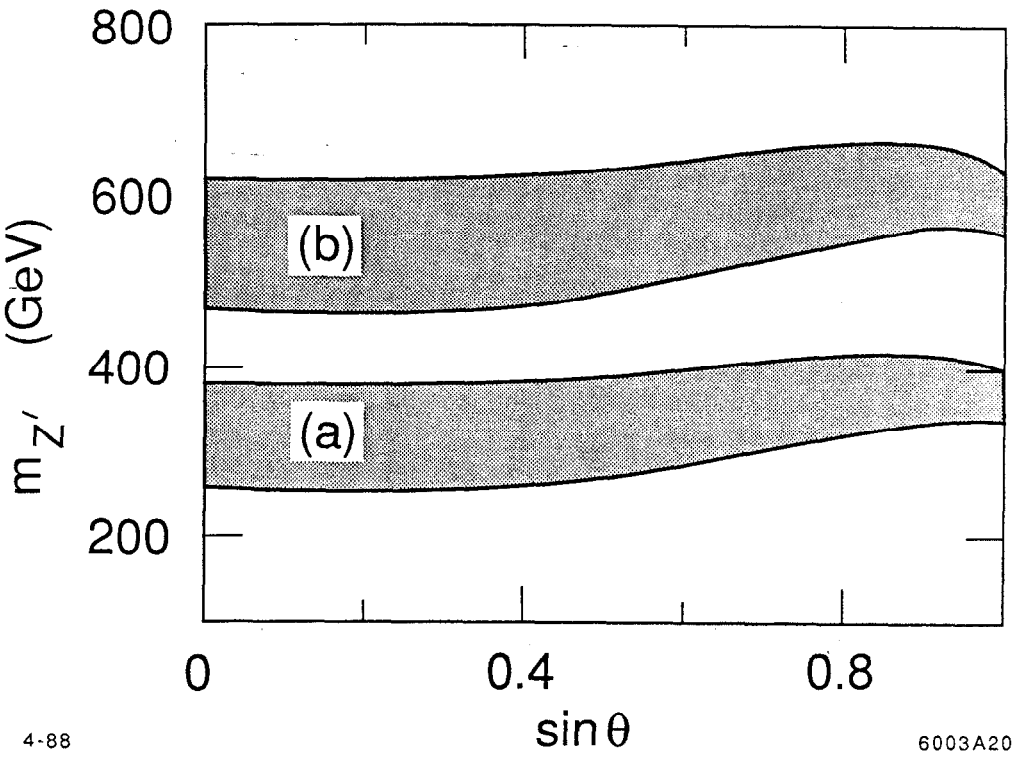

Figure 54. Mass limits for a Z' boson producing 5 events of $p\bar{p} \to Z' + X$, $Z' \to e^+e^-$ at the Tevatron collider (a) for $\sqrt{s}$= 1.8 TeV, $\int \mathcal{L} = 10^{37}$, (b) for $\sqrt{s}$ = 2 TeV, $\int \mathcal{L} = 10^{38}$, from ref. 7. The coupling scheme is that of eq. (6.1). In each region, the upper bound assumes that the Z' decays only to known fermions, and the lower bound assumes that the Z'decay to all of the states in the **27** of E_6.

boson mass of 600 GeV.[64] A stronger bound comes from the radiative corrections that such a boson would make in the K^0–$\overline{K^0}$ mass matrix. These corrections are known to be anomalously large and lead to a lower bound on the mass of a $(V+A)$ charged boson of order 2 TeV.[65]

While current experiments put little constraint on the presence of new neutral

vector bosons, many theoretical extensions of the standard model cry out for such particles. While the minimal grand unified theory, based on the group $SU(5)$, does not have room for an extra neutral boson, the most common alternative choices for a grand unifying group, $SO(10)$ and E_6, have natural candidates. In these theories, one can arrange that the extra bosons are very heavy, but it is often more natural to place one or both at the weak scale. In grand unified theories with a left-right symmetric $SU(2)_L \times SU(2)_R$ structure at some scale, the extra neutral boson in this extended weak group may survive to low energies. The recent phenomenological exploration of superstrings has brought new force to speculations about new Z^0 bosons; in this setting, the grand unification group E_6 arises in a natural way, and in the simplest scenarios for phenomenology at least one extra neutral vector boson is left massless until one includes the effects of weak-interaction symmetry breaking.[66,67]

In the discussion to follow, we will focus, for definiteness, on a particular scheme for the properties of the new Z^0, set out by Langacker, Robinett, and Rosner.[68] Following the motivation of the previous paragraph, we will assume that the new boson arises from some sort of E_6 grand unification. This grand unifying group contains two new neutral bosons; we will choose an arbitary linear combination of these, parametrized by an angle θ. By varying θ, we sweep through a wide class of distinct models for the couplings of the new boson. Robinett and Rosner[69] have argued that, under some general conditions, the coupling constant renormalization for this new boson from the grand unification scale to the weak scale is just proportional to the renormalization of the standard model hypercharge coupling g'; we will use this assumption to specify the coupling constant of the new boson. Finally, we will ignore the mixing of the new boson with the familiar Z^0; we have noted already that this last assumption is required phenomenologically. The neutral boson of left-right symmetric theories is excluded from this scheme by the assumption about coupling constant renormalization. Generally, this latter choice gives even larger effects than those which follow from the Langacker-Robinett-Rosner scheme.

Table 10. Quantum numbers of the **27** of E_6.

$SU(3) \times SU(2)_L$	**Y**	χ	ψ	(ID)
$(\mathbf{3},\mathbf{2})$	1/6	-1	1	(u_L, d_L)
$(\overline{\mathbf{3}},\mathbf{1})$	$-2/3$	-1	1	$(\overline{u_R})$
$(\overline{\mathbf{3}},\mathbf{1})$	1/3	3	1	$(\overline{d_R})$
$(\mathbf{1},\mathbf{2})$	$-1/2$	3	1	(ν_L, e_L^-)
$(\mathbf{1},\mathbf{1})$	1	-1	1	$(\overline{e_R^-})$
$(\mathbf{1},\mathbf{1})$	0	-5	1	$(\overline{\nu_R})$
$(\mathbf{3},\mathbf{1})$	$-1/3$	2	-2	(D_L)
$(\overline{\mathbf{3}},\mathbf{1})$	1/3	-2	-2	$(\overline{D_R})$
$(\mathbf{1},\mathbf{2})$	$-1/2$	-2	-2	(N_L, E_L)
$(\mathbf{1},\mathbf{2})$	1/2	2	-2	$(\overline{N_R}, \overline{E_R})$
$(\mathbf{1},\mathbf{1})$	0	0	4	S

This model leads to a neutral current Lagrangian of the form

$$\begin{aligned} \mathcal{L}_{\rm NC} \;=\; & eA_\mu\, J^\mu_{EM} \;+\; \frac{e}{\sin^2\theta_w \cos^2\theta_w}\, Z_\mu\, J^\mu_Z \\ & + \frac{e}{\cos^2\theta_w}\, Z'_\mu\, J^\mu_{Q'}\;, \end{aligned} \tag{6.1}$$

where the new bosons Z' couples to the charge Q' given by

$$Q' \;=\; \left[\frac{1}{2\sqrt{6}}\sin\theta\cdot\chi \;-\; \frac{1}{6}\sqrt{\frac{5}{2}}\cdot\cos\theta\cdot\psi\right]\;. \tag{6.2}$$

This charge is built from two quantum numbers χ and ψ which characterize the coupling of each fermion to the two new neutral bosons of E_6. The values of

χ and ψ for a standard generation of quarks and leptons are presented in Table 10. Actually, the fundamental matter multiplet in E_6 grand unification is a 27-dimensional multiplet, including also a number of states with exotic weak quantum numbers. These states are also listed in Table 10.

The charge χ gives the coupling to the neutral boson which is contained in the $SO(10)$ subgroup of E_6; the charge ψ is the coupling to the boson orthogonal to this $SO(10)$ subgroup. These pure couplings give two special, distinct models. In addition to these two cases, much attention has been given to the case $\sin\theta = \sqrt{3/8}$, since this linear combination appeared as the couplings of the Z' in the first examples of superstring phenomenology.[70] These three cases give the coupling schemes labelled χ, ψ, and η in Fig. 53. Curiously, the η case gives particularly weak couplings to conventional fermions and thus provides a conservative estimate of the effect of the Z'.

6.2. Properties of a New Z^0

Let us first consider the method of search for a Z' resonance at an e^+e^- collider, and other effects of the new boson which could be measured off resonance. We will then turn to the expected properties of the resonance itself.

The most obvious property of the new Z^0 is the fact that it creates an enormous resonance in e^+e^- annihilation, with a peak height given by

$$\sigma(e^+e^- \to Z^{0\prime}) = \frac{12\pi}{M_{Z'}^2} \frac{\Gamma(Z^{0\prime} \to e^+e^-)}{\Gamma_{\rm tot}} = \frac{9}{\alpha^2} BR(Z^{0\prime} \to e^+e^-)\,\mathrm{R}\,. \quad (6.3)$$

We will see below that the branching ratio of the resonance is to e^+e^- is typically about 5%, so that (6.3) predicts a peak cross section of order 10^4 R. As an example of this behavior, we show in Fig. 55 the predicted total cross section for e^+e^- annihilation to μ pairs and to hadrons for a Z' with the superstring-inspired (η) couplings and a mass of 600 GeV. While at first it appears that one must scan to locate the resonance, this is not actually necessary. Even at a collider with definite

center of mass energy, the process of radiation of a collinear photon followed by annihilation at the resonance would be substantial, as we saw in Section 3 for the analogous effect producing the familiar Z^0. Further, in a realistic design, this effect is substantially enhanced by beamstrahlung.

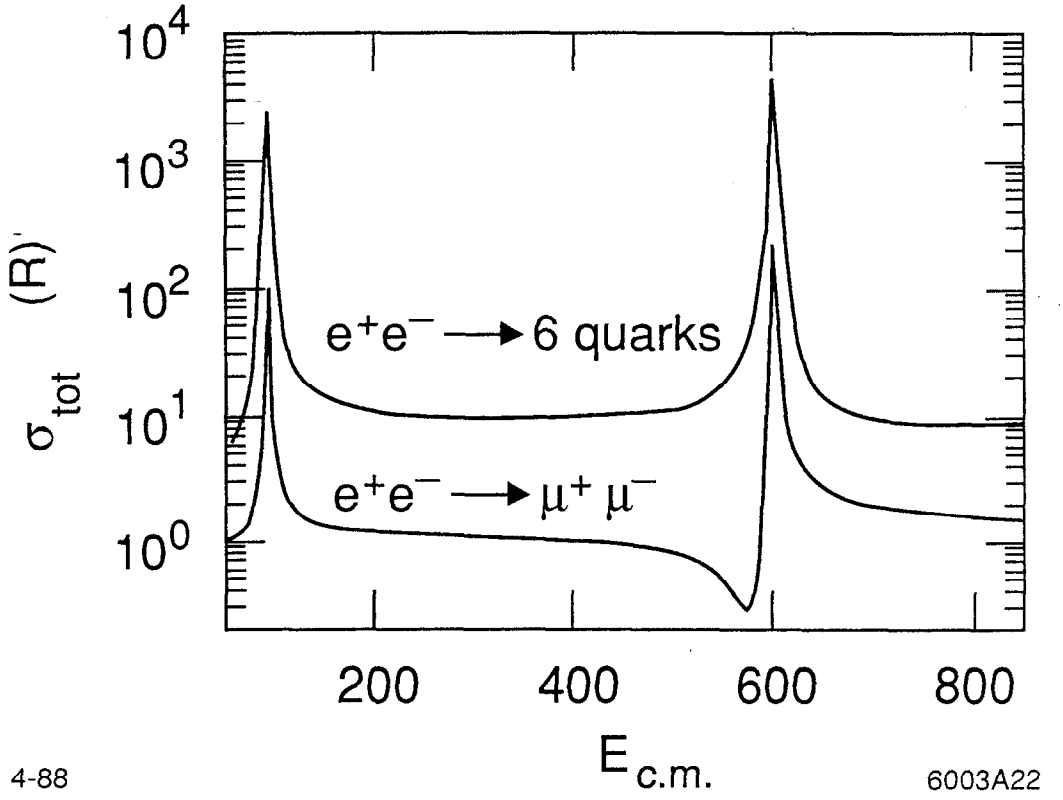

Figure 55. Total cross section for e^+e^- annihilation to hadrons and to $\mu^+\mu^-$, including the effects of a Z' (with η couplings) at a mass of 600 GeV.

Fig. 56 shows the distribution of quark pair production events as a function of the hadronic invariant mass which would be measured in a calorimeter, computed for the beamstrahlung spectrum used in Section 3. Even at as low a mass as 400 GeV, the new Z^0 included in the calculation stands out above the continuum by more than 2 orders of magnitude.

Even away from the resonance, the Z' has significant effects on the basic asymmetries of $e^+e^- \to f\overline{f}$, since the relative couplings of the new Z^0 to left- and right-handed fermions generally differ significantly from those of the familiar Z^0 and the photon. The forward-backward asymmetries to leptons and to b and t quarks,

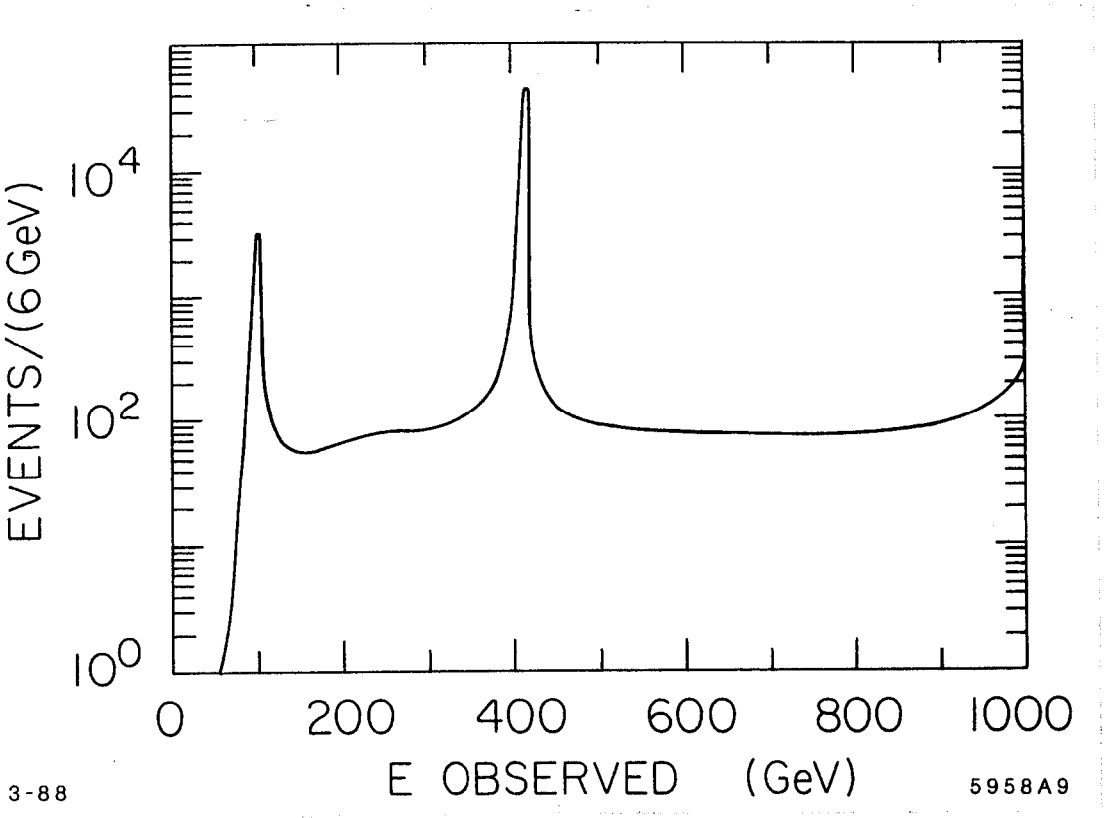

Figure 56. Distribution of observed hadronic invariant masses resulting from e^+e^- annihilation to hadrons, including the effects of a Z' of mass 400 GeV, computed with the $\delta = 0.26$ beamstrahlung spectrum shown in Fig. 4.

which differ substantially from zero already in the standard model, receive large, interfering contributions from the new exchange. In Fig. 57, we have plotted these effects as a function of energy for a Z' at 600 GeV, for the three cases χ, ψ, η of the couplings to fermions. Note that the asymmetries to the three final states give independent information constraining the Z' couplings.

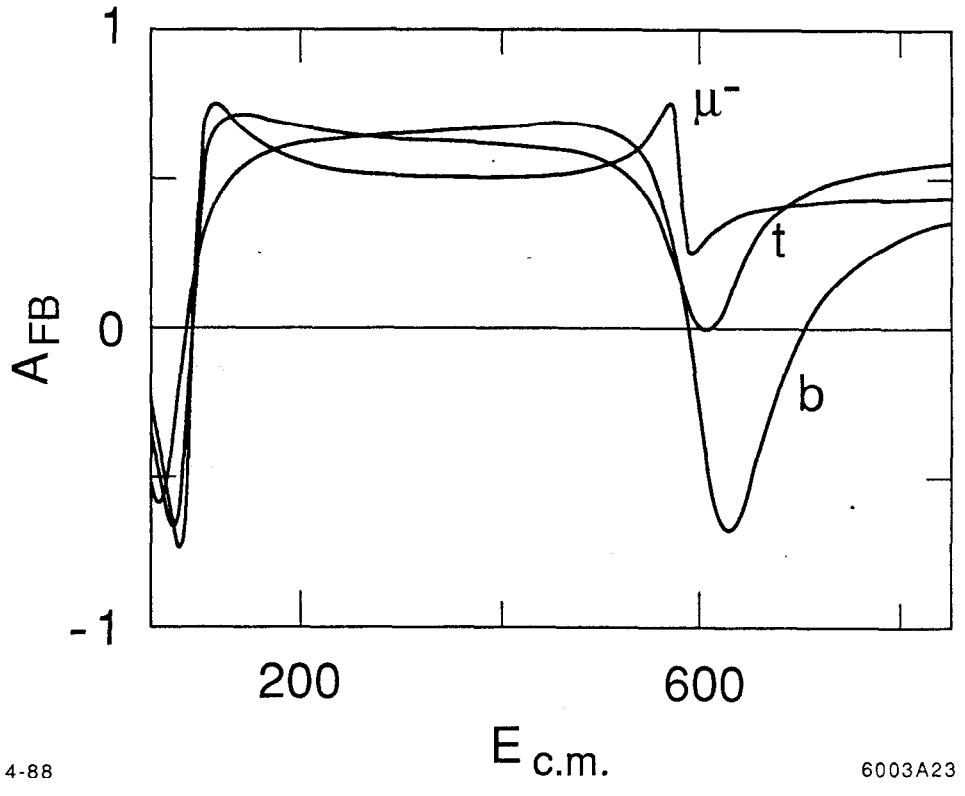

Figure 57. Forward-backward asymmetries for the production of μ, b, and t pairs, including the effects of a Z' (with η couplings) of mass 600 GeV.

If polarized electrons are used, the polarization asymmetry to these three final states gives three additional measureable parameters. The behavior of the three polarization asymmetries, over the same range of energy, is shown in Fig. 58.

If no Z' is found below 1 TeV, the values of the six asymmetries in $e^+e^- \to f\overline{f}$ can be used to search for a new vector boson at still higher energies. The perturbation of the asymmetries by such a resonance is of order 1 for a Z' below 1.5 TeV, and, if the asymmetries can be measured to $\pm 1\%$, any Z' below 4 TeV would produce a visible effect. In Figs. 59 and 60, we plot the expectations for two of these asymmetries, the lepton polarization asymmetry and the t quark forward-backward asymmetry, measured at 1 TeV, as a function of the mass of the Z'.

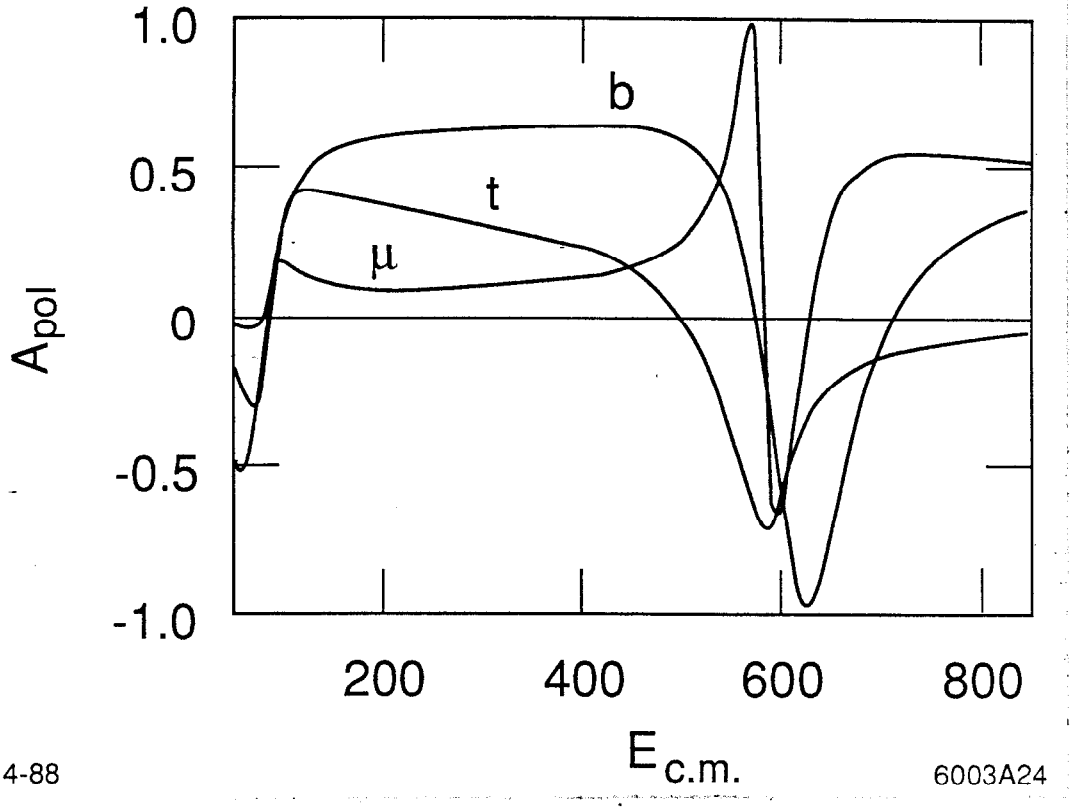

Figure 58. Polarization asymmetries for the production of μ, b, and t pairs, including the effects of a Z' (with η couplings) of mass 600 GeV.

Again, we emphasize that these two observables, and the other four as well, are theoretically independent of one another and so each one gives a new constraint.

Figs. 61 and 62 demonstrate this point in another way by plotting two asymmetries against one another for the three canonical choices of the Z' couplings.The three cases are clearly distinguished in any regime where the deviation from the standard model is visible in the first place. It is, of course, quite likely that a Z' of mass below 4 TeV will first be observed at a hadron collider.

However, it is not possible in that case to measure even the coupling to leptons without invoking extra theoretical assumptions. Asymmetry experiments in e^+e^- annihilation will complement the discovery of the resonance by pinning down some and possibly all of the Z' couplings to quarks and leptons.

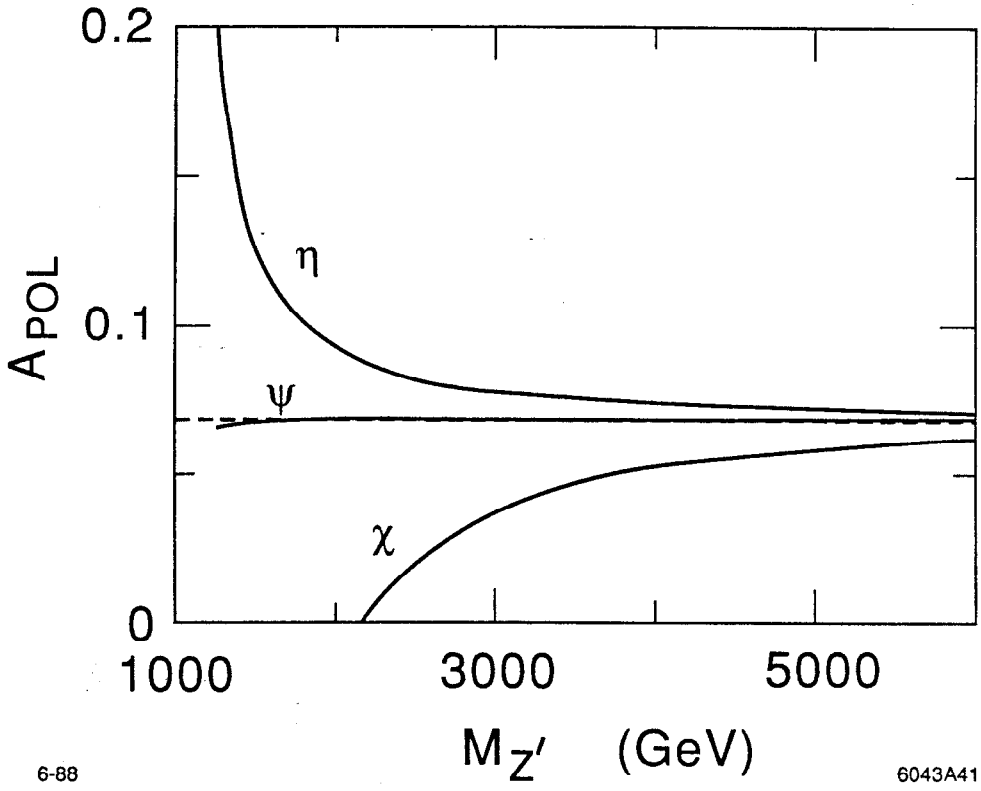

Figure 59. Polarization asymmetry for lepton pair production at $\sqrt{s} = 1$ TeV, including the effects of a heavy Z', computed for the three coupling schemes defined at the end of section 6.1.

6.3. Properties of a New Z^0 on Resonance

If a new Z^0 is found in the region where it is accessible to e^+e^- annihilation-experiments on resonance, those experiments will provide a much more sensitive characterization of the couplings of the new boson. In the process of fermion pair-production at the new resonance, the standard contributions from photon and Z^0 exchange are negligible, and so the relative rates of production reflect directly the couplings of the Z' to the various species.

In the class of models presented above, the partial width of the new Z^0 to a given fermion species is given by

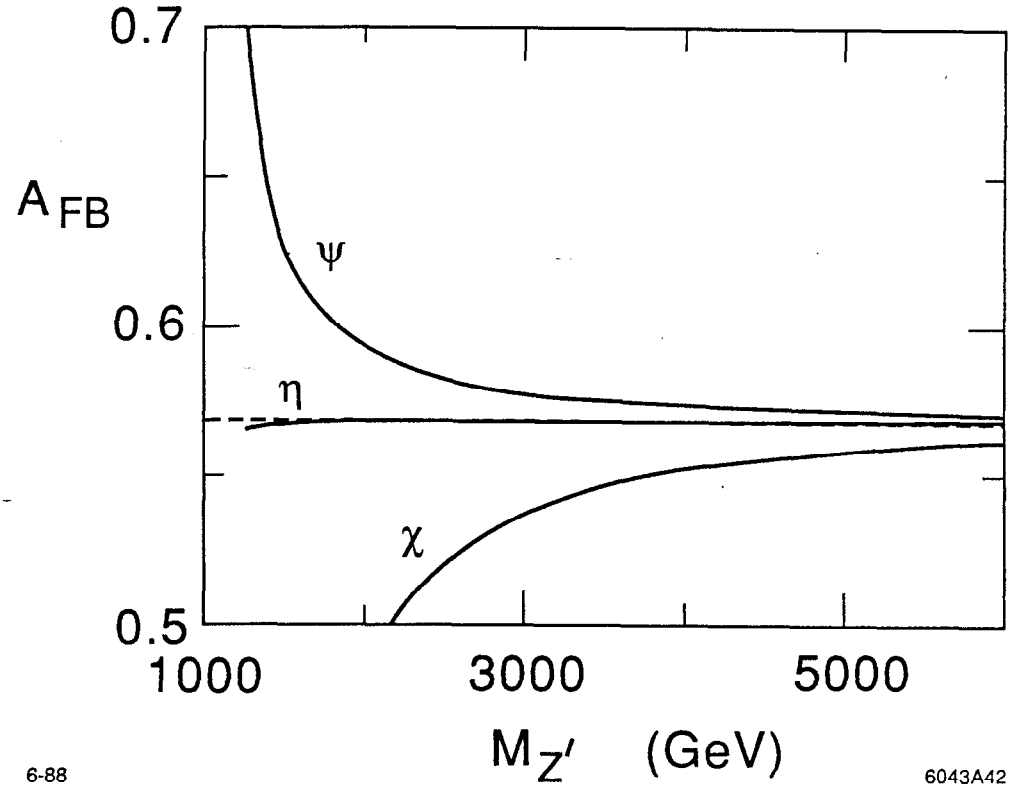

Figure 60. Forward-backward asymmetry for t quark pair production at $\sqrt{s} = 1$ TeV, including the effects of a heavy Z'.

$$\begin{aligned}\Gamma(Z^{0\prime} \to f\overline{f}) &= \frac{\alpha}{6\cos^2\theta_w} m_{Z'} \cdot (Q')^2 \\ &= (0.78\,\mathrm{GeV}) \cdot \left(\frac{m_{Z'}}{500\,\mathrm{GeV}}\right) \cdot \left[\frac{\sin\theta}{2\sqrt{6}}\chi - \frac{\cos\theta}{6}\sqrt{\frac{5}{2}}\psi\right]^2 .\end{aligned} \tag{6.4}$$

Note that (6.4) counts left- and right-handed fermions separately; these two contributions must be added to find the observable partial width. The total width of the resonance depends on whether the new Z^0 decays only to conventional fermions; in models of extended grand unification, it is not unlikely that at least some of the exotic states from Table 10 will be light enough to be pair-produced. For definiteness, though, let us consider the case in which none of the exotic states appear. For this case, the relative branching ratios for the fermions of the standard model

are presented in Fig. 63, and the total width is graphed as a function of the mixing angle θ in Fig. 64.

The enormous size of the peak cross section makes the new Z^0, like the familiar one, an outpost at high center of mass energy at which one can perform the whole

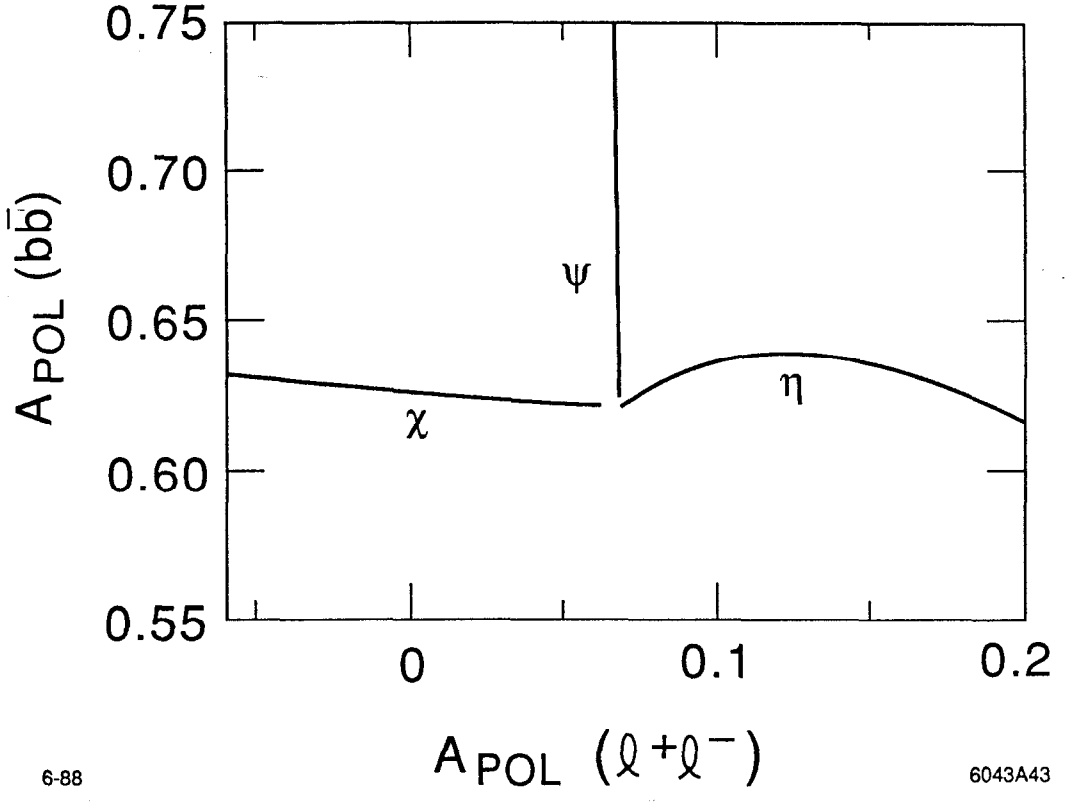

Figure 61. Comparison of the polarization asymmetry predicted for lepton and for b quark pair production at $\sqrt{s} = 1$ TeV in models with a Z' of mass between 1 and 6 TeV. The three curves correspond to the three coupling schemes defined at the end of Section 6.1.

range of e^+e^- annihilation experiments with large event samples. Like the familiar Z^0, experiments at the new Z^0 will provide precision tests of QCD and the electroweak interactions and high-sensitivity searches for new massive particles. The rate is sufficiently high that even processes forbidden in the limit of zero mixing

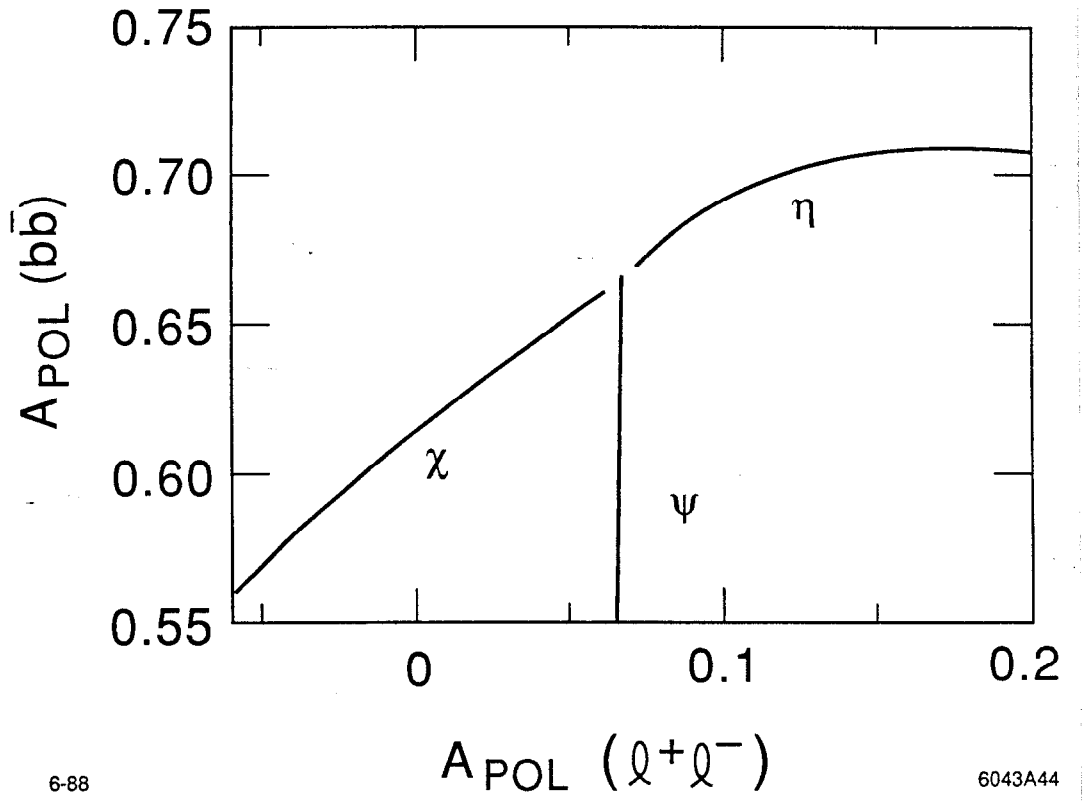

Figure 62. Comparison of the polarization asymmetry for lepton pair production and the forward-backward asymmetry for b quark pair production, at $\sqrt{s} = 1$ TeV, predicted in models with a Z' of mass between 1 and 6 TeV.

between the new Z^0 and the familiar one may be measureable if the mixing is not strictly zero. In fact, the amplitudes for the Z' to decay to conventional W pairs and to a Z^0 plus a Higgs boson are proportional to the Z^0–Z' mixing angle. Dib and Gilman[71] have estimated the event rates for these decays and have found that they are quite substantial, even for mixing angles of the size required by Fig. 53. Their results for the case of a new Z' at a mass of 400 GeV, with η couplings, are shown in Fig. 65.

To make a precision determination of the various couplings of the Z', one can study the asymmetries of fermion pair production. On resonance, there are only three independent asymmetries. All polarization asymmetries are essentially equal

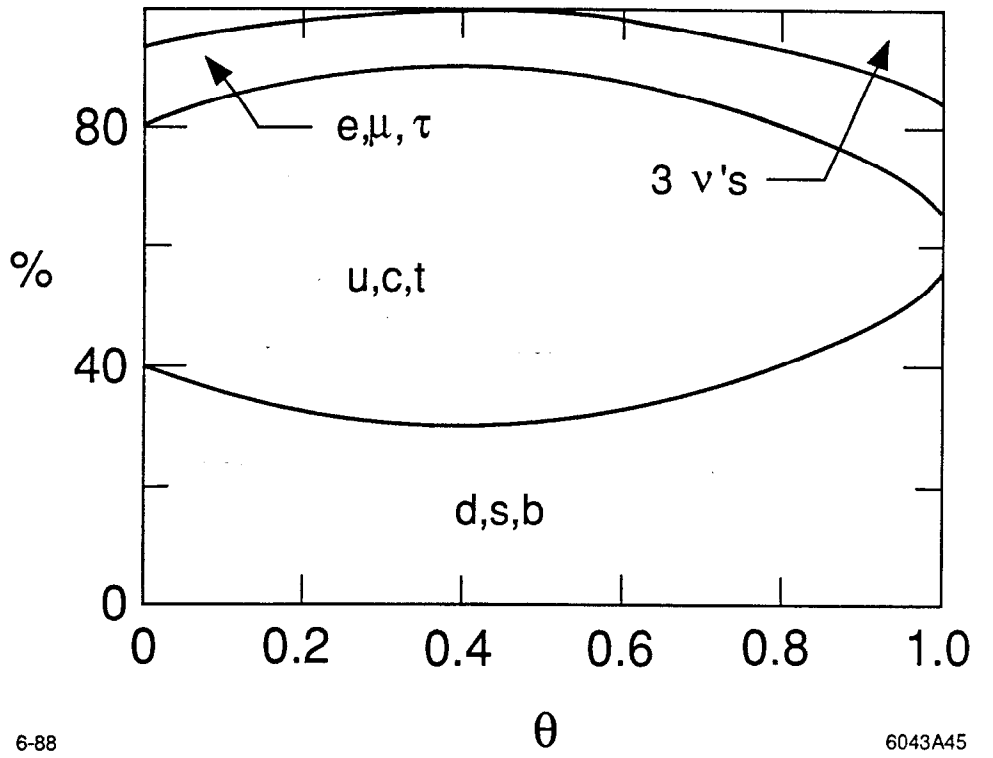

Figure 63. Branching fractions of a Z' to quarks and leptons, using the couplings of eq. (6.1). The figure assumes that these are the only major decay modes.

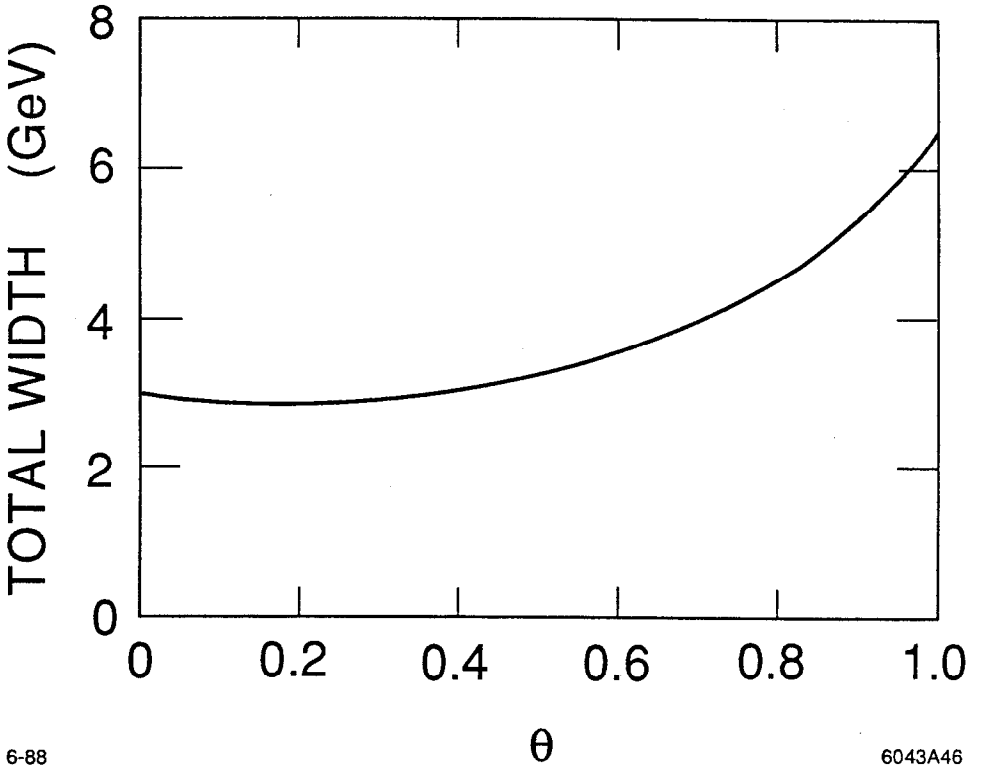

Figure 64. Total width of the Z', under the assumptions of Fig. 63.

and given by

$$A_{\rm pol} \;=\; \frac{(Q'_{eL})^2 - (Q'_{eR})^2}{(Q'_{eL})^2 + (Q'_{eR})^2} \;. \tag{6.5}$$

The lepton forward-backward asymmetry is connected to this quantity by the simple relation

$$A_{FB} \;=\; 0.75\big(A_{\rm pol}\big)^2 \;, \tag{6.6}$$

as on the familiar Z^0. The forward-backward asymmetries to b and t, given by

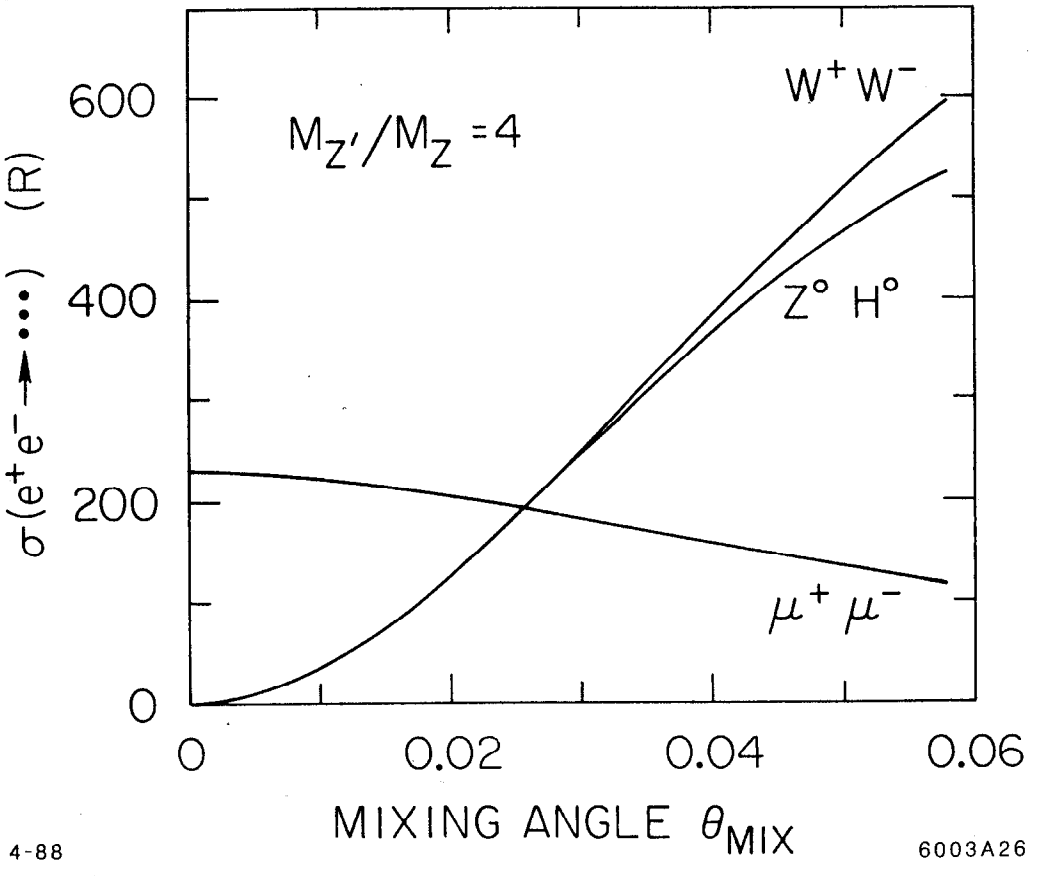

Figure 65. Cross sections for $e^+e^- \to Z' \to W^+W^-$ and $e^+e^- \to Z' \to H^0Z^0$, at the resonance peak, from ref. 71.

$$A_{FB} = 0.75 \frac{((Q'_{eL}Q'_{fL})^2 + (Q'_{eR}Q'_{fR})^2) - ((Q'_{eL}Q'_{fR})^2 + (Q'_{eR}Q'_{fL})^2)}{(Q'_{eL}Q'_{fL})^2 + (Q'_{eR}Q'_{fR})^2 + (Q'_{eL}Q'_{fR})^2 + (Q'_{eR}Q'_{fR})^2} \quad (6.7)$$

do provide new information.

In the class of models we have been considering, the forward-backward asymmetry to t quarks vanishes, since the coupling of the t to the new Z^0 is purely axial

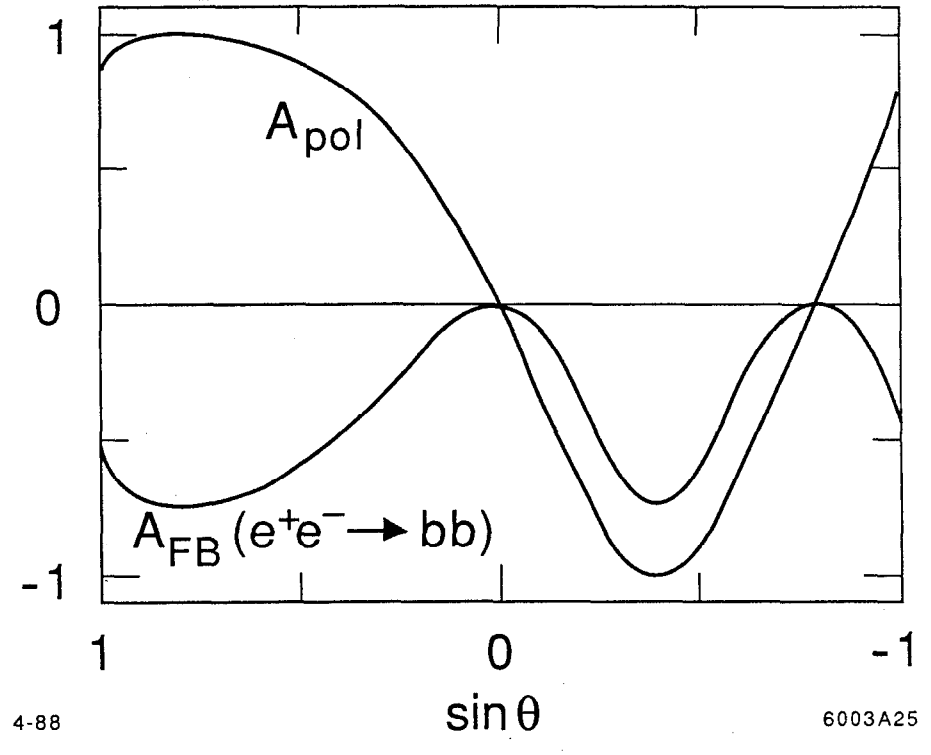

Figure 66. The polarization asymmetry and the forward-backward asymmetry for b quark pair production at the Z' resonance, for a Z' coupling according to eq. (6.1).

for any value of θ. Fig. 66 shows the values of the reamining two asymmetries as a function of θ. Lynn, Stuart, and Cvetič[72] have considered the comparison of these asymmetries for more general coupling schemes of the Z'.

As an example of their analysis, we present in Fig. 67 the comparison of the b quark forward-backward and polarization asymmetries for the various models that

they consider. It is clear that these asymmetries combine into an incisive tool for analyzing the nature of the new resonance.

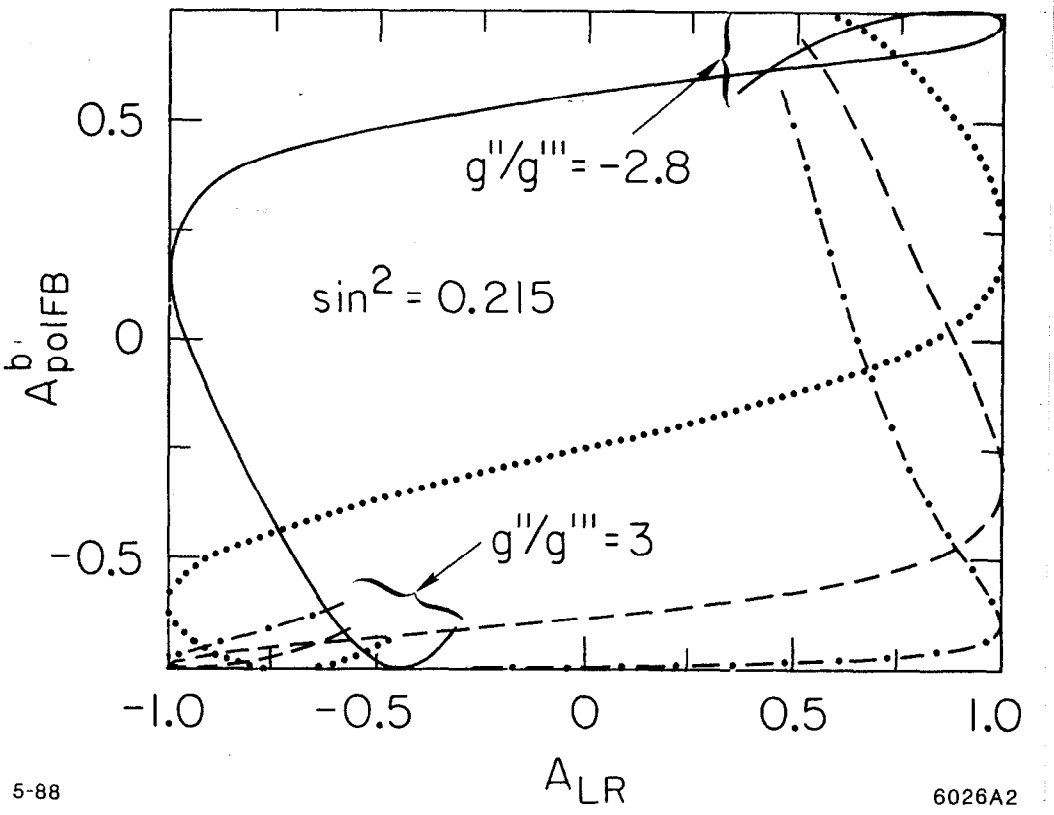

Figure 67. Comparison of the polarization asymmetry and the forward-backward asymmetry for b quark pair production at the Z' resonance, for variety of schemes for the Z'coupling considered in ref. 72.

7. W Boson Pair-Production

We have already emphasized in Section 3 that W boson pair production is a prominent process in high-energy e^+e^- physics, with the largest total cross section of any single annihilation process. In Sections 4 and 5, we encountered W pair production as a background to new physics. But it is important to note that W pair production is, in its own right, a process of great physical interest. Generically, for charged massive vector bosons, the tree-level pair production cross section violates unitarity. This phenomenon, in fact, presented a serious and longstanding problem to the theory of weak interactions. It was resolved only when gauge-theory models of the weak interactions were invented, and the resolution of the problem required the detailed structure of weak boson couplings given by the gauge theories.[73] This unusual feature makes the cross section for $e^+e^- \to W^+W^-$ especially sensitive to corrections to the form of the W couplings, stemming either from modifications of the standard model or from radiative corrections due to new heavy species.

It is not difficult to understand the feature of the $e^+e^- \to W^+W^-$ amplitude which leads to this sensitive dependence on the couplings. At leading order, W pair production arises from the Feynman diagrams of Fig. 68. The contribution from the first of these diagrams, with s-channel photon exchange, is very easy to estimate; it should give roughly the standard result for scalar boson pair-production, times a product of polarization vectors.

$$\frac{d\sigma}{d\cos\theta} \sim \frac{\pi\alpha^2}{4s}\sin^2\theta \cdot |\epsilon(k_+)\cdot\epsilon(k_-)|^2 \ , \tag{7.1}$$

in units of R, where $\epsilon^\mu(k_+)$ and $\epsilon^\mu(k_-)$ are the polarization vectors for the produced W bosons. If the W bosons are transversely polarized, their dot product is of

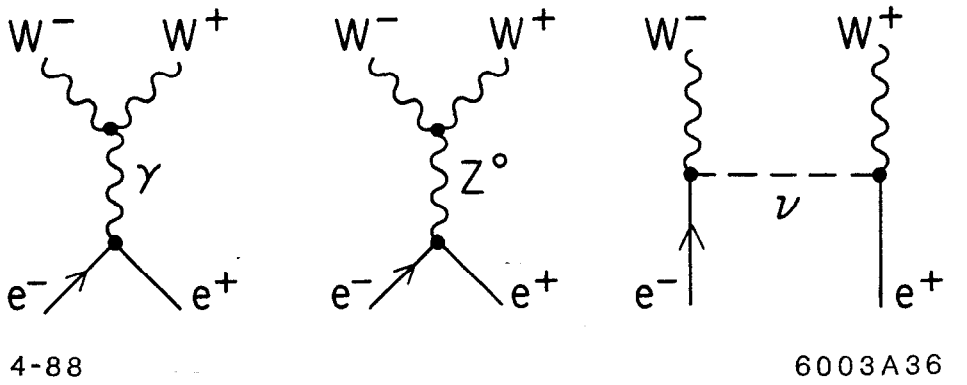

Figure 68. Feynman diagrams contributing to $e^+e^- \to W^+W^-$ in leading order.

order 1, but massive W bosons also possess a longitudinal polarization state, with polarization vector

$$\epsilon(k_+) \;=\; (\frac{k_+}{m_W}, 0, 0, \frac{E_+}{m_W}) \;. \tag{7.2}$$

The Lorentz scalar product of the two longitudinal polarization vectors is of order s/m_W^2, and so the differential cross section grows proportional to s^2 in units of R or proportional to s in absolute units. This behavior violates unitarity. In a generic theory of W bosons, one can do nothing but watch the cross section increases until the W bosons become a strongly-coupled system at high energy. However, in the standard weak interaction gauge theory, the unitarity-violating terms in the three diagrams shown in Fig. 68 conspire to cancel exactly, producing a differential cross section which is asymptotically constant in units of R. This means that any small corrections to the standard model which do not obey the unitarity cancellation can have dramatically magnified effects. Let us now discuss how to parametrize such effects, and how to measure them.

7.1. Phenomenology of W Boson Pair-Production

The cross section for $e^+e^- \to W^+W^-$ is built up as a composite of several components. In one view, the process is built up from the interference of s- and t-channel exchanges, as shown in Fig. 68. In another view, the process can be thought of as the sum of the pair-production of transverse and longitudinally polarized W bosons, with a small addition of the mixed combinations. The two major processes have quite different physics: The production of transversely polarized W bosons is quite similar to the reaction $e^+e^- \to \gamma\gamma$ and has a pronounced forward peak due to the t-channel ν exchange contribution. The production of longitudinally polarized W bosons is complicated by the unitarity cancellation described in the previous paragraph but, after this cancellation, it has a smooth angular dependence, proportional to $\sin^2\theta$ at high energies. To discuss W pair production concretely, we should present a formalism which allows us to disentangle these contributions.

Hagiwara, Peccei, Zeppenfeld, and Hikasa[74] have shown that the structure of W pair production is conveniently analyzed in terms of form factors for the $WW\gamma$ and WWZ vertices. The contribution of the s-channel diagrams, containing arbitrary values for the possible form factors, can be superposed on the contribution from the neutrino exchange diagram. This latter contribution, which involves a well-studied coupling at low momentum transfer, is relatively insensitive to new physics. Let us set up the kinematics of W pair production following this method, but using the slightly different conventions of ref. 75.

To begin, let us parametrize the WWV vertex, for $V = \gamma$ or Z, in terms of form factors f_i^V. For the kinematics shown in Fig. 69, we write the vertex as

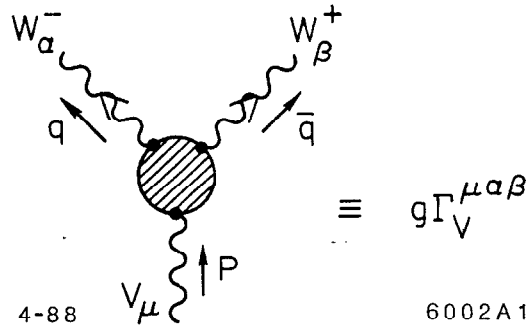

Figure 69. Vertex functions used to define the WWV form factors.

$$
\begin{aligned}
\Gamma_V^{\mu\alpha\beta}(q,\bar{q},P) \;&\equiv\; \sum_{i=1}^{7} f_i^V \cdot T_i \\
&= f_1^V \cdot (q-\bar{q})^\mu g^{\alpha\beta} \;-\; f_2^V \cdot \frac{(q-\bar{q})^\mu P^\alpha P^\beta}{m_W^2} \\
&+ f_3^V \cdot (P^\alpha g^{\mu\beta} - P^\beta g^{\mu\alpha}) \;+\; f_4^V \cdot i(P^\alpha g^{\mu\beta} + P^\beta g^{\mu\alpha}) \\
&+ f_5^V \cdot \epsilon^{\mu\alpha\beta\rho}(q-\bar{q})_\rho \;+\; f_6^V \cdot i\epsilon^{\mu\alpha\beta\rho}P_\rho \\
&+ f_7^V \cdot (-i)\frac{(q-\bar{q})^\mu \epsilon^{\alpha\beta\rho\sigma}P_\rho (q-\bar{q})_\sigma}{m_W^2}
\end{aligned}
\tag{7.3}
$$

The form factors are dimensionless functions of s. The three form factors f_4, f_6, and f_7 multiply CP-violating structures and will be ignored from here on. The s-channel exchanges of γ and Z^0 are added coherently by defining the combinations

$$
F_i \;=\; Q f_i^A \;+\; \frac{(I_3 - \sin^2\theta_w\, Q)}{\sin^2\theta_w}\left(\frac{s}{s-m_Z^2}\right) f_i^Z \;,\; i = 1,\cdots,7, \tag{7.4}
$$

where I_3 and Q are the weak isospin and electric charge of the annihilating fermions. In the standard model, at tree level,

$$
\begin{aligned}
\text{for } e_L^- : \quad F_1 \;&=\; \frac{1}{2}F_3 \;=\; -1 \;+\; \left(-\frac{1}{2\sin^2\theta_w}+1\right)\frac{s}{s-m_Z^2} \\
\text{for } e_R^- : \quad F_1 \;&=\; \frac{1}{2}F_3 \;=\; -1 \;+\; \frac{s}{s-m_Z^2}\;.
\end{aligned}
\tag{7.5}
$$

and all other form factors are zero.

The differential cross sections for annihilation of polarized electrons and positrons into W^+W^- are given in terms of the form factors by

$$\begin{aligned}
\frac{d\sigma}{d\cos\theta} &= \frac{\pi\alpha^2}{2s}\cdot\beta\cdot\Sigma\ ; \\
\Sigma_{TT} &= 2\sin^2\theta\left[\mid A_1\mid^2 -(A_1A_2^* + A_2A_1^*)\cos\theta + |A_2|^2(1+2\cos^2\theta)\right] \\
\Sigma_{TL} = \Sigma_{LT} &= \mid A_3\mid^2(1+\cos^2\theta) + (A_3A_4^* + A_4A_3^*)\cos\theta\sin^2\theta + |A_4|^2\sin^4\theta \\
\Sigma_{LL} &= \mid A_5\mid^2\sin^2\theta,
\end{aligned} \tag{7.6}$$

where the subscripts T and L denote transverse and longitudinal polarization of the W bosons. Two possible states of initial polarization contribute. For $e_R^- + e_L^+$, the neutrino-exchange diagram does not contribute and so the coefficients A_j are built entirely from the F_i:

$$\begin{aligned}
A_1 &= \beta\cdot F_1 \\
A_2 &= 0 \\
A_3 &= \frac{\beta^2\sqrt{s}}{m_W}\left[\frac{F_3}{2} + \frac{\beta\cos\theta}{2}\cdot F_5\right] \\
A_4 &= +\frac{\beta^2\sqrt{s}}{2m_W}\cdot F_5 \\
A_5 &= \beta\frac{s}{m_W^2}\left[\frac{F_3}{2} - \left(\frac{1}{2} - \frac{m_W^2}{s}\right)\cdot F_1 + \frac{\beta^2}{4}\frac{s}{m_W^2}\cdot F_2\right]
\end{aligned} \tag{7.7}$$

where β is the W velocity: $\beta = (1-4m_W^2/s)^{\frac{1}{2}}$. For $e_L^- + e_R^+$, we must add the

contribution of the neutrino-exchange diagram to form

$$
\begin{aligned}
A_1 =& \beta \cdot F_1 + \frac{\beta}{2\sin^2\theta_w \mathcal{D}} \\
A_2 =& \frac{1}{2\sin^2\theta_w \mathcal{D}} \\
A_3 =& \frac{\beta\sqrt{s}}{m_W}\left[\frac{F_3}{2} - \frac{\beta\cos\theta}{2}\cdot F_5 + \frac{1}{2\sin^2\theta_w} + \frac{m_W^2}{\sin^2\theta_w \beta^2 s}\left(1 - \frac{2m_W^2}{s\mathcal{D}}\right)\right] \\
A_4 =& -\frac{\beta^2\sqrt{s}}{2m_W}\cdot F_5 + \frac{m_W}{\sin^2\theta_w\sqrt{s}\mathcal{D}} \\
A_5 =& \beta\frac{s}{m_W^2}\left[\frac{F_3}{2} - \left(\frac{1}{2} - \frac{m_W^2}{s}\right)\cdot F_1 + \frac{\beta^2}{4}\frac{s}{m_W^2}\cdot F_2 + \frac{1}{4\sin^2\theta_w}\right. \\
& \left. + \frac{1}{\beta^2\sin^2\theta_w}\frac{m_W^2}{s}\left(1 - \frac{2m_W^2}{s\mathcal{D}}\right)\right]
\end{aligned}
\tag{7.8}
$$

where β is as above and

$$
\mathcal{D} = \frac{1}{2}(1 + \beta^2 - 2\beta\cos\theta). \tag{7.9}
$$

The various cross sections to different W polarizations states, computed at 1 TeV for polarized electrons on unpolarized positrons, are shown in Fig. 70. Note that the annihilation cross sections for e_R^- are very small throughout the whole angular range. The final states with mixed (LT) W polarization can also be ignored to a first approximation. This leaves as the two major components of the cross section the transverse and longitudinal W pair production, whose forms we have described at the beginning of this section. Since the production of longitudinal bosons is more sensitive to the effects of new physics, it is important to note that the cross section for transverse W production is larger over the whole angular range. The longitudinal W pairs make up only about 25% of the cross section in the backward hemisphere and are completely swamped in the forward peak.

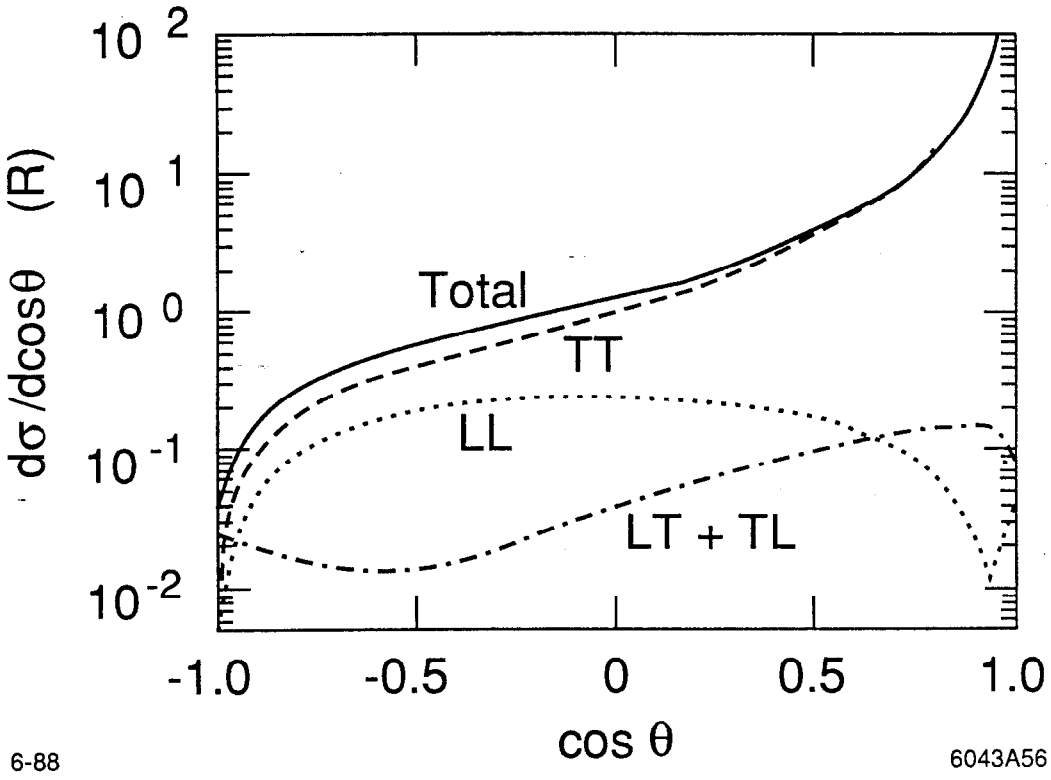

Figure 70. Differential cross sections for $e^+e^- \to W^+W^-$ corresponding to W boson states of definite polarization, (as in eq. (7.6)), computed at $\sqrt{s} = 1$ TeV.

To separate the longitudinal and transverse production experimentally, one needs to measure some additional parameter of the produced particles. The most convenient probe makes use of the lepton emitted in the decay $W \to \ell\overline{\nu}$. Let χ be the angle between the lepton momentum and the W momentum, measured in the W rest frame. The angular distribution in χ peaks about $\cos\chi = 0$ for longitudinally polarized W bosons, and at forward or backward angles for transversely polarized bosons. Further, the parity violation of the W couplings distinguishes the two transverse polarization states, making the decay lepton an even more effective polarimeter. We will argue in the next section that, even in the presence of beamstrahlung, the full kinematics of W pair-production and decay can be reconstructed for events with a leptonic decay on one side and a hadronic decay on the other. This topology accounts for about 40% of all W pair events and so provides

a large sample for analysis. The explicit formula for the χ distribution in terms of the form factors F_i is the following:

$$\begin{aligned}
&\frac{d\sigma}{d\cos\theta d\cos\chi}(e^+e^- \to W^+\ell^-\overline{\nu}) \\
&= \frac{3\pi\alpha^2}{8s}\cdot\beta\cdot \mathrm{BR}(W^-\to\ell^-\overline{\nu}) \\
&\qquad \cdot\Big[\Sigma_{TT}\cdot(1-\frac{1}{2}\sin^2\chi)\pm 4\cos\theta\sin^2\theta|A_2|^2\cdot\cos\chi \\
&\qquad +\Sigma_{LT}\cdot(1+\frac{1}{2}\sin^2\chi)\pm\left(2\cos\theta|A_3|^2+\sin^2\theta(A_3A_4^*+A_4A_3^*)\right)\cdot\cos\chi \\
&\qquad +\Sigma_{LL}\cdot\sin^2\chi\Big],
\end{aligned} \tag{7.10}$$

where the A_j are the same coefficients that appeared in (7.6) and the upper (lower) signs refer to $e_L^-e_R^+$ ($e_R^-e_L^+$). The same formula gives the χ distribution in $e^+e^-\to W^-\ell^+\nu$ from each polarization state. In Fig. 71, we plot the χ distributions predicted by the standard model tree level cross section at three values of $\cos\theta$. The figure shows clearly the dominance of the transverse polarization state at forward angles, and the increasing importance of the longitudinal polarization state near $\cos\theta = 0$.

To give an idea of the sensitivity of the W cross section to new physics, let us consider the effects of three modifications of the W form factors from the standard model form. As a first example, we consider a deviation of the WWV couplings from their gauge-theory form of a sort that might be generated by a W substructure. We will study one particular case here; a more extensive analysis along these lines has been presented in ref. 76. Let us assume that the W boson has a small anomalous magnetic moment, and that this magnetic moment is of fundamental character, so that it is visible at large Q^2. As a model of this effect, we may modify

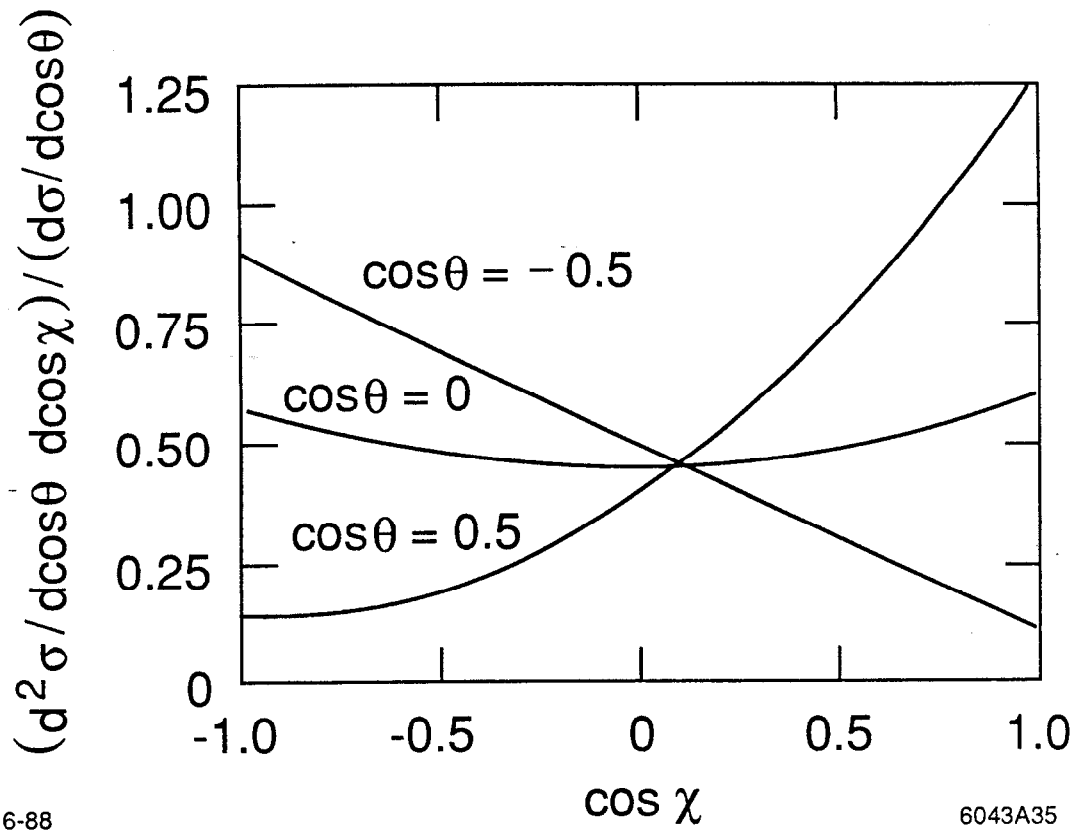

Figure 71. Distribution of lepton decay angles χ for pair produced W bosons, computed at $\sqrt{s} = 1$ TeV and three values of $\cos\theta$. Each curve is normalized to enclose a total area of 1.

the W form factors according to

$$\begin{aligned} F_1 &= \frac{1}{\sin^2\theta_w} I_3 \frac{s}{s - m_W^2} + Q\left(1 - \frac{s}{s - m_Z^2}\right) \\ F_3 &= F_1 \cdot \left(1 + \frac{g-2}{2}\right) . \end{aligned} \tag{7.11}$$

Note that we have assumed the same modification of the photon and Z^0 vertices; this insures that the amplitude for $e_R^- e_L^+$ annihilation still substantially cancels. This choice is, then, a conservative one. Inserting the expresssions (7.11) into (7.6), we see that the unitarity cancellation is not complete in the $e_L^- e_R^+$ amplitude, and so

the amplitude for longitudinal W production is enhanced by a factor proportional to

$$(g-2)\cdot\frac{s}{m_W^2}\,. \tag{7.12}$$

This enhancement can be substantial even for small values of $(g-2)$. Fig. 72 shown the size of this effect at .1 TeV; the effect of the nonzero $(g-2)$ is both to raise the differential cross section and to distort it into the $\sin^2\theta$ pattern characteristic of longitudinal W production.

The second modification that we will consider is one which assumes the gauge boson couplings of the standard model but adds in a new generation of heavy quarks and leptons. This situation is especially interesting in the case that the new fermions are too heavy to be pair-produced at a 1 TeV e^+e^- collider. However heavy these fermions might be, they can affect the process of W pair production through radiative corrections. Ordinarily, one thinks of radiative corrections as contributing only small effects, but the situation here is an especially favorable one. In a parity-conserving field theory, radiative corrections at an energy $\sqrt{s}$ due to heavy particles of mass M are always suppressed by a factor (s/M^2).[77]

However, in theories with chiral gauge couplings, this suppression is often absent. This is the situation for radiative corrections to the W boson mass and the Z^0 polarization asymmetry in standard weak interaction theory. For W pair production, we must take account of a further effect. Except for corrections to the external legs, the radiative corrections to the W pair production amplitude affect only the s-channel diagrams, correcting the intermediate boson propagators and the 3-boson vertices. Though these two contributions should cancel to preserve unitarity at asymptotic s, there is no reason to expect a unitarity cancellation among the loop corrections for $s < M^2$, even when $s >> m_W^2$. Thus, the radiative corrections to W pair production due to new heavy fermions should be of order

$$\frac{\alpha}{\pi}\cdot\frac{s}{m_W^2}\,, \tag{7.13}$$

a substantial enhancement.

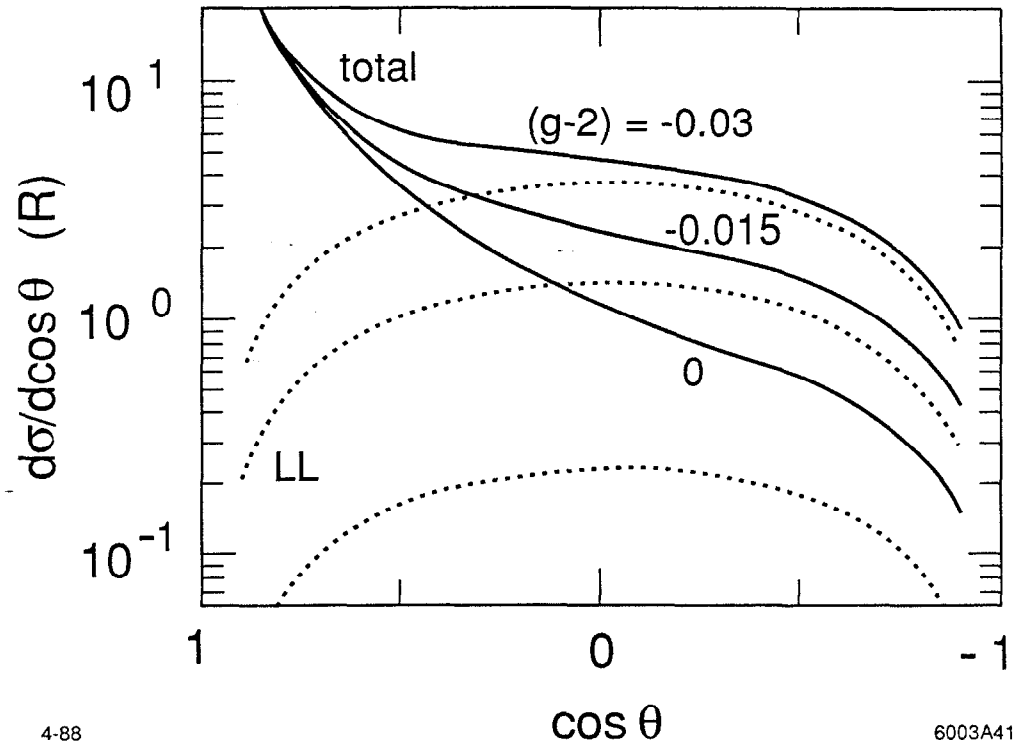

Figure 72. Effect on the differential cross section for $e^+e^- \to W^+W^-$ of an anomalous magnetic moment for the W boson, introduced according to eq. (7.11). The curves are drawn for $\sqrt{s}$= 1 TeV, $\cos\theta = 0$. The dotted curves show the contribution from longitudinal W bosons only.

The corrections to the W form factors due to a new heavy generation have been computed in ref. 75. The results of this calculation are shown in Figs. 73–75. Fig. 73 shows the effect on the differential cross section at $\cos\theta = 0$ of a new heavy generation. We should note that, though our results are quantitative for fermions of mass less than 400 GeV, they are only qualitative above that point because they ignore the strong couplings of such heavy fermions to the Higgs sector. However, they indicate substantial, and approximately mass-independent corrections, for fermions of mass well above the value necessary to be seen directly at the e^+e^- collider.

For the 750 GeV curve in Fig. 73, the enhancement is roughly 5% of the total cross section for $\cos\theta < 0.4$. Since the enhancement (7.13) is associated with the

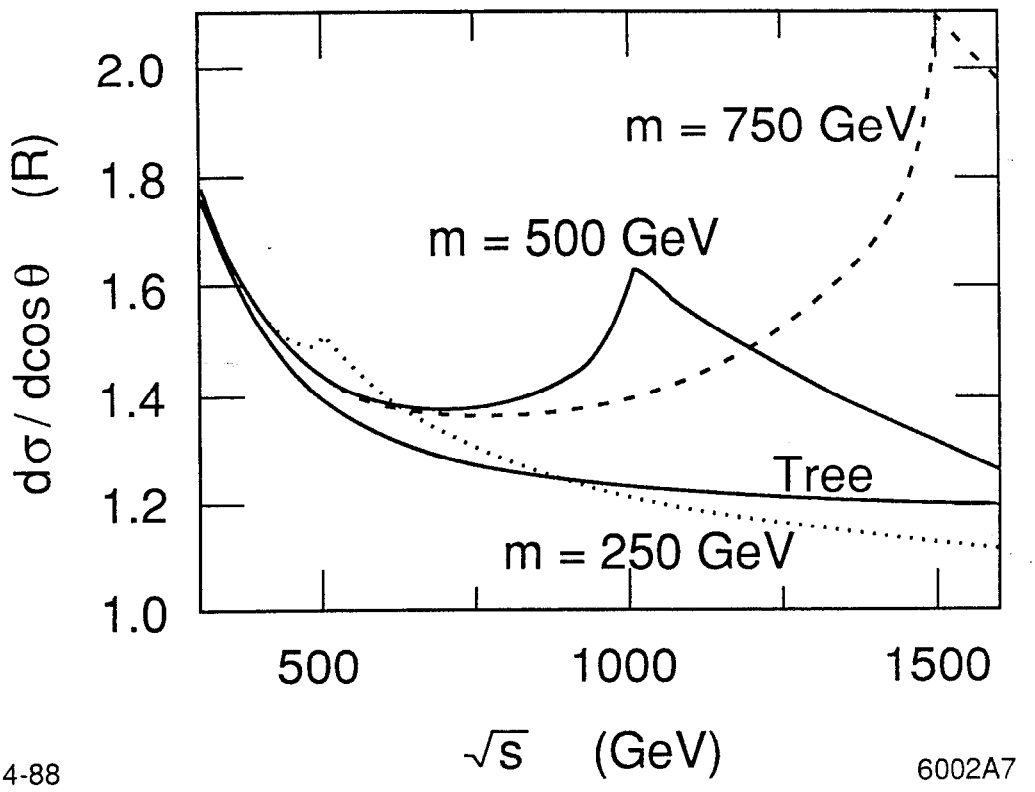

Figure 73. Effect on the differential cross section for $e^+e^- \to W^+W^-$, at $\cos\theta = 0$, of an additional generation of heavy quarks and leptons. The heavy fermions are assumed to be degenerate, with the indicated masses.

failure of a unitarity cancellation, it should act almost entirely on the production of longitudinally polarized W bosons. Thus, the effect should also be visible, in an orthogonal way, in the χ distribution. Fig. 74 shows this effect of heavy fermion radiative corrections on the χ distribution at $\cos\theta = 0$ and 1 TeV in the center of mass. Fig. 75 shows the effect on the differential cross section of a generation of fermions with 100 MeV isospin splitting; the effect is quite similar to that from degenerate fermions, with only some splitting of the threshold peak.

The last of our three examples is another case of using measurements at 1 TeV to survey new phenomena at still higher energies.

To understand this case, one must recall that, in the Higgs mechanism, the lon-

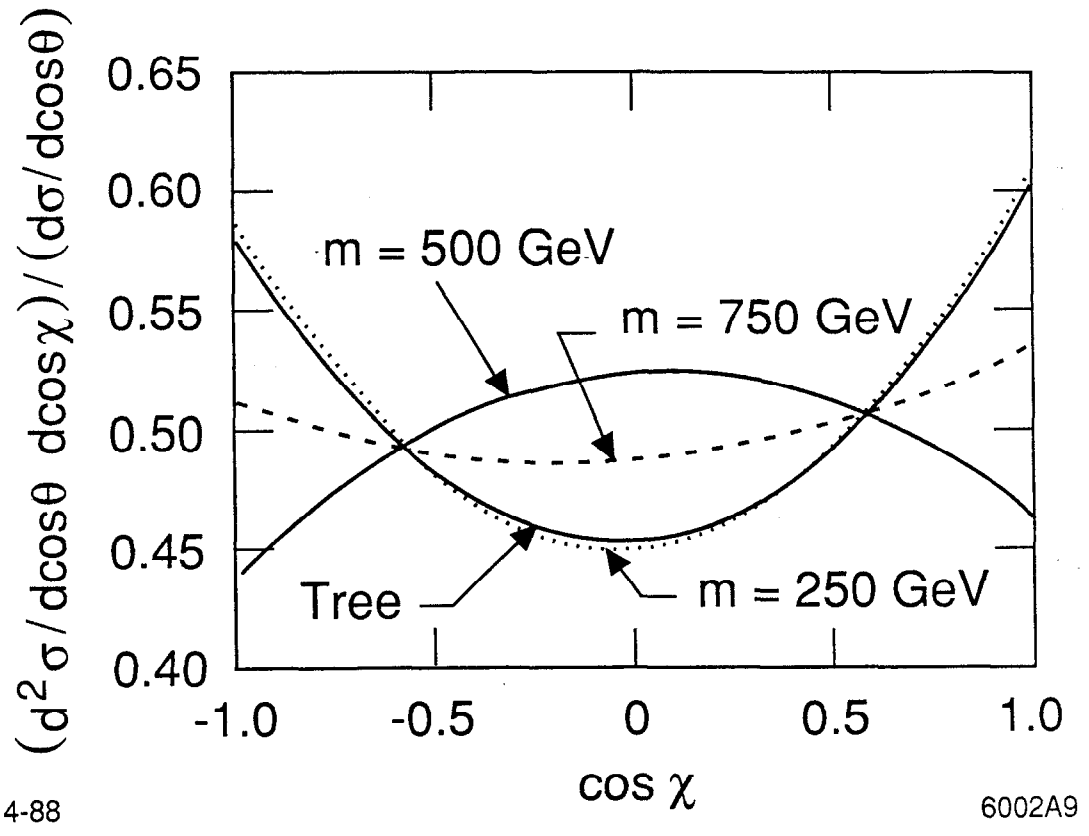

Figure 74. Effect of a new heavy generation of fermions on the distribution of lepton decay angles χ, at $\sqrt{s} = 1$ TeV and $\cos\theta = 0$. The curves are normalized as in Fig. 71.

gitudinal polarization states of massive vector bosons arise from the Higgs sector. This means that if the Higgs sector becomes strongly coupled above 1 TeV, longitudinal W bosons will share in these strong interactions. In technicolor models of the weak-interaction symmetry breaking, the Higgs sector is a strongly coupled gauge theory similar to the conventional strong interactions, with a rho resonance at 1.8 TeV (or lower, in more elaborate models). This state appears as a resonance in the $I = J = 1$ channel of two longitudinal W bosons. Including this resonance as a final-state interaction in $e^+e^- \to W^+W^-$, with a mass and width scaled from the conventional strong interactions,[78] we find the effect on the differential cross section at $\cos\theta = 0$ shown in Fig. 76. Since the entire effect comes from the production of longitudinal W bosons, we might expect that this effect is also visible in

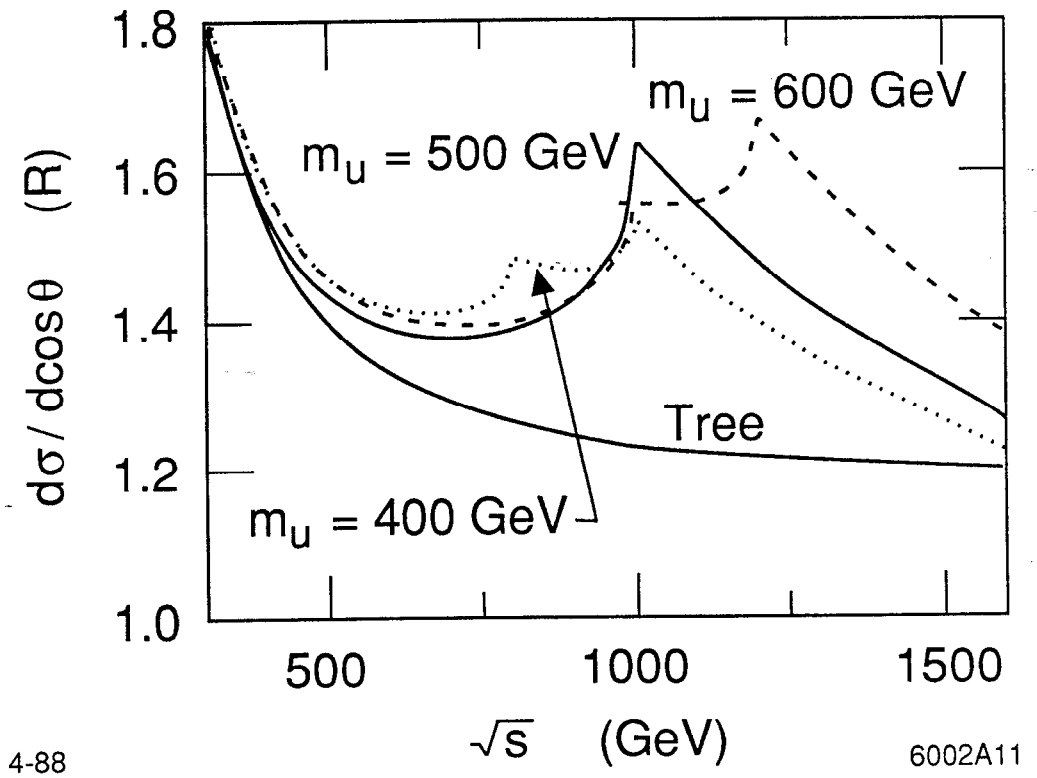

Figure 75. Effect on the differential cross section for $e^+e^- \to W^+W^-$, at $\cos\theta = 0$, of an additional generation of heavy quarks and leptons, computed for $m_D = 500$ GeV, $m_U = 400, 500, 600$ GeV.

the χ distribution, and we show that in Fig. 77. In this example and the previous one, we can see clearly that the differential cross section for $e^+e^- \to W^+W^-$ is a powerful tool not only for scanning downward from the center of mass energy of an e^+e^- collider, but also for scanning upward to new phenomena above 1 TeV.

7.2. Determination of the W^+W^- Differential Cross Section

To realize the potential of the experiments discussed in the previous section, it is necessary to be able to measure the W boson pair-production cross section accurately in the presence of realistic smearing effects and substantial beamstrahlung. In this section, we will argue that this task is actually quite straightforward, and that strong constraints can be placed on the models just discussed with a data

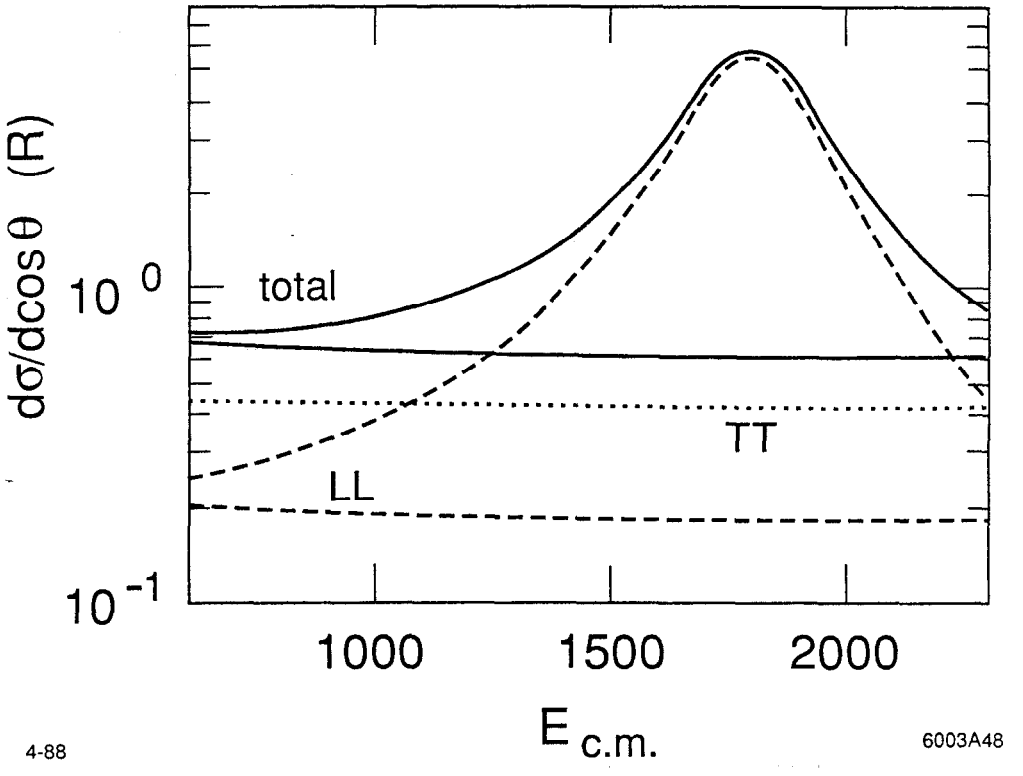

Figure 76. Effect of the technicolor rho resonance, in the minimal scheme of technicolor, on the differential cross section for $e^+e^- \to W^+W^-$ at $\cos\theta = -0.5$. The dashed line indicates the contribution from longitudinally polarized W bosons alone.

sample of 30 fb^{-1}.

The analysis that we will present should be considered only a first attempt to extract the full information which is available. In principle, one can extract the angular distribution for W pair production either from events in which both W's decay hadronically or from events in which one W decays hadronically and one leptonically. The case of hadronic decays on both sides has slightly higher background. It also has the important disadvantage that it is not straightforward to measure the charge of each W and thus to resolve whether the W^- is produced forward or backward. Since the angular distribution of W's has a large forward peak due to conventional transverse boson production, one loses some of the the power to discriminate models if one cannot distinguish backward from forward

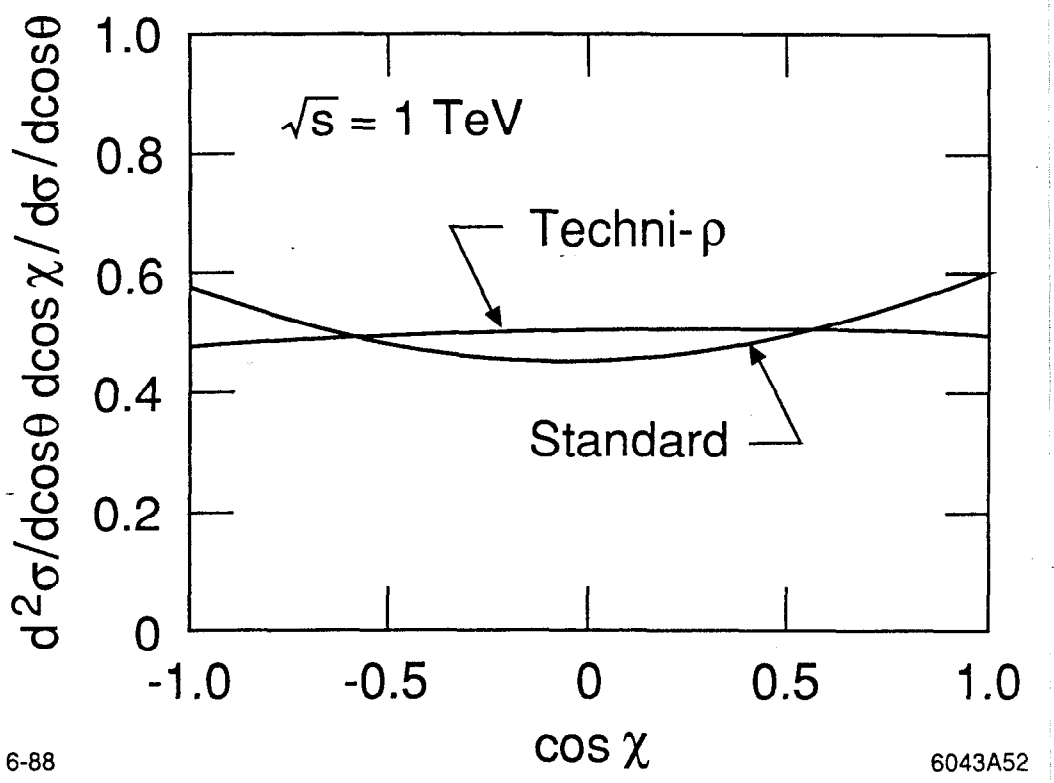

Figure 77. Effect of the presence of the technicolor rho resonance on the distibution of lepton decay angles χ, at $\cos\theta = 0$ and $\sqrt{s} = 1$ TeV. The curves are normalized as in Fig. 71.

production. Our studies suggest that one can determine the charge of each W, making the wrong choice in only a few percent of the cases, by dividing the event into hemispheres and counting the charge in each hemisphere.[8] However, this analysis will concentrate on events with leptons on one side, for which the assignment of the W signs is completely clear. In addition, this analysis concentrates on the $\cos\theta$ distribution of W pairs; we have not attempted to extract the additional information available in the $\cos\chi$ distribution.

The most important complication in this measurement is the beamstrahlung, which leads to substantial smearing of the center of mass energy of annihilation, and to arbitrary boosts along the beam axis (which we take to be the z axis) when particles of unequal energy collide. If we did not correct for this effect, it would

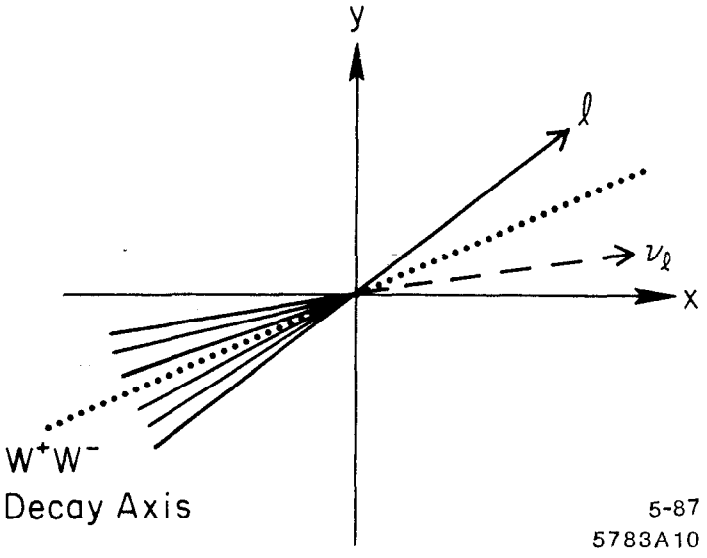

Figure 78. Transverse plane of an $e^+e^- \to W^+W^-$ event with one leptonic and one hadronic decay. The transverse momentum of the neutrino must be chosen so that the transverse momentum of the leptons balances that of the hadrons.

produce a severe distortion of the measured angular distribution of W pairs.

To study this problem, we re-examined the W pair events generated according to the standard model through the simulation described in Section 3. The simulation used the beamstrahlung spectrum with $\delta = 0.26$ shown in Fig. 4. Smearing due to the detector was modelled as described in Section 3. In this event sample, we sought to isolate events containing a a di-jet from the decay of one W, and an isolated lepton and escaping neutrino from the other W.

We begin by analyzing each event in the plane transverse to the beam axis. The configuration expected for a W^+W^- event is shown in Fig. 78. The analysis makes use of $\ell = e$ or μ only. An isolated lepton is required by demanding that there be less than 2 GeV of additional energy within a 30° cone centered on the lepton. We then perform a cluster analysis with a minimum separation of 15 GeV between clusters. Each cluster is required to have $|\cos\theta| < 0.75$, and it is demanded that there be two clusters with a combined invariant mass within 10 GeV of the W mass. The invariant mass of the leptonic decay is insensitive to boosts along the

z-axis; thus,

$$M_{\ell\nu}^2 = M_W^2 = (E_\ell + E_\nu)^2 - (p_{\ell x} + p_{\nu x})^2 - (p_{\ell y} + p_{\nu y})^2 - (p_{\ell z} + p_{\nu z})^2.$$

Using this equation, and knowing that the transverse momentum of the hadronic side must be balanced by the transverse momentum on the leptonic side, one can derive a quadratic equation for $p_{\nu z}$. We reject events which give imaginary values of $p_{\nu z}$. In cases where there are two real solutions, we resolve the quadratic ambiguity by choosing the smaller value of $|p_\nu|$. We then boost the event along the z-axis so that $\sum \vec{p}_z = 0$, where the sum includes p_ν. Finally, using the sign of the lepton charge, we determine θ as the angle between the W^+ and the incoming e^- beam in the center of mass frame.

This analysis is almost completely clean. The background from quark-pair production is less than 0.1%; another 0.1% comes from Z-pair production. The branching fractions of W-decay show that 25% of W's produced should result in one W decaying into hadrons and the other decaying into e or μ. This analysis results in an efficiency of 22% to find these W-pairs in the region of interest. This fairly low efficiency is caused by the stringent cuts to keep the angular distribution uncontaminated by backgrounds. Figs. 79 and 80 show the resultant measured angular distribution with the overall luminousity normalization fit to the theory curves to compare shapes only. The statistical errors correspond to a data set of 30 fb^{-1}. The roll-off of the measured points for $\cos\theta > 0.65$ is due to some particles escaping through the simulated 10° hole in the detector.

To quantify the sensitivity of this analysis to new physics, we fit the Monte Carlo data to theoretical angular distributions in the region $|\cos\theta| < 0.65$. The generator used to produce the four-vectors contained the standard model only. By forming a χ^2 between the data and the standard model distribution, we found that the data is consistent with the input distribution at the 90% confidence level, as expected. The presence of a new heavy generation of fermions changes the differential cross section as shown in Fig. 79. Fitting the overall luminousity

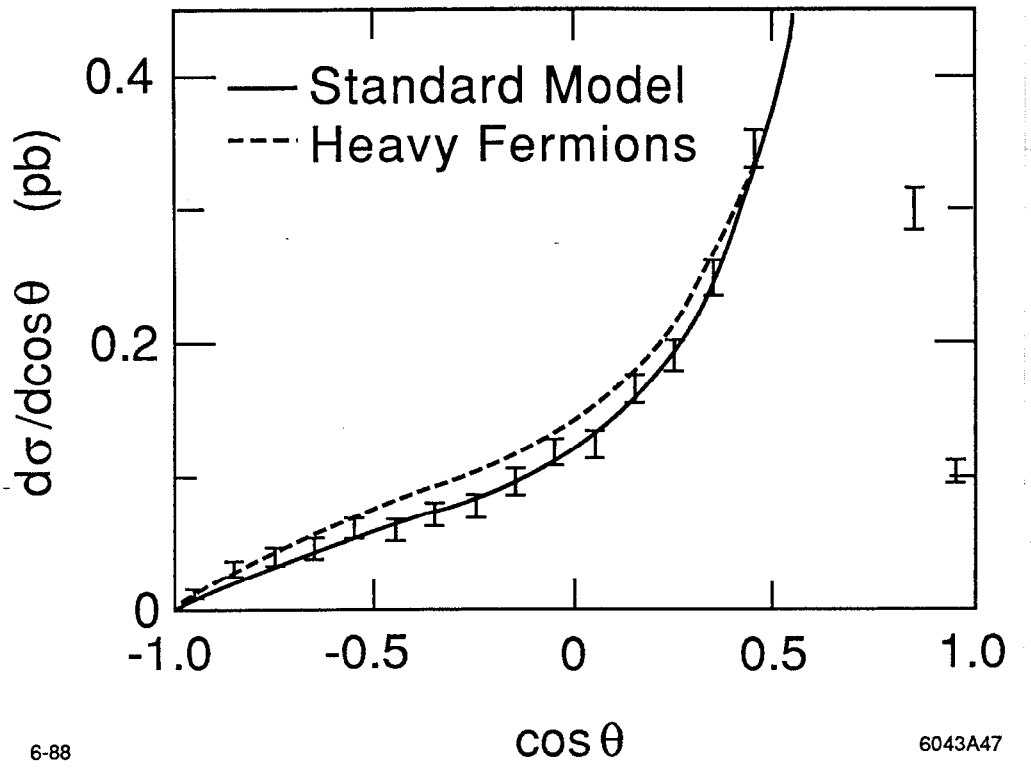

Figure 79. The reconstructed angular distribution of W pairs from events in which one W decays hadronically and the other W decays leptonically. The solid line shows the input (standard model) distribution; the dashed curve indicates the prediction for a new heavy fermion generation with mass 600 GeV.

normalization of the data to curves for different fermion masses, given by the calculations of ref. 75, we were able to exclude a new heavy generation of fermions of mass less than 700 GeV at the 95% confidence level. This demonstrates the ability of this measurement to detect masses of fermions greater than half the center of mass energy. In a similar way, we fit the Monte Carlo distributions to the model discussed in the previous section which gave an anomalous magnetic moment for the W. We found that a value of $(g-2)$ of greater than 0.03 could be excluded at the 95% confidence level using a data set of 30 fb^{-1}.

The variation of the differential cross section with new physics lies almost completely in the contribution of the longitudinally polarized W's. We have argued

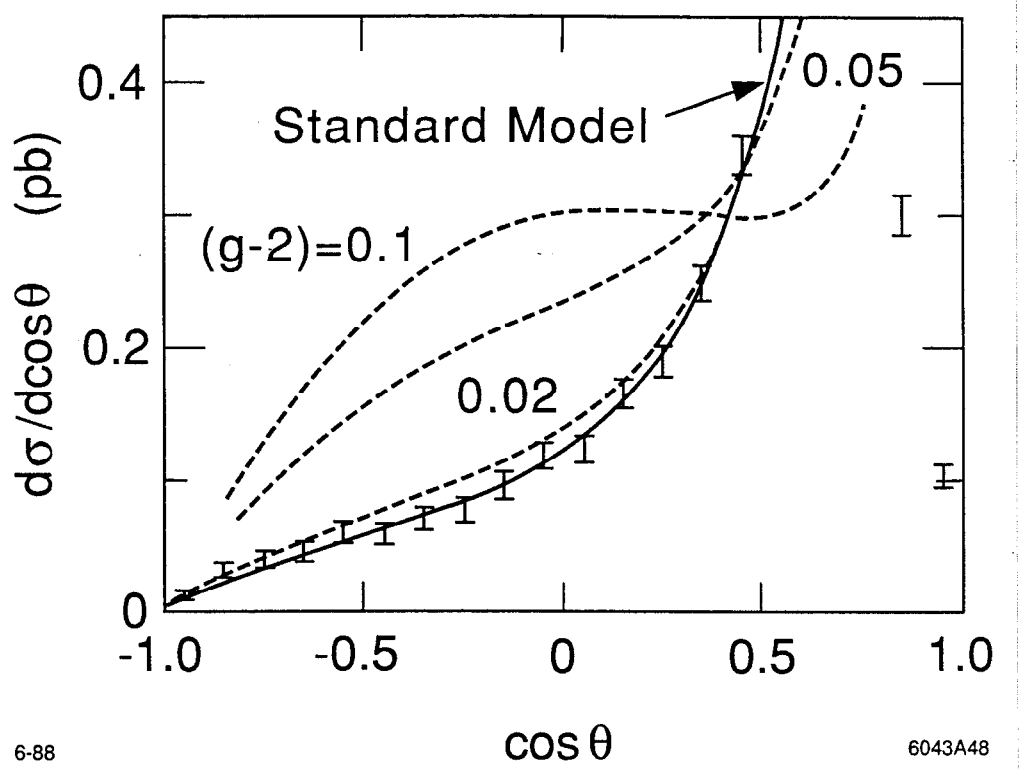

Figure 80. The reconstructed angular distribution of W pairs from events in which one W decays hadronically and the other W decays leptonically. The solid line shows the input distribution and the dashed curve shows the predictions for W anomalous magnetic moment, in the model of eq. (7.11).

in the previous section that the fraction of longitudinal W bosons in the sample is enhanced by cutting on the decay angle χ to select a region near $\cos\chi = 0$. Our preliminary studies show that it may be possible, by measuring the χ distribution, to determine directly the cross section for producing longitudinally polarized W's. This quantity would be of direct interest in probing variations of the standard model. We regard this as an important issue for further investigation.

8. TeV Multiplet Searches I: Supersymmetry

Thus far in this report, we have been discussing searches for components of the weak-interaction gauge theory or direct manifestations of corrections to this theory at high energies. However, as we made clear in Chapter 2, the new physics which should appear at energies beyond the Z^0 may be considerably more complex in character. If one postulates a new set of forces which cause the spontaneous breaking of the weak interaction symmetry, this set of forces will have their own intricate dynamics and will produce their own spectrum of particles. In this case, we expect a whole multiplet of new particle states. In the last two chapters of this report, we would like to discuss two examples of new particle types which might be associated with such an extended Higgs sector and to explain with care how these particles can be discovered at a 1 TeV e^+e^- collider.

The first of our examples will be the extension of the standard model by the inclusion of supersymmetry, a fundamental symmetry between boson and fermion states. Supersymmetric theories are the most highly developed examples of the weak-coupling scenario for the Higgs sector discussed in Chapter 2. They are the only known models of the weak-coupling type which can incorporate grand unification at very high energies and naturally maintain the large separation between the energy scale of this grand unification and the scale of weak interaction symmetry breaking. In principle, one can imagine a model with fundamental supersymmetry which is broken at the grand unification scale or the Planck scale, but in order for supersymmetry to be relevant to the Higgs problem, it must remain an exact symmetry down to energies of order 1 TeV. Models of this type, often called models of "low-energy supersymmetry", will be our focus here.

If supersymmetry is still essentially exact at 1 TeV, we should find a complete

multiplet containing the known elementary particles and their supersymmetry partners at energies below this scale. Beyond this general constraint, though, not much is known about where the new states should be found. Bounds from current experiments imply that squarks and gluinos must be heavier than about 60 GeV,[79] and (charged) sleptons are heavier than about 20 GeV.[80] Other limits exist, although they are rather complicated, since they usually depend on other assumptions, such as the existence of at least one extremely light superpartner. Thus there is still much freedom in the supersymmetric approach, and it is unclear at what mass supersymmetric particles will be first discovered.

Despite the uncertainty of the supersymmetric masses, there is one particle in the supersymmetric picture which must be rather light— the lightest neutral scalar Higgs boson. In the minimal supersymmetric extension of the standard model (with only Higgs doublets), it can be proved[25,26] that one scalar Higgs must exist which is lighter than the Z. In non-minimal models, this result is somewhat modified. Nevertheless, if a few very reasonable assumptions are made, it can be shown that in a wide class of non-minimal supersymmetric models with Higgs singlets as well as Higgs doublets, the lightest scalar Higgs must still have mass less than $\mathcal{O}(m_Z)$.[27] Thus, the non-observation of a Higgs boson at LEP-II would put rather tight constraints on the possible supersymmetric parameters. Furthermore, the above argument would suggest that if the "low-energy" supersymmetric approach is correct, then one is guaranteed that the Higgs boson should be discovered at the e^+e^- collider we consider here if it has not already been seen at the lower energy e^+e^- colliders. This fact will also have consequences for the search for supersymmetric particles, as we shall see below.

Thus, the first evidence for supersymmetry which will be discovered may well be a light scalar Higgs boson! Of course, a convincing discovery of supersymmetry requires the observation of the supersymmetric partners of the known elementary particles. Three logical possibilities exist. First, supersymmetric particles may have already been discovered at a lower energy collider. Second, supersymmetric particles may be too heavy to be detected at LEP-II or the Tevatron, but will be

observable at 1 TeV. Finally, supersymmetric particles may be still heavier (say, on the order of 1 TeV in mass) and could only be discovered after a further step in energy. This suggests two possible roles for a 1 TeV collider in the investigation of supersymmetry. If no evidence (apart from the possible discovery of a light Higgs scalar) has been uncovered at lower energy colliders, then this machine becomes a tool for the possible discovery of supersymmetry. On the other hand, if we imagine that the first concrete evidence for supersymmetry has already been obtained elsewhere, then the primary function of this collider would be to quantify the evidence for supersymmetry, and begin to assemble more detailed information of the supersymmetric parameters.

8.1. General Expectations for the Spectrum of Superparticles

The standard picture of "low-energy" supersymmetry which has emerged over the last few years is as follows.[81] Supersymmetry is a necessary ingredient for the consistent unification of particle physics and gravity, which takes place around the Planck scale. In recent years, the superstring[82] has attracted a great deal of theoretical attention, as a candidate theory for the unification of particle physics, gravity and quantum mechanics. It is premature to draw any detailed conclusions as to the impact of superstrings on low-energy physics. Nevertheless, the general structure seems fairly straightforward. At the Planck scale, the effective field theory Lagrangian is that of $N = 1$ supergravity. This Lagrangian is in general very complicated, since it is non-renormalizible. But if we ignore interactions of gravitational strength, the resulting effective Lagrangian simplifies considerably. This Lagrangian contains two pieces: one piece with an exact global $N = 1$ supersymmetry, and a second piece consisting of soft supersymmetry breaking terms. If supersymmetry is relevant for explaining the scale of electroweak interactions, then the mass parameters which occur in the soft supersymmetry breaking terms must be of order 1 TeV or below. The goal of any collider which hopes to discover supersymmetry is then to measure the coefficients of these soft supersymmetry breaking terms.

The above description is oversimplified, in that it tacitly assumes that there are only two relevant scales: the Planck scale and the electroweak scale. More complicated models are easily constructed, in which various intermediate scales play important roles. Such questions involve details of model-building, which will initially have a minor impact on the phenomenology. More important is the question of the appropriate electroweak gauge group. In certain approaches inspired by superstring theory,[66] it has been argued that the "low-energy" gauge group must be some subgroup of E_6 which is larger than rank-four. This suggested the possibility that the appropriate electroweak gauge group at the TeV scale is larger than $SU(2) \times U(1)$. In addition to implying the existence of additional Z-bosons, such approaches implied the existence of new fermions (and their supersymmetric partners) in order to fill up the E_6 multiplets. The possibility of extra Z^0 bosons has been considered separately in Chpater 6 of this report. In our analysis of supersymmetry, we shall ignore such enlargements of the low-energy gauge group. Clearly, the discovery of a larger low-energy gauge group will have vast implications for the search for new physics.

We will take a minimalist approach to the study of supersymmetric phenomenology by working with the minimal supersymmetric extension of the standard model.[83] In this model, one takes the standard model as it is known today (including the as yet undiscovered t-quark) and simply adds the corresponding supersymmetric partners. The Higgs sector must be enlarged to two Higgs doublets[25,84] in order to allow for the proper generation of mass for both up-type and down-type quarks and leptons, but no additional Higgs multiplets are added.

Let us discuss some generalities of the mass spectrum expected in a low-energy supersymmetric model. What we present below should only be regarded as a general guide. No model exists today which is so compelling as to rule out other approaches. The basic assumption of the low-energy supersymmetric approach, as summarized above, is that supersymmetry is responsible for the electroweak scale. This implies, very roughly, that supersymmetric particles should have masses within an order of magnitude of the W and Z mass. This is not a very useful

statement as it stands, although at the present time it can only be marginally improved. We quickly survey here the various sectors of supersymmetric particles.

First, consider that gaugino/higgsino sector. This consists of the gluino, two charginos and four neutralinos. The charginos and neutralinos are mass eigenstates which are model-dependent linear combinations of charged and neutral gauginos and higgsinos. In the minimal supersymmetric model, the corresponding mass matrices depend on three unknown mass scales—μ, M_2, and M_1—and on the ratio of the vacuum expectation values of the two Higgs fields,

$$\tan\beta = v_2/v_1 \tag{8.1}$$

where v_1 is the vacuum expectation value of the Higgs field which couples to d-type quarks, and v_2 is the analogous quantity for u-type quarks. Here μ is a supersymmetric Higgs mass parameter and M_2 and M_1 are gaugino mass parameters associated with the $SU(2)$ and $U(1)$ subgroups of the standard model. We will follow the common practice of reducing the number of free parameters by assuming that these latter two mass parameters are related to the gaugino mass of the $SU(3)$ standard model subgroup, M_3 (the gluino mass), by requiring that all three mass scales are equal at some grand unification scale. Then, at the electroweak scale, all three mass parameters can be expressed in terms of one of them, which we choose to be $M_2 \equiv M$. The other two mass scales are given by

$$M_3 \equiv M_{\tilde{g}} = (g_s^2/g^2)M \qquad M_1 \equiv (3/5)M' = (g'^2/g^2)M. \tag{8.2}$$

We will assume that the lightest neutralino is actually the lightest of all superpartners, a state we call the LSP. This assumption has important consequences for phenomenology, which we will detail below. In our specific model, this assumption is true over almost the entire range of parameters. The eigenstates of the neutralino and chargino mass matrices are rather complicated for low values of M and $|\mu|$. However, in this case, these states would be discovered at SLC or LEP.

This leads us to focus on those areas of parameter space where the chargino and neutralino masses are heavy, and there, as we will soon show, the form of the mass eigenstates simplifies immensely.

Our general procedure will be to examine the variation of the phenomenology as a function of M (with $M' = \frac{5}{3}M\tan^2\theta_W \simeq \frac{1}{2}M$ according to eq. (8.2)). This leaves two remaining parameters: μ and $\tan\beta$. There is a slight theoretical prejudice as to the value of $\tan\beta$. This basically arises due to the relation:

$$\lambda_t = \frac{gm_t}{\sqrt{2}m_W \sin\beta} \,. \tag{8.3}$$

which expresses the relation between the top-quark Yukawa coupling (λ_t) and the top-quark mass. Thus, the large top-quark mass can be explained, in part, by a maximal value of $\sin\beta$. Although this argument is clearly oversimplified, it does accurately portray the general tendency of models (where the large top-quark mass is an input) to favor values of $\tan\beta$ above 1. One might conclude that very large values of $\tan\beta$ should be favored. However, one runs into various technical problems when $\tan\beta$ exceeds some number of order 5 or 10. As a result, typical models tend to have $\tan\beta$ somewhere between 1 and 5. In this report, we have fixed $\tan\beta = 2$. One should not draw any deep conclusion from this choice. In fact, in almost all instances, our results are extremely insensitive to the precise value of $\tan\beta$ chosen. Finally, we remark that some arbitrary phase choices have been fixed to avoid introducing new CP-violating phases into the theory. This choice is a simply a matter of convenience, since at present there are no significant experimental constraints on these phases for the mass range of interests to our study. By our choices of phase, $\tan\beta$ and M are positive and μ can be of either sign.

Let us now examine briefly the masses of the charginos and neutralinos as a function of the free parameters M, μ and $\tan\beta$. We are particularly interested in those masses which correspond to charginos and neutralinos which would not have been discovered at SLC or LEP, but can be discovered at the higher energies.

The dependence on $\tan\beta$ is extremely weak in the mass regions of interest, so we will only show graphs corresponding to $\tan\beta = 2$. Furthermore, in this region of interest, the lightest of the six states is the neutral state $\widetilde{\chi}_1^0$. We shall assume that this state is the lightest supersymmetric particle (LSP), which is stable, and behaves in a detector like a neutrino. As a result, the process $e^+e^- \to \widetilde{\chi}_1^0\widetilde{\chi}_1^0$,

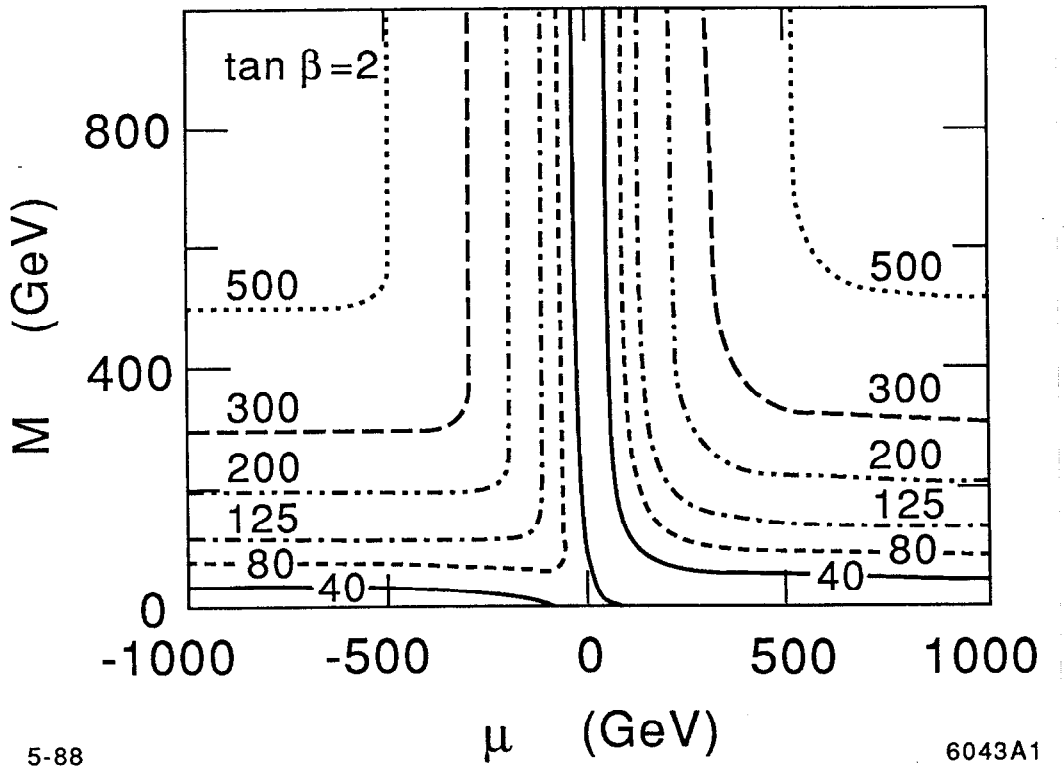

Figure 81. Contours of constant $\widetilde{\chi}_1^+$ mass, where $\widetilde{\chi}_1^+$ is the lighter of the two chargino states, computed in the M-μ plane for $\tan\beta = 2$. The chargino mass (in GeV) labels each contour.

is undetectable, and we must search for, *e.g.*, $e^+e^- \to \widetilde{\chi}_1^0\widetilde{\chi}_2^0$ in order to detect evidence for neutralino production. In the latter case, $\widetilde{\chi}_2^0$ decays directly to $\widetilde{\chi}_1^0$ and associated quark jets or a lepton pair. (We will emphasize later that over a large region of parameter space, the $\widetilde{\chi}_2^0$ decays with nearly 100% branching ratio[85] into

$\widetilde{\chi}_1^0 H_2^0$, where H_2^0 is the lightest Higgs scalar of the supersymmetric model.) One can also search for $e^+e^- \to \widetilde{\chi}_1^+\widetilde{\chi}_1^-$, since the charginos can be detected via their decay into $\widetilde{\chi}_1^0$ and associated quark jets or a lepton pair. Thus, the most relevant mass parameters to examine are: the mass of the lightest chargino ($M_{\widetilde{\chi}_1^+}$) and the sum of the masses of the two lightest neutralinos ($M_{\widetilde{\chi}_1^0} + M_{\widetilde{\chi}_2^0}$). These are shown

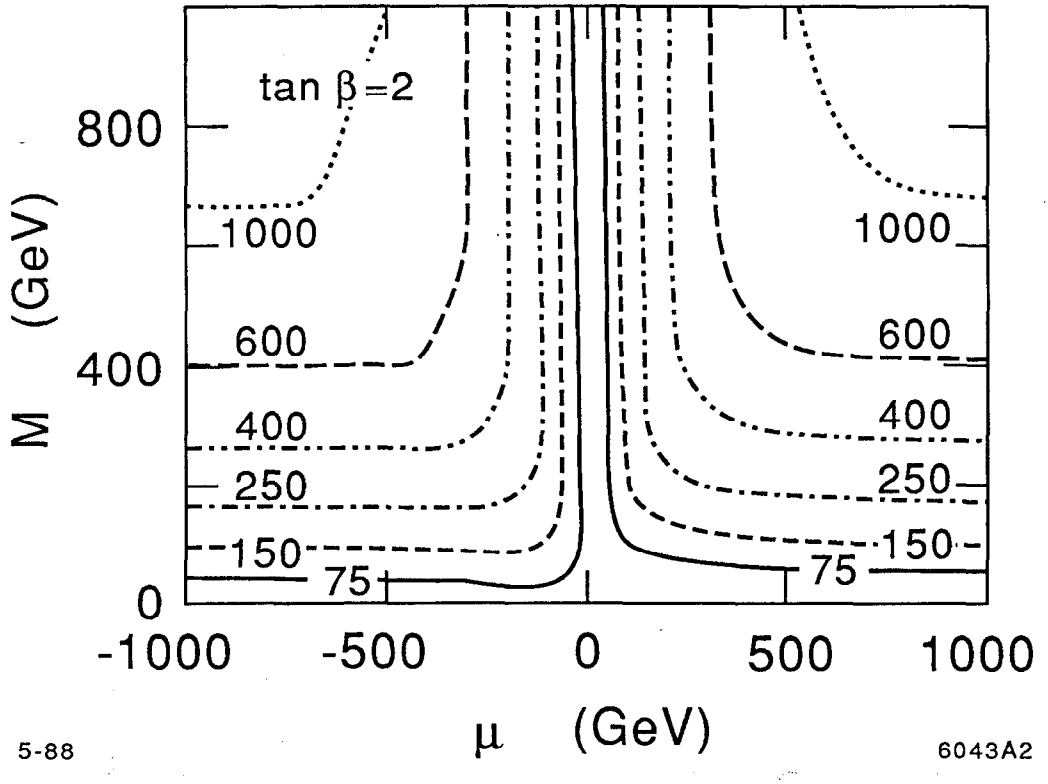

Figure 82. Contours of constant values of the *sum* of the masses of $\widetilde{\chi}_1^0$ and $\widetilde{\chi}_2^0$, where $\widetilde{\chi}_1^0$ and $\widetilde{\chi}_2^0$ are the two lightest neutralino states. Again, the contours are given in the M-μ plane for $\tan\beta = 2$. The sum of the two masses (in GeV) labels each contour.

as contours in Figs. 81 and 82. On each plot, the lowest mass contour shown corresponds to the likely upper limit of discovery attainable at SLC and LEP-I, and the second lowest contour is the corresponding upper limit likely to be obtained at LEP-II. The next three contours span the mass range that can be studied in

higher energy experiments, with the highest mass contour corresponding to the kinematical limit for production at $\sqrt{s} = 1$ TeV. The systematics of the contours at large M and $|\mu|$ are quite simple.[85,86] If $|\mu| > M$, with $|\mu| \gg m_Z$, then $\widetilde{\chi}_1^0$, $\widetilde{\chi}_2^0$ and $\widetilde{\chi}_1^+$ are approximately pure gaugino states with $\widetilde{\chi}_1^0 \simeq \widetilde{B}$, $\widetilde{\chi}_2^0 \simeq \widetilde{W}_3$, and $\widetilde{\chi}_1^+ \simeq \widetilde{W}^+$. The corresponding masses are: $M_{\widetilde{\chi}_1^0} \simeq M'$ and $M_{\widetilde{\chi}_2^0} \simeq M_{\widetilde{\chi}_1^+} \simeq M$. If $M > M' > |\mu|$, with M, $M' \gg m_Z$, then all the aforementioned states are approximately pure higgsino states with the mass of each state roughly degenerate with mass $|\mu|$. (In this latter case, $\widetilde{\chi}_1^0$ does remain the LSP, and there is enough phase space for $\widetilde{\chi}_2^0$ and $\widetilde{\chi}_1^+$ to decay into $\widetilde{\chi}_1^0$ and light quark jets or leptons.) Thus, in Fig. 81, high mass contour lines should be roughly rectangular, with intercept $|\mu| \simeq M_{\widetilde{\chi}_1^+}$ at large M and intercept $M \simeq M_{\widetilde{\chi}_1^+}$ at large $|\mu|$. In Fig. 82, high mass contour lines should also be roughly rectangular, with intercept $|\mu| \simeq (M_{\widetilde{\chi}_1^0} + M_{\widetilde{\chi}_2^0})/2$ at large M and intercept $M \simeq \frac{2}{3}(M_{\widetilde{\chi}_1^0} + M_{\widetilde{\chi}_2^0})$ at large $|\mu|$. (In the latter, we approximated $M' \simeq \frac{1}{2}M$.) Actually, in Fig. 82, one expects deviation from the behavior just described, in the region $M > |\mu| > M'$; for further details see ref. 85. It should be noted that the term "photino" has not been used in the above discussion. The photino exists as an approximate mass eigenstate only when $M - M' \ll m_Z$. Using the result of eq. (8.2), this implies that $M \ll 2m_Z$. This is *not* the parameter region of interest to us here. In the region of larger M, there is no neutralino state which is approximately a pure photino.

We next turn to the squark/slepton sector of the model. Let $\widetilde{f}_L$ and $\widetilde{f}_R$ be the scalar partners of the left and right-handed fermion f. One complication which arises is that $\widetilde{f}_L$ and $\widetilde{f}_R$ are not mass-eigenstates. There is $\widetilde{f}_L$-$\widetilde{f}_R$ mixing which is proportional in strength to:

$$M_{LR}^2 = \begin{cases} m_d(A_D + \mu \tan\beta), & \text{for "down"-type } f; \\ m_u(A_U + \mu \cot\beta), & \text{for "up"-type } f. \end{cases} \tag{8.4}$$

where A_D and A_U are (unknown) soft supersymmetry breaking mass parameters, presumably of order m_W. The supersymmetric Higgs mass μ is also presumably of order m_W (to within an order of magnitude), and $\tan\beta$ is of $\mathcal{O}(1)$. Due to the

appearance of the *fermion* mass in eq. (8.4), one expects M_{LR} to be small compared to the diagonal squark (and slepton) masses, with the possible exception of the top-squark, where m_t can be appreciable. Even so, as the squark and slepton masses are raised, the importance of the mixing term diminishes. Henceforth, we shall simply neglect the mixing term, in which case the squark and slepton masses are given by:

$$M^2_{\tilde{u}_L} = M^2_{\tilde{Q}} + m^2_u + m^2_Z \cos 2\beta(\tfrac{1}{2} - \tfrac{2}{3}\sin^2\theta_W) \tag{8.5}$$

$$M^2_{\tilde{u}_R} = M^2_{\tilde{U}} + m^2_u + \tfrac{2}{3}m^2_Z \cos 2\beta \sin^2\theta_W \tag{8.6}$$

$$M^2_{\tilde{d}_L} = M^2_{\tilde{Q}} + m^2_d - m^2_Z \cos 2\beta(\tfrac{1}{2} - \tfrac{1}{3}\sin^2\theta_W) \tag{8.7}$$

$$M^2_{\tilde{d}_R} = M^2_{\tilde{D}} + m^2_d - \tfrac{1}{3}m^2_Z \cos 2\beta \sin^2\theta_W \tag{8.8}$$

$$M^2_{\tilde{\nu}} = M^2_{\tilde{L}} + \tfrac{1}{2}m^2_Z \cos 2\beta \tag{8.9}$$

$$M^2_{\tilde{e}_L} = M^2_{\tilde{L}} + m^2_e - m^2_Z \cos 2\beta(\tfrac{1}{2} - \sin^2\theta_W) \tag{8.10}$$

$$M^2_{\tilde{e}_R} = M^2_{\tilde{E}} + m^2_e - m^2_Z \cos 2\beta \sin^2\theta_W \tag{8.11}$$

In the above equations, we have used the notation of the first generation fermions. Identical formulae can be written down for higher generations. The soft supersymmetry breaking parameters $M_{\tilde{Q}}$, $M_{\tilde{U}}$, $M_{\tilde{D}}$, $M_{\tilde{L}}$ and $M_{\tilde{E}}$ are unknown. (We have suppressed generational indices. Further complications such as intergenerational mixing are possible, although there are some constraints from the nonobservation of flavor changing neutral currents.) Again, one expects these parameters to be roughly the size of m_W, to within an order of magnitude. From numerous model-building exercises (based on "low-energy" supergravity or inspired by the

superstring), one typically finds:

$$M_{\tilde{L}} \approx M_{\tilde{E}} < M_{\tilde{Q}} \approx M_{\tilde{U}} \approx M_{\tilde{D}} \tag{8.12}$$

with the squark masses somewhere between a factor of 1—4 larger than the slepton masses. Again, we have suppressed generational labels. The first two generations are thought to be close to being degenerate in mass. However, renormaliztion group evolution can effect the third generation soft supersymmetry breaking masses. Typically, one finds $M_{\tilde{Q}_3}$ and $M_{\tilde{U}_3}$ reduced by a factor of 1—3 from the other soft supersymmetry breaking masses because of renormalization effects due to a heavy top quark mass. For simplicity, we can summarize our expectations as follows: the gross features of the squark/slepton spectrum indicate twelve degenerate squarks which are somewhat heavier than nine degenerate sleptons; differences among the three generations are ignored in the first approximation.

At this point, we have observed no connection between the squark/slepton masses and the gaugino/higgsino masses. In principle, these mass scales are independent. In typical model building, one often finds a general trend that $M_{\tilde{g}} \lesssim M_{\tilde{q}}$. We shall regard this statement as being suggestive only and far from definitive. However, if we make such an assumption, then from eq. (8.2), it follows that $M \simeq \frac{1}{4} M_{\tilde{g}}$. Hence, the above inequality would imply that $M_{\tilde{q}} \gtrsim 4M$. From Figs. 81 and 82, it follows that LEP-II could rule out values of M up to about 100 GeV. This would in turn limit squark masses to be above about 400 GeV, if no evidence is found for supersymmetry at colliders during the next decade. From this observation, we deduce two conclusions. If supersymmetry has not been found at any lower energy colliders, the most promising direction for supersymmetry detection at a 1 TeV collider lies in the neutralino/chargino sector. If on the other hand, supersymmetry is discovered at an earlier collider, we expect that signals will be seen in many different channels. In this case, one would want to use the high energy collider as a precision tool to measure supersymmetric particle properties in finer detail in the relatively clean e^+e^- environment.

8.2. Neutralino and Chargino Production

As outlined above, it is not inconceivable that squarks and sleptons of a "low-energy" supersymmetric model are too heavy to be produced at a 1 TeV e^+e^- collider. In that case, one must look to the charginos and the neutralinos for the first direct evidence for supersymmetry. We begin by surveying parameter space in the minimal supersymmetric extension of the standard model. We then compute all relevant cross sections and deduce some simple approximate forms. In order to evaluate the maximum discovery potential of the collider, we examine in detail via Monte Carlo the case of neutralino pair production in the next section and thereby obtain the efficiency for supersymmetric detection via a particular class of events containing hadronic jets and large missing transverse energy. This allows us to estimate the discovery limit of neutralinos as a function of the supersymmetric parameters.

We begin by surveying the cross sections for:

$$e^+e^- \to \widetilde{\chi}_i^0 \widetilde{\chi}_j^0 \tag{8.13}$$

$$e^+e^- \to \widetilde{\chi}_i^+ \widetilde{\chi}_j^- \tag{8.14}$$

We have computed the differential and total cross sections for these processes independently and checked them against the results which already appear in the literature (see ref. 87–89). In presenting our results below, we shall give total cross sections (before cuts) in units of R. We will refer to these total cross sections a values of R for supersymmetric processes. Our analysis proceeds as follows: We survey the range of possible supersymmetric parameters by computing cross sections for the above processes as a function of M and $|\mu|$, at a fixed $\tan\beta$. Note that having specified M, the value of M' is fixed by eq. (8.2). The results presented below are quite insensitive to $\tan\beta$. Thus, we shall only present graphs with $\tan\beta = 2$. As we move around in the M–μ plane, both masses and mixing angles of the neutralino and chargino states change. The variation of masses has already

been exhibited in Figs. 81 and 82. For each value of M and μ, we diagonalize the chargino and neutralino mass matrices numerically and compute the corresponding masses and mixing angles. Both sets of quantities appear in the Feynman rules for the various chargino and neutralino interactions.[83] All the cross sections for processes (8.13) and (8.14) are then computed. Two additional parameters must be provided in order to complete the above program—the mass of the selectron and the sneutrino. These parameters must be specified because of the contribution of slepton exchange to the production of charginos and neutralinos. According to our philosophy of heavy slepton masses discussed at the end of the last section, we shall fix $M_{\tilde{\nu}} = M_{\tilde{e}} = 500$ GeV, which implies that selectrons cannot be pair-produced at 1 TeV. The reader should be warned that the slepton mass is held fixed even as M is varied, in the graphs presented below. Choosing the slepton mass to vary with M (if one wished to insure a gluino mass which was smaller than the squark mass) would lead to slightly different results.

In Figs. 83 and 84, we exhibit contours of constant total (normalized) cross section R as a function of M and μ. The corresponding chargino and neutralino masses should be read off of Figs. 81 and 82. The chargino cross sections are clearly larger; this is almost entirely due to the one-photon s-channel exchange which would give $R \simeq 1$ if the final state masses were neglected. The $\widetilde{\chi}_1^0\widetilde{\chi}_2^0$ cross section never exceeds $R = 0.6$; the maximum value of this cross section can depend sensitively on $M_{\tilde{e}}$, as we will show in more detail below. To gain an understanding of these plots, we have explicitly computed the cross sections in the following two asymptotic limits:

$$\mathbf{I}: \quad \sqrt{s} \gg |\mu| \gg M \tag{8.15}$$

$$\mathbf{II}: \quad \sqrt{s} \gg M \gg |\mu| \tag{8.16}$$

In limiting case **I**,

$$R(\widetilde{\chi}_1^+\widetilde{\chi}_1^-) = \frac{1}{8\sin^4\theta_W}\left(1 + \frac{3r_\nu}{2}\left[2 + \frac{1}{1+r_\nu} + 2(1+r_\nu)\log\left(\frac{r_\nu}{1+r_\nu}\right)\right]\right) \tag{8.17}$$

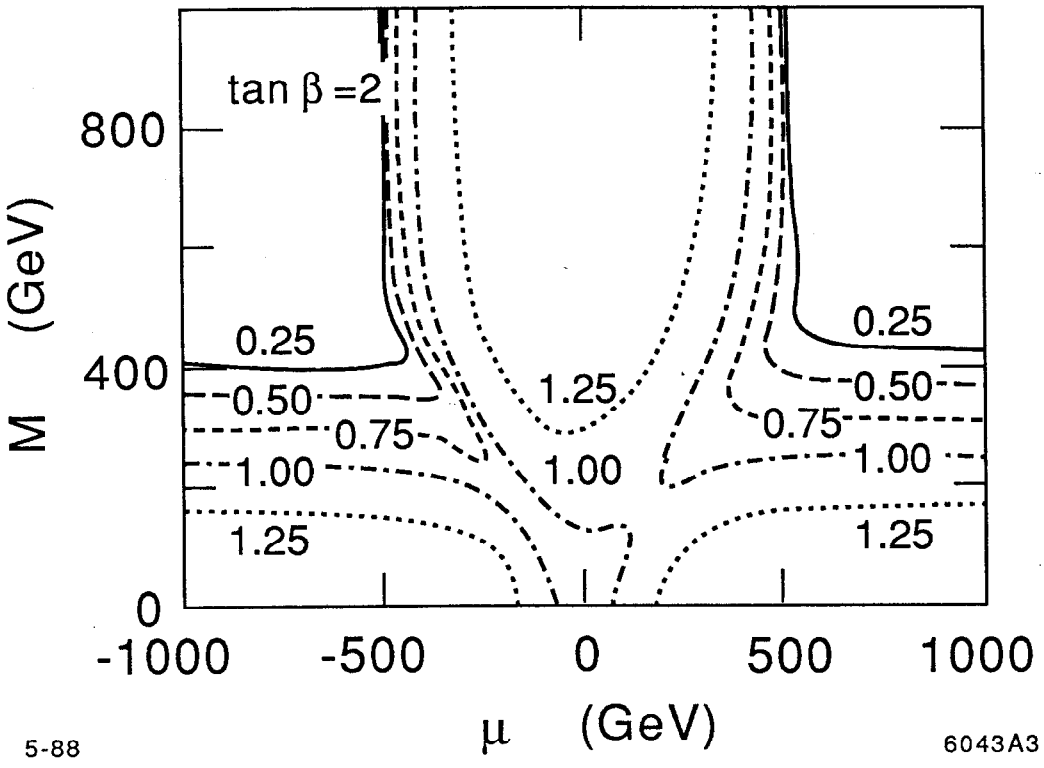

Figure 83. Contours of constant R for $e^+e^- \to \widetilde{\chi}_1^+\widetilde{\chi}_1^-$, at $\sqrt{s} = 1$ TeV. We take $\tan\beta = 2$ and $M_{\tilde{\nu}} = 500$ GeV. The total cross section, in units of R, labels each contour.

$$R(\widetilde{\chi}_1^0\widetilde{\chi}_2^0) = \frac{3}{32\sin^2\theta_W\cos^2\theta_W}\left[1 + \frac{r_e}{1+r_e} + 2r_e\log\left(\frac{r_e}{1+r_e}\right)\right] \tag{8.18}$$

where,

$$r_\nu \equiv \frac{M_{\tilde{\nu}}^2}{s}, \qquad r_e \equiv \frac{M_{\tilde{e}}^2}{s} \tag{8.19}$$

In limiting case **I**, $\widetilde{\chi}_1^0$, $\widetilde{\chi}_2^0$, and $\widetilde{\chi}_1^+$ are all pure gauginos. As a result, s-channel Z exchange is highly suppressed in this limit. Using $r_\nu = r_e = 1/4$ in eqs. (8.17) and (8.18) gives:

$$R(\widetilde{\chi}_1^+\widetilde{\chi}_1^-) = 1.47, \qquad \text{in limiting case } \mathbf{I}. \tag{8.20}$$

$$R(\widetilde{\chi}_1^0\widetilde{\chi}_2^0) = 0.24, \qquad \text{in limiting case } \mathbf{I}. \tag{8.21}$$

Interestingly, in $\widetilde{\chi}_1^+\widetilde{\chi}_1^-$ production, the contribution due to $\tilde{\nu}$-exchange (and its

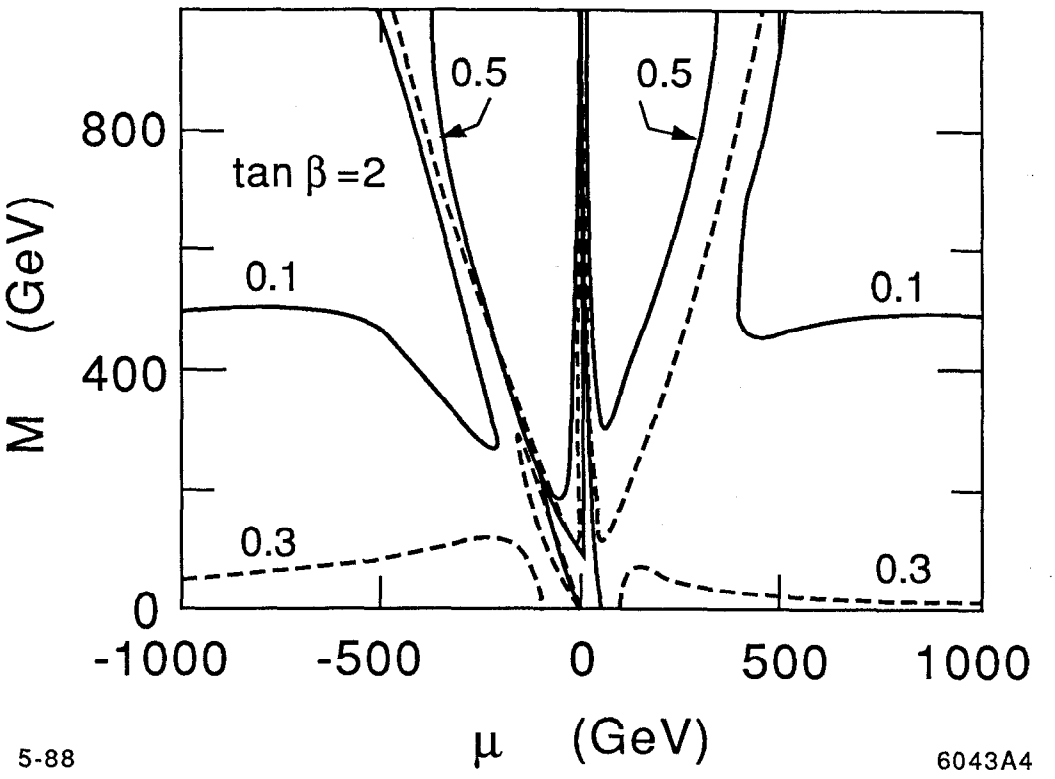

Figure 84. Contours of constant R for $e^+e^- \to \widetilde{\chi}_1^0\widetilde{\chi}_2^0$, at $\sqrt{s} = 1$ TeV. We take $\tan\beta = 2$ and $M_{\tilde{e}} = 500$ GeV. The total cross section, in units of R, labels each contour.

interference with γ and Z exchange), is maximally negative near $r_\nu = 1/4$, which was chosen above.

In limiting case **II**,

$$R(\widetilde{\chi}_1^+\widetilde{\chi}_1^-) = 1 + \frac{\cos 2\theta_W(1 - 4\sin^2\theta_W)}{\sin^2 2\theta_W} + \frac{\cos^2 2\theta_W(\cos^2 2\theta_W + 4\sin^4\theta_W)}{2\sin^4 2\theta_W} \quad (8.22)$$

$$R(\widetilde{\chi}_1^0\widetilde{\chi}_2^0) = \frac{1 + (1 - 4\sin^2\theta_W)^2}{4\sin^4 2\theta_W} \quad (8.23)$$

In limiting case **II**, $\widetilde{\chi}_1^0$, $\widetilde{\chi}_2^0$, and $\widetilde{\chi}_1^+$ are all pure higgsinos. Thus slepton exchange is highly suppressed and the results are insensitive to the choice of the slepton

masses. Evaluating these results numerically gives:

$$R(\widetilde{\chi}_1^+\widetilde{\chi}_1^-) = 1.38, \qquad \text{in limiting case } \mathbf{II}. \tag{8.24}$$

$$R(\widetilde{\chi}_1^0\widetilde{\chi}_2^0) = 0.57, \qquad \text{in limiting case } \mathbf{II}. \tag{8.25}$$

(These values include the factor (3.11) from the renormalization of α.) Although

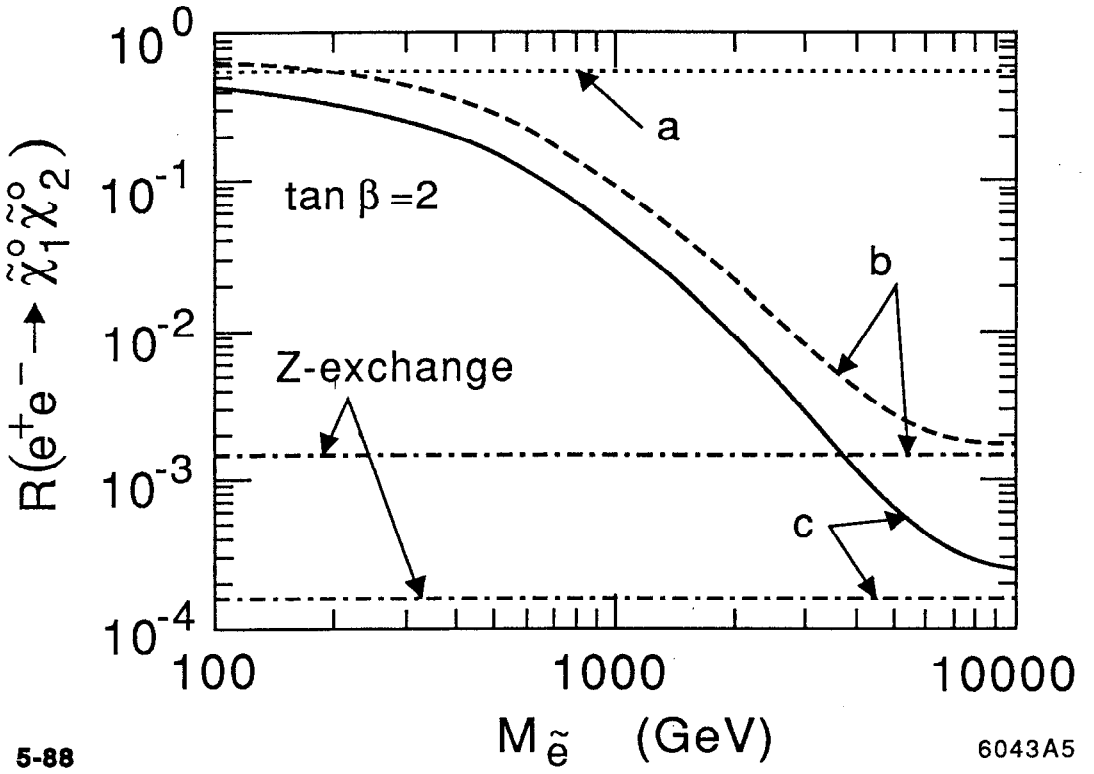

Figure 85. Dependence of the cross section for $e^+e^- \to \widetilde{\chi}_1^0\widetilde{\chi}_2^0$ (in units of R) on the selectron mass, for $\sqrt{s} = 1$ TeV. Three representative parameter choices are shown: (a) $M = 700$ GeV, $\mu = 200$ GeV, (b) $M = 200$ GeV, $\mu = 160$ GeV, (c) $M = 300$ GeV, $\mu = 400$ GeV. Both the total cross section and the contribution due to Z-exchange are shown in two of the cases. For case (a), the $\tilde{e}$-exchange contribution is quite small, so that the difference between the Z-exchange contribution and the total cross section is not discernable on the graph.

the asymptotic numerical results quoted above are not that accurate in the sub-asymptotic ranges covered in Figs. 83 and 84, nevertheless the above numbers (with phase space corrections due to final state masses included) give a surprisingly accurate picture of the gross structure of the cross section contour plots.

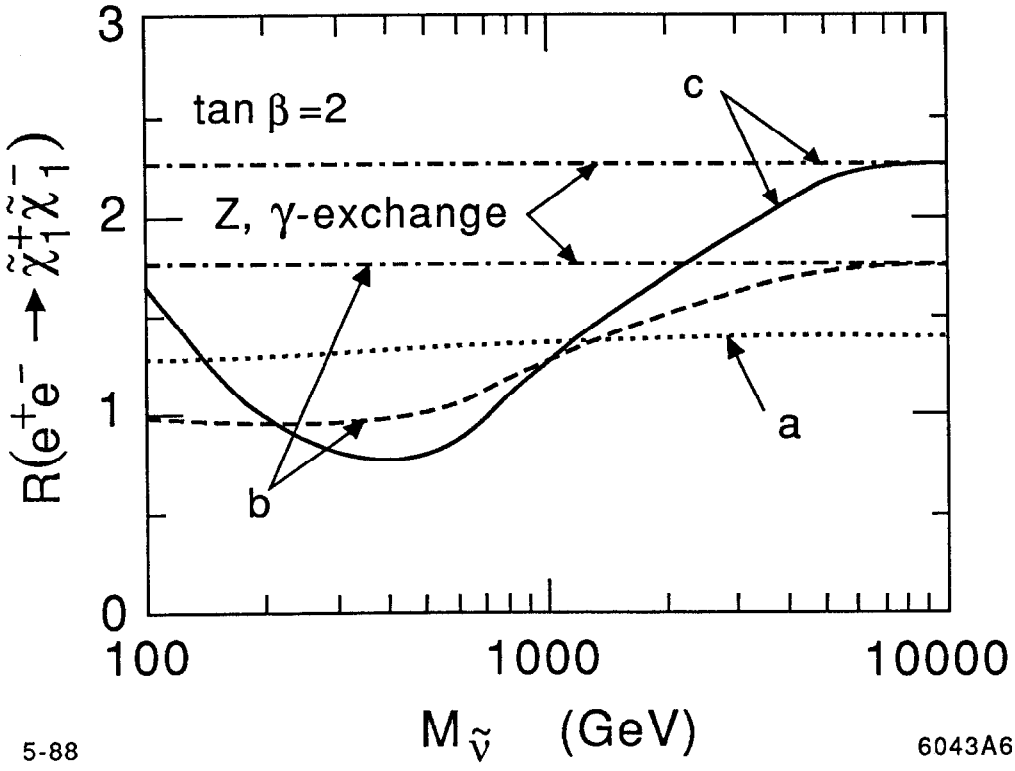

Figure 86. Dependence of the cross section for $e^+e^- \to \tilde{\chi}_1^+\tilde{\chi}_1^-$ (in units of R) on the sneutrino mass, for $\sqrt{s} = 1$ TeV. The results are shown for the three parameter choices of Fig. 85. Both the total cross section and the contribution due to Z,γ-exchange are shown in two of the cases. For case (a), the $\tilde{\nu}$-exchange contribution is rather small, so that the difference between the Z,γ-exchange contribution and the total cross section is not shown on the graph.

Next, we investigate the sensitivity to the slepton mass. From the analysis just presented, it is clear that the sensitivity to slepton mass is greatest for $e^+e^- \to \tilde{\chi}_1^0\tilde{\chi}_2^0$ in the region of parameter space in which $|\mu| > M$. Some representative

parameter choices are shown in Fig. 85. For comparison, we also display the contribution due to Z-exchange. Note that even for fairly large selectron mass (say, $M_{\tilde{e}} = 1$ TeV), the selectron-exchange dominates the Z-exchange in the $|\mu| > M$ region. Based on this graph, one can roughly surmise how the contours of Fig. 84 would be modified in this region of parameter space as $M_{\tilde{e}}$ varies. On the

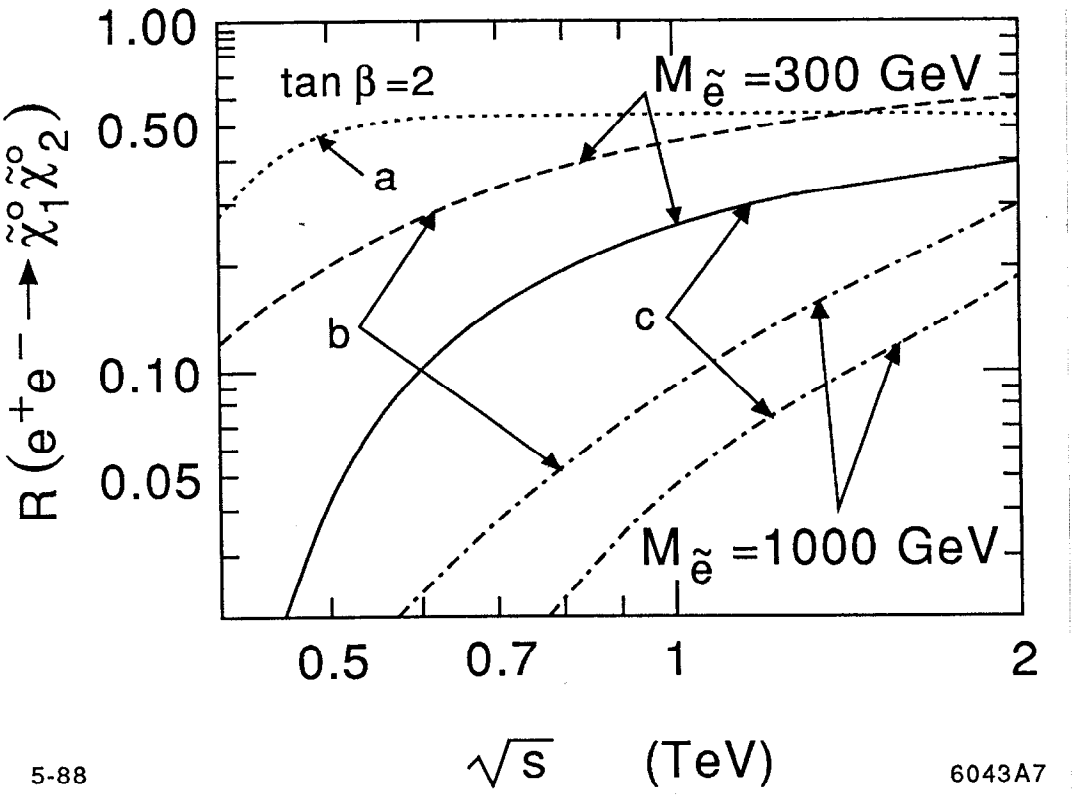

Figure 87. Dependence of the total cross section for $e^+e^- \to \widetilde{\chi}_1^0\widetilde{\chi}_2^0$, in units of R, on the center of mass energy. The results are show for the three parameter choices of Fig. 85. In two of the cases, curves for $M_{\tilde{e}} = 300$ GeV and 1000 GeV are shown. In case (a), there is essentially no dependence on the selectron mass, as Fig. 85 already illustrated.

other hand, the cross section for $e^+e^- \to \widetilde{\chi}_1^+\widetilde{\chi}_1^-$ is less sensitive to the sneutrino mass. This is illustrated in Fig. 86 (note the *linear* vertical scale). In fact, the

sum of the direct and interference terms involving $\tilde{\nu}$-exchange is negative, so that the total cross section is reduced from the Z,γ-exchange contribution. As before, in the region where $M \gg |\mu|$, the charginos are nearly pure higgsinos and the slepton-exchange becomes negligible.

Finally, for completeness, we have briefly examined the energy dependence of the results. All graphs so far have corresponded to a center of mass energy of

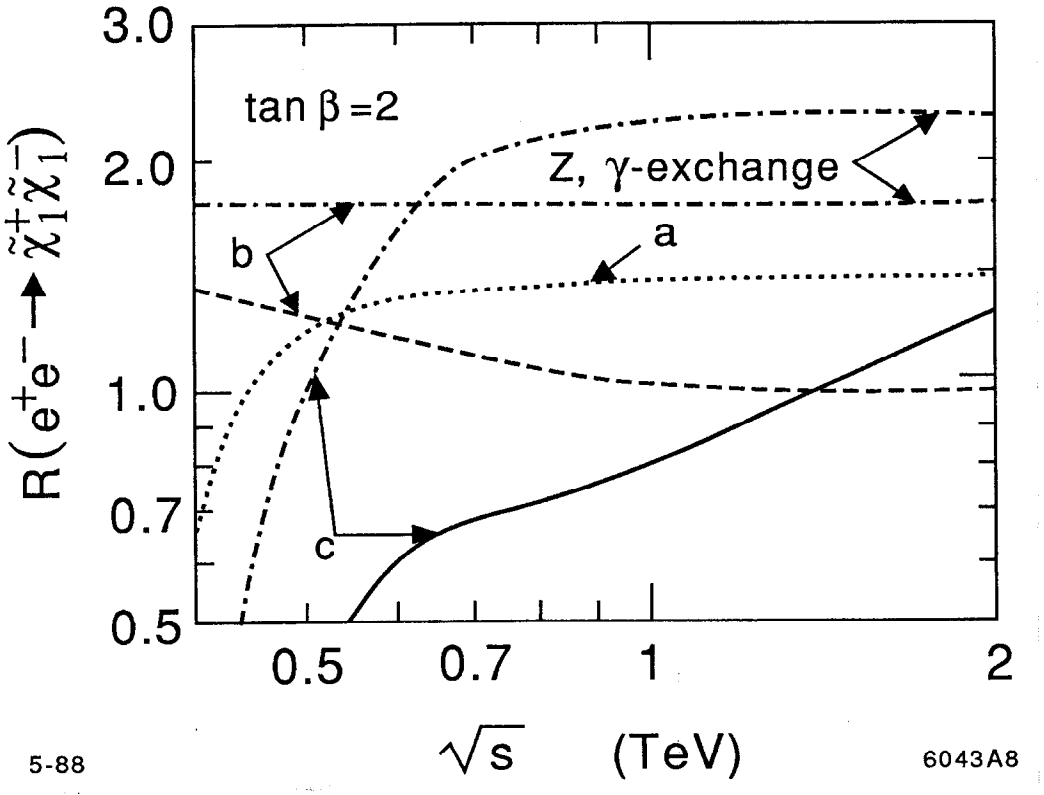

Figure 88. Dependence of the total cross section (in units of R) for $e^+e^- \to \tilde{\chi}_1^+\tilde{\chi}_1^-$ on the center of mass energy. The results are shown for the three parameter choices of Fig. 85. The sneutrino mass is fixed to $M_{\tilde{\nu}} = 500$ GeV. In two of the cases shown, the contribution due to Z,γ-exchange is shown separately. In case (a), there is essentially no difference between the Z,γ-contribution and the total cross section, since sneutrino exchange is negligible for this choice of parameters.

1 TeV. In Figs. 87 and 88, we display the cross sections for $e^+e^- \to \tilde{\chi}_1^0\tilde{\chi}_2^0$ and

$\widetilde{\chi}_1^+\widetilde{\chi}_1^-$ as a function of $\sqrt{s}$, for two different choices of slepton mass (for various choices of M, $|\mu|$, and $\tan\beta = 2$). Once again, we have plotted the normalized cross sections R in order to indicate the scaling behavior of these cross sections once $\sqrt{s}$ is sufficiently larger than the final state masses. In order to ascertain the $\sqrt{s}$ dependence on the discovery potential for supersymmetry, we have recomputed the contour plot for $\sigma_T(e^+e^- \to \widetilde{\chi}_1^0\widetilde{\chi}_2^0)$ at $\sqrt{s} = 600$ GeV. As before, we have fixed

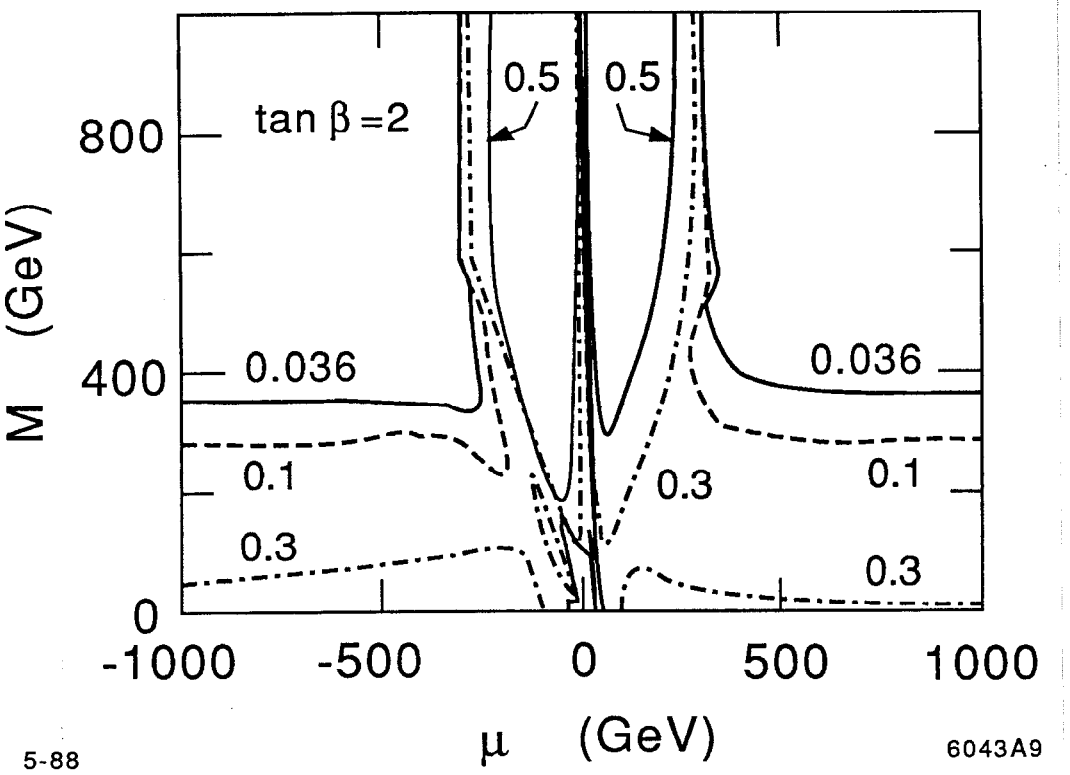

Figure 89. Contours of constant R for $e^+e^- \to \widetilde{\chi}_1^0\widetilde{\chi}_2^0$, at $\sqrt{s} = 600$ GeV. We take $\tan\beta = 2$ and $M_{\tilde{e}} = 300$ GeV. The total cross section, in units of R, labels each contour.

the selectron mass to be $M_{\tilde{e}} = \frac{1}{2}\sqrt{s}$. (This leads to somewhat larger values of the cross section in the $|\mu| > M$ region, compared with using the previous value of $M_{\tilde{e}} = 500$ GeV.) The result, shown in Fig. 89 should be compared with the corresponding plot at $\sqrt{s} = 1$ TeV, shown in Fig. 84. In comparing these two

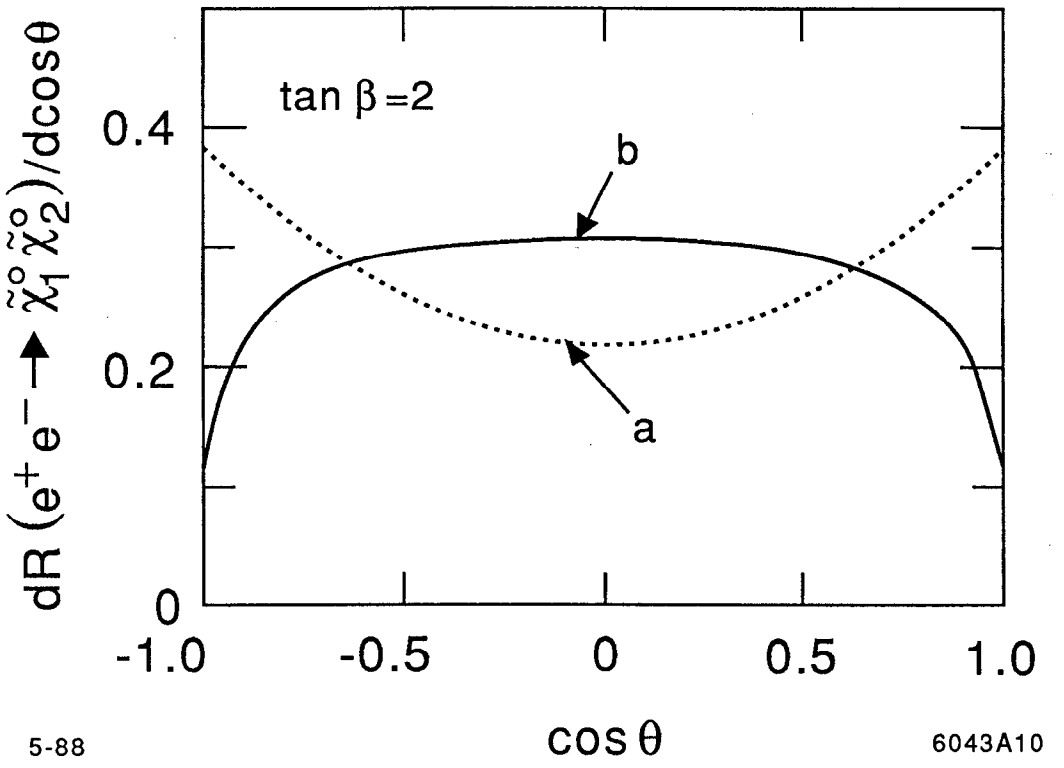

Figure 90. Angular distribution for $e^+e^- \to \widetilde{\chi}_1^0\widetilde{\chi}_2^0$ at $\sqrt{s} = 1$ TeV, for the parameter choices (a) and (b) of Fig. 85. In case (a), $\tilde{e}$-exchange is negligible, and the angular distribution shown is characteristic of Z-exchange. In case (b), $\tilde{e}$-exchange dominates Z-exchange, and the angular distribution shown is characteristic of the scalar-exchange.

plots, one should take care to note that the normalized cross sections R have been plotted. In particular, the $R = 0.036$ contour of Fig. 89 and the $R = 0.1$ contour of Fig. 84 correspond to the same total cross section in picobarns.

In addition to the total cross sections, we will need to make use of the differential cross sections and the decay rates of the charginos and neutralinos. The differential cross sections can be found in ref. 87; the decay rates and branching ratios have been studied in detail in ref. 85. All results were derived independently for this study. Some typical angular distributions are shown in Figs. 90 and 91. The peculiar shape of the distribution of $\widetilde{\chi}_1^+\widetilde{\chi}_1^-$ production is due to the destructive interference of the $\tilde{\nu}$-exchange and Z,γ-exchange contributions. The $\tilde{\nu}$-exchange is

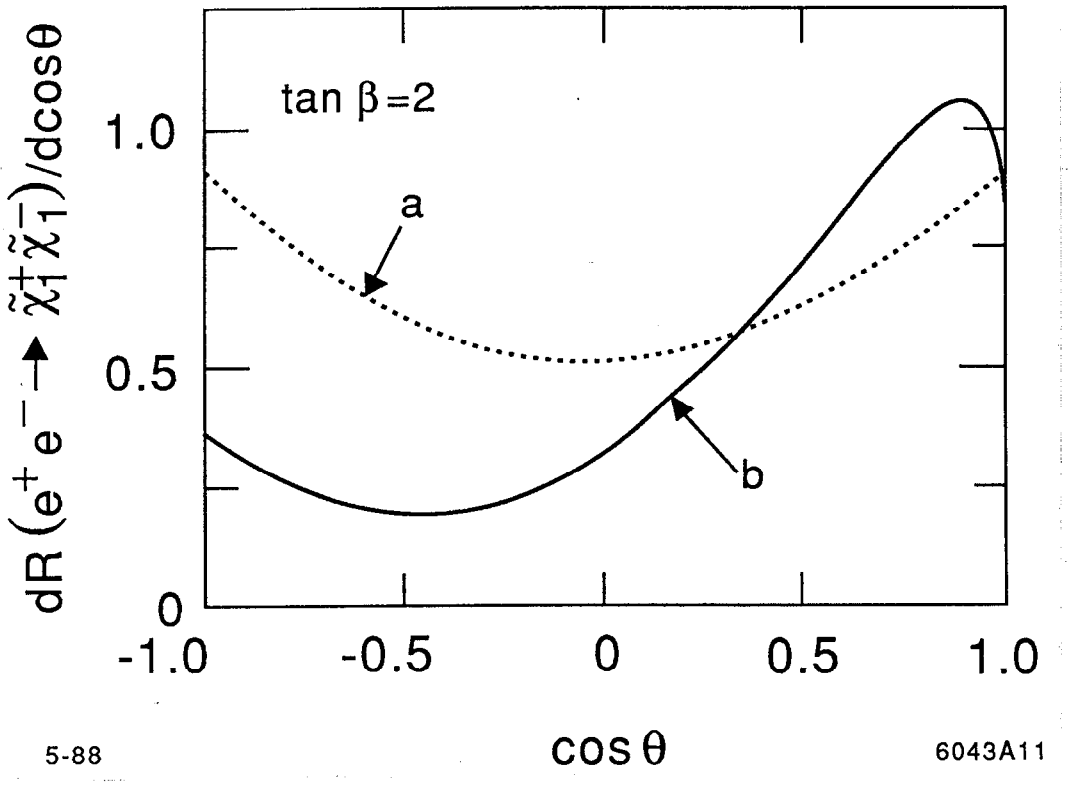

Figure 91. Angular distribution for $e^+e^- \to \tilde{\chi}_1^+\tilde{\chi}_1^-$ at $\sqrt{s} = 1$ TeV, for the parameter choices (a) and (b) of Fig. 85. In case (a), $\tilde{\nu}$-exchange is negligible, and the angular distribution shown is characteristic of Z,γ-exchange. In case (b), $\tilde{\nu}$-exchange is significant and is largest in the backwards direction, where it interferes destructively with the contribution due to Z,γ-exchange.

asymmetric in $\cos\theta$, and for large $M_{\tilde{\nu}}$ the destructive interference is greatest near $\cos\theta = -1$. However, none of the angular distributions exhibit strong forward or backward peaking (unless the mass of the scalar exchanged is close to zero). Overall, these results show that the loss of efficiency in signal detection due to forward (or backward) production down the beam hole should be rather minimal.

Examining the possible decay modes of $\tilde{\chi}_2^0$ leads to a rather interesting observation. In the region of parameter space of relevance to our study, we often found that $\tilde{\chi}_2^0$ decayed with nearly 100% branching ratio into $\tilde{\chi}_1^0 H_2^0$, where H_2^0 is the Higgs scalar of the supersymmetric model which must be lighter than the Z. This

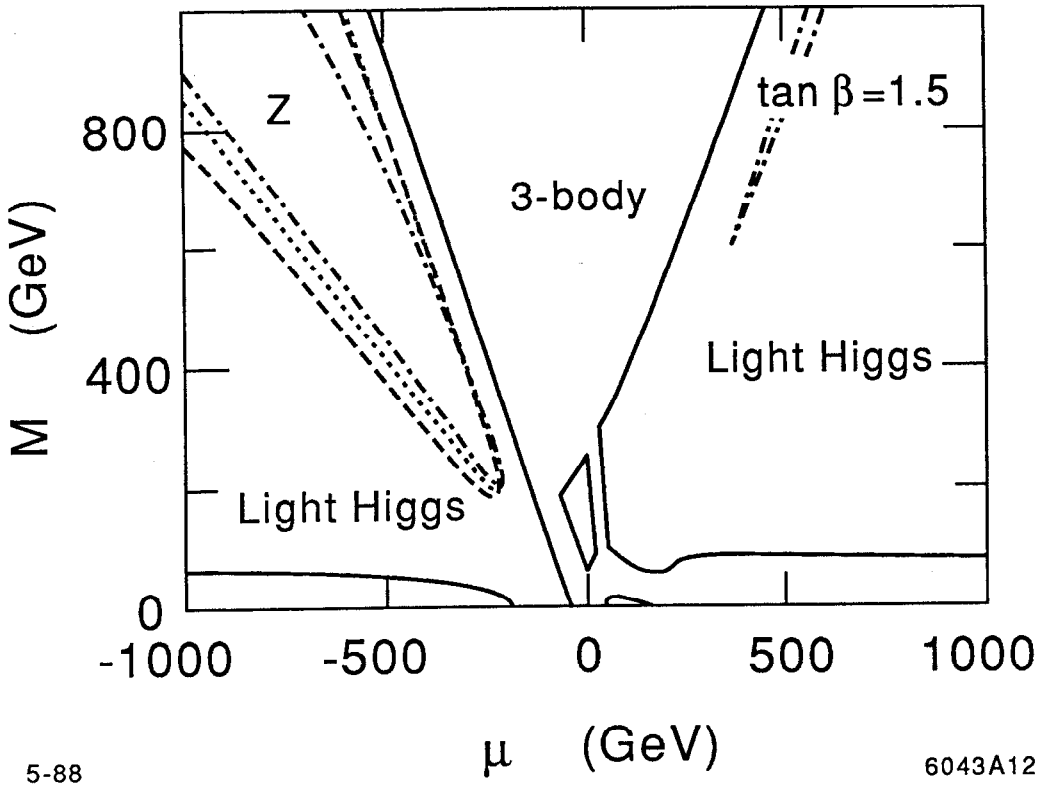

Figure 92. Three distinct regions of $\widetilde{\chi}_2^0$ decay are exhibited as a function of M and μ. In the region denoted by "3-body", no two-body modes are kinematically allowed. In the region "Light Higgs", two body decays into Higgs bosons, which are lighter than the Z, dominate. In the region "Z", three contours are shown corresponding to: $BR(\widetilde{\chi}_2^0 \to \widetilde{\chi}_1^0 Z)$ = 10% (dashed contour); 20% (dotted contour); and 50% (dashdot contour). In addition, there is a very narrow region with positive μ values, indicated by the dashdot contour, where $BR(\widetilde{\chi}_2^0 \to \widetilde{\chi}_1^0 Z) \simeq 100\%$. Unmarked areas alternate between the first two regions described above. We have chosen $\tan\beta = 1.5$, and m_{H^+} = 500 GeV, which implies that the mass of the light scalar Higgs boson is $m_{H_2^0} = 35.2$ GeV.

is illustrated by the contour plot shown in Fig. 92, based on a calculation taken from ref. 85. The contours of Fig. 92 have been obtained for a charged Higgs boson mass equal to 500 GeV. (Given m_{H^+} and $\tan\beta$, all the remaining Higgs masses in the minimal supersymmetric masses are fixed.[90]) Note that in Fig. 92, the value $\tan\beta = 1.5$ has been used. The results for $\tan\beta = 2$ would be only slightly changed; the main effect being the slight decrease in the overall area of the

"Light Higgs" region due to a somewhat larger value of $m_{H_2^0}$. In general, as $m_{H_2^0}$ is reduced, the "Light Higgs" region in Fig. 92 increases in size at the expense of the region where three-body decays dominate. Note that the region where the branching ratio for $\widetilde{\chi}_2^0 \to \widetilde{\chi}_1^0 Z$ is significant is confined to the area where μ is negative and $M \gtrsim |\mu| \gtrsim M'$. In the corresponding area with positive μ, although $\widetilde{\chi}_2^0 \to \widetilde{\chi}_1^0 Z$ is kinematically allowed, the amplitude turns out to be rather suppressed. (See ref. 85 for further discussion.) The region where the latter decay is appreciable is rather insensitive to the choice of the Higgs mass.

8.3. Observation of Neutralino Pair Production

We now turn to a Monte Carlo analysis of neutralino production. We decided to focus first on neutralino production rather than chargino production for a number of reasons. First, the signature for $e^+e^- \to \widetilde{\chi}_1^0\widetilde{\chi}_2^0$ is expected to be quite clean. As explained above, one finds that over a large region of supersymmetric parameter space, that $BR(\widetilde{\chi}_2^0 \to \widetilde{\chi}_1^0 H_2^0) \simeq 100\%$. The H_2^0 is presumed to decay dominantly into $b\overline{b}$ jets, and the primary and secondary $\widetilde{\chi}_1^0$'s (*i.e.* the LSP's) escape the detectors, resulting in substantial missing transverse energy. In other regions of parameter space (particularly when $M > |\mu|$), direct three body decays of $\widetilde{\chi}_2^0$ are most important. The majority of these decays end up with the LSP plus hadronic jets ($\widetilde{\chi}_2^0 \to \widetilde{\chi}_1^0 + q\overline{q}$). The precise ratio of hadronic to leptonic final states depends on the masses of the squarks and sleptons which mediate one of the diagrams which contributes to the three-body neutralino decay. The signature in both cases is rather similar: We expect to find events with hadronic jets and substantial missing energy due to the two LSP's which escape. The second reason for focusing first on neutralino decay is one of phase space kinematics. From Figs. 81 and 82, one sees that an area of supersymmetric parameter space does exist (where $|\mu| > M$) where $e^+e^- \to \widetilde{\chi}_1^0\widetilde{\chi}_2^0$ is kinematically allowed, but chargino production is forbidden. The third reason is that neutralino production provides a challenge to the power and efficiency of searches in e^+e^- reactions. As we noted in the previous section, the cross sections for $\widetilde{\chi}_1^0\widetilde{\chi}_2^0$ production are quite small, with

R-values less than 0.6. Thus, we regard the neutralino Monte Carlo as a real test of how far we can push the supersymmetry discovery limits.

In constructing our Monte Carlo simulation, we made use of the model detector described in Chapter 3. We assumed 10 fb^{-1} of data, and studied the cases of $\sqrt{s}$ = 600 GeV and 1 TeV. The standard beamstrahlung spectrum of Fig. 4 was employed in the generation of background events. (We did not incorporate the beamstrahlung in the generation of the signal events. Since the most important feature of $\widetilde{\chi}_1^0\widetilde{\chi}_2^0$ production is missing *transverse* energy, the only possible significant effect of beamstrahlung is to reduce the center of mass energy of a given event. Since a large fraction of all events still occurs near $\sqrt{s} = 2E_{beam}$, the overall effect of beamstrahlung on our signal rate is small.) Our analysis method was devised to take advantage of the basic features of neutralino pair production: unbalanced quark jets and substantial missing transverse energy.

Signal events and background events described below were put through the following sets of cuts:

1. Each event is divided up into two hemispheres and a thrust axis is determined. Let θ_{thr} be the polar angle of the thrust axis relative to the beam direction. The event is kept if $|\cos\theta_{thr}| < 0.6$. This cut insures that the majority of hadronic activity is away from the forward direction (and the beam hole).

2. The missing mass M_{miss} is computed for the event. The event is kept if $M_{miss} > \frac{2}{3}\sqrt{s}$. Such an event is guaranteed to have at least two energetic undetected particles at large angles with respect to each other. This cut is very helpful in eliminating a large part of the ZZ background to be discussed below.

3. The tracks of each event are partitioned according to their thrust hemispheres. The momenta in each hemisphere are summed vectorially, and 180° minus the transverse angle between these two vectors is called the acoplanarity ($\phi_{acop} = 180° - \phi_T$). We require that $\phi_{acop} > 90°$, which ensures that undetected particles produced in an event are emitted at large polar angle

with respect to the beam direction.

4. The visible energy of the event is denoted by E_{vis}. In order to get rid of events in which energetic undetected particles are emitted in the forward direction, we demand that $E_{vis} > 0.1\sqrt{s}$. This helps to cut out backgrounds due to two-photon events or events where there was a very large beamstrahlung photon emitted.

5. The largest background which survived the four cuts above were events due to $e^+e^- \to e^\pm \nu W^\mp$, in which the outgoing $e^\pm$ is emitted in the forward direction and hence was not detected. Note that in such events, the number of visible tracks which result from the W decay must be odd. On the other hand, the $\widetilde{\chi}_1^0\widetilde{\chi}_2^0$ events would lead to a neutral final state and hence an even number of charged tracks. Thus, we add one further cut and demand that only events with an even number of detected charged tracks be kept. It is important to note that, in this counting, we ignored tracks in the 10° hole around the beam direction.

The most important background events were due to two sources: (i) γW fusion (the dominant background being $e^+e^- \to e^\pm \nu W^\mp$), and (ii) $e^+e^- \to ZZ$ (in particular, when one of the Z's decays into a neutrino pair). We begin by showing histograms of the total visible mass (M_{vis}) of the background events of types (i) and (ii) described above, normalized to an integrated luminosity of 10 fb^{-1}. First, we exhibit in Fig. 93(a)-(b) the dramatic effect of the cut on charged tracks on the $e^+e^- \to e^\pm \nu W^\mp$ events. In Fig. 93(a), we display the histogram prior to the cut on charged tracks (cut #5 above), and Fig. 93(b) displays the same histogram after this cut is made. Notice the difference in vertical scale between the two histograms. The few remaining events are naturally clustered around $M_{vis} = m_W$ and present little trouble in the remaining analysis. The charged track cut is clearly crucial in eliminating this background. In Fig. 93(c), we display the histogram for ZZ background events (after all cuts). Note that the signal which makes it through in this case is rather small and is clustered around $M_{vis} = m_Z$. Our conclusion

is that under the series of cuts described above, it is very difficult for standard model events to get through. Thus, these cuts present a rather clean filter for beyond-the-standard-model physics.

We next ran Monte Carlo events for $e^+e^- \to \widetilde{\chi}_1^0\widetilde{\chi}_2^0$ through the same set of cuts. In Table 11, we present a summary of the various parameter choices we studied. (All masses are given in GeV units.) Two particular parameter choices are examined at both $\sqrt{s} = 600$ and 1000 GeV; the remaining cases are all at the higher energy. Note that we sometimes chose smaller values of the selectron mass than previously advertised, which resulted in slightly larger cross sections. In Table 12, we summarize the effects of the cuts on the $\widetilde{\chi}_1^0\widetilde{\chi}_2^0$ signal.

Typical histograms of M_{vis} for the $\widetilde{\chi}_1^0\widetilde{\chi}_2^0$ events (normalized to 10 fb^{-1}) are presented in Fig. 94(a)–(g) for the seven cases listed in Tables 11 and 12. We note that the efficiency of the cuts (*i.e.*, the ratio of the number of events surviving the cuts to the total number of events computed from the total cross section) is fairly constant—roughly 25%—over the parameter space which was surveyed in Table 12. Furthermore, the effect of the cut on charged tracks on the $\widetilde{\chi}_1^0\widetilde{\chi}_2^0$ events was rather weak; about 65% of the signal was retained (roughly independent of the supersymmetric parameters). Case (f) corresponds to the smallest cross section studied: $R = 0.09$. After all cuts, we end up with 21 events. The background is estimated to be about 22 events, of which 13 are $e^+e^- \to e^\pm\nu W^\mp$ and 9 are $e^+e^- \to ZZ$. The $e^\pm\nu W^\mp$ are tightly clustered around the W mass (as shown in Fig. 93(b)) and can be easily subtracted. The ZZ events are a little more spread out (see Fig. 93(c)), but they can also be efficiently subtracted. We conclude that signals down to $R = 0.1$ at an integrated luminosity of 10 fb^{-1} should be clearly detectable.

In all cases studied above, $BR(\widetilde{\chi}_2^0 \to \widetilde{\chi}_1^0 H_2^0)$ was close to 100%. From Table 11, we see that $m_{H_2^0} \approx 50$ GeV, which explains the origin of the peaking of the histograms around $M_{vis} = 50$ GeV in Fig. 94(a)-(f). We concocted one peculiar example (case (g)) in which the lightest scalar Higgs boson was close in mass to that

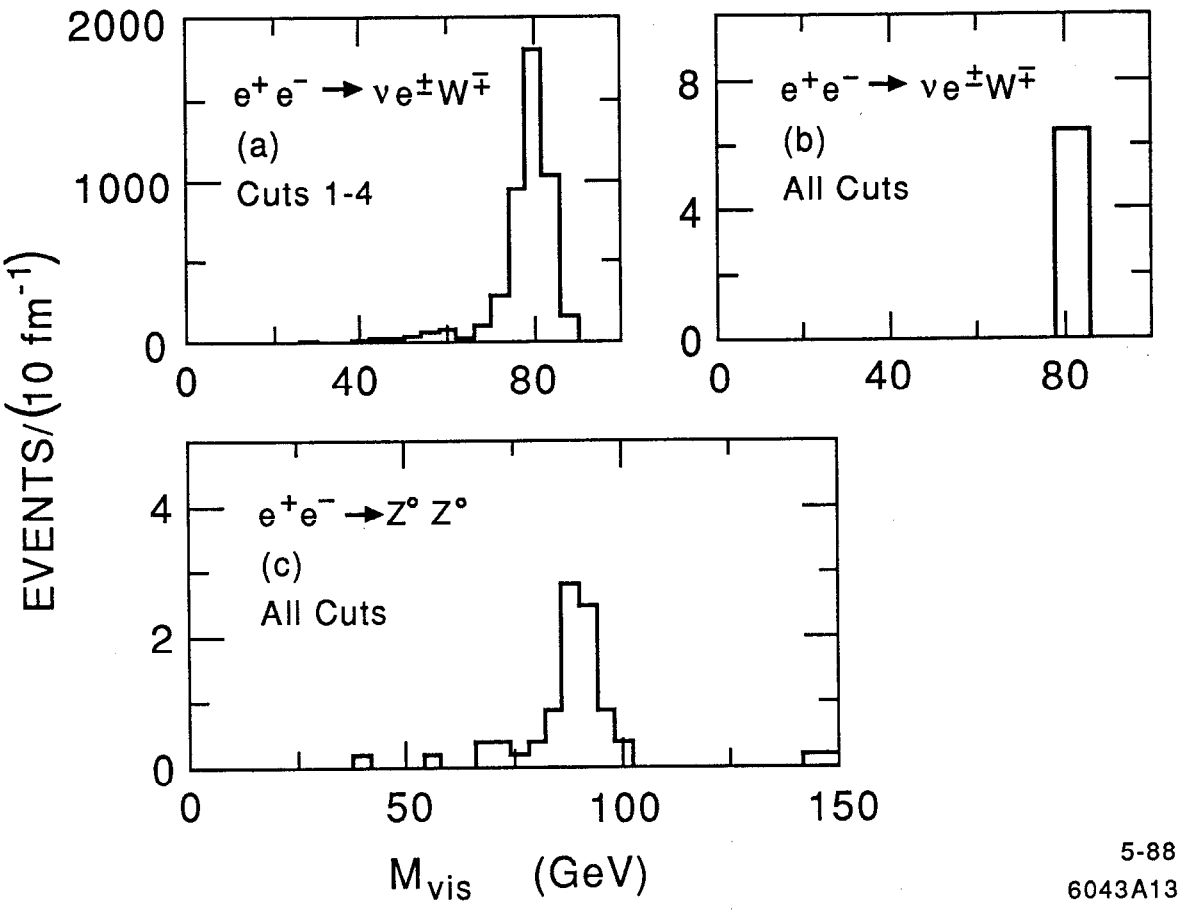

Figure 93. The visible mass, M_{vis}, observed in the major standard model backgrounds to neutralino production. In (a) and (b), $e^+e^- \rightarrow e^{\pm}\nu W^{\mp}$ events are shown, and in (c) $e^+e^- \rightarrow ZZ$ events are shown. Events passing the first four cuts described in the text are shown in histogram (a). Events passing all five cuts are shown in histograms (b) and (c). The effects of beamstrahlung are incorporated in all the histograms exhibited in this figure.

Table 11. Summary of parameters for $e^+e^- \rightarrow \tilde{\chi}_1^0 \tilde{\chi}_2^0$ Monte Carlo Runs.

Run	$\sqrt{s}$	M	μ	$\tan\beta$	$M_{\tilde{\chi}_1^0}$	$M_{\tilde{\chi}_2^0}$	$M_{\tilde{e}}$	m_{H^+}	$m_{H_2^0}$
1	600	200	160	2	66	131	200	200	51.4
2	600	300	400	2	142	262	300	300	54.0
3	1000	200	160	2	66	131	200	200	51.4
4	1000	300	400	2	142	262	300	300	54.0
5	1000	400	700	2	196	382	400	400	54.8
6	1000	500	600	2	244	460	500	500	55.2
7	1000	300	400	0.05	147	276	300	300	92.5

Table 12. Summary of results for $e^+e^- \rightarrow \tilde{\chi}_1^0 \tilde{\chi}_2^0$ Monte Carlo runs, based on 10 fm^{-1} of data.

Run	$\sqrt{s}$	R	Number of Events Before Cuts	Number of Events After Cuts 1–4	Number of Events After All Cuts	Efficiency
1	600	0.39	950	353	237	25%
2	600	0.10	240	69	46	19%
3	1000	0.55	480	213	139	29%
4	1000	0.26	225	79	53	24%
5	1000	0.19	162	58	39	24%
6	1000	0.09	79	31	21	27%
7	1000	0.25	216	73	49	23%

of the Z. As a result, M_{vis} peaks in the same region as the background (see Fig. 94(g)), and our sensitivity for detection of a signal is somewhat reduced. However, this is a rather artificial choice (we had to choose $\tan\beta = 0.05$). In any case, we presume that the lightest Higgs scalar mass will have been measured by the time the neutralino search is carried out. One may also be concerned that we did not survey parameters for which $BR(\widetilde{\chi}_2^0 \to \widetilde{\chi}_1^0 Z)$ is large. In such a case, the resulting M_{vis} distribution would also peak near m_Z. However, by comparing Figs. 84 and 92, we observe that $BR(\widetilde{\chi}_2^0 \to \widetilde{\chi}_1^0 Z) \lesssim 10\%$ in the region where $R \geq 0.1$. Hence, $\widetilde{\chi}_2^0$ decays with final state Z's will only be truly relevant at collider energies larger than 1 TeV. Finally, we note that we have not yet examined regions of parameter space where three-body decays are dominant. In such a region, we expect the M_{vis} distribution to be peaked at even smaller masses (compared to those shown in Fig. 94); this should present no special problems for isolating the signal.

Given the rather constant efficiency observed in Table 12, we estimate that the discovery limit for neutralinos at a 1 TeV e^+e^- collider (assuming 10 fb^{-1} of data) should be approximately given by the $R = 0.1$ contour of Fig. 84. At $\sqrt{s} = 600$ GeV, we can tolerate somewhat smaller values of R, perhaps as low as $R = 0.04$, assuming the same integrated luminosity as above. It remains to examine in detail the events isolated by our Monte Carlo analysis, in order to determine whether further information can be ascertained (*e.g.*, the masses and mixing angles of the two neutralinos produced and their couplings to standard model particles). This is presently under investigation.

We end this section with a few comments regarding chargino production. As demonstrated earlier, the cross section for $\widetilde{\chi}_1^+\widetilde{\chi}_1^-$ production is typically 5 times larger than the corresponding cross section for $\widetilde{\chi}_1^0\widetilde{\chi}_2^0$ production. Nevertheless, as suggested above, the $\widetilde{\chi}_1^0\widetilde{\chi}_2^0$ signal is particularly clean; very severe cuts can be made which eliminate almost entirely the standard model background, while reducing the signal by about a factor of 4. The detection techniques for $\widetilde{\chi}_1^+\widetilde{\chi}_1^-$ will require a little more finesse. We have not yet completed this analysis. Nevertheless, one should note the similarities of the chargino search to that of a new heavy lepton. Although

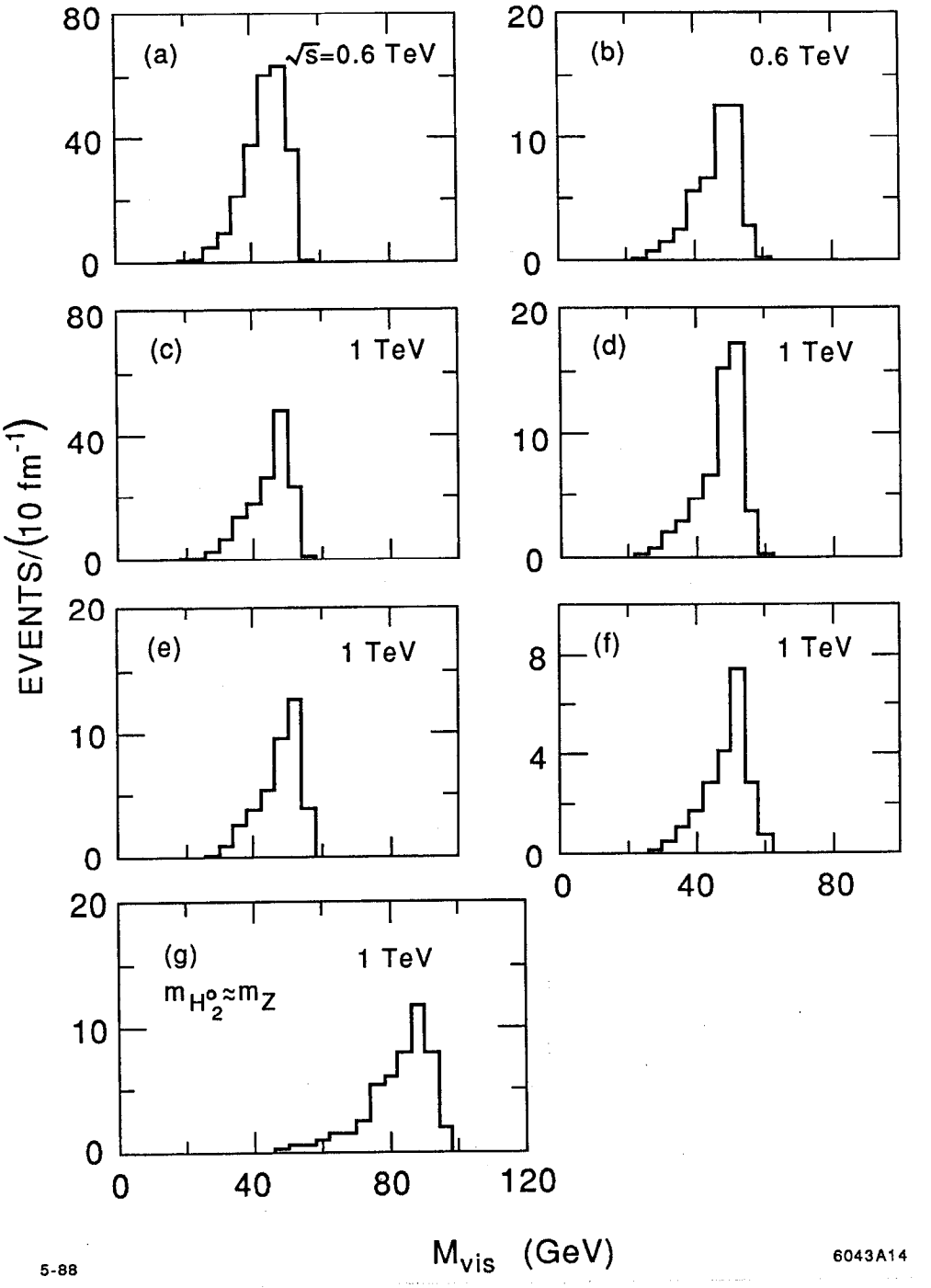

Figure 94. The visible mass, M_{vis}, is plotted for $e^+e^- \to \widetilde{\chi}_1^0\widetilde{\chi}_2^0$ events which pass all five cuts described in the text. Seven representative parameter choices, which are summarized in Table 11, are shown here. The total number of signal events which pass the cuts is summarized in Table 12.

the details of the production distribution are likely to be somewhat different, the gross features of the search technique should be rather similar. Thus, we anticipate that the discovery limits for charginos will be rather similar to those obtained for a new heavy lepton in Chapter 4.

8.4. Detection of Squarks and Sleptons

If evidence for supersymmetry is found at other colliders, it would be desirable to utilize the 1 TeV e^+e^- collider we are considering here for a detailed study of the supersymmetric particle production. The cleaner environment of e^+e^- physics should allow one to measure masses, angular distributions, asymmetries, polarization, etc. with far greater precision than is possible at a hadron collider. These studies have not been completed. Nevertheless, a few remarks at this point may be useful. From the theoretical survey of supersymmetric masses presented above, it seems likely that at least five (perhaps six) flavors of squarks are rather close in mass. Similarly, we expect that the sleptons are all also close together in mass, although this mass scale may be distinct from that of the squarks. As a result, each squark (of charge e_q in units of e) contributes $\frac{3}{4}e_q^2\beta^3$ units of R in cross sections due to one-photon exchange. This would be summed over all degenerate flavors, and multiplied by 2, counting both L and R-type squarks. (For sleptons, the color factor of 3 is removed; of course, only the charged sleptons are produced by one-photon exchange.) In addition, one must add Z-exchange, which slightly modifies the resulting cross sections. (Explicit expressions for the cross sections can be obtained from ref. 89.) The $\tilde{q}\bar{\tilde{q}}$ cross section, as a function of the (common) squark mass is illustrated in Fig. 95. The complication for squark and slepton detection arises in the decay patterns. The simplest possible decay is $\tilde{q} \to q\tilde{\chi}_1^0$. The $\tilde{\chi}_1^0$ is the LSP, which escapes the detectors. Such a signature is not all that different from that of a chargino or a new heavy lepton which is detected via its hadronic decay mode. In fact, in the case of the squark decay, which is a *two-body* decay, there is greater potential for a larger missing transverse energy which would make the signature somewhat cleaner. The complication in squark decay arises

when one considers other possible squark decay modes. Depending on the relative masses between the squark sector and the chargino/neutralino sector, one will have to consider possible decays into charginos and higher mass neutralino states: $\widetilde{q} \to q'\widetilde{\chi}_j^+$ (j = 1,2), and $\widetilde{q} \to q\widetilde{\chi}_j^0$ (j = 2,3,4). The possible number of scenarios due to the various possible decay chains becomes large as one surveys the entire range of parameter space. Despite the large number of open channels, it turns out

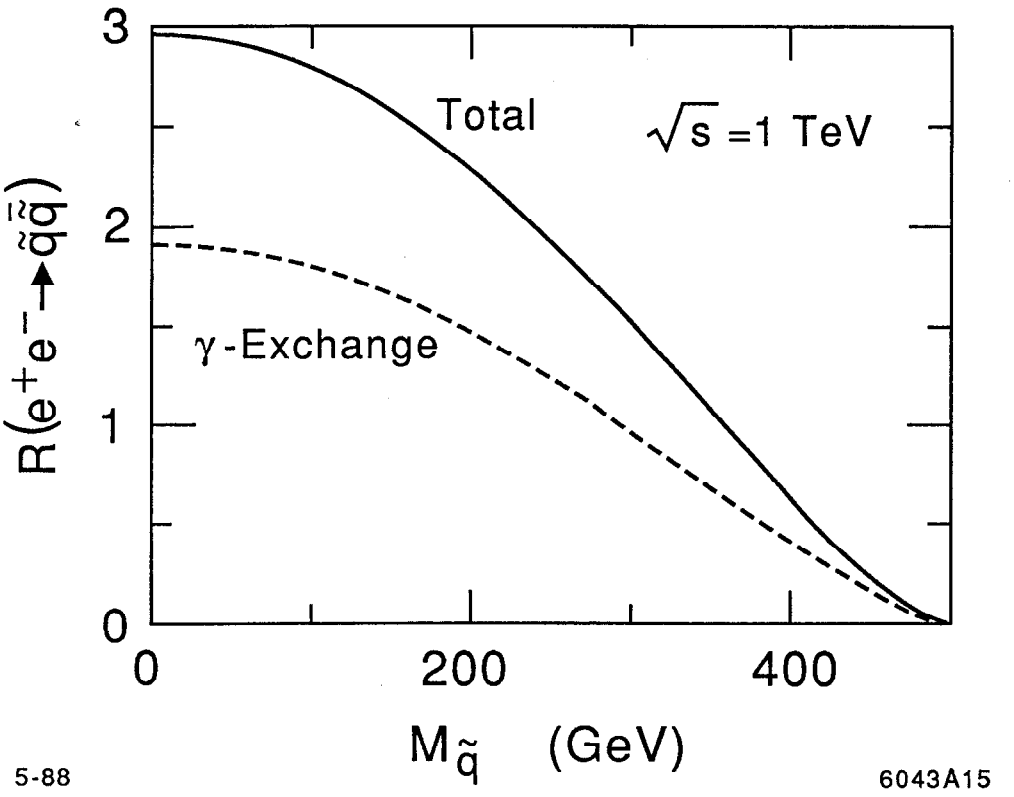

Figure 95. Total cross section for $e^+e^- \to \tilde{q}\bar{\tilde{q}}$ (in units of R) at $\sqrt{s}$ = 1 TeV, summed over two generations of L and R-type (mass-degenerate) squarks. The total cross section and the contribution due to one-photon exchange is plotted against the common squark mass, $M_{\tilde{q}}$.

that[91] the branching ratio for $\widetilde{q} \to q\widetilde{\chi}_1^0$ (averaged over one generation of L and R-type squarks) remains high (at least 50%) in the range of parameters of interest

to our study. (This should be contrasted with gluino decay, in which the branching ratio for the direct decay into the LSP quickly drops to about 14% for the heavier gluino.[92]) Thus, we tentatively conclude that there will be sufficient cross section for the production of squarks (and sleptons), which subsequently decay directly into the LSP, to allow for their detection and study at a 1 TeV e^+e^- collider, as long as the total normalized $\tilde{q}\bar{\tilde{q}}$ cross section, summed over all degenerate species, is of order 1 in units of R. More detailed conclusions await further analysis and study.

9. TeV Multiplet Searches II: Charged Higgs Bosons

Our second example of extra novel states associated with the Higgs sector will be that of charged scalar bosons. Such particles arise in a wide variety of contexts. In theories in which the Higgs particles are elementary, these states are the fundamental $SU(2) \times U(1)$ partners of the scalar Higgs boson. In theories in which the Higgs particles are composite, it is usually possible also to make composite charged objects. In technicolor models, these states are the analogues of π^+ and K^+ for the new set of strong interactions. The number and masses of charged Higgs particles are crucial identifiers of the nature of the Higgs sector responsible for $SU(2) \times U(1)$ breaking. But it is known that it will be very difficult to find charged Higgs particles at a high energy hadron collider.[93] In this section, we will show that it is quite straightforward to discover these particles at a 1 TeV e^+e^- collider.

The simplest models with charged Higgs bosons, and the one we will use to parametrize our discussion here, is a model with fundamental Higgs bosons in two SU(2) Higgs doublets:

$$\phi_1 = \begin{pmatrix} \phi_1^+ \\ \phi_1^0 \end{pmatrix}, \qquad \phi_2 = \begin{pmatrix} \phi_2^+ \\ \phi_2^0 \end{pmatrix}, \tag{9.1}$$

where ϕ_1^+, ϕ_1^0, ϕ_2^+ and ϕ_2^0 are complex fields. Therefore there are initially eight fields. The vacuum expectation values (VEV's) are

$$< \phi_1 >= \begin{pmatrix} 0 \\ v_1/\sqrt{2} \end{pmatrix}, \qquad < \phi_2 >= \begin{pmatrix} 0 \\ v_2/\sqrt{2} \end{pmatrix}. \tag{9.2}$$

Assuming no CP violation, the relative phase between the two vacuum expectation values may be set to zero. The effective vacuum expectation value for this

non-minimal model (v) is derived from the sum in quadrature of the individual VEV's, hence $m_W = g \cdot v/2 = g \cdot \sqrt{(v_1^2 + v_2^2)}/2$. Since the ρ parameter ($\rho = m_W^2/m_Z^2 \cos^2\theta_w$) is experimentally consistent with unity, ($\rho = 1.006 \pm 0.008$)[94] the Higgs multiplets are likely to be SU(2) doublets (also any number of SU(2) singlets are allowed). At least two Higgs doublets are necessary for "low energy" supersymmetric models.[83] We have also noted that extra charged Higgs bosons appear in more general models of the Higgs sector, including technicolor models.[28] For models with two Higgs doublets, there are three physical neutral Higgs bosons (H_1^0, H_2^0, H_3^0) and two charged Higgs bosons (H^+ and H^-). Originally there are four neutral and four charged fields but one neutral field and two charged fields are absorbed to give mass to the Z^0 and to $W^\pm$ by the Higgs mechanism. The mass eigenstates of the physical Higgs bosons can be mixtures of the weak eigenstates. There are two mixing angles for two Higgs doublets since the charged and neutral sector do not mix. One of the mixing angles is related to the ratio of the vacuum expectation values. In general, the physical Higgs bosons in the two doublet model are given by[95]

$$\begin{aligned} H^\pm &= -\phi_1^\pm \sin b + \phi_2^\pm \cos b, \\ H_1^0 &= \sqrt{2}[(Re\phi_1^0 - v_1)\cos a + (Re\phi_2^0 - v_2)\sin a], \\ H_2^0 &= \sqrt{2}[-(Re\phi_1^0 - v_1)\sin a + (Re\phi_2^0 - v_2)\cos a], \\ H_3^0 &= \sqrt{2}[-Im\phi_1^0 \sin b + Im\phi_2^0 \cos b]. \end{aligned} \tag{9.3}$$

The mixing angle b is defined by $\tan b = v_2/v_1$. The other angle a is also an arbitrary parameter.

Among the neutral Higgs bosons, H_3^0 is a pseudoscalar and the other two are scalars, if their parities are defined through their couplings with fermions. More precisely, if CP is a good symmetry, we can distinguish the CP-odd state H_3^0 from H_1^0 and H_2^0, which are CP-even. The interactions of Higgs bosons with fermions can be determined from the fermion mass term in the Lagrangian; these couplings are model dependent. An important constraint on the Higgs couplings is that flavor

changing neutral currents (FCNC) should not be induced by the neutral Higgs bosons (or at least that FCNC should be suppressed to within the experimentally allowed level). FCNC due to Higgs exchange are absent if fermions with the same electric and weak charges are allowed to couple only to one of the two Higgs doublets (only to ϕ_1^0 or only to ϕ_2^0).

The charged Higgs bosons are expected to be heavier than the W bosons in the minimal supersymmetric extension of the standard model,[84] but in general the mass is unknown. In the two-doublet model, the couplings of the charged Higgs bosons depends only on one mixing angle b ($\tan b = v_2/v_1$). The couplings of the charged Higgs boson to fermions are also constrained by the absence of FCNC mentioned above. There are two typical models which can avoid the FCNC which might be induced by the neutral Higgs bosons:

(1) All the fermions couple only to one of the Higgs doublets and do not couple to the other one. In this case, the relative ratios of the coupling constants of the charged Higgs boson to fermions are proportional to the fermion mass.

(2) Fermions with weak isospin $I_3 = 1/2$ couple only to one of the Higgs doublets and those with $I_3 = -1/2$ couple only to the other doublet. The relative ratios of the coupling constants depend on both the ratio of the vacuum expectation values and the fermion masses.

Of course, many other choices are possible. But in general, the coupling $H^{\pm}tb$ is larger than that for $H^{\pm}cs$ and the coupling for $H^{\pm}cs$ is larger than for $H^{\pm}ud$.

Before we begin our analysis of searches for $H^{\pm}$ at this new collider, let us review the present mass limits on the $H^{\pm}$ and the further searches expected in the near future. Charged Higgs bosons have been looked for at the PEP and PETRA e^+e^- colliders. Most of the region up to $\sim$ 19 GeV is excluded independent of the charged Higgs decay modes.[11,36,96,97] Limits below the bottom quark mass are obtained by the CLEO group[98] using the b quark decays, $b \to c + H^{\pm}$ or $u + H^{\pm}$. Techniques similar to those used at PEP and PETRA can be applied to search for a charged Higgs boson in the mass range available to SLC and LEP.[99]

If the charged Higgs mass cannot be reached by SLC/LEP or even by LEP-II, then we could in principle look for $H^{\pm}$ at the large hadron colliders (SSC or LHC). In pp collisions, a charged Higgs boson may be produced by the reaction $b+g \to t+H^-$ (and the charge conjugate process); the cross section is typically O(1-100 pb).[93] In general, though the standard neutral Higgs boson can be produced via WW- or ZZ-fusion processes, the charged Higgs boson cannot be produced via WZ-fusion processes in any Higgs doublet model, since there is no tree-level HWZ-coupling. The most promising decay mode to look for is $H^- \to \tau\overline{\nu}_\tau$, since the QCD background is not very high. However, the background from the process $b+g \to t+W^-$ with just the same event signature as the signal and a much higher cross section makes the search seem hopeless.[93] It is even more difficult to look for the decay mode $H^+ \to t+\overline{b}$, because of the higher QCD background. Therefore, although the cross section is not small, it seems to be very difficult to search for the charged Higgs bosons at hadron colliders.[100]*

On the other hand, at high energy e^+e^- colliders, the background conditions are far better and the events are cleaner since there are no spectator jets. In this chapter, we will demonstrate that it will not be difficult at all to find the charged Higgs bosons at a 1 TeV e^+e^- collider of the type that we consider in this report.

9.1. Phenomenology

The charged Higgs bosons (H^+H^-) are pair-produced in e^+e^- annihilation via virtual γ or Z^0 exchange as shown in Fig. 96(a) and 96(b). The total cross section for the process $e^+e^- \to \gamma,\ Z^0 \to H^+H^-$ is given by

$$\frac{d\sigma}{d\cos\theta} = \frac{\pi\alpha^2}{8s}\beta^3 \left[\left| 1 - \frac{(-\frac{1}{2}+\sin^2\theta_w)(\cos^2\theta_w)}{\sin^2\theta_w\cos^2\theta_w}\ \frac{s}{s-m_z^2} \right|^2 + \left| 1 - \frac{(\sin^2\theta_w)(\cos^2\theta_w)}{\sin^2\theta_w\cos^2\theta_w}\ \frac{s}{s-m_z^2} \right|^2 \right] \sin^2\theta\ . \tag{9.4}$$

* The case of charged Higgs boson production from heavy quark decay at the SSC (for example, $g+g \to t+\bar{t} \to bH^+ + \bar{b}H^-$) is under study.[101]

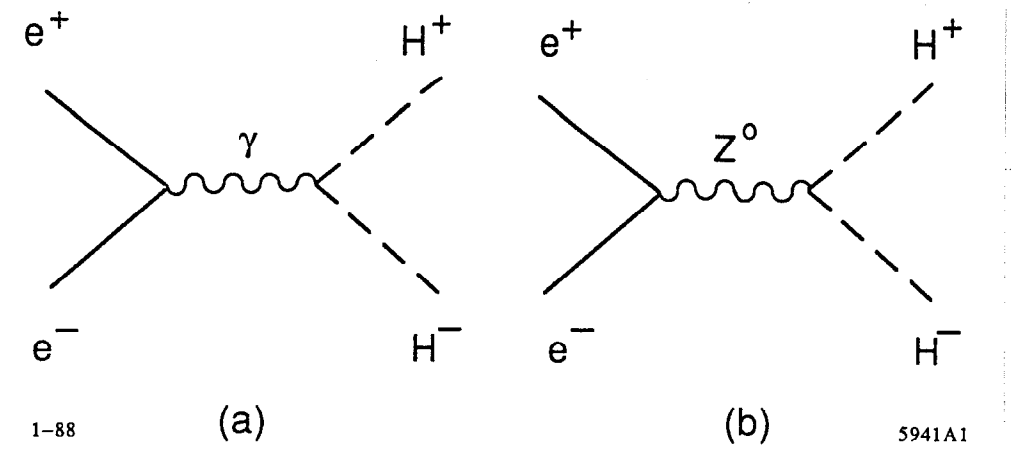

Figure 96. Feynman diagrams for charged Higgs pair production in e^+e^- annihilation.

where $\beta = (1 - 4M^2_{H\pm}/s)^{\frac{1}{2}}$.

The cross section relative to that for standard model pair production events at a 1 TeV e^+e^- collider is

$$\frac{R_{H^+H^-}}{R_{hadrons} + R_{W^+W^-} + R_{Z^0Z^0}} \approx \frac{0.30 \cdot \beta^3}{7 + 20 + 1} \approx 0.01 \cdot \beta^3. \tag{9.5}$$

(This formula does not take into account the large effects due to radiative corrections and beamstrahlung.) After a cut on the polar angle ($|\cos\theta| < 0.6$) the above ratio is about $0.03 \cdot \beta^3$. At PEP and PETRA energies, the relative cross section is

$$\frac{R_{H^+H^-}}{R_{hadrons}} \approx \frac{0.25 \cdot \beta^3}{4} \approx 0.063 \cdot \beta^3. \tag{9.6}$$

For $|\cos\theta| < 0.6$, the ratio is $0.10 \cdot \beta^3$. But although this naive estimate of the signal to background ratio gives a smaller value at the high energy colliders than at PETRA, the background situation is actually better at high energy since jet reconstruction is easier there.

The possible decay modes of the charged Higgs boson are $H^+ \to t\bar{b}$, $c\bar{s}$ or $\tau^+\nu_\tau$ as shown in Fig. 97(a), (b), and (c). The decay process $H^+ \to t\bar{b}$ is the

dominant mode for most of the parameter space, if it is kinematically allowed. If the mode $H^+ \to t\bar{b}$ is not allowed, the decay rate to $\tau^+\nu_\tau$ can be significant. For

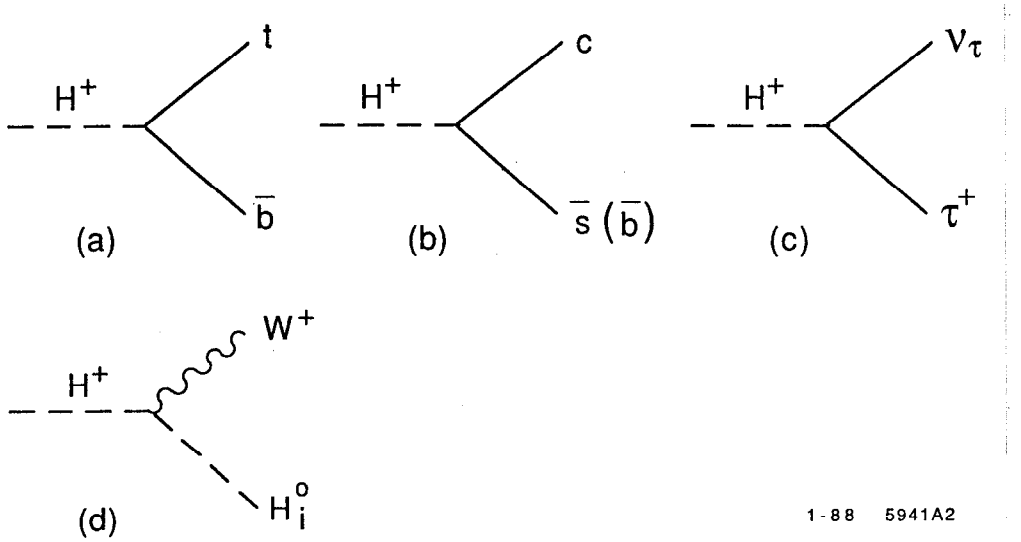

Figure 97. Feynman diagrams for the charged Higgs boson decay processes.

two doublet models the branching fraction depends on the ratio of the vacuum expectation values. If the ratio of the vacuum expectation values is close to unity, the branching fraction of $H^+ \to \tau^+\nu_\tau$ can be as large as 30%.

The other possibility for the charged Higgs decay is $H^+ \to H_i^0 + W^+$ (Fig. 97(d)), where H_i^0 is one of the physical neutral Higgs bosons. We also consider this decay mode in our discussion. This process is important because the lightest neutral Higgs boson may not be detected at LEP-II if the ZZH_i^0 coupling is suppressed. For H_3^0 (the CP odd pseudoscalar state), the ZZH_3^0 and WWH_3^0 couplings are actually forbidden, so that H_3^0 cannot be produced in the process $e^+e^- \to Z^0H_3^0$ or from WW- or ZZ-fusion. Thus this state may first be seen in $H^\pm$ decay.

Note that the charged Higgs bosons do not couple to $W^+ + Z^0$ at the tree level, if they are members of SU(2) doublets. Therefore, even if kinematically allowed,

the $H^+ \to W^+ + Z^0$ decay mode is highly suppressed.

9.2. Search for $H^+ \to t\bar{b}$

We first consider the case $M_{H^\pm} > m_t + m_b$. In this case, the dominant reaction of Higgs production and decay is $e^+e^- \to H^+H^- \to t\bar{b} + b\bar{t}$. The charged Higgs events then have approximately a four jet structure. Reconstruction of the jets and calculation of jet-jet invariant masses are the key points of this analysis. The experimental methods which are described here are essentially generalizations of those developed for PETRA[102] and for the SLC.[99] These methods can be applied at higher energy colliders if beamstrahlung effects are not too severe. Our standard beamstrahlung spectrum is turns out to be perfectly acceptable from this point of view.

In general, the Monte Carlo studies reported in this chapter assume the standard detector defined in Chapter 3. They also include the effects of beamstrahlung, using spectrum shown in Fig. 4, in computations of signal and background.

To reconstruct the jet structure of the H^+H^- events, we apply a cluster algorithm. This analysis is based on the variable d_{ij}, which defines the 'distance' between two particles (or clusters):

$$d_{ij}^2 = (|\vec{p_i}||\vec{p_j}| - \vec{p_i}\cdot\vec{p_j})(4|\vec{p_i}||\vec{p_j}|)/(|\vec{p_i}| + |\vec{p_j}|)^2. \tag{9.7}$$

This variable, which is standard for the Lund cluster algorithm,[103] is similar but not identical to the variable y_{ij} defined in (3.15). Since there are 4 jets in the lowest order for the processes $H^+H^- \to b\bar{t}t\bar{b}$, the number of reconstructed clusters is forced to equal four. The basic scheme goes as follows. Initially, each observed particle is assumed to be a cluster by itself. Then the two clusters with the smallest 'distance' d_{ij}^2 are combined by adding vectorially their 4-momenta. This is repeated until the number of clusters is reduced to four.[99]

To resolve the combinatorial problem of pairing clusters, we rely on the beam energy constraint. Even with initial state radiation and beamstrahlung effects,

most of the events with large visible energy and with good longitudinal momentum balance can be reconstructed using the beam energy constraint. For any heavy particles which are pair produced, the event shape is little modified by beamstrahlung and initial state radiation since the events cannot be produced after hard radiation. After finding four clusters (j1, j2, j3, j4), the energy of the clusters are calculated assuming that the velocity of the clusters $\vec{\beta}_i$ is as observed;[102]

$$\begin{aligned} \sum E_i &= \sqrt{s}, \\ \sum E_i \vec{\beta}_i &= \vec{0}. \end{aligned} \tag{9.8}$$

The calculated energy E_i can be negative for badly reconstructed events. Since we force the total longitudinal momentum to be zero, the individual cluster energies may be given incorrectly by the E_i in events with significant beamstrahlung. However, our analysis will show that this method nevertheless gives a good value for the mass of the pair-produced particles.

Once the E_i are found, we can search for the best combinations of two clusters for forming the H^+ and H^-. Within the three pairings of clusters (12)(34),(13)(24), and (14)(23), the pairing is selected which minimizes the quantity

$$\chi^2 = \left(\frac{\sqrt{s}/2 - E_i - E_j}{\sqrt{s}/2}\right)^2 + \alpha\left[\left(\frac{M_{ij} - M_{H^\pm}}{M_{H^\pm}}\right)^2 + \left(\frac{M_{kl} - M_{H^\pm}}{M_{H^\pm}}\right)^2\right]. \tag{9.9}$$

The parameter α is optimized so that the reconstructed mass resolution is small for H^+H^- events and, simultaneously, the mass distribution for the background is reasonably wide in order to maximize the signal to background ratio. We use the value $\alpha = 0.25$.

To enhance the H^+H^- signal relative to ordinary multihadron background, and to WW- and ZZ-background, we apply the following cuts: (These cuts are optimized for a 200 GeV $H^\pm$ and $\sqrt{s} = 600$ GeV.)

(1) $N_{ch} > 6$, where N_{ch} is the measured charged multiplicity.

(2) $E_{\rm vis} > 0.7 \cdot \sqrt{s}$, where $E_{\rm vis}$ is the total visible energy obtained by the electromagnetic and the hadron calorimeter (muon momenta are added).

(3) $|\Sigma p_z|/E_{\rm vis} < 0.2$, where Σp_z is the sum of the longitudinal momenta measured in the same way as the visible energy.

The cuts (2) and (3) reject events with large momentum imbalance along the beam direction due to beamstrahlung and initial state radiation effects.

(4) $|\cos\theta_{H^\pm}| < 0.70$, where $\theta_{H^\pm}$ is the reconstructed polar angle of the $H^\pm$ momentum.

(5) The reconstructed energy of each cluster ($E_i, i = 1,2,3,4$) should exceed 30 GeV.

(6) The difference between the $H^\pm$ and $H^\mp$ energies must be smaller than 20 GeV.

(7) The difference between the two reconstructed dijet masses must be smaller than 40 GeV.

(8) The minimum angle (ψ_{min}) between any pair of cluster momenta should be greater than 50°.

The expected ψ_{min} distributions are shown for H^+H^- events assuming $M_H^\pm$ = 150 GeV in Fig. 98(a), for multihadron events in Fig. 98(b) and for W^+W^- events in Fig. 98(c).

After the cuts (1)-(8), the distributions of the averaged invariant mass of the two reconstructed Higgs bosons are shown in Fig. 99(a) for H^+H^- events for $M_H^\pm$ = 150 GeV. The assumed charged Higgs mass of 200 GeV is used for the χ^2 calculation in eqn.(1). Hence a small enhancement is seen even above 200 GeV, but this is not a problem for reconstructing the charged Higgs mass of 150 GeV. In Fig. 99(b), (c), (d) and (e), the same plots are shown for QCD background, for W^+W^- events, for Z^0Z^0 events, and for the sum of the above three background distributions, respectively. The numbers of events in the figures correspond to an integrated luminosity of 10 fb^{-1}. (The bin size of the plots for the background

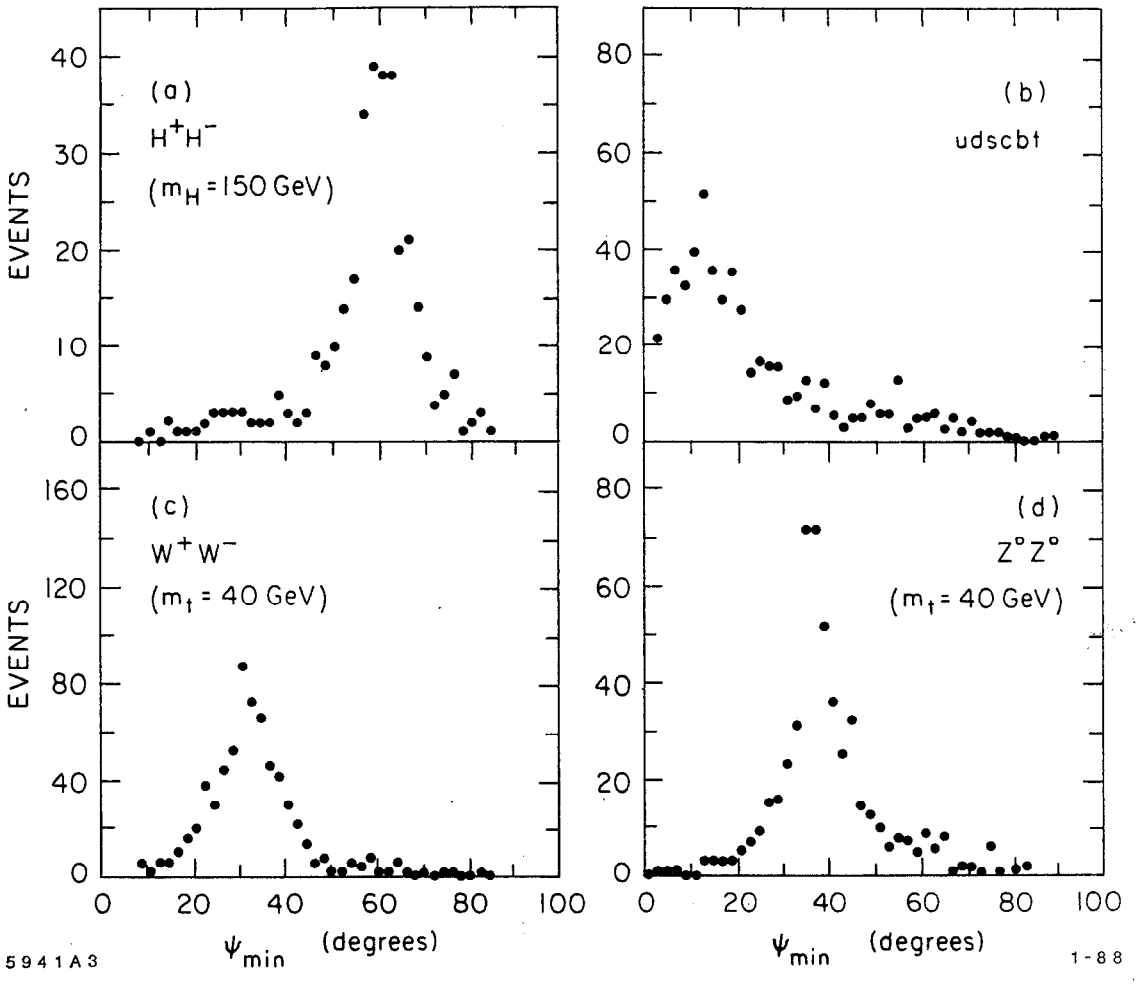

Figure 98. The distribution of the minimum angle between any pair of the cluster momenta, after the cuts (1)-(7), at $\sqrt{s}$ = 600 GeV (a) for $H^+H^- \rightarrow b\bar{t}t\bar{b}$ events for $M_{H^\pm}$ = 150 GeV and m_t = 60 GeV, with an integrated luminosity of 15 fb^{-1}; (b) for multihadron events (Lund shower model), with an integrated luminosity of 2.5 fb^{-1}; (c) for for W^+W^- events, with an integrated luminosity of 2.5 fb^{-1}; (d) for Z^0Z^0 events, with an integrated luminosity of 20 fb^{-1}.

processes ((b)-(e)) is twice as large as for the signal (a), but the integrated numbers of events are normalized correctly so that the plots can be compared by overlaying the figures. The peaks in the background plot are due to statistical fluctuations because of the small statistics of the Monte Carlo events.) It is not difficult to distinguish the charged Higgs boson production from the background. The mass resolution is determined by the jet energy calculation and hence it depends very much on the missing neutrino momenta and on the energy resolution assumed in our basic model of the the hadron calorimeter.

Since each H^+H^- event contains four B-hadrons which have a relatively long lifetime (about 1 ps), we can enhance the ratio of signal to background by selecting multi-B events using a vertex detector. In principle, the new collider should allow a very sophisticated vertex detector, but in this analysis we assumed only a modest impact parameter resolution of 40 μm, together with a beam spot size $< 1\mu m$. In this context, we apply the following additional cut:

(9) At least three charged particles are required to have momentum greater than 1 GeV and have impact parameter between 200 μm and 2 mm.

The larger impact parameter cut of 2 mm reduces the contamination from charged particles coming from K_S- or Λ-decays. After the cut (9), the reconstructed Higgs mass (defined as the average of the two dijet masses in an event) is shown in Fig. 100(a) for the case of a 150 GeV $H^{\pm}$. The corresponding background contributions are shown in Fig. 100(b). Comparing to Fig. 99, we see that the background is largely reduced.

In Figs. 101 and 102, we show the results of the same analysis for $M_{H^{\pm}} =$ 120 GeV and 200 GeV, respectively, at $\sqrt{s} = 600$ GeV. A weaker cut on the minimum angle cut between any pair of clusters ($\psi_{min} > 40°$) is applied for the case of $M_{H^{\pm}} = 120$ GeV. For $\sqrt{s} = 1$ TeV, and for an $H^{\pm}$ mass of 300 GeV, we find the mass plot of Fig. 103(a). This figure, like all of the previous ones, assumes a top quark mass of 60 GeV. Increasing the t mass to 120 GeV gives the mass plot shown in Fig. 103(b). The corresponding background plot is shown in Fig. 103(c).

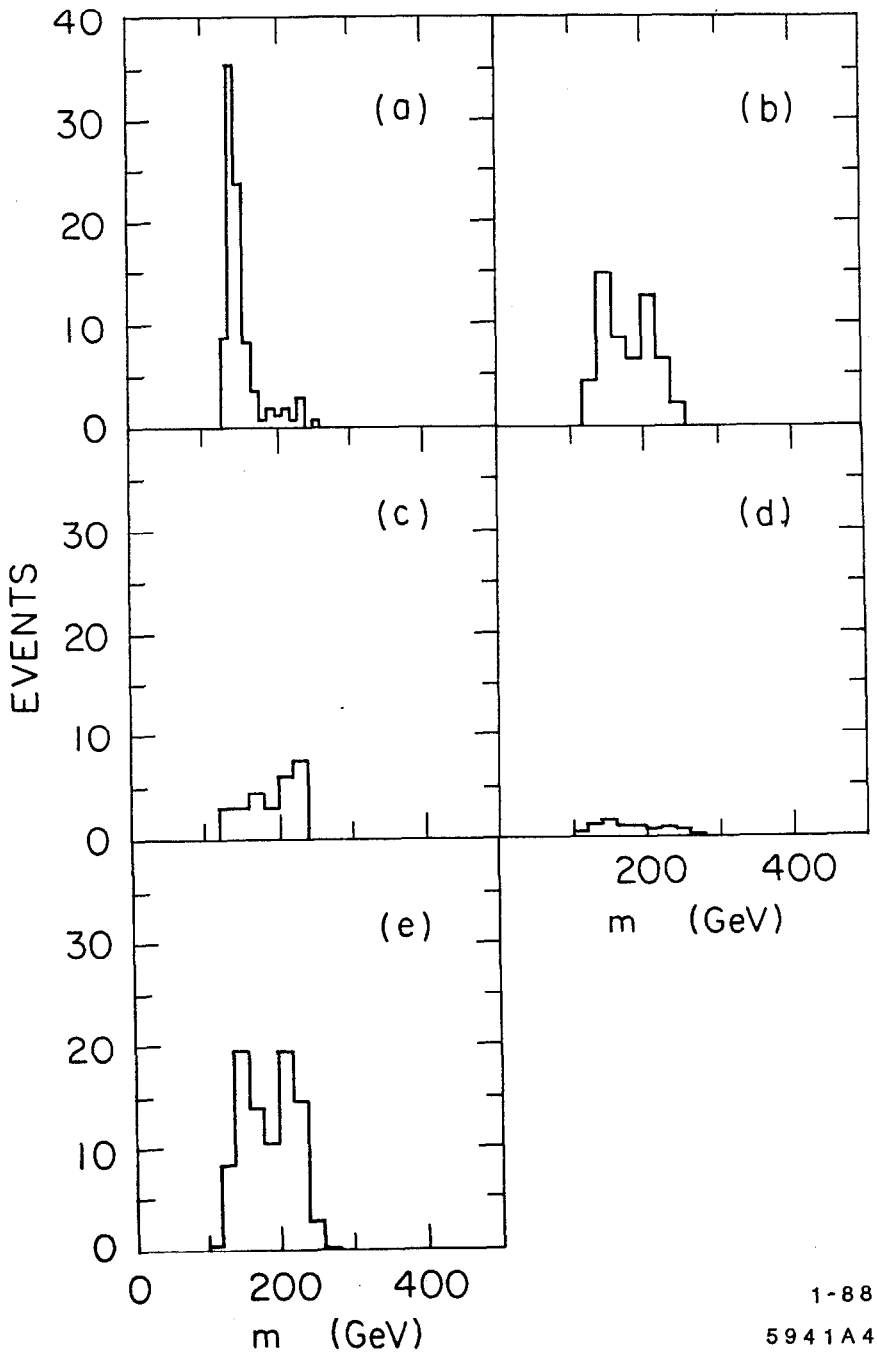

Figure 99. Reconstructed invariant mass distribution (defined as the average of the two dijet masses) for the events passing all the cuts except for the impact parameter cut (9): (a) for $H^+H^- \to b\bar{t}t\bar{b}$, with $M_{H^\pm} = 150$ GeV and $m_t = 60$ GeV, (b) for multihadron events (Lund shower model); (c) for W^+W^- events, (d) for Z^0Z^0 events; (e) for the sum of (b), (c) and (d). The cuts are optimized for a 200 GeV charged Higgs boson.

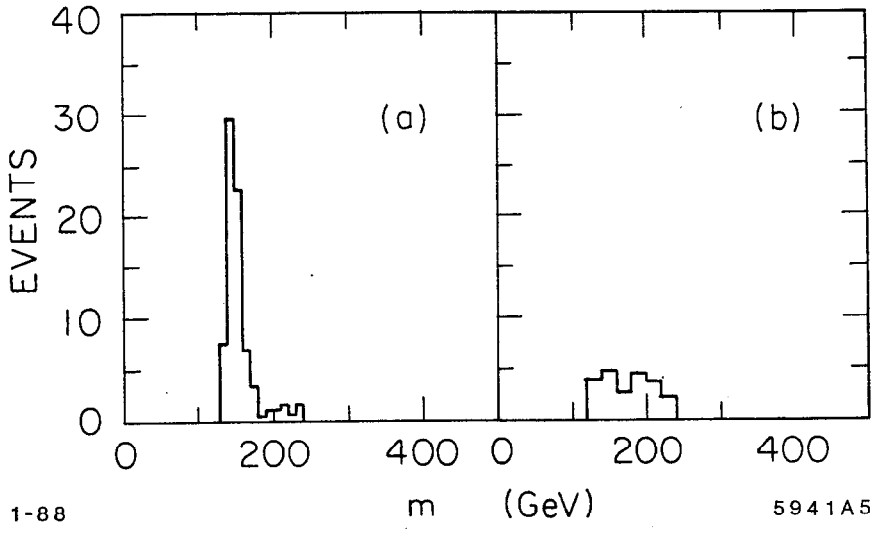

Figure 100. Reconstructed invariant mass distribution for the events passing all the cuts (1)-(9): (a) for $H^+H^- \rightarrow b\bar{t}t\bar{b}$ with $M_{H^\pm} = 150$ GeV and $m_t = 60$ GeV; (b) for the sum of $q\bar{q}$, W^+W^- and Z^0Z^0 events. The cuts are optimized for a 200 GeV charged Higgs boson.

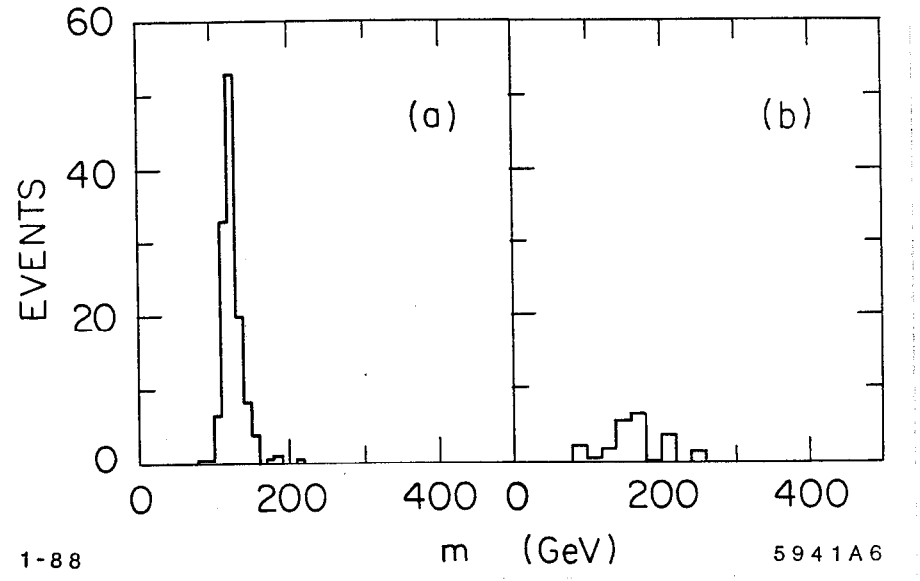

Figure 101. Reconstructed invariant mass distribution at $\sqrt{s} = 600$ GeV, after applying all the cuts: (a) for the process $H^+H^- \rightarrow b\bar{t}t\bar{b}$ with $M_{H^\pm} = 120$ GeV and $m_t = 40$ GeV; (b) for the corresponding background (sum of QCD, W^+W^- and Z^0Z^0). The cuts are optimized for $M_{H^\pm} = 120$ GeV.

Since the top decays into a bottom quark and an on shell W boson in this case, the events do not have a four jet structure. The Higgs mass peak is broader and the efficiency is worse, but the peak is still significant. All the plots are based on the integrated luminosity of 10 fb^{-1} for both $\sqrt{s}$ = 600 GeV and 1 TeV.

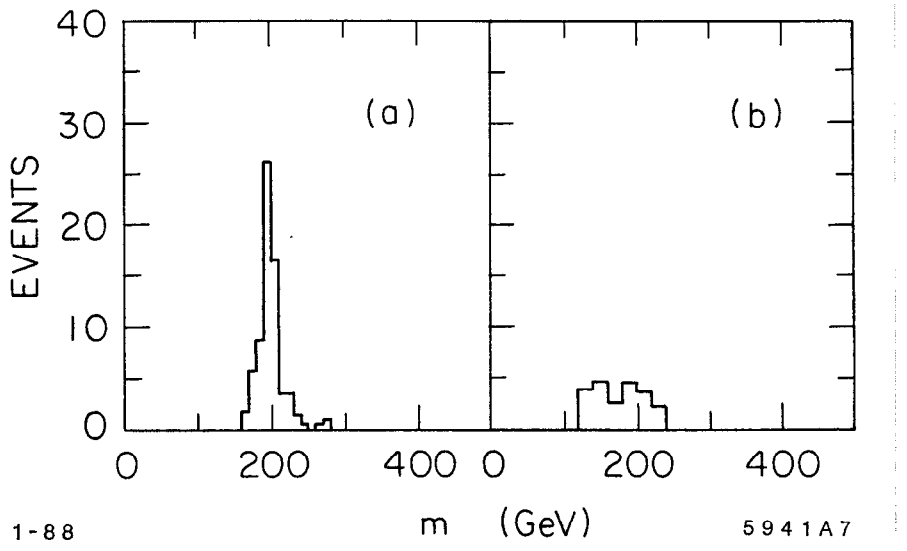

Figure 102. Reconstructed invariant mass distribution at $\sqrt{s}$ = 600 GeV, after applying all the cuts: (a) for the process $H^+H^- \rightarrow b\bar{t}t\bar{b}$ with $M_{H\pm}$ = 200 GeV and m_t = 60 GeV; (b) for the corresponding background (sum of QCD, W^+W^- and Z^0Z^0). The cuts are optimized for $M_{H\pm}$ = 200 GeV.

The QCD background for all of these analyses is estimated using the Lund QCD shower model (version 6.3)[45]This model has the uncertainties discussed in Section 3.3. However, even if the QCD background were a factor of two larger, this analysis demonstrates that we would still have no problem finding the charged Higgs signal for the decay scheme $H^+ \rightarrow t + \bar{b}$.

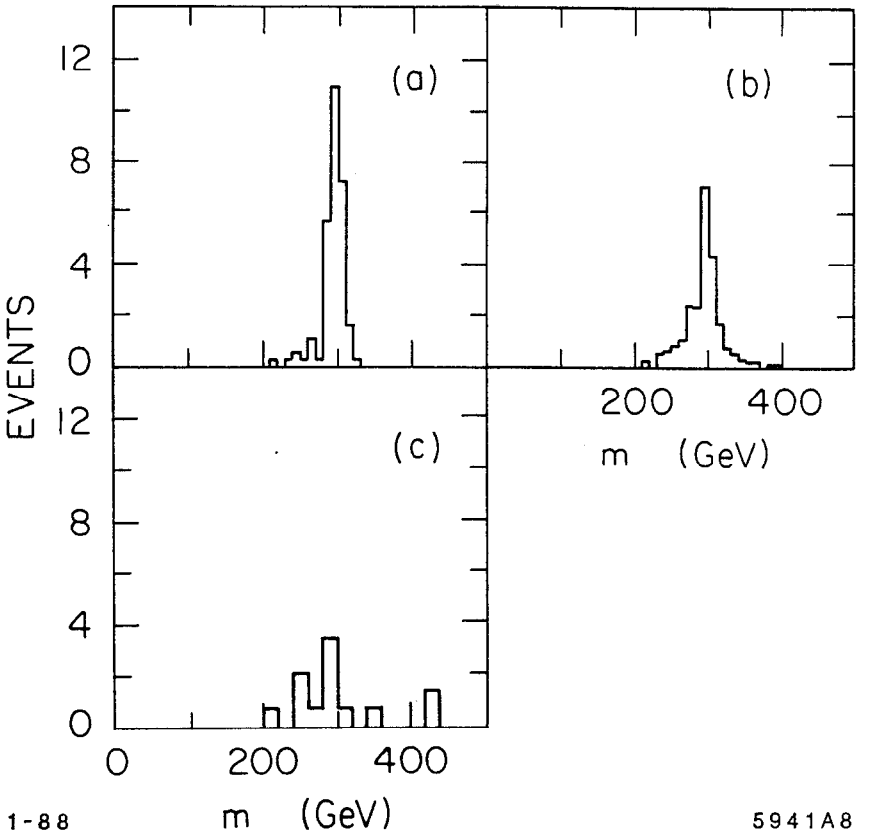

Figure 103. Reconstructed invariant mass distribution at $\sqrt{s} = 1$ TeV, after applying all the cuts: (a) for the process $H^+H^- \to b\bar{t}t\bar{b}$ with $M_{H^\pm} = 300$ GeV and $m_t = 60$ GeV; (b) for the process $H^+H^- \to b\bar{t}t\bar{b}$ with $M_{H^\pm} = 300$ GeV and $m_t = 120$ GeV; (c) for the corresponding background (sum of QCD, W^+W^- and Z^0Z^0). The cuts are optimized for $M_{H^\pm} = 300$ GeV.

9.3. Searches for $H^\pm$ in Other Modes

If the H^+ is forbidden kinematically from decaying to $t\bar{b}$, perhaps because the top quark is very heavy, there are a number of other processes which can be used to discover the charged Higgs boson. In this section, we will discuss the three most important of these.

Let us first consider $H^\pm$ decay schemes involving the τ lepton: $e^+e^- \to H^+H^- \to \tau^+\nu_\tau + s\bar{c}$ $(b\bar{c})$ or the charge conjugate. If the $H^\pm \to t + b$ decay

is kinematically forbidden, this $\tau\nu+$ hadrons topology becomes very interesting, since the decay branching fraction for the mode $H^- \to \tau^-\overline{\nu}_\tau$ can be as large as 30%. The branching fraction depends on the ratio of the vacuum expectation values.

This mode has already been looked for at PETRA and PEP. We can try similar cuts to those applied by JADE at PETRA,[96] rescaled for $\sqrt{s} = 1$ TeV. These cuts are the following:

(1) $N_{ch} \geq 2$, where N_{ch} is the visible charged multiplicity,

(2) $0.30 \cdot \sqrt{s} < E_{\rm vis} < \sqrt{s}$,

(3) $|\cos\theta_{th}| < 0.7$, where θ_{th} is the polar angle of the thrust axis,

(4) $\phi_{acop} > 20°$, where ϕ_{acop} is the acoplanarity angle of the event, defined by the thrust axes in the two hemispheres.

(5) Each thrust hemisphere is required to have at least one charged particle and an energy of at least 10 GeV. The invariant mass of the four vector sum in one of the thrust hemispheres M_1 must be larger than 150 GeV and that for the other hemisphere M_2 must be smaller than 5 GeV.

The last cut efficiently rejects W^+W^- and Z^0Z^0 events. After all the cuts (1)-(5), the detection efficiency for the H^+H^- events is about 5 % for $M_{H^\pm} = 200$ GeV and for $BR(H^- \to \tau^-\overline{\nu}_\tau) = 0.30$. The number of events expected after all the cuts is about 15, for an integrated luminosity of 10 fb^{-1}, $M_{H^\pm} = 200$ GeV and $B(H^- \to \tau^-\overline{\nu}_\tau) = 0.30$. None of the background events from multihadrons, W^+W^- or Z^0Z^0 events pass the cuts in the Monte Carlo analysis. Because of the limited Monte Carlo statistics of the background events, the 68% C.L. upper limit on the number of background events is 2. After selecting the events, the higher one of the two hemisphere masses corrected by the hemisphere visible energy

$$m = M_1(\sqrt{s}/2)/E_1 \ ,$$

is plotted in Fig. 104, where M_1 is the larger hemisphere mass and E_1 is the

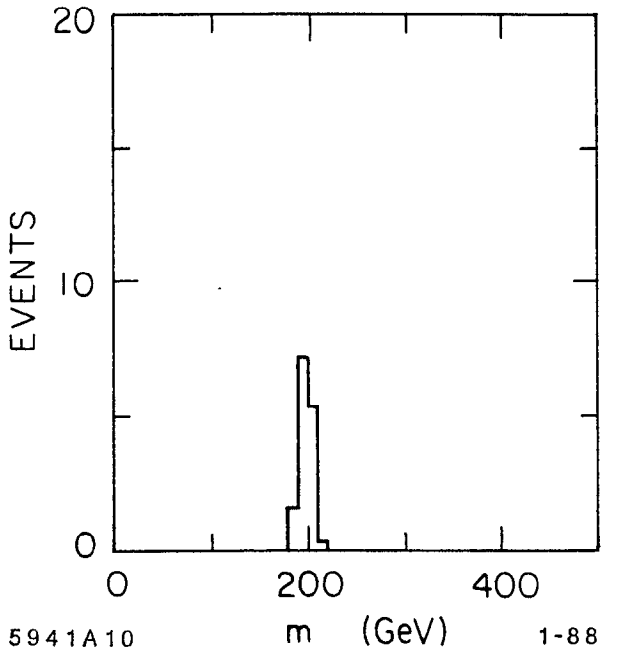

Figure 104. Plot of the corrected larger hemisphere mass ($m = M_+(\sqrt{s}/2)/E_+$) after all the cuts, computed for for H^+H^- events with $M_{H^\pm} = 200$ GeV, $\sqrt{s} = 600$ GeV, and an integrated luminosity of 10 fb^{-1}. We take $BR(H^+ \to \tau^+\nu_\tau) = 0.30$, $BR(H^+ \to c\bar{b}) = 0.05$, and $BR(H^+ \to c\bar{s}) = 0.65$. In the Monte Carlo studies no background events are survived after the cuts. Because of the limited statistics for the background calculation, the 68% C.L. of the background events in the plot is set to be 2.

corresponding visible energy in the hemisphere. A sharp peak is seen in the plot.

We can also look for charged Higgs bosons in top quark decays, since the decay channel $t \to H^+ + b$ is fully competitive with the main decay mode $t \to W^+ + b$. The ratio of the two decay widths is give by:[101]

$$\frac{\Gamma(t \to H^+b)}{\Gamma(t \to W^+b)} = \frac{p_{H+}}{p_{W+}} \frac{m_t^2(m_t^2 - M_{H+}^2)}{(m_t^2 + 2m_W^2)(m_t^2 - m_W^2)} \cot^2 b, \qquad (9.10)$$

where p_{H+} and p_{W+} are the center of mass momenta of the H^+ and W^+ for the respective decays. The cross section of $t\bar{t}$ events is greater than that for charged Higgs boson pair production by approximately an order of magnitude. For $M_{H^\pm} =$

200 GeV and $\sqrt{s} = 600$ GeV, we have

$$\sigma(e^+e^- \to H^+H^-) \approx 0.3\beta^3 \text{ R} \approx 0.12 \text{ R}\,, \tag{9.11}$$

while the cross section for $t\bar{t}$ is about 1 unit of R. Since there are now other high-mass hadronic states being produced, we concentrate on the decay mode $H^+ \to \tau^+\nu_\tau$. The signature of the τ from the charged Higgs decay is an isolated charged pion with or without accompanying π^0's (electromagnetic shower energy). On the other hand, the signature of the ordinary top quark decay ($t \to W^+ + b$) is an isolated lepton (e or μ). Of course, isolated charged pions are also produced from the chain $t \to W^+ + b \to \tau^+\nu_\tau + b \to \pi^+\overline{\nu}_\tau(+\pi^{0\prime}\text{s})\ \nu_\tau + b$. This probability is, however, about a factor of five lower than the probability of having an isolated e or μ. Therefore, by comparing the ratio of the number of isolated charged pions to the number of the isolated leptons (e's or μ's) to the same ratio expected for ordinary top decays into W^+ alone we can observe, in principle, a signal for the decay $t \to b + H^+$ *

The ratio, however, cannot be studied in the absence of the other cuts, since the isolated leptons or isolated charged pions can also come from W^+W^- or Z^0Z^0 events. Therefore, the event topology requirements are also needed to reject the background. We propose the following set of cuts:

(1) $E_{\text{vis}} > 0.5\sqrt{s}$,

(2) $|\cos\theta_{th}| < 0.8$, where θ_{th} is the polar angle of the thrust axis,

(3) Each thrust hemisphere is required to have at least three charged particles.

This cut efficiently rejects W^+W^- and Z^0Z^0 events which contain isolated charged particles.

(4) $M_{\text{out}} = \left(\sqrt{s}/E_{\text{vis}}\right) \cdot \Sigma p_T^{\text{out}} > 80$ GeV, where p_T^{out} is the transverse momentum of each particle from the plane defined by the two major sphericity axes.[104]

---

* This method was first tried for charged Higgs boson searches in $t\bar{t}$ production at SSC.[101] The background calculation for the QCD processes at SSC is not yet completed.

Table 13. Comparison of number of isolated leptons and isolated charged pions, for $M_{H^\pm} = 150$ GeV, $m_t = 200$ GeV and $\int \mathcal{L} = 10$ fm^{-1}.

Process	Total Events	Isolated Leptons	Isolated $\pi^\pm$	$\pi^\pm / \ell^\pm$
$t \to W^\pm$ or $H^\pm + b$	3,436	272	171	0.629 ± 0.061
$t \to W^\pm + b$ (no $H^\pm$)	3,436	445	104	0.234 ± 0.025
Light quark pair ($udscb$)	93,647	4.3	4.0	
W^+W^-	65,100	48	26	
Z^0Z^0	3,858	7.2	5.3	

In the sample of events obtained by the above cuts, the inclusive numbers of isolated leptons (e's and μ's) or isolated charged pions are counted. The isolation condition for the charged particle is

(5) The momentum must be larger than 2 GeV. The isolation parameter[105] $\rho = \sqrt{2|\vec{p}_i|(1-\cos\theta_{Ji})}$ must satisfy the condition $\rho > 3.0$ GeV$^{1/2}$, where $\vec{p}_i$ is the isolated charged particle momentum and θ_{Ji} is the angle between the isolated charged particle i and the nearest jet J, which is defined by the Lund jet algorithm.[103]

After the cuts, the numbers of isolated leptons or isolated charged pions are given in Table 13. For the first row, $\Gamma(t \to H^+ + b) = \Gamma(t \to W^+ + b)$ is assumed. The numbers of events are based on the cross section with initial state radiation (the maximum initial state photon energy is 99% of $\sqrt{s}/2$) and beamstrahlung.

If the background is taken into account, the ratio ($\#\ \pi^\pm$ / $\#\ \ell^\pm$) for $BR(t \to W^+b) = 1.0$ (no charged Higgs boson below top mass) is 0.276 ± 0.026 and for the case $BR(t \to H^+b) = 0.5$ the number is 0.622 ± 0.055. These two numbers differ by more than five standard deviations. The ratios are not very sensitive to the top mass as long as the number of isolated $\pi^\pm$ and $\ell^\pm$ from the background is small compared with those from the top quark decays. For a 250 GeV top quark and

a 150 GeV $H^{\pm}$, the effect is still more than four standard deviations if $BR(t \rightarrow H^{+}b) = 0.5$. Perfect e, μ and $\pi^{\pm}$ identification is assumed here. Since there are not many isolated charged tracks, reasonably conservative values of the e μ and charged pion misidentification probabilities do not significantly change the result. For example with the lepton detection efficiency $P(\ell \rightarrow \ell) = 0.9$, the charged pion efficiency $P(\pi \rightarrow \pi) = 0.9$, the lepton misidentification probability $P(\ell \rightarrow \pi) = 0.01$, and the pion misidentification probability $P(\pi \rightarrow \ell) = 0.01$, the ratio ($\#\ \pi^{\pm}$ / $\#\ \ell^{\pm}$) for $BR(t \rightarrow W^{+}b) = 1.0$ is 0.286 ± 0.028, and for the case $BR(t \rightarrow H^{+}b) = 0.5$ the number is 0.629 ± 0.058. The efficiencies and misidentification probabilities are defined within the acceptance of our model detector.

Finally, we consider the possible decay of the charged Higgs boson into a W boson and a neutral Higgs. If there is a light neutral Higgs boson, charged Higgs bosons may decay into W plus this light neutral Higgs boson. For the scalar Higgs bosons (CP even states), the decay branching fraction of the process $H^{+} \rightarrow W^{+}H_i^0$ ($i = 1, 2$) may be suppressed due to the Higgs mixing. If the lightest Higgs is pseudoscalar (CP odd state H_3^0), there is no such suppression for two doublet models. This case is more interesting because a pseudoscalar Higgs cannot be produced from the process $e^{+}e^{-} \rightarrow Z^0 H_3^0$ or from WW- or ZZ-fusion since there is no tree level ZZH_3^0- or WWH_3^0-coupling. The decay branching fraction of $H^{+} \rightarrow W^{+}H_i^0$ depends on the top mass but it can be the dominant decay mode if H_i^0 is light enough. The dominant decay mode of the H_i^0 is normally $b\bar{b}$. For simplicity, $M_{H^{\pm}} = 150$ GeV, $BR(H^{+} \rightarrow W^{+}H_i^0) = 1$, $M_{H_i^0} = 25$ GeV, and $BR(H_i^0 \rightarrow b\bar{b}) = 1$ are assumed. B-tagging techniques can be used to select these events since each event contains at least four B-hadrons.

The most promising process, having a distinctive event topology and the advantage of charged Higgs mass reconstruction, is when one W decays leptonically and the other W decays hadronically. This gives events of the form $e^{+}e^{-} \rightarrow H^{+}H^{-} \rightarrow H_i^0 W^{+} + H_i^0 W^{-} \rightarrow b\bar{b} + \ell^{\pm}\nu_{\ell} + b\bar{b} + q\bar{q}'$. The events are selected by requiring an isolated lepton from a W decay and also requiring tracks with a large impact parameter (B-tagging).

The events are selected by using the same set of cuts for the $t\bar{t}$ selection discussed in the previous section (cuts (1)-(4)). Also an isolated charged lepton is required. The isolation condition is just as in the previous section (cut (5)).

Since the event signature is one isolated lepton plus four jets (two H_3^0 jets and two jets from W-decay), the selected events are forced to form four clusters after removal of the isolated lepton. The events must have a W boson, so one of the pairs of jets is required to sum to the W mass. That is, we place the additonal cut:

(6) A combination of two jets (i and j) exits and satisfies

$$|M_{ij} - m_W| < 5 \text{ GeV} .$$

After all the cuts, the higher hemisphere mass corrected by the hemisphere visible energy $M_1(\sqrt{s}/E_1)$ is plotted in Fig. 105(a). The corresponding background is shown in Fig.105(b). One can see a clean peak of about 50 events at 150 GeV.

It should be noted that H_3^0 can be found at LEP-II if both the H_3^0 and $H^\pm$ are so light that the $W^\pm$ can decay into $H^\pm H_3^0$.[106] Since the branching fraction is not large, $O(1\%)$, the best process to look at is $e^+e^- \to W^+W^-$ with one W decaying subsequently into $H^\pm H_3^0 \to \tau^\pm \nu_\tau + b\bar{b}$ and the other W decaying leptonically. Since only the H_3^0 decays hadronically in the event the H_3^0 mass can be reconstructed. Measuring the momentum spectrum of the H_3^0 allows the $H^\pm$ mass to be determined.

The general conclusions of our study of charged Higgs boson searches are the following:

(1) With a 1 TeV e^+e^- linear collider and an integrated luminosity of 10 fb^{-1}, we can detect production of charged Higgs bosons and determine its mass for $H^\pm$ masses of less than 80 % of the beam energy and a dominant decay mode of $H^+ \to t + \bar{b}$.

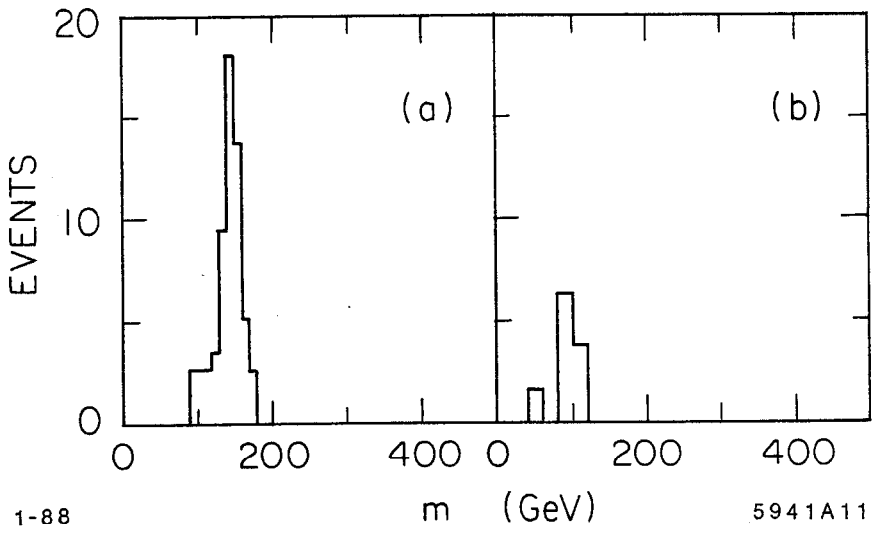

Figure 105. Plot of the corrected larger hemisphere mass ($m = M_+(\sqrt{s}/2)/E_+$) after all the cuts: (a) for H^+H^- events at $\sqrt{s} = 600$ GeV with integrated luminosity of 10 fb^{-1}, $M_{H^\pm} = 150$ GeV, $BR(H^+ \to W^+H_3^0) = 1.00$, $M_{H_3^0} = 25$ GeV and $BR(H_3^0 \to b\bar{b}) = 1.00$; (b) the corresponding background plot for the sum of QCD processes, W^+W^- and Z^0Z^0, again with 10 fb^{-1}.

(2) If the charged Higgs boson is sufficiently lighter than the top quark, the top quark decays to $H^+ + b$. We can detect the signal of the charged Higgs boson both through its direct pair production and in the top quark decay.

(3) If there is a light neutral Higgs boson, a charged Higgs boson may decay into W plus the neutral Higgs with a large branching fraction. Even if neutral Higgs bosons cannot be produced via the process $e^+e^- \to Z^0H_i^0$, or WW-or ZZ-fusion (for example, the CP odd state), the neutral higgs boson can be produced and detected in the decay $H^\pm \to W^\pm H_i^0$.

(4) It is necessary to understand the higher order QCD processes and to improve the QCD shower models, and to test them at lower energies. Also processes containing weak vector bosons must be experimentally understood.

(5) Beamstrahlung effects must be moderate. We have to compromise between the integrated luminosity and the beamstrahlung effect. But the realistic

spectrum which we assumed for our Monte Carlo studies proved to be are perfectly acceptable for studies of charged Higgs boson production.

10. Conclusions

In this report, we have presented a number of the central experiments which might be conducted at a e^+e^- collider operating in the energy region 600 GeV – 1 TeV. We have discussed the the significance of these experiments to the progress of high energy physics, and we have demonstrated that these experiments can be carried out with realistic detectors and in the environment which one might anticipate from the collider design. We have concentrated on the most important issue of the search for manifestations of the Higgs boson sector and other indications of new physics beyond the standard model. But along this line, we have sketched a rich experimental program, with great potential for major discoveries.

We analyzed in detail four classes of experiments which probe for physics beyond the standard model. We first considered searches for new quarks and leptons; our conclusion here was that these objects could be identified from event samples of a few fb^{-1}. We exhibited very efficient search procedures for isolating these states; this analysis suggests that one can go on to measure branching ratios and decay parameters for these new states.

We then studied experiments which can isolate the neutral Higgs boson of the standard model. Outside of a small range around the mass of the W, we found that this search could be done in a completely straightforward way by utilizing the WW fusion process of Higgs production. The technique reconstructs the Higgs boson from its major decay modes and could be used to study the decays of the Higgs in more detail. This search required larger event samples, of order 30 fb^{-1}.

We studied searches for modifications of the gauge theory of weak interactions at high energy. We discussed the effect on e^+e^- annihilation processes of the presence of a new Z^0 resonance. This effect is of course dramatic if the new

resonance lies within the energy range of the collider, but we found observable effects also from resonances a factor of 3 higher in mass. This discussion also illustrated the use of longitudinal polarization of the electron beam as a sensitive diagnostic tool. We discussed precision tests of the weak interaction couplings in the process $e^+e^- \to W^+W^-$. We showed that, assuming an event sample of 30 fb^{-1}, one can measure the differential cross section for W pair production with sufficient accuracy to be sensitive to the radiative corrections which would signal new heavy fermions or a strongly-coupled Higgs sector.

Finally, we analyzed searches for two specific manifestations of larger new sectors of physics beyond the standard model. We found that the pair-production of neutral supersymmetric particles can be isolated in event samples of 10 fb^{-1}. Our analysis makes clear that a wide variety of the states predicted by theories of supersymmetry can be discovered at this high-energy collider. We also found that charged Higgs bosons can be isolated in events samples of 10 fb^{-1}, by direct reconstruction of these states from their major hadronic decays.

The integrated luminosity samples called for in this summary of our results are large by the current standards of high energy physics. This is the result of the well-known feature of any point-like process that cross sections decrease dramatically with energy, proportional to E_{CM}^{-2}. This feature presents a challenge to accelerator designers, to construct machines which deliver e^+e^- luminosities in excess of 10^{33} $\text{cm}^{-2}\text{sec}^{-1}$. This problem is an inseparable part of the challenge of e^+e^- physics. In this report, we have documented the experimental advantages that make this problem worth solving. We have shown that the experimental environment of an e^+e^- collider remains exceptionally clean at these high energies, even in the presence of those compromises in beam energy spread and access to forward angles which might be necessary to achieve a high luminosity.

We have, then, seen the breadth and clarity of view into the fundamental processes of physics which a 1 TeV e^+e^- collider will provide. We look forward to the coming era of e^+e^- experimentation in this high energy regime, and to the

realization of the great promise which this experimental program offers.

REFERENCES

1. F. Bulos, *et. al.*, in *Proceedings of the 1982 DPF Summer Study on Elementary Particles and Future Facilities (Snowmass, Colo.)*, R. Donaldson, R. Gustafson, and F. Paige, eds. (Fermilab, 1982).
2. J. Ellis, in *Proceedings of the XIV International Symposium on Multiparticle Dynamics,* P. Yager and J. F. Gunion, eds. (World Scientific, Singapore, 1984).
3. M. E. Peskin, in *Physics in Collision 4,* A. Seiden, ed. (Éditions Frontières, Gif-sur-Yvette, 1984).
4. J. Dorfan and R. J. Van Kooten, in *The Fourth Family of Quarks and Leptons,* D. B. Cline and A. Soni, eds. Ann. N. Y. Acad. Sci., vol. 518 (1987).
5. G. Altarelli in *Proceedings of the Workshop on Physics at Future Accelerators (La Thuile),* J. H. Mulvey, ed. (CERN, Geneva, 1987).
6. J. Ellis and F. Pauss, in *Proceedings of the Workshop on Physics at Future Accelerators (La Thuile),* J. H. Mulvey, ed. (CERN, Geneva, 1987).
7. M. E. Peskin, in *Proceedings of the Fifteenth SLAC Summer Institute on Particle Physics (August, 1987)*, E. C. Brennan, ed. SLAC–Report–328 (1988).
8. G.J. Feldman, in *Proceedings of the Fifteenth SLAC Summer Institute on Particle Physics (August, 1987)*, E. C. Brennan, ed. SLAC–Report–328 (1988).
9. S. L. Wu, *Phys. Rep.* **107,** 59 (1984).
10. P. Duinker, *Rev. Mod. Phys.* **54,** 325 (1982).
11. S. Komamiya, in *Proceedings of the 1985 International Symposium on Lepton and Photon Interactions at High Energies*, M. Konuma and K. Takahashi, eds. (Nissha, Kyoto, 1986).

12. E. Eichten, I. Hinchliffe, K. D. Lane, and C. Quigg, *Rev. Mod. Phys.* **56,** 579 (1984).

13. G. Ekspong and K. Hultqvist, USIP Report 82-05 (1982); W. Innes, in *Proceedings of the Second Mark II Workshop on SLC Physics (Granlibakken),* G. Feldman, ed. SLAC-Report-306 (1986)

14. J. Boucrot, *et. al.*, CERN preprint CERN-EP/87-40 (1987).

15. R. Cahn, *et. al.*, in *Proceedings of the Workshop on Experiments, Detectors, and Experimental Areas for the Supercollider (Berkeley),* R. Donaldson and M. G. D. Gilchriese, eds. (World Scientific, Singapore, 1988).

16. M. Chanowitz and M. K. Gaillard, *Nucl. Phys.* **B261,** 379 (1985).

17. J. F. Gunion, G. L. Kane, and J. Wudka, *Nucl. Phys.* **B299,** 231 (1988).

18. M. S. Chanowitz, in *Proceedings of the Salt Lake City Meeting (APS-DPF, 1987),* C. DeTar and J. Ball, eds. (World Scientific, Singapore, 1987).

19. M. Chanowitz, M. A. Furman, and I. Hinchliffe, *Phys. Lett.* **78B,** 285 (1978), *Nucl. Phys.* **B153,** 402 (1979).

20. E. Eichten, in *High Energy Physics 1985* (Proceedings of the Yale Theoretical Advanced Study Institute). M. Bowick and F. Gürsey, eds. (World Scientific Press, Singapore, 1986).

21. B. Pendleton and G. Ross, *Phys. Lett.* **98B,** 291 (1981).

22. C. Hill, *Phys. Rev.* **D24,** 691 (1981).

23. M. Claudson, L. J. Hall, and I. Hinchliffe, *Nucl. Phys.* **B228,** 501 (1983).

24. C. Preitschopf, unpublished.

25. K. Inoue, A. Kakuto, H. Komatsu, and S. Takeshita, *Prog. Theor. Phys.* **68,** 927 (1982) (E: **70,** 330, (1983)); **71,** 413 (1984).

26. R. Flores and M. Sher, *Annals of Physics (NY)* **148,** 95 (1983).

27. H. E. Haber and M. Sher, *Phys. Rev.* **D35,** 2206 (1987); M. Drees, *Phys. Rev.* **D35,** 2910 (1987); J. F. Gunion, L. Roszkowski and H. E. Haber, *Phys. Lett.* **189B,** 409 (1987); J. Ellis, D. V. Nanopoulos, S. T. Petcov, and F. Zwirner, *Nucl. Phys.* **B283,** 93 (1987).

28. E. Farhi and L. Susskind, *Phys. Rep.* **74,** 277 (1981).

29. M. E. Peskin, *Nucl Phys.* **B175,** 197 (1980); J. P. Preskill, *Nucl. Phys.* **B177,** 21 (1981).

30. E. J. Eichten, K. D. Lane, and M. E. Peskin, *Phys. Rev. Lett.* **50,** 811 (1983).

31. B. Schrempp, F. Schrempp, N. Wermes, and D. Zeppenfeld, *Nucl. Phys.* **B296,** 1 (1988).

32. B. W. Lee, C. Quigg, and H. Thacker, *Phys. Rev.* **D16,** 1519 (1977).

33. D. P. Barber, *et. al.*, *Phys. Rev. Lett.* **45,** 1904 (1980).

34. H.-J. Behrend, *et. al.*, *Phys. Lett.* **114B,** 287 (1982).

35. B. Adeva, *et. al.*, *Phys. Lett.* **115B,** 345 (1982).

36. M. Althoff, *et. al.*, *Phys. Lett.* **122B,** 95 (1983).

37. K. Yokoya, *Nucl. Instrum. Methods* **A251,** 1 (1986); P. Chen, SLAC-PUB-4293 (1987).

38. SLD Design Report, SLAC–Report–273 (1984).

39. F. A. Berends, R. Kleiss, and S. Jadach, *Nucl. Phys.* **B202,** 63 (1982); *Comp. Phys. Comm.* **29,** 185 (1983).

40. M. Katuya, *Phys. Lett.* **124B,** 421 (1983).

41. We are grateful to K.-K. Gan for this observation.

42. I. Hinchliffe, in *Proceedings of the 1982 DPF Summer Study on Elementary Particles and Future Facilities (Snowmass, Colo.),* R. Donaldson, R. Gustafson, and F. Paige, eds. (Fermilab, 1982).

43. O. P. Sushkov, V. V. Flambauer, and I. B. Khriplovich, *Sov. J. Nucl. Phys.* **20,** 537 (1975).

44. W. Alles, Ch. Boyer, and A. Buras, *Nucl. Phys.* **B119,** 125 (1977).

45. T. Sjostrand and M. Bengtsson, Computer Phys. Comm. 43, 367 (1987); *Nucl. Phys.* **B289,** 810 (1987).

46. A. Petersen, *et. al.*, SLAC-PUB-4290 (1987).

47. G. Marchesini and B.R. Webber, *Nucl. Phys.* **B238,** 1 (1984); B.R. Webber, *Nucl. Phys.* **B238,** 492 (1984).

48. This program is described in M. Davier, *et. al.*, in *Proceedings of the ECFA Workshop on LEP200 (Aachen)*, A. Bohm and W. Hoogland, eds. (CERN, Geneva, 1987).

49. R. Ansari, *et. al.*, *Phys. Lett.* **186B,** 452 (1987).

50. J. F. Gunion, Z. Kunszt, and M. Soldate, *Phys. Lett.* **163B,** 389 (1985) (E: **168B,** 427 (1986)); W. J. Stirling, R. Kleiss, and S. D. Ellis, *Phys. Lett.* **163B,** 261 (1985).

51. J. F. Gunion and M. Soldate, *Phys. Rev.* **D34,** 826 (1986); R. Kleiss and W. J. Stirling, *Phys. Lett.* **200B,** 193 (1988).

52. J. C. Pati and A. Salam, *Phys. Lett.* **58B,** 333 (1975).

53. G. Senjanović, F. Wilczek, and A. Zee, *Phys. Lett.* **141B,** 389 (1984).

54. T. Banks and M. Karliner, *Nucl. Phys.* **B281,** 399 (1987).

55. J. L. Rosner, *Comments on Nucl. and Part. Phys.* **15,** 195 (1986); V. D. Angelopoulos, J. Ellis, H. Kowalski, D. V. Nanopoulos, N. D. Tracas, and F. Zwirner, *Nucl. Phys.* **B292,** 59 (1987).

56. J. Bagger, S. Dimopoulos, and E. Massó, *Nucl. Phys.* **B253,** 397 (1985).

57. J. F. Gunion and A. Tofighi-Niaki, *Phys. Rev.* **D36,** 2671 (1987).

58. J. Gunion, P. Kalyniak, M. Soldate, and P. Galison, *Phys. Rev.* **D34,** 101 (1986).

59. R. Cahn, *Nucl. Phys.* **B255,** 341 (1985).

60. E. Gabrielli, in *Proceedings of the Workshop on Physics at Future Accelerators (La Thuile),* J. H. Mulvey, ed. (CERN, Geneva, 1987).

61. M. E. Peskin, unpublished.

62. R. Ansari, *et. al.*, *Phys. Lett.* **195B,** 613 (1987).

63. U. Amaldi, *et. al.*, *Phys. Rev.* **D36,** 1385 (1987).

64. A. Jodido, *et. al.*, *Phys. Rev.* **D34,** 1967 (1986) (E: **D37,** 237 (1988)).

65. G. Beall, M. Bander, and A. Soni, *Phys. Rev. Lett.* **48,** 848 (1982).

66. P. Candelas, G. Horowitz, A. Strominger, and E. Witten, *Nucl Phys.* **B258,** 46 (1985).

67. M. Dine, V. Kaplunovsky, M. Mangano, C. Nappi, and N. Seiberg, *Nucl. Phys.* **B259,** 549 (1985).

68. P. Langacker, R. W. Robinett, and J. L. Rosner, *Phys. Rev.* **D30,** 1470 (1984).

69. R. W. Robinett and J. L. Rosner, *Phys. Rev.* **D26,** 2396 (1982).

70. E. Witten, *Nucl. Phys.* **B258,** 75 (1985).

71. C. Dib and F. J. Gilman, *Phys. Rev.* **D36,** 1337 (1987).

72. B. W. Lynn, R. G. Stuart, and M. Cvetič, SLAC-PUB-4624 (1988).

73. J. M. Cornwall, D. N. Levin and G. Tiktopoulos, *Phys. Rev.* **D10,** 1145 (1974) (E: **D11,** 972 (1975)).

74. K. Hagiwara, R. D. Peccei, D. Zeppenfeld, and K. Hikasa, *Nucl. Phys.* **B262,** 233 (1987).

75. C. Ahn, M. E. Peskin, B. W. Lynn, and S. Selipsky, SLAC-PUB-4600 (1988).

76. M. Kuroda, F. M. Renard, and D. Schildknecht, *Phys. Lett.***183B,** 366 (1987).

77. T. Applequist and J. Carazzone, *Phys. Rev.* **D11,** 2856 (1975).

78. K. Lane, in *Proceedings of the 1982 DPF Summer Study on Elementary Particles and Future Facilities (Snowmass, Colo.),* R. Donaldson, R. Gustafson, and F. Paige, eds. (Fermilab, 1982).

79. C. Albajar *et. al.*, *Phys. Lett.* **198B,** 261 (1987).

80. See, *e.g.*, H.J. Behrend *et. al.*, *Z. Phys.* **C35,** 181 (1987).

81. H.P. Nilles, *Phys. Rep.* **110,** 1 (1984).

82. M.B. Green, J.S. Schwarz and E.Witten, *Superstring Theory.* (Cambridge University Press, Cambridge, 1987).

83. H. E. Haber and G. L. Kane, *Phys. Rep.* **117,** 75 (1985).

84. J.F. Gunion and H.E. Haber, *Nucl. Phys.* **B272,** 1 (1986).

85. J.F. Gunion and H.E. Haber, *Phys. Rev.* **D37,** 2512 (1988).

86. M. Drees, C.S. Kim, and X. Tata, *Phys. Rev.* **D37,** 784 (1988).

87. A. Bartl, H. Fraas and W. Majerotto, *Z. Phys.* **C30,** 441 (1986); *Nucl. Phys.* **B278,** 1 (1986).

88. J.-M. Frere and G.L. Kane, *Nucl. Phys.* **223,** 331 (1983); J. Ellis, J.-M. Frere, J.S. Hagelin, G.L. Kane and S.T. Petcov, *Phys. Lett.* **132B,** 436 (1983).

89. S. Dawson, E. Eichten and C. Quigg, *Phys. Rev.* **D31,** 1581 (1985).

90. J.F. Gunion and H.E. Haber, *Nucl. Phys.* **B278,** 449 (1986).

91. H. Baer, V. Barger, D. Karatas and X. Tata, *Phys. Rev.* **D36,** 96 (1987); R.M. Barnett and H.E. Haber, unpublished.

92. R.M. Barnett, J.F. Gunion and H.E. Haber, *Phys. Rev. Lett.* **60,** 401 (1988); *Phys. Rev.* **D37,** 1892 (1988).

93. J.F. Gunion, H.E. Haber, F.E. Paige, W.-K. Tung and S.S.D. Willenbrock, *Nucl. Phys.* **B294,** 621 (1987).

94. G. Altarelli, in *Proceedings of the XXIII International Conference on High-Energy Physics (Berkeley),* S. C. Loken, ed. (World Scientific, Singapore, 1987).

95. H.E. Haber, G.L. Kane and T. Sterling, *Nucl. Phys.* **B161,** 493 (1979).

96. W. Bartel, *et. al., Phys. Lett.* **114B,** 211 (1982); *Z. Physik* **C31,** 359 (1986).

97. H.-J. Behrend, *et. al., Phys. Lett.* **193B,** 376 (1987).

98. A. Chen, *et. al., Phys. Lett.* **122B,** 317 (1983).

99. S. Komamiya, in *Proceedings of the Third Mark-II Workshop on SLC Physics, Pajara Dunes,* G. J. Feldman, ed. SLAC-Report-315 (1987).

100. H.-U. Bengtsson, S. Komamiya and H. Yamamoto, *Int. J. Mod. Physics* **A2,** 1055 (1987).

101. J.F. Gunion, H.E. Haber, S. Komamiya, H. Yamamoto and A. Barbaro-Galtieri, in *Proceedings of the Workshop on Experiments, Detectors, and Experimental Areas for the Supercollider (Berkeley),* R. Donaldson and M. G. D. Gilchriese, eds. (World Scientific, Singapore, 1988).

102. T.L. Barklow, Ph. D. thesis, University of Wisconsin (Madison) RX-1030 (1983).

103. T. Sjostrand, Computer Phys. Comm. 27(1982)234, ibid. 28(1983)229, ibid. 39(1986)347.

104. R. Marshall, *Z. Physik* **C26,** 291 (1984).

105. T.L. Barklow, in *Proceedings of the Second Mark-II Workshop on SLC Physics (Granlibakken),* G. J. Feldman, ed. SLAC-Report-306 (1986).

106. S. Nandi, OSU-RN-200 (1987).